# Investigations on Flagellar Biogenesis, Motility and Signal Transduction of *Halobacterium salinarum*

**Wilfried Staudinger**

aus

Heilbronn

2007

## Erklärung

Diese Dissertation wurde im Sinne von § 13 Abs. 3 der Promotionsordnung vom 29. Januar 1998 von Herrn Prof. Dr. Dieter Oesterhelt betreut.

## Ehrenwörtliche Versicherung

Diese Dissertation wurde selbständig und ohne unerlaubte Hilfe angefertigt.

München, am 22. April 2008

. . . . . . . . . . . . . . . . . . .
Wilfried Staudinger

Dissertation eingereicht am: 09.11.2007

1. Gutachter: Prof. Dr. Dieter Oesterhelt

2. Gutachter: Prof. Dr. Wolfgang Marwan

Mündliche Prüfung am: 17.03.2008

This dissertation was generated at the Max Planck Institute of Biochemistry, in the Department of Membrane Biochemistry under the guidance of Prof. Dr. Dieter Oesterhelt.

**Parts of this work were published previously or are in preparation for publication:**

Poster presentation at the Gordon Conference on Sensory Transduction In Microorganisms, Ventura, CA, USA, January 22-27, 2006. Behavioral analysis of chemotaxis gene mutants from *H. salinarum*.

del Rosario, R. C., Staudinger, W. F., Streif, S., Pfeiffer, F., Mendoza, E., and Oesterhelt D. (2007). Modeling the CheY$^{(D10K,Y100W)}$ *H. salinarum* mutant: sensitivity analysis allows choice of parameter to be modified in the phototaxis model. *IET Systems Biology*, 1(4):207-221.

Koch, M. K., Staudinger, W. F., Siedler, F., and Oesterhelt, D. (2007). Physiological sites of deamidation and methyl esterification in sensory transducers of *H. salinarum*. In preparation.

Streif, S., Staudinger, W. F., Joanidopoulos, K., Seel, M., Marwan, W., and Oesterhelt, D. (2007). Quantitative analysis of signal transduction in motile and phototactic archaea by computerized light stimulation and tracking. In preparation.

*Meinen Eltern*

*"Die beste und sicherste Tarnung ist immer noch die blanke und nackte Wahrheit. Die glaubt niemand!"*

**Max Frisch**
schweizer Schriftsteller (1911 - 1991)

# Contents

# List of Figures

# List of Tables

# 1 Summary

The extremely halophilic archaeon *Halobacterium salinarum* thrives in salt lakes and solar salterns. To survive in these hostile environments *H. salinarum* on the one hand employs a variety of bioenergetic strategies e.g. photosynthesis by the proton pump bacteriorhodopsin. On the other hand, *H. salinarum* employs a bacteria-like two-component chemotaxis- and phototaxis system to search its environment for optimal nutrient and light conditions in a trial and error fashion.

*H. salinarum* cells are propelled by one to two polarly inserted semi-rigid right handed helical flagellar bundle(s) that consist of five to ten filaments. Monopolarly flagellated cells swim forth by clockwise (CW) and back by counterclockwise (CCW) rotation of the flagellar bundle. Swimming phases are interrupted by a short stop that is followed by a change of flagellar rotational direction. In unstimulated cells, the average durations of CW and CCW swimming phases are equal which results in a random walk. A biased random walk which directs the cells to favorable conditions arises by shortened swimming phases upon negative stimulation and prolonged swimming phases upon positive stimulation. In contrast, peritrichously flagellated *E. coli* cells alternate between swimming by CCW and tumbling by CW rotation of their flagellar motors.

At the beginning of this study, it was known that despite their superficial similarity, bacterial and archaeal flagellar motility are different with respect to flagellar biogenesis and molecular composition and function of the flagellar motor. In the complete genome of *H. salinarum*, homologs to proteins of the bacterial flagellar motility system are absent. However, a so-called *fla* gene cluster had been found and the phenotype of a *flaI* mutant had shown that FlaI is involved in flagellar biogenesis. A bioinformatic analysis presented in this study indicated that the function of the Fla proteins may not be restricted to flagellar biogenesis. In particular, the analysis showed that:

1. FlaI is a putative ATPase.

2. FlaJ is predicted to be a membrane-spanning protein with 8 transmembrane helices.

3. Both FlaI and FlaJ are homologs to proteins of the type II secretory pathway and the type IV pili system.

4. FlaH is a putative ATPase without homology to proteins of the type II secretory pathway and the type IV pili system.

5. While FlaI and FlaJ are most likely involved in flagellar biogenesis, FlaH is a candidate for a flagellar motor protein. This implies that:

   a) the ATPase site of FlaH is not required for flagellar biogenesis but for energization of the flagellar motor.

  b) ATP rather than protons is the driving force of the *H. salinarum* flagellar motor.

6. FlaD and FlaCE both have a FlaD/E domain.

7. FlaCE is a fusion protein with a N-terminal FlaD/E and a C-terminal FlaC domain.

In order to investigate the function of the FlaJ, FlaD, FlaCE and FlaJ proteins, mutants carrying single in-frame deletions of the corresponding genes were generated. The presence of flagella and the motility of these mutants and an already existing *flaH* deletion mutant was investigated with swarm plates, computerized cell tracking, high intensity dark-field microscopy and electron microscopy. The following results were obtained:

1. The *flaJ* and *flaH* mutants were devoid of flagella and belonged to the Fla⁻ mutant class.

2. The *flaCE* mutant was immotile, had a single filament and belonged to the Mot⁻ mutant class.

3. The *flaD* mutant also had a single filament, but showed residual motility and belonged to the Mot⁻ mutant class.

As both the *flaCE* and the *flaD* mutants had only one filament, that lack of the FlaDE domain may be responsible for this phenotype. The paralysis of the single filament in case of the *flaCE* mutant may then be attributed to lack of the FlaC domain, which in turn means that FlaCE is involved in flagellar rotation. Considering the results of the bioinformatic analysis, the non-flagellated phenotype of the *flaH* mutant suggests that FlaH has a dual role. It may act as scaffold protein that is involved in energization of the flagellar motor by ATP hydrolysis.

*H. salinarum* flagellar filaments consist of five flagellins. However, in the genome a gene coding for a further flagellin homolog, *flgXXX* was identified. FlgXXX might have escaped previous detection due to its low abundance. To test this hypothesis the motility of a *flgXXX* mutant was investigated with swarm plates. Deletion of *flgXXX* had neither an influence on flagellar biogenesis nor on motility, which makes it very unlikely that FlgXXX is a component of the *H. salinarum* filament.

*H. salinarum* senses stimuli like amino acids, oxygen, compatible osmolytes, light and membrane potential by a set of eighteen membrane spanning and soluble receptors (Htrs) that are homologous to the *E. coli* methyl accepting chemotaxis proteins (MCPs). In *E. coli*, stimuli sensed by MCPs are intracellularly relayed to the flagellar motor by chemotaxis (Che) proteins. CheW couples the autophosphorylating histidine kinase CheA to MCPs and CheA phosphorylates the response regulator CheY. Phosphorylated CheY (CheY-P) binds to the motor switch to induce tumbling of the cells. CheR and CheB confer adaptation to persisting stimuli by adding and removing methyl groups on MCPs, respectively and CheZ terminates the signal by dephosphorylating CheY-P. Analysis of the complete genome revealed that *H. salinarum* has an extended set of chemotaxis genes which codes for one homolog each of CheA, CheY, CheB and CheR and in addition

codes for two CheW homologs, three homologs to *B. subtilis* CheC and one homolog to *B. subtilis* CheD. In *B. subtilis*, CheC is the CheY-P phosphatase instead of CheZ and CheD is a MCP deamidase instead of CheB.

Before this study, the function of *H. salinarum* CheA and CheY and the phenotypes of *cheY*, *cheA*, *cheB*, *cheC1*, *cheW1* and *cheW2* knockout mutants had been analyzed. However, except for homologies, nothing was known about the function of the remaining chemotaxis proteins. In order to address this question, *cheR*, *cheC3* and *cheD* knockout mutants were generated and analyzed with respect to their swimming behavior and their ability to perform chemo- and phototaxis. The knockouts of *cheB* and *cheC1* had to be repeated as the genotype of the previous mutants turned out to be ambiguous and the reported phenotype of the mutants was potentially influenced by polar effects.

In order to find out more about the effect of CheY-P on the motor switch of *H. salinarum*, the wild type *cheY* allele was replaced by a *cheY*$^{\text{D10K,Y100W}}$ (*cheY*$^{**}$) allele. Due to its effect in *E. coli*, CheY$^{**}$ was expected to mimic non-hydrolyzable, permanently activated CheY-P. A comparison of the phenotypes of this mutant and a *cheY* knockout mutant that lacks both CheY as such and CheY-P should give interesting insights into the properties of the *H. salinarum* motor switch. Spontaneous reversal frequencies and phototaxis of the mutants were analyzed with a computerized cell tracking system. The rotational bias of the mutants was determined by high-intensity dark-field microscopy and their ability to perform chemotaxis was analyzed by a swarm plate assay. The availability of the *cheR* and *cheB* mutants allowed a comparison of the Htr methylation states in these mutants and in wild type cells by a mass spectrometric approach. The following results were obtained:

1. CheR is the methyltransferase and CheB is the methylesterase for Htrs.

2. CheB but not CheD is the deamidase for Htr2 and Htr4.

3. All Che proteins investigated in this study were essential for efficient photo- and chemotaxis of *H. salinarum*.

4. Except the *cheB* mutant, all other mutants had reduced spontaneous reversal frequencies; none of the mutants including the *cheB* mutant had an increased spontaneous reversal frequency.

5. All mutants except the *cheC1* mutant had CW biases deviant from the wild type 50% CW. The CW biases of the mutants ranged from 30% to 99% CCW.

6. The *cheC1* mutant had a wild type like bias in contrast to the previously reported 88% CW bias.

7. Unlike previously reported, the *cheB* mutant

   a) had a wild type spontaneous reversal frequency instead of drastically elevated reversal frequency.

   b) had a 30% CW bias instead of a 50% wild type bias.

   c) responded to photostimuli, albeit with reduced efficiency.

8. The $cheY^{**}$ mutant was indistinguishable from the $cheY$ knockout mutant with respect to spontaneous reversal frequency, 99% CW bias and the complete absence of photo- and chemotaxis.

9. Phototactic and chemotactic efficiencies of the mutants correlated only weakly, which is exemplified by the observations that

    a) all mutants except the $cheY^{**}$ mutant were able to perform at least residual chemotaxis.

    b) the $cheC3$ mutant showed only weak response to photostimuli, but exhibited the best chemotactic response of all mutants.

    c) the $cheR$ mutant did not respond to photostimuli, but showed a chemotactic response comparable to that of the phototactic $cheB$ mutant.

The observed low to wild-type like spontaneous reversal frequencies and altered CW biases of the mutants were unexpected for the following reasons. When the effect of CheY-P on the *E. coli* flagellar motor is transferred to the swimming behavior of *H. salinarum*, one would expect that low CheY-P steady state concentrations like in a $cheR$ mutant result in decreased switching frequency and high CheY-P steady state concentrations like in the $cheB$ and the $cheY^{**}$ mutants result in high switching frequencies. CheY-P is not expected to affect the CW bias. However, modeling of *H. salinarum* motor switching and its sensory control had shown that *E. coli* motor models cannot be applied to *H. salinarum*. Indeed the low to wild-type like switching frequencies of the mutants were consistent with the *H. salinarum* motor model. In the model, temporarily elevated CheY-P concentrations induce motor switching, but both permanently increased and permanently decreased steady state CheY-P concentrations lower the switching probability. As the model parameters are symmetric with respect to CW and CCW rotational modes, CW biases deviant from 50% could not be explained. This gave rise to the idea that the *H. salinarum* motor is actually pseudosymmetric, i.e. parameters for CW and CCW mode are actually different, but at intermediate, wild type CheY-P steady state concentrations the motor behaves symmetrically. Only at high or low CheY-P steady state concentrations the asymmetry becomes apparent. These considerations resulted in a modified motor model that was able to explain the 99% CW of the $cheY^{**}$ mutant and was still able to reproduce all data which were the basis of the previous model.

The weak correlation of the mutants´ chemo- and phototactic efficiencies is a new and unexpected aspect of *H. salinarum* signal transduction. One explanation is the presence of a methylation-independent adaptation system that works at low stimulus concentrations. Another explanation is the existence of alternative Htr-mediated signal transduction pathways. These pathways may consist of an invariant core of chemotaxis proteins that is differentially supplemented by additional chemotaxis proteins. To settle these interesting issues, further studies are required.

# 2 Introduction

## 2.1 The organism *Halobacterium salinarum* and its lifestyle

### 2.1.1 Taxonomic classification

*Halobacterium salinarum*[1] is an extremely halophilic organism that belongs to the domain *Archaea* (phylum: *Euryarchaeota*, class: *Halobacteria*, order: *Halobacteriales*, family: *Halobacteriaceae*, genus: *Halobacterium*) (Garrity et al., 2004). The *Archaea* were introduced in the 1970s by Carl Woese as a new, distinct domain besides the *Bacteria* and *Eukarya* on the basis of 16S rRNA sequences (Woese and Fox, 1977; Woese et al., 1990). Woese chose the term Archaea, because the organisms that were first assigned to this new domain were adapted to extreme conditions that might have existed on the early (Archaean) earth. However, it is known today that archaea are not exclusively extremophiles, but are found in most diverse habitats and may constitute as much as 20% of the total biomass (DeLong and Pace, 2001). Archaea share similarities with both Bacteria and Eukarya. It is often stated - although slightly oversimplified - that operational genes that are associated with central metabolism, energy conversion and biosynthesis are of bacterial origin, whereas those associated with information processing such as transcription and translation are of eukaryotic nature (see Allers and Mevarech (2005) and references therein). On the other hand, a closed circular chromosome and polycistronic messages are bacterial features. The presence of a high fraction (up to 50%) of genes in archaeal genomes without clear function underscores that there is more to archaea than just a combination of bacterial and eukaryotic properties.

Even before archaea were recognized as a new domain, special features like a peculiar spectrum of antibiotic sensitivity, the presence of N-linked glycoproteins and a cell envelope structure obviously distinct from bacterial ones, were noted. With the exception of *Ignicoccus* species, archaea do not possess a true periplasmic space. Halophilic and most mesophilic archaeal cells are enclosed by a typical lipid bilayer, albeit of special lipid content, but lack a peptidoglycan layer. Instead, the lipid bilayer is surrounded by a cell surface glycoprotein layer (S-layer). The S-layer of *Haloferax volocanii* and *H. salinarum* is a crystalline lattice of hexagonally arranged subunits that form dome-shaped structures and it contains pores permeable to solutes and small proteins (Kessel et al., 1988; Trachtenberg et al., 2000). S-layers are not restricted to archaea, but in contrast to bacterial S-layers, their archaeal counterparts are directly anchored to the cytoplasmic membrane.

---

[1]Over the years, the species name was changed from initially *Halobacterium halobium* to *Halobacterium salinarium* and finally to *Halobacterium salinarum*. The species also includes strains previously called *Halobacterium cutirubrum* and *Halobacterium* sp. NRC-1.

While lipids of bacteria and eukaryotes consist of fatty acids that are covalently linked to glycerol via ester bonds, archaeal membrane lipids consist of phytanyl groups (saturated $C_{20}$ alkyl chains derived from isoprenyl groups) that are linked to the glycerol backbone via a chemically more inert ether bond (Langworthy and Pond, 1986). Membrane lipids of *H. salinarum* are almost exclusively derived from *sn*-2,3 Diphytanylglycerol-diether (archaeol) (Kates, 1996).

## 2.1.2 The habitat of *H. salinarum*

As an extremely halophilic organism *H. salinarum* is not salt-tolerant, but rather requires high salt concentrations to survive. Depending on the presence of other stabilizing ions, especially divalent cations like $Mg^{2+}$ and $Ca^{2+}$, 3 - 5 M NaCl are required for growth and maintenance of cell shape (Stoeckenius and Rowen, 1967). Laboratory strains are routinely grown at 40°C in peptone medium containing 4.3 M NaCl and minor amounts of KCl and $MgCl_2$ (Oesterhelt and Krippahl, 1983). The natural habitats of *H. salinarum* are salt lakes and solar salterns. Besides their high salinity, these habitats are characterized by intense illumination and high temperatures altogether leading to a low oxygen tension. An especially striking feature of these habitats is their red color, which is caused by the growth of halophilic organisms (Figure 2.1). Many of these organisms produce carotenoids such as bacterioruberin to protect themselves against photooxidative damage. In addition, *H. salinarum* produces the purple pigment bacteriorhodopsin in large amounts, which it uses to perform a second kind of photosynthesis (see 2.1.4).



**Figure 2.1: Picture of a solar saltern on Lanzarote, Spain, 1992.**
The red color is caused by growth of halophilic organisms e.g. *H. salinarum*.

Although a number of defined media were described for *H. salinarum*, its exact nutritional demands seem to be rather complex and there are indications that even complex medium does not contain all constituents needed for optimal growth. However, it seems to be clear that *H. salinarum* mainly uses amino acids as carbon source and it is thought

that these amino acids are released from other halophilic organisms upon their death e.g. from the green alga *Dunaliella salina*.

*H. salinarum* has developed several strategies to cope with the hostile conditions of its habitat, some of which will be discussed in the following.

### 2.1.3 Adaptation to hypersaline conditions

Most halophilic bacteria, e.g. *Halomonas elongata*, maintain their osmotic balance despite high extracellular salt concentrations by uptake or synthesis of compatible osmolytes such as glycerol, glycine-betaine or ectoine (Grammann et al., 2002). In contrast, halophilic archaea like *H. salinarum* and *Natronomonas pharaonis* employ a "salt-in" strategy: high sodium concentrations outside the cell are counterbalanced by even higher potassium concentrations in the cytosol (Engel and Catchpole, 2005; Falb et al., 2005). As a consequence proteins of *H. salinarum* have to be adapted to remain soluble in high salt concentrations. Halophilic proteins are characterized by a high abundance of negatively charged, acidic residues which increases stability and enhances solubility in order to prevent precipitation (salting-out). Thus, in *H. salinarum* the majority of all proteins have p$I$ values between 3.5 and 5.5 (Tebbe et al., 2005; Klein et al., 2005). Usually the acidic residues are found on the solvent-exposed surface of the proteins. In addition to intrinsically halophilic proteins, there are more than 200 proteins in *H. salinarum*, probably acquired from bacteria via lateral gene transfer that were rendered halophilic by insertion of a stretch of acidic amino acids (`http://www.halolex.mpg.de`). The plant-type ferredoxin of *H. salinarum* is a typical example of this strategy (Marg et al., 2005).

A related issue is protein folding and secretion at high salinity. Halophilic archaea make extensive use of the twin-arginine translocation (Tat) pathway (reviewed by Albers et al. (2006)). In the Tat pathway, proteins are translocated across the membrane in their fully folded state. The Tat pathway owes its name to an almost invariant pair of arginine residues within a semi-conserved S-R-R-X-F-L-K (X is for any amino acid) motif contained in the signal sequence of the target proteins. It is present in most bacteria and archaea, but predominant in haloarchaea like *H. salinarum* and was shown to be essential for viability of *H. volcanii* under aerobic growth conditions (Rose et al., 2002; Dilks et al., 2005).

### 2.1.4 Energy metabolism

Due to the challenging living conditions of *H. salinarum*, several alternative pathways for energy production and storage evolved in this organism. *H. salinarum* is capable of oxidative phosphorylation by aerobic and anaerobic respiration, substrate level phosphorylation by fermentation of L-arginine and photophosphorylation by retinal protein based photosynthesis mediated by bacteriorhodopsin in combination with the ATP synthase.

*H. salinarum* degrades organic compounds via the TCA cycle using oxygen as terminal electron acceptor (Ghosh and Sonawat, 1998). In case of oxygen shortage which is quite common in saturated brines, trimethylamine $N$-oxide (TMAO), dimethylsulfoxide (DMSO) and to some extent fumarate can be used as alternative terminal electron acceptors (Oren and Trüper, 1990; Oren, 1991).

L-arginine is fermented via the arginine-deiminase (ADI) pathway (Hartmann et al., 1980; Ruepp and Soppa, 1996). First, arginine is taken up by an arginine:ornithine antiport and gets degraded to citrulline by the arginine deiminase. Then, catalyzed by the catabolic ornithine transcarbamylase, citrulline reacts with inorganic phosphate to carbamoyl phosphate and ornithine that in turn drives the antiport. In the last step, carbamate kinase transfers phosphate from carbamoylphosphate to ADP, leading to the production of one mole ATP from one mole arginine in total.

In case of shortage of organic nutrients, *H. salinarum* can still grow phototrophically with light as sole energy source. The photobiology of *H. salinarum* is dominated by the four retinal-containing seven-transmembrane-helix proteins bacteriorhodopsin (BR), halorhodopsin (HR) and the two sensory rhodopsins I and II (SRI and SRII)(reviewed by Oesterhelt (1998)).

BR acts as light-driven outward directed proton pump that mediates photophosphorylation. The chromophore retinal is bound in the space between the seven membrane-spanning helices (A-G) to a lysine in helix G forming a Schiff base. Light activation of BR triggers a photocycle in which retinal is isomerized from all-*trans* to 13-*cis* and back accompanied by de- and reprotonation of the Schiff base and conformational changes in the protein. This leads to proton release to the extracellular space against the membrane potential followed by proton uptake from the intracellular space. Following their gradient, the extruded protons flow back into the cell thereby driving ATP synthesis by the ATPase (see Schäfer et al. (1999) and references therein). Via the actions of a sodium:proton antiport and a potassium uniport, the proton gradient may also be used to charge a potassium/sodium "battery" that is discharged in the darkness to maintain the ATP level (Wagner et al., 1978).

HR acts as a light-driven inwardly directed chloride pump (Schobert and Lanyi, 1982). As in the case of proton pumping by BR, chloride pumping changes the membrane potential and thus energizes the system. However, this cannot lead to sustained photophosphorylation as the halobacterial ATPase specifically utilizes protons for ATP synthesis. Rather, it is thought that the active import of chloride ions by the action of HR helps to maintain the high intracellular chloride concentrations required for osmotic balance of the cells especially during growth.

## 2.1.5 Morphology and swimming behavior of *H. salinarum*

*H. salinarum* cells are rod shaped, 2 - 6 µm long, approximately 0.4 - 0.7 µm wide and usually polarly flagellated. However, flagella emerging from random sites are sometimes observed, especially on unusually long, filamentous cells. Monopolarly and bipolarly flagellated cells are observed in any growth phase, but while in the logarithmic phase the majority of the cells are monopolarly flagellated, bipolarly flagellated cells are predominant in the stationary phase (Alam and Oesterhelt, 1984). Five to ten flagella form a semi-rigid, right handed helical bundle. Cells are pushed forward by clockwise (CW) and pulled backward by counterclockwise (CCW) rotation of the flagellar bundle as revealed by high-intensity dark-field microscopy.

CW rotation leads to a more efficient locomotion than CCW rotation (Marwan et al., 1991). The rotatory principle of the halobacterial flagellar motor was shown in a classical
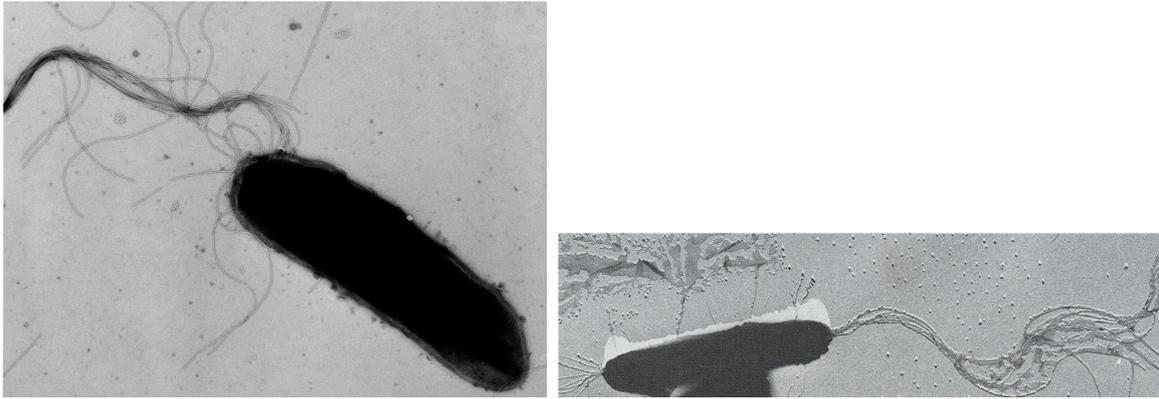
**(A)** Monopolarly flagellated *H. salinarum* cell.      **(B)** Bipolarly flagellated *H. salinarum* cell.

**Figure 2.2: Electron micrographs of mono and bipolarly flagellated *H. salinarum* cells**. Cells are typically 2 - 6 µm long and 0.4 - 0.7 µm wide. **(A)** Monopolarly flagellated, uranyl acetate stained cell. The micrograph was taken by Harald Engelhardt (Staudinger, 2001). **(B)** Bipolarly flagellated, platinum/carbon shadowed cell. It is frequently observed that one flagellar bundle is shorter than the other. The micrograph is taken from Alam and Oesterhelt (1984). An example of a laterally flagellated cell is given in Figure 3.6 (C).

assay developed by Silverman and Simon (1974): when *H. salinarum* cells are tethered to a glass surface via their flagella, the cell body rotates either CW or CCW and rotation is sometimes spontaneously interrupted by a short stop phase of several hundred milliseconds, followed by a change in rotational direction (Alam and Oesterhelt, 1984; Marwan et al., 1991). Switching the rotational sense does not dissociate the flagellar bundle into single filaments. In contrast, the peritrichously distributed, left handed helical flagellar filaments of the bacterial prototypes *E. coli*, *S. typhimurium* and *B. subtilis* form a cooperative bundle upon CCW rotation leading to effective forward swimming, but fall apart upon CW rotation or pausing, leading to tumbling of the cells (Fig. 2.8). The fact that flagella of the peritrichously flagellate halophilic archaeon *Haloarcula quadrata* do not disentangle upon switching demonstrates, that the stability of bundle association does not depend on the mode of flagellation, but is a property of archaeal flagellar filaments (Alam et al., 1984). Figure 2.3 shows the principle swimming modes of mono- and bipolarly flagellated *H. salinarum* cells and indicates that bipolarly flagellated cells are capable of all swimming modes of monopolarly flagellated cells, even if the two flagellar bundles do not act in a coordinated fashion.

Whether the filaments of a bundle are driven by their own spatially separated motors or all end on a single rotary unit is still an open question. In any case, it seems that the individual filaments act synchronously as cells swim with almost constant speed, before they stop all of a sudden (Marwan et al., 1991).

Without stimulus, the cells change their swimming direction by switching the rotational sense of the flagellar bundle every 10 - 20 s on average, depending on the observation conditions. During the short stop phase, the cells are usually slightly displaced by Brownian motion. Thereby, the cells do not swim back and forth the same paths all the time, but perform a so-called random walk. However, over time unstimulated cells do not change their spatial position. The random walk becomes a biased random walk as soon as the

cells are stimulated: attractant stimuli like nutrients suppress motor switching, leading to prolonged swimming in the current direction whereas repellent stimuli e.g. harmful substances lead to premature switching. Thus, the cells search their environment for optimal thriving conditions in a trial and error fashion and accumulate at sites that offer such conditions.



**A**

**B**

| right bundle <br> left bundle | CW | CCW | stop |
|---|---|---|---|
| **CW** | stop | right | right |
| **CCW** | left | stop | left |
| **stop** | left | right | stop |
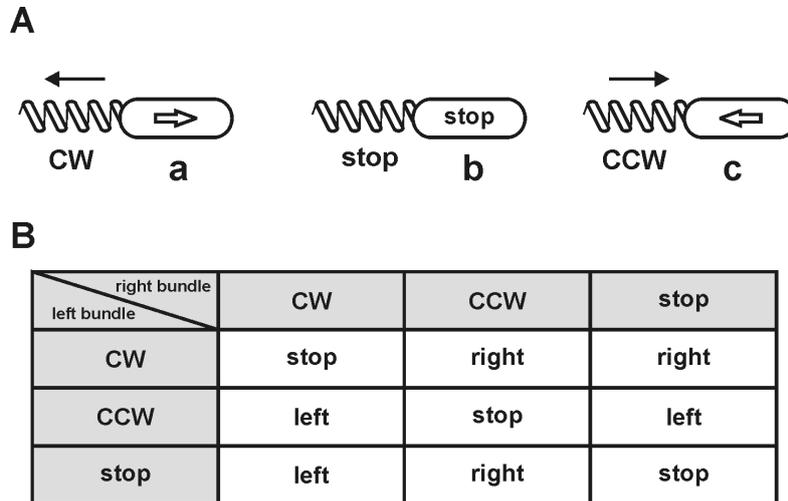
**Figure 2.3: Sketches of the principal swimming modes observed in *H. salinarum* cells.** **(A)** Monopolar cells, **(a)** move forward by clockwise rotation; **(b)** stop or **(c)** swim backward by counter-clockwise rotation of their right-handed helical flagella. The definition proposed by Macnab and Ornston (1977) for light-wave propagation of flagella and cell body movement is adopted. The swimming direction of the cell is indicated by open arrows, the direction of light wave propagation is indicated by solid arrows. After a stop **(b)**, the cells reverse their swimming direction. **(B)** Bipolarly flagellated cells show all possible combinations of rotation of the two flagellar bundles resulting in 9 modes: 3 modes that result in a stop, 3 possibilities that result in swimming to the right and 3 possibilities that result in swimming to the left. Figure and figure captions are modified from Alam and Oesterhelt (1984).

## 2.2 Structure and biogenesis of archaeal flagella

### 2.2.1 Archaeal and bacterial flagella are only superficially similar

Archaeal and bacterial flagellar filaments share many morphological, functional and phenomenological properties. They are both semi-rigid, helical, polymorphic motility structures that form bundles and are driven by a rotatory motor. It is therefore not surprising that initially composition and assembly of these motility organelles were believed to be largely identical. The structure of the bacterial flagellum and the processes involved in its assembly e.g. gene regulation and protein secretion have been studied in great detail (reviewed by Macnab (2003, 1999)). Recently, much effort has been made to obtain even more structural detail which resulted in X-ray structures of the filament protein and highly resolved EM structures of the whole organelle from frozen-hydrated cells (Samatey et al., 2001; Murphy et al., 2006). Compared to this detailed knowledge, research on the archaeal motility structure is still in its infancy. Nevertheless, the data available so far

clearly show, that composition and assembly of this machine and probably even the way it is powered are significantly distinct from its bacterial counterpart.

## 2.2.2 Structure, function and assembly of bacterial flagella

The bacterial flagellum comprises three main substructures, the filament, the hook and the basal body (Fig. 2.4). The filament is usually composed of one protein, flagellin FliC and is terminated at its tip by a capping protein FliD (HAP2)[2]. The junction to the more flexible hook, that consists of a single protein, FlgE, is accomplished by the hook associated proteins FlgK (HAP1)[2] and FlgL (HAP3)[2].

The basal body fulfils three functions: it anchors the flagellum to the membranes and cell wall, converts a transmembrane ion gradient into a rotational motion that can be switched between CW and CCW states and exports structural proteins for flagellum assembly. In Gram-negative bacteria like *E. coli* three ring-like structures anchor the flagellum to the cytoplasmic membrane (MS ring), the peptidoglycan layer (P ring) and the outer membrane (L ring). Gram-positive bacteria like *B. subtilis* lack the P and L rings. The motor consists of stator and rotor. The stator is made by MotAB complexes that embrace the rotor and form a proton conducting channel (Braun et al., 2004). While MotA is anchored to the cytoplasmic membrane, MotB is also anchored to the peptidoglycan layer. The rotor is a ring-like structure (also called C ring) that extends to the cytoplasm and consists of several proteins including the switch proteins FliG, FliM, FliN and, in the case of *B. subtilis*, additionally FliY (Bischoff and Ordal, 1992). FliG interacts with the MotAB complexes to convert the transmembrane proton gradient into rotation and the whole switch complex allows the motor to switch between CW and CCW rotation (Park et al., 2006b; Brown et al., 2007). Rotation of the C-ring is transferred to the hook via a thin rod that spans the MS, P and L rings.

Assembly of the flagellum starts from the base and the MS ring is the first partial structure observable by electron microscopy (Aizawa, 1996). At a later stage however, the flagellins are transported through the hollow core of the growing filament and assembled at its tip, a process in which the capping protein HAP2 plays an essential role (Yonekura et al., 2000; Hughes and Aldridge, 2001). Mutants that lack HAP2 secrete flagellin, but fail to assemble it. Flagellin export occurs by a specialized type III export apparatus that resides in the interface of the C and the MS ring.

## 2.2.3 Structure and morphology of archaeal flagella

Archaeal flagellar filaments have a diameter of 10 - 14 nm and are therefore only about half as thick as their bacterial counterparts. More importantly, the *H. salinarum* filament lacks a central channel, which excludes assembly of newly synthesized flagellins at the tip (Cohen-Krausz and Trachtenberg, 2002; Trachtenberg et al., 2005). So far any attempts to isolate an intact archaeal flagellar motor failed. Methods that were established to isolate bacterial flagella with the motor attached e.g. solubilization of the cell

---

[2]Protein names in front of parentheses are according to the nomenclature of Iino et al. (1988), while names in parentheses are alternative, commonly used protein names.
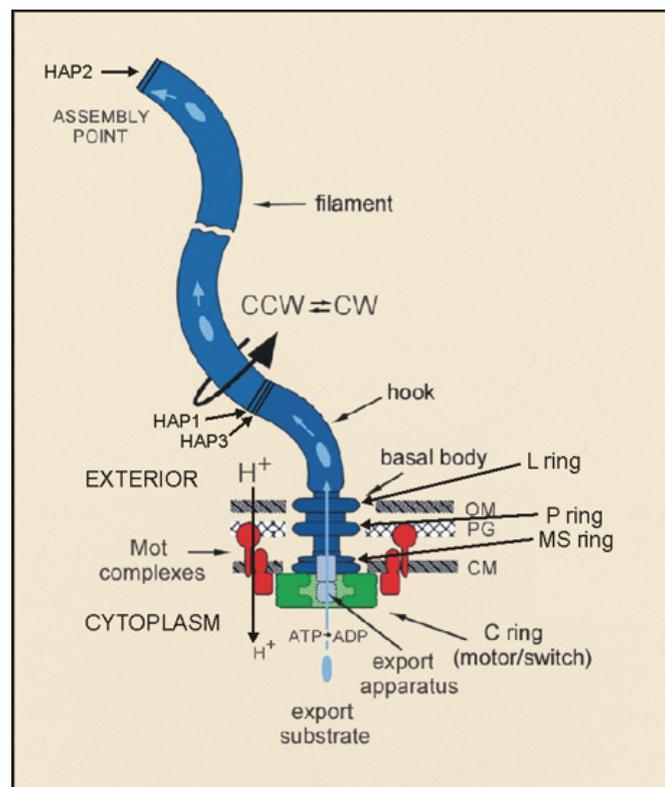
**Figure 2.4: Sketch of the bacterial flagellum**. The flagellum is the motor organelle for bacterial propulsion. Driven by a transmembrane proton gradient ($H^+ \rightarrow H^+$), it rotates both CCW and CW; The motor consists of stators or Mot complexes (red) and a rotor or C ring (green), which also serves as the CCW $\rightleftharpoons$ CW switch. As well as being the organelle of motility, the flagellum is a specialized type III export apparatus (lilac), translocating subunits of its substrates (pale blue) in an ATP-dependent manner across the plane of the cytoplasmic membrane (CM) and delivering them into a central channel in the basal body-hook-filament structure where they eventually reach their assembly point at the distal end of the structure. PG, peptidoglycan layer; OM, outer membrane. Figure and figure captions are slightly modified from Macnab (1999).

membrane with Triton X-100 proved to be difficult as the archaeal motor structures seem to be sensitive to this detergent (Thomas et al., 2001a), which may reflect a different mode of anchoring in the cell membrane. Solubilization or phase separation with Triton X-114 yielded somewhat better results. So far hook-like structures were observed in *Methanococcus voltae*, but in contrast to their bacterial counterparts, they were of quite variable lengths (Bardy et al., 2002). Knob-like structures that resemble basal bodies were also observed in several *Methanococcus* species, but the well defined rings (MS, P, L and C) of the bacterial basal body were missing (Kalmokoff et al., 1988). Only in the case of *Methanococcus thermolithotrophicus* and *Methanospirillum hungatei* two rings similar to those of Gram-positive bacteria were reported (Cruden et al., 1989). Notably these preparations included cell-lysis with Triton X-100. Solubilization of *H. salinarum* cell envelopes with Triton X-114 yielded a roundish structure termed "polar cap" with many flagella attached (Kupper et al., 1994). In thin-sections of *H. salinarum* cells a "discoid lamellar structure" was observed at the poles and in close proximity to the flagella emerging from there (Speranskii et al., 1996; Metlina, 2004). Whether the poorly defined anchoring structures seen in most cases are an archaeal feature or rather represent the part of the structure that is resistant to detergent treatment, is still an open question.

## 2.2.4 Archaeal flagellar and type IV pili biogenesis share similarities

Interestingly, none of the archaeal genomes sequenced so far, codes for homologs to the proteins involved in the bacterial flagellar structure or assembly system. Both, archaea and bacteria, employ homologous proteins for chemotaxis including the response regulator CheY. Since in both domains phosphorylated CheY (CheY-P) is thought to bind to switch proteins of the flagellar motor to influence swimming behavior, it is quite astonishing that no homolog to the bacterial switch proteins was found. Instead many similarities to bacterial type II secretion systems (T2SS) and especially to the biogenesis of type IV pili (T4P) were found.

Type IV pili are 5 - 7 nm thick filaments that are found at the poles of many mostly Gram-negative pathogenic bacteria, e.g. *Pseudomonas aeruginosa*, and allow them to adhere to and to translocate over moist surfaces in a flagella-independent manner known as "twitching motility" (Mattick, 2002). Twitching motility plays an important role in host colonization and biofilm formation by a wide range of pathogens and in fruiting body formation of *Myxococcus xanthus*.

The type II secretory pathway is the main terminal branch of the general secretory pathway. It is found in Gram-negative bacteria and is responsible for the release of "virulence factors" like degradative enzymes (proteases, cellulases, pectinases) and toxins (aerolysin, cholera toxin) (Thanassi and Hultgren, 2000). In addition, it was shown that the main pilin-like protein (also called pseudopilin) assembles into a pseudopilus upon overexpression (Sauvonnet et al., 2000).

Common, homologous constituents of the type II secretory pathway, type IV pili- and archaeal flagellar biogenesis are (1) a major (pseudo)prepilin/preflagellin, (2) several minor (pseudo)prepilins/preflagellins, (3) a (pseudo)prepilin/preflagellin peptidase, (4)

an ATPase, (5) a multispanning transmembrane (TM) protein and (6) several additional as yet uncharacterized proteins. An outer membrane secretin present in the type II secretory pathway and type IV pili biogenesis is absent in the archaeal flagellar biogenesis (Peabody et al., 2003). Figure 2.5 summarizes these similarities in a speculative model for the archaeal flagellum.
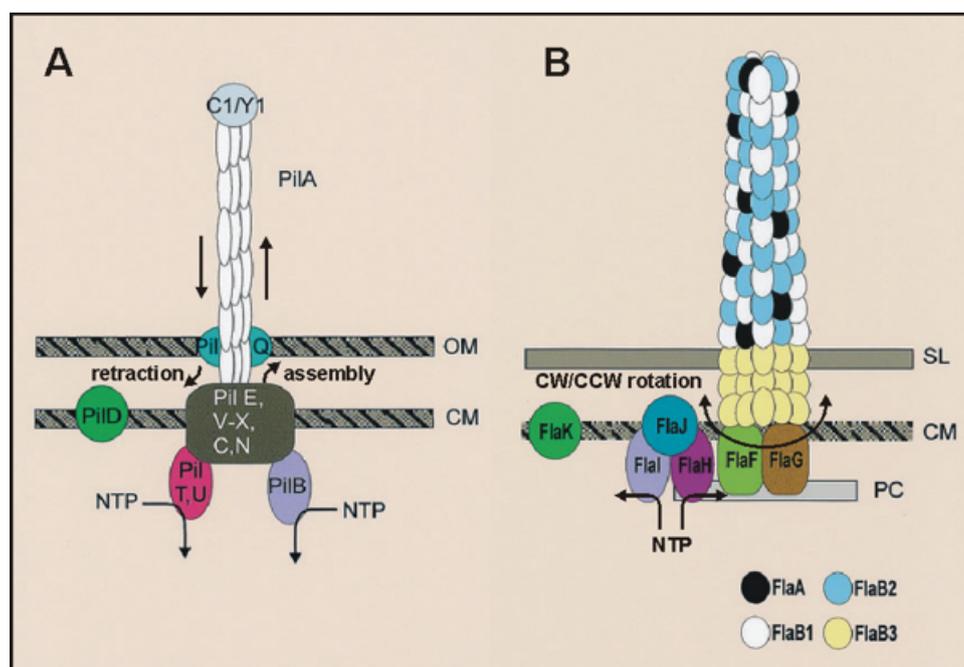


**Figure 2.5: Schematic speculative representation of (A) type IV pilus and (B) archaeal (*M. voltae*) flagellum**. Note that the similarities between the two systems as indicated by these sketches must be restricted to assembly, because the way these structures confer motility is fundamentally different: assembly and retraction in case of pili and rotation in case of archaeal flagella. Elementary structures of the archaeal flagellum like stator and rotor are omitted. **(A)** Type IV pilus. The major pilin (PilA) as well as pilin-like proteins (PilE and PilV–X) are synthesized as preproteins with the leader peptide cleaved by a prepilin peptidase, PilD. PilD is also responsible for methylation of the PilA N-terminal amino acid. The secretin PilQ is required for the type IV pilus to cross the outer membrane (OM). NTP binding proteins (PilT/U and PilB, respectively) are required to provide energy for retraction and assembly. PilC1 or it homolog PilY1 seem to function as tip adhesins required for binding of adhesins to epithelial and endothelial cells. The diameter of the filament is approximately 6 nm. **(B)** Archaeal flagellum, represented by a *M. voltae* flagellum. Flagellin subunits are synthesized as preproteins, with the leader peptide cleaved by the preflagellin peptidase FlaK prior to the incorporation of the flagellins into the filament. Flagellin FlaB3 localizes proximal to the cell surface and may form the hook section of the flagellar filament. FlaI and FlaH are putative NTP-binding proteins. The identification and function of other components of the archaeal flagellum remains unknown. Diameter of the filament is approximately 12 nm. SL, S layer; OM, outer membrane; CM, cytoplasmic membrane; PC, polar cap; CW, clockwise; CCW, counterclockwise. Figures and figure captions are modified from Bardy et al. (2003b).

## Archaeal flagella consist of multiple flagellins that are posttranslationally processed

Archaeal flagella usually consist of two to five flagellins (Thomas et al., 2001a). In *H. salinarum* five highly homologous flagellins were identified (Gerl and Sumper, 1988; Gerl et al., 1989). The corresponding genes are tandemly arranged in two flagellin operons *flgB1-flgB3* and *flgA1-flgA2* that are separated by approximately 40 kb. Mutational studies revealed that despite their high homology, the different flagellins seem to have distinct functions (Tarasov et al., 2000). It has been suggested that the helicity of archaeal flagella is caused by the presence of structurally distinct flagellins rather than the ability of a single flagellin to exist in different conformations (Pyatibratov et al., 2002; Samatey et al., 2001). *M. voltae* possesses four flagellins, two of which (FlaB1 and FlaB2) were shown to be the major components of the flagellar filament (Kalmokoff and Jarrell, 1991). FlaA was later identified as a minor component of the filament and FlaB3 was enriched in a curved region that could represent a kind of hook (Bardy et al., 2002).

Archaeal flagellins are known to undergo two posttranslational modifications: N-terminal cleavage of a signal peptide and glycosylation. Besides their high homology between different archaeal species, archaeal flagellins and bacterial type IV pilins are similar in that they possess a positively charged leader peptide that is followed by a hydrophobic region of approximately twenty amino acids (Faguy et al., 1994). Like in type IV pili, an N-terminal signal peptide of the archaeal flagellins is cleaved off by a peptidase (Thomas et al., 2001b). A preflagellin peptidase activity was first shown in membranes of methanogens e.g. *M. voltae* (Correia and Jarrell, 2000). Based on these results, the cleavage site of flagellins of various archaea including *H. salinarum* were deduced and the amino acids that are important for processing were determined for *M. voltae* FlaB2 (Thomas et al., 2001b). The enzyme responsible for this preflagellin peptidase activity (FlaK) was finally identified in *Methanococcus maripaludis* (Bardy and Jarrell, 2002). Two of five conserved aspartate residues (D18 and D79) were shown to be essential for the function of the heterologously expressed *M. voltae* FlaK (Bardy and Jarrell, 2003), indicating that like the prepilin peptidases, FlaK belongs to a novel aspartic acid protease family (LaPointe and Taylor, 2000). Unlike in other classes of signal peptides, the signal peptide is cleaved off in front of the hydrophobic region. The preflagellin peptidase is a membrane bound enzyme topologically similar to the prepilin peptidase of the type IV pili system (Bardy and Jarrell, 2002, 2003). While the prepilin peptidase is a bifunctional enzyme that N-methylates the pilin after cleavage, N-methylation is not a feature of the archaeal preflagellin peptidase. *H. salinarum* strain R1 also possesses a putative preflagellin peptidase, OE4201R, which possesses the two conserved aspartate residues (D25 and D92, *H. salinarum* numbering) that were shown to be essential for the activity of the *M. voltae* enzyme.

Glycosylation occurs extracellularly. Addition of EDTA, which cannot enter the cells and removes $Mg^{2+}$ from the growth medium, leads to production of flagellins that are reduced in their apparent molecular weight (MW) by approximately 7 kDa (Sumper, 1987). The same apparent MW loss is observed after chemical deglycosylation with anhydrous hydrogen fluoride. All flagellins of *H. salinarum* contain the same sulfated glycans that are N-glycosidically linked to an asparagine residue within a **Asn**-X-(Thr/Ser) motif that

is common to all *N*-linked glycopeptides analyzed so far. The glycoconjugates are of the type

$$\text{Asn} \rightarrow 1\text{Glc4} \rightarrow 1\text{HexUA4} \rightarrow 1\text{HexUA4} \rightarrow (1\text{HexUA or } 1\text{Glc}),$$

with HexUA being either glucuronic or iduronic acid in a stoichiometry of 3:1 and all HexUA being sulfated (Wieland et al., 1985, 1986). The discovery of the Asn-Glc linkage came as a surprise, because previously the only *N*-glycosicid linkage known from Eukarya was Asn-*N*-GlcNAc (Kornfeld and Kornfeld, 1985). In *H. salinarum*, the oligosaccharide moiety is transferred to the Asn residue via a dolichol monophosphate intermediate (Lechner et al., 1985b). Although the glycans attached to the flagellins of *H. salinarum* and *M. voltae* are different, in both organisms the same glycans are also found attached to the cell-surface glycoprotein (CSG) of their S-layers, which indicates that glycan assembly pathways for flagellins and the CSG are at least partially shared (Sumper, 1987; Voisin et al., 2005). The halobacterial CSG is known to contain further sulfated as well as non-sulfated glycans, but it is assumed that the sulfated glycans arise from a common pool of precursors (Lechner et al., 1985a,b). Genes responsible for biosynthesis and attachment of glycans were recently identified in *M. voltae* and a model for glycan assembly and attachment to the flagellins was proposed (Chaban et al., 2006) (Fig. 2.6). The model might at least partially be applicable to *H. salinarum* as homologs of the glycosyl transferase AglA and the oligosaccharyl transferase AglB are also encoded in the genome of *H. salinarum*.

The sequence in which N-terminal cleavage and glycosylation of the flagellins occurs is not clear, but it was shown that these two events are independent of each other (Bardy and Jarrell, 2003; Chaban et al., 2006).
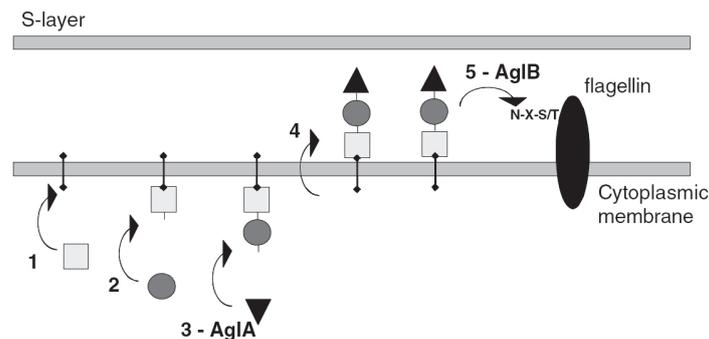


**Figure 2.6: Proposed model for flagellin and S-layer *N*-linked glycan assembly and attachment in *M. voltae*.** Steps 1–3 diagram the assembly of the trisaccharide via glycosyl transferases (AglA for step 3) onto a lipid carrier at the cytoplasmic face of the cytoplasmic membrane. Step 4 represents the translocation of the glycan to the exterior of the membrane via a flippase enzyme. Finally, step 5 shows the attachment of the complete glycan to the target protein via an STT3 oligosaccharyl transferase (AglB). Figure and figure caption are as published by Chaban et al. (2006).

## The archaeal *fla* gene cluster is involved in flagellar biogenesis

The ATPase and the multispanning TM protein that the archaeal flagellar biogenesis has in common with the type two secretion system (T2SS) and type four pili (T4P) biogenesis are encoded by genes that are part of so-called *fla* (***fl**agella **a**ccessory*)[3] gene clusters and are named *flaI* and *flaJ*, respectively. So far *flaH*, *flaI* and *flaJ* were found in the genomes of all sequenced archaea that are known to be flagellated, emphasizing the importance of these genes. FlaH possesses a putative ATPase domain and in contrast to FlaI and FlaJ it seems to lack a corresponding counterpart in the T2SS and in T4P biogenesis. The presence of the other genes that constitute archaeal *fla* gene clusters seems to be less conserved (Klein, 2005). Gene arrangement and location of *fla* gene clusters and their neighboring genes is quite variable, however, in most cases *fla* gene clusters are located in close proximity to flagellin operons (Thomas et al. (2001a) and supplemental Fig. S6, in Falb et al. (2005)). In *M. voltae* some of the *fla* genes are cotranscribed with the flagellin genes *flaB1-B3*, giving rise to the idea that the *fla* genes are involved in flagellar biosynthesis (Kalmokoff and Jarrell, 1991). Indeed, insertional inactivation of *flaH* in *M. voltae* led to non-flagellated cells (Thomas et al., 2001c). However, in this study polar effects on transcription of the subsequent *flaI* and *flaJ* genes could not be excluded. Nonetheless this result showed that at least one of the genes *flaHIJ* is essential for flagellar biogenesis. In frame deletion of *flaI* in *H. salinarum* resulted in non-flagellated cells and thus showed that FlaI is essential for flagellar biogenesis (Patenge et al., 2001), a result that was later also found for a *M. voltae* non-polar insertional *flaI* mutant (Thomas et al., 2002). The same study showed that deletion of *flaJ* also results in non-flagellated cells. In all those studies transcription of the flagellin genes was not influenced, indicating that FlaI and FlaJ are not involved in regulation of flagellin expression but rather in flagellar biogenesis. In the *M. voltae flaI* and *flaJ* mutants, non-secreted flagellins were N-terminally processed and localized to the membrane like in wild type cells. On immunoblots of the *H. salinarum flaI* mutant culture supernatant, however, two effects were seen: (1) the detected flagellin bands were of reduced intensity and (2) the apparent MW of the flagellins was reduced by approx. 7 kDa, indicating that those flagellins were not glycosylated (see 2.2.4). The reduced apparent MW of the flagellins was not observed in immunoblots of crude extracts. It was hypothesized that FlaI is needed for proper assembly of flagellins into the filament and that flagellins that are not assembled and glycosylated are degraded. Immunoblots of *M. voltae* membrane and cytosolic fractions and a filament preparation with some rudimentary basal structure attached revealed that FlaC, FlaD, FlaE and FlaH are only found in the membrane fraction. Thus these proteins seem to be membrane associated rather than being a part of the filament (Thomas and Jarrell, 2001). Interestingly, the *M. voltae flaD* gene codes for two proteins of different length. The short FlaD seems to be transcribed from a second ribosome binding site within *flaD*. Fig 2.7 shows a schematic comparison of the *H. salinarum* and *M. voltae fla* gene clusters (Patenge et al., 2001).

---

[3]Unfortunately the current nomenclature of flagellin and flagella accessory genes is inconsistent. Although Gerl and Sumper (1985) introduced the prefix "flg" for flagellin genes and Patenge et al. (2001) introduced the prefix "fla" for flagella accessory genes, some groups use the prefix "fla" for flagellin genes as well as for flagella accessory genes.
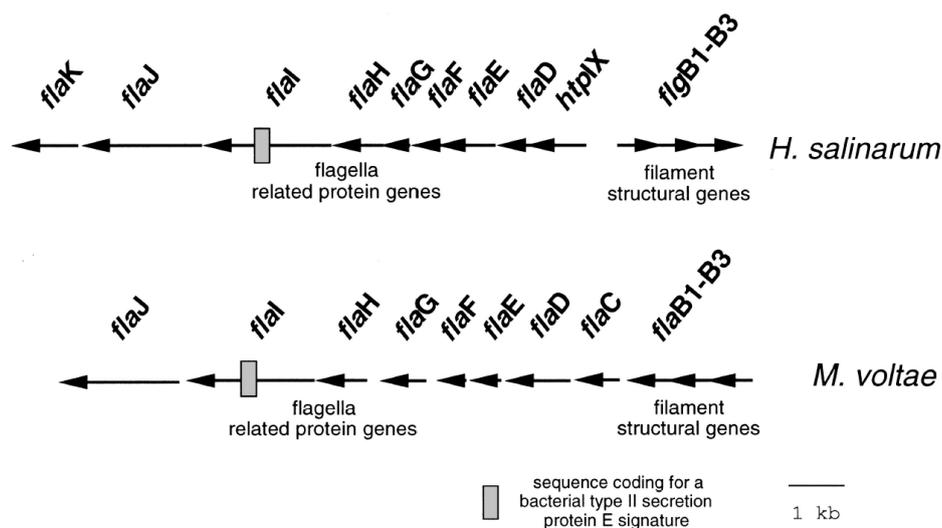
**Figure 2.7: Schematic comparison of the organization of flagella-related protein genes in *H. salinarum* and *M. voltae*.** One of the genes (*flaI*) contains a sequence that codes for a protein signature that is specific for members of the bacterial type II secretion protein superfamily. Figure and figure captions are as published by Patenge et al. (2001).

## Concluding remarks on the similarities of the archaeal flagellar system and type IV pili biogenesis

The lack of a central channel for flagellin transport in the archaeal flagellar filament and the similarities to T4P biogenesis convincingly support the notion that archaeal flagella like T4P are assembled from the base. However, twitching motility is based on extension and retraction of the pili, whereas the archaeal flagellar assembly is a rotatory unit. Thus the similarities between T4P and archaeal flagella must be restricted to biogenesis. It is reasonable to assume that the flagella start to rotate as soon as the anchoring structures and a part of the filament are assembled and that flagellins have to be replaced from time to time. How the flagellins can be incorporate into the base of a rotating structure is an interesting question.

Due to the superficial similarity to the bacterial flagella, it has always been assumed that archaeal flagella are driven by a proton gradient. However, already in the pre-genomic era, there was experimental evidence that this is probably not the case. When *H. salinarum* cells are starved and kept in the dark, they lose their motility. Upon illumination with orange light, the cells gradually regain their previous motility on a minutes time scale (see Fig. 1 in Bibikov et al. (1991)). This phenomenon is called "photokinesis" and is only observed in BR containing cells. The relatively slow onset of photokinesis is not consistent with a protein gradient as the driving force of the flagellar motor. If the flagellar motor were driven by protons photokinesis would be expected to start instantly as a proton gradient is established by BR within milliseconds. The obvious alternative energy source is ATP. This would be consistent with the photokinesis results as the establishment of a sufficiently high ATP level by the proton-driven ATPase is expected to take minutes. The obvious differences to the bacterial flagellar system

and especially the lack of homologs to the proton conducting motor proteins MotA and MotB further challenges the idea that the archaeal flagellar motor is driven by a proton gradient.

## 2.3 Signal Transduction

Signal transduction (ST) can in principle be classified in two categories: (1) intercellular ST, that allows cells to transmit and exchange signals among each other and (2) intracellular ST, in which environmental and cell-internal stimuli are sensed and processed by the cell, but not "communicated" to neighboring cells. In eukaryotic multicellular organisms intercellular ST constitutes the largest portion of signaling pathways, yet especially in such organisms, inter- and intracellular ST are highly interconnected. Originally intercellular signaling seemed to be restricted to higher organisms. Most prokaryotic organisms seem to live as isolated entities and accordingly the majority signaling pathways found in prokaryotes serve to respond to environmental stimuli like light, oxygen, pH and nutrients. On the other hand, it is known that prokaryotic organisms are able to grow to high cell densities and to form communities, implying that cell-to-cell communication might be advantageous even for unicellular prokaryotic organisms. Indeed, in the last 10 - 15 years a phenomenon known as quorum sensing has been observed in a growing number of bacteria (reviewed by Henke and Bassler (2004)) and in the meantime was also observed in the halophilic archaeon *Natronococcus occultus* (Paggi et al., 2003). In quorum sensing the cells communicate by secretion of signaling substances called autoinducers. When a certain threshold concentration is reached, these autoinducers regulate and synchronize gene expression and behavior of the whole cell population. Quorum sensing controls secretion of virulence factors, formation of biofilms, conjugation, sporulation and bioluminescence (Miller and Bassler, 2001). Quorum sensing also occurs between distinct bacterial species and there is a growing body of evidence that in symbiotic and pathogenic relationships between bacteria and eukaryotes, the eukaryotic host is able to sense autoinducers and to respond to them.

### 2.3.1 Two-component systems in prokaryotic signal transduction

Most prokaryotic organisms live in dynamically changing environments. In order to cope with this situation, they evolved systems to sense and respond to environmental stimuli. While most sensory pathways in eukaryotic organisms rely on serine, threonine or tyrosine kinases, the most common pathways in prokaryotes are based on a histidine-aspartate phosphorelay (HAP) system (reviewed by Wadhams and Armitage (2004). Despite their dominance in prokaryotes, HAP systems are also found in many lower eukaryotes and even plants. HAP systems consist of at least two components, a dimeric histidine protein kinase (HPK) and a response regulator (RR), and are therefore also known as two-component systems. They affect behavior by addressing two different targets, transcription and motility systems.

In transcription regulation, the dimeric HPK usually is a sensor kinase, in which an N-terminal region spans the membrane at least twice and thus has a periplasmic por-

tion that is able to sense extracellular stimuli. A cytoplasmic so-called HAMP[4] domain (*h*istidine kinases, *a*denylyl cyclases, *m*ethyl-accepting chemotaxis proteins and *p*hosphatases) links the N-terminal domain with a dimerization and a kinase domain that interacts with its cognate RR. In response to an activating stimulus, one monomer that has ATP bound to its kinase domain transfers the $\gamma$-phosphate to a His residue on the other domain. The phosphate is then transferred to a conserved Asp in the RR, which leads to activation of the RR output domain.

In prokaryotic chemotaxis, the dual function of the sensor kinase, sensing and autophosphorylation has been split into two separate protein modules. This allows sensing of numerous stimuli via highly homologous transducers that relay the signal to a joint histidine kinase, CheA. The reason for the evolution of this modified HPK system may be that all these stimuli must be integrated to yield an unambiguous output to the motility system. The sensing modules have most likely evolved by gene duplication followed by modification of the sensing domain to allow for sensing of various signals. For a deeper insight into the structure of prokaryotic transducers see 2.3.10 and associated Figure 2.14.

## 2.3.2 Bacterial chemotaxis as a paradigm of signal transduction

Bacterial chemotaxis is the biased movement towards increasing concentrations of favorable and away from increasing concentrations of harmful chemicals. It is one of the best established signal transduction pathways and has been most extensively studied in the enterobacterial model organisms *E. coli* and *Salmonella enterica* serovar Typhimurium. Today, mechanistic details of all steps of the pathway and crystal structures of most pathway components are available. Thus, chemotaxis in *E. coli* has become a paradigm for signal transduction. The relative simplicity of the pathway and the wealth of data makes bacterial chemotaxis an attractive objective and test case for modeling approaches. Although differences to other sensory pathways clearly exist, it is nevertheless anticipated that some basic principle applicable to sensory pathways in general may emerge from such studies. In this context, signal processing, sensitivity and robustness of the pathway are issues that attract most of the attention.

While chemotaxis in *E. coli* and *S. typhimurium* are largely identical, chemotaxis in *B. subtilis* proved to be more complex. Genome sequencing projects revealed that the simple signal transduction network of *E. coli* chemotaxis is rather an exception. Most chemotactic microorganisms, including the archaeon *H. salinarum*, do not only possess far more putative chemoreceptors than *E. coli*, merely reflecting adaptation to different, more challenging environments, but also an extended set of chemotaxis proteins.

## 2.3.3 Principles of prokaryotic taxis

Despite differences in the network structure of various prokaryotic chemotaxis systems, there are principles that apply to all of them. In active search for optimal conditions,

---

[4]The HAMP domain is widely distributed in histidine protein kinases, adenylyl cyclases, chemoreceptors and phosphatases. It consists of two amphipathic helices and is thought to play an important role in signaling (Aravind and Ponting, 1999; Appleman et al., 2003; Appleman and Stewart, 2003). A NMR structure of an archaeal HAMP domain was recently published (Hulko et al., 2006).

prokaryotic organisms perform a random walk that becomes biased upon stimulation. No absolute stimulus strengths (e.g. the absolute concentration of a chemical) are sensed but rather changes in stimulus strength. Cells are attracted by both - increased stimulus strength of an attractant and decreased stimulus strength of a repellent and they are repelled by both - decreased stimulus strength of an attractant and increased stimulus strength of a repellent. It is widely accepted that due to their small size, bacteria and archaea detect temporal rather than spatial changes (Macnab and Koshland, 1972; Berg and Purcell, 1977), although a contrasting view exists (Thar and Kühl, 2003). Thus, a kind of "short-term memory" that allows for comparison of current and previous stimulus strength, is needed. This is achieved by an adaptation system that makes the cells return to their unbiased random walk in presence of a persisting stimulus.

## 2.3.4  Chemotaxis in *E. coli*

### Swimming behavior of *E. coli*

*E. coli* cells are peritrichously flagellated. CCW rotation of the flagellar motors leads to formation of a flagellar bundle that effectively propels the cells through the medium. Such "smooth" runs are interrupted by shorter intervals of a "tumbling" motion that is caused by dissociation of the flagellar bundle upon switching of the flagellar motors to CW rotation. Theses tumbles randomly reorient the cells, thereby giving them a new swimming direction.
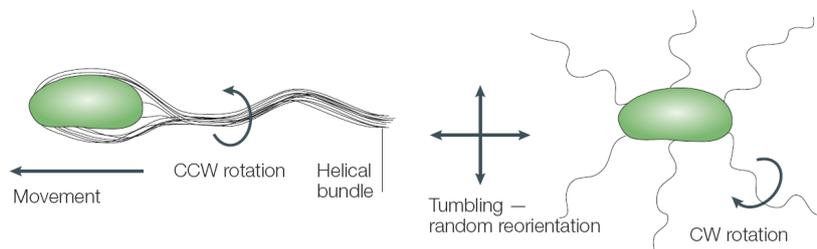


**Figure 2.8: Swimming behavior of *E. coli*.** In case of unbiased swimming, smooth runs of approx. 1 s (CCW rotation of the flagellar motors) are interrupted by tumbles of approx. 0.1 s. The figure is taken from Butler and Camilli (2005).

### The chemotaxis pathway of *E. coli*

In *E. coli* chemicals are sensed by receptor dimers that are called **m**ethyl accepting **c**hemotaxis **p**roteins (MCPs) due to the presence of a methylation region (see Fig. 2.14). This region contains 4 - 5 methylatable glutamates, some of which are encoded as glutamines. The MCP dimers form a ternary signaling complex together with CheW monomers and CheA dimers (Gegner et al., 1992; Schuster et al., 1993). Repellent stimulation activates the HPK CheA to autophosphorylate itself *in trans* using ATP as substrate (Hess et al., 1987, 1988a; Borkovich et al., 1989). The exact role of CheW in this process is unclear, but it seems to be clear that CheW promotes efficient signal

transfer from the MCP to CheA. Following this step, the pathway branches. CheA-P transfers its phosphate group to the RRs CheY and less efficiently to CheB (Hess et al., 1988b). Phosphorylated CheY (CheY-P) then diffuses to the flagellar motor where it binds to the switch protein FliM. Deletion of either CheA or CheY results in smooth swimming, non-chemotactic cells, which led to the conclusion that the default rotational mode of the *E. coli* motor is CCW (smooth swimming) and CheY-P is the switch factor that induces CW rotation (tumbling) (Parkinson, 1976, 1978). CheZ helps to extinguish the signal by reducing the half-life of CheY-P from 2 s to 200 ms (Lukat et al., 1991). Adaptation to a persisting stimulus is conferred by CheR and CheB. CheR is a constitutively active methyltransferase that methylates the glutamates in the methylation region using *S*-adenosylmethionine as substrate. CheB is a bifunctional deamidase/methylesterase that gets activated about 100-fold upon phosphorylation by CheA (Lupas and Stock, 1989). CheB-P demethylates the same glutamate residues that are methylated by CheR. The methyl groups are released as volatile methanol. Methylation of MCPs increases and demethylation decreases activity of the signaling complex (Ninfa et al., 1991; Borkovich et al., 1992). Thus, adaptation seems to be achieved by counterbalancing ligand occupancy- and methylation state of the MCP. Phosphorylation of CheB leads to a negative feedback loop that resets activity of the signaling complex to prestimulus values, because increased MCP activity leads to increased levels of CheA-P and CheY-P but at the same time to increased CheB activity. The second function of CheB is deamidation of glutamines in the methylation region, thereby rendering them methylatable (Rollins and Dahlquist, 1981; Kehry et al., 1983a). Glutamines have about the same MCP activating effect as methyl esterified glutamates, suggesting that the charge state of the methylatable residues is involved in the regulation of MCP activity. As expected from the described pathway, in *E. coli* attractant stimulation leads to a decrease of methanol release, while repellent stimulation leads to increased methanol release. Deletion of *cheR* and *cheB* result in smooth and tumbling cells, respectively. It is now widely accepted that CheB and CheR are required for chemotaxis, although contrasting observations were reported (Stock et al., 1985). However, it turned out that phosphorylation of CheB is not a prerequisite for adaptation (Alon et al., 1999). A recent study suggests, that CheB-P feedback loop compensates for gene expression noise in the signal transduction pathway to provide robustness (Kollmann et al., 2005). First successful models of *E. coli* chemotaxis assume that CheB only acts on active signaling complexes (Barkai and Leibler, 1997). Subsequent models assumed that in addition CheR only acts on inactive signaling complexes (Morton-Firth et al., 1999; Barkai et al., 2001).

### A closer look at the chemotaxis proteins

CheA is a 5 domain protein (P1 - P5). P1 is the phosphorylation domain that contains the phosphorylation site His48 and is responsible for phospho-transfer to CheY and CheB, P2 is the CheY and CheB binding domain, P3 is the dimerization domain, P4 is the catalytic domain responsible for ATP binding and autophosphorylation and P5 is the regulatory domain that couples CheA to CheW and the MCPs. CheA is expressed in two forms, full length CheA (CheA$_L$) and short CheA (CheA$_S$). CheA$_S$ is transcribed from a second internal transcription site and lacks the first 97 amino acids that are part

of the P1-domain and include the phosphorylation site. CheA$_S$ is only found in enteric bacteria that contain CheZ and CheZ binds to CheA$_S$, but not to CheA$_L$. It appears that recruiting of CheZ to the receptor cluster is the main function of CheA$_S$. The CheA$_L$ and CheA$_S$ are present *in vivo* in a 50% ratio (Li and Hazelbauer, 2004). CheW contains two domains with homology to the CheA P5 domain. It was therefore speculated that CheA and CheW may compete for MCP binding sites. CheY and CheB both have an RR domain and get phosphorylated at Asp57 and Asp56, respectively. Removal of the N-terminal domain activates CheB (Lupas and Stock, 1989). Thus phosphorylation of CheB abrogates the inhibitory effect of the N-terminal domain on the catalytic effector domain. CheR and to a lesser extent CheB are tethered to a C-terminal NWETF motif that is present in the high abundant *E. coli* MCPs but not in the low abundant MCPs and does not locate to the methylation region (see also 2.3.9). The interactions of the *E. coli* chemotaxis proteins are summarized in Fig. 2.15.

## 2.3.5 Chemotaxis in *B. subtilis*

*E. coli* and *B. subtilis* are similar in their chemotactic behavior. They are both peritrichously flagellated, alternate in swimming between runs and tumbles, perform a random walk that is biased by stimuli and show similar excitation and adaptation speeds (Kirby et al., 1999; Sourjik and Berg, 2002b). However, the underlying network structure and strategy to perform chemotaxis are different. This section focuses on the differences to *E. coli* chemotaxis.

### *B. subtilis* employs an extended set of chemotaxis proteins

From a genomic point of view, the most prominent difference is that the genome of *B. subtilis* codes for an extended set of chemotaxis proteins (Kunst et al., 1997). With CheW, CheA, CheY, CheR and CheB, *B. subtilis* has an almost complete set of homologs to the *E. coli* chemotaxis proteins. In addition, CheC, CheD, CheV and FliY, which is part of the *B. subtilis* motor switch complex, are involved in chemotaxis. CheZ is the only *E. coli* chemotaxis protein that has no homolog in the *B. subtilis* system. There are remarkable differences between *E. coli* and *B. subtilis* in excitation, adaptation and signal termination, the key steps of prokaryotic chemotaxis.

### Excitation

In contrast to *E. coli*, deletion of either *cheA* or *cheY* both cause tumbling of *B. subtilis* cells, suggesting that the default rotational mode of the *B. subtilis* flagellar motor is CW (Fuhrer and Ordal, 1991; Bischoff et al., 1993). On the other hand, unlike in *E. coli*, stimulation of the receptor complex by attractant addition leads to increased CheA-P and CheY-P levels (Garrity and Ordal, 1997), suggesting that *E. coli* and *B. subtilis* transducers exhibit opposite response behavior (for differences between *E. coli* and *B. subtilis* receptors see also 2.3.9, p. 36). Taken together, the opposite default flagellar rotational modes and CheA/CheY phosphorylation rates in *E. coli* and *B. subtilis* lead to prolonged swimming phases after attractant addition and increased tumbling rate after repellent

stimulation. Besides CheW, CheV is found in the *B. subtilis* transducer/kinase complex. CheV is a two-domain protein with an N-terminal CheW like domain and a C-terminal CheY like two-component receiver domain. CheV and CheW are partially redundant in their function as deletion of either gene has only a minor effect. However, double mutants lacking both genes are non-chemotactic (Rosario et al., 1994). The CheY like domain of CheV gets phosphorylated by CheA at D235. A CheV D235A mutant that cannot be phosphorylated, is still able to respond, but only partially adapts. Thus, CheV phosphorylation is required for adaptation, but not for CheV mediated coupling of transducers to CheA (Karatan et al., 2001).

### *B. subtilis* has a methylation-independent adaptation system

In *B. subtilis*, adaptation is accomplished by a methylation-dependent as well as a methylation-independent system. At low attractant concentrations the methylation-independent system is sufficient to achieve adaptation. Adaptation to high attractant concentration requires the methylation-dependent system. Several lines of evidence point to the existence of a methylation-independent adaptation system. Taking into account that signaling of the *B. subtilis* receptor complex is inverted compared to *E. coli*, the corresponding *B. subtilis cheB* and *cheR* mutants are expected to swim smooth and tumble, respectively and to be unable to respond and adapt to stimuli. In three different papers, the response of a *B. subtilis cheB* mutant to a proline analogue (sensed by McpC) and asparagine (sensed by McpB) was reported (Kirsch et al., 1993a; Kirby et al., 2000; Zimmer et al., 2002). They all show that a *cheB* mutant exhibits a wild-type prestimulus CCW rotational bias. At low attractant concentration, the mutant excites and adapts to attractant addition like wild type. At high attractant concentration, the mutant still excites normally to attractant addition, it even transiently adapts, but fails to maintain the adapted state. The studies disagree however, whether the mutant is capable to respond and adapt to attractant removal. A strain that produces a McpB mutant protein that lacks functional methylation sites, nevertheless releases methanol and shows normal chemotaxis to high concentrations of asparagine (Zimmer et al., 2002). Obviously this happens by the assistance of other receptors as the phenomenon only appears if a sufficient number of other receptors is present. The assistance in adaptation to high attractant concentrations by other receptors is not only accompanied by methanol release, but seems to be methylation-dependent. Deletion of *cheB* in the *mcpB* mutant strain abolishes chemotaxis to high asparagine concentration. On the other hand, adaptation to low asparagine concentrations in the McpB mutant strain neither requires the presence of CheB, nor the assistance by other receptors, consistent with the existence of a methylation-independent adaptation system that works at low stimulus concentrations. The phenotype of the *cheR* mutant is less clear. Two subpopulations with extreme CW bias (tumbly) and less extreme CW bias that make up 33% and 66% of the whole cell population, respectively, were observed (Kirsch et al., 1993b). While the mutant senses and adapts to both attractant addition and removal, it only senses addition of repellent, but does not adapt. Repellent removal only restores the CCW prestimulus bias, a true response is not seen.

## Selective methylation changes occur in methylation-dependent adaptation

Another notable difference between *E. coli* and *B. subtilis* is that even their methylation-dependent adaptation systems seem to work differently. Taking into account that in contrast to *E. coli* the *B. subtilis* receptor complex is activated by attractant addition, an inverted *E. coli* methanol release pattern would be expected, i.e. increased methanol release upon attractant addition and decreased methanol production below the basal level upon attractant removal. However, *B. subtilis* cells release methanol both upon positive and negative stimulation (Kirby et al., 1997). Fast net demethylation of transducers is followed by a slower net remethylation. By this way, the overall methylation level of transducers before stimulation and after completed adaptation is the same. Methanol release upon negative stimulation requires CheY or more specifically CheY-P as a $cheY^{\text{D54A}}$ mutant, in which CheY cannot be phosphorylated has the same phenotype as a *cheY* deletion mutant. In both cases a methanol release pattern that would be expected in analogy to the *E. coli* system was observed (Kirby et al., 1997, 1999). These observations led the authors to propose a negative feedback of CheY-P on the receptor complex.

Zimmer et al. (2000) identified 3 of 4 possible glutamate residues of McpB to be responsible for methanol release. E371, which is encoded as Q, releases methanol only in response to addition of the attractant Asn, E637 releases methanol only in response to Asn removal and E630 releases methanol in both cases. A substitution of Glu to Asp results in a non-methylatable residue with a fixed negative charge. While a $mcpB^{\text{E630D}}$ mutant has a low CCW prestimulus bias and is unable to adapt to Asn addition, a $mcpB^{\text{E637D}}$ mutant has the opposite phenotype. In both cases, an additional Q371D mutation did not affect the phenotype of the mutants. Obviously E371 has no significant effect on adaptation. The phenotypes of the mutants imply that methylation of E630 increases receptor activity, whereas methylation of E637 decreases receptor activity. Based on their results the authors proposed an electrostatic model for *B. subtilis* adaptation, that is capable to explain the methanol release pattern. After attractant addition, the activating residue E630 gets demethylated and the inhibiting residue gets methylated. Adaptation to attractant removal inverts the process.

## The roles of CheD, CheC and FliY

The involvement of CheC and CheD in chemotaxis is quite complex. On the one hand, there are indications that CheC and CheD can act independently, on the other hand, they were found to interact and mutually regulate their activities.

Deletion of *cheD* and *cheC* leads to undermethylated and about twofold overmethylated transducers, respectively (Rosario et al., 1995). In binding studies with GST-tagged CheC and CheD and yeast two hybrid assays CheC and CheD were shown to interact (Rosario and Ordal, 1996; Kirby et al., 2001). However, more detailed analyses of *cheD*, *cheC* and *cheCcheD* double mutants in combination with yeast two hybrid assays revealed the following: (1) CheD is absolutely required for McpC-mediated signaling, but not for McpB mediated signaling (2) In a similar manner, deletion of *cheC* has a much stronger effect on McpC-mediated signaling than on McpB-mediated signaling (3) CheD, but not CheC, is necessary for the generation of wild-type CheA autophosphorylation

levels; (4) CheC is necessary for adaptation to positive McpB mediated stimulation, and (5) CheC interacts directly with CheA, whereas CheD does not (Kirby et al., 2001). The authors concluded that although CheC and CheD interact, they can act independently to affect chemotaxis in *B. subtilis*. The notion is supported by the fact that in many organisms in which a CheD homolog is found, a CheC homolog is missing.

Later studies showed that CheD and CheC interact to reciprocally regulate their activities in at least two processes, dephosphorylation of CheY-P and transducer modification by deamidation and demethylation. It was for a long time speculated why *B. subtilis* lacks a homolog to the *E. coli* CheY-P phosphatase CheZ, until it was found that actually *B. subtilis* has two CheY-P phosphatases, FliY and CheC (Szurmant et al., 2003, 2004). Together with CheX, which is not present in *B. subtilis*, FliY and CheC belong to a widespread family of CheY-P phosphatases (see Fig. 2.9).
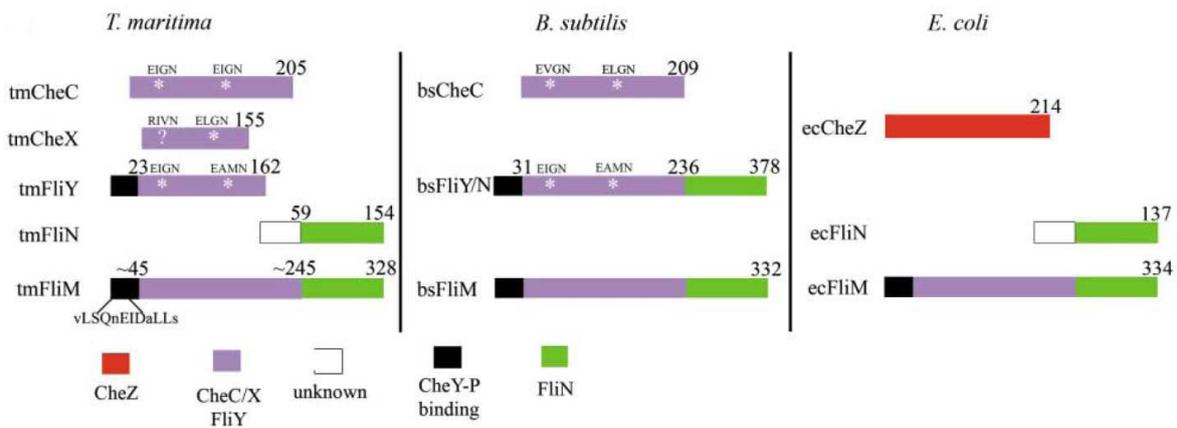


**Figure 2.9: The CheC family and related proteins**. Domain organization for the family of protein aspartate-phosphatases and related proteins in three different bacteria, *T. maritima*, *B. subtilis*, and *E. coli*. Purple segments represent the CheC homology region; green segments represent the FliN homology region (PDB code: 1O6A). FliY/N and FliM contain an N-terminal peptide that binds CheY-P (black). CheC, CheX, and FliY/N contain dephosphorylation centers (white stars with conserved residues above), but FliM does not. Most FliY/N proteins follow the domain architecture of bsFliY/N. TmFliY is abnormally short. The structurally unrelated CheY-phosphatase CheZ found in $\beta$ and $\gamma$-proteobacteria is shown in red. Figure and caption are from Park et al. (2004).

Interestingly, FliM has a domain with homology to CheC, but does not have CheY-P phosphatase activity. FliY is part of the *B. subtilis* flagellar switch and its copy number was determined to be approx. 500 per cell. *B. subtilis* lacks a separate FliN switch protein. Instead a FliN domain is fused to the C-terminal region of FliY, which explains why *B. subtilis* FliY is also referred to as FliY/N. FliY and FliM share an N-terminal CheY-P binding peptide of approx. 16 amino acids that is not present in CheC and CheX. CheC was found to have a weak CheY-P phosphatase activity that is about 5-fold enhanced in the presence of CheD. CheC is the lowest abundant chemotaxis with a copy number of 20 molecules per cell (Szurmant et al., 2004). *Thermotoga maritima* has all three phosphatases. In contrast to CheC, CheX does not require CheD to achieve its full activity. Crystal structures of the *T. maritima* proteins revealed that while CheC is a monomer, CheX is an obligatory dimer. CheC and CheX monomers have a common fold

and internal 2-fold symmetry. In CheX, the CheC $\alpha 2$ and $\alpha 2´$ helices are replaced by two $\beta$ strands $\beta_x$ and $\beta_x´$ (Park et al., 2004). Comparison of the CheX dimer structure with the crystal structure of the *T. maritima* CheC:CheD complex shows that the CheX $\beta_x´$ strand and the CheC $\alpha 2´$ helix form the dimerization and CheC:CheD interaction surfaces, respectively (Chao et al., 2006).

The other facet of the CheD-CheC interaction is transducer modification. As *B. subtilis* CheB was found to complement a *E. coli cheB* mutant (Kirsch et al., 1993a), it was assumed, that *B. subtilis* CheB deamidates Gln residues to methylatable Glu. However, in *B. subtilis* deamidation of McpA and probably also McpB and McpC is catalyzed by CheD (Kristich and Ordal, 2002). A study performed with *T. maritima* CheD and transducers revealed that CheD also demethylates selected Glu residues that fit the CheB substrate recognition motif. It seems that *T. maritima* CheB and CheD have distinct substrate sites on different receptors with some overlap of specificity (Chao et al., 2006). CheC inhibits transducer deamidation by mimicking the transducer substrate with its $\alpha 2´$ helix. Indeed mutation of CheC A150 to Q150, that resides at the position of the substrate Q in the $\alpha 2´$ helix, leads to deamidation of this residue.

## A model for *B. subtilis* chemotaxis

Based on models for *E. coli* chemotaxis, Rao et al. (2004) built a model for *B. subtilis* chemotaxis that could reproduce many experimental data. To build their model they proposed an involvement of CheV in methylation-independent adaptation and merged the previously proposed negative feedback of CheY-P on the receptor complex with the observation that selective methylation changes occur in methylation-dependent adaptation.

It is known from *E. coli* that the stoichiometry of CheW in the transducer complex has a strong influence on the number of functional complexes (Gegner et al., 1992). The number of active CheV can be dynamically regulated by phosphorylation which in turn could regulate the number of functional transducer complexes. For simplicity the model assumes that phosphorylated CheV disrupts the transducer complex. Thus, CheV-P forms a negative methylation-independent feedback loop.

In case of the negative CheY-P feedback loop, the authors proposed that CheY-P may act as a switch for selection of the methylation site. The inhibiting residue E637 is preferentially methylated by CheR when CheY-P binds to the receptor. Otherwise the activating residue E630 is methylated. The authors further note that like in the *E. coli* models activity dependent demethylation by CheB is required for robust adaptation. How CheB distinguishes between active and inactive transducers is not clear. According to the model, activation of CheB by phosphorylation and the use of CheY-P as a switch, was not sufficient.
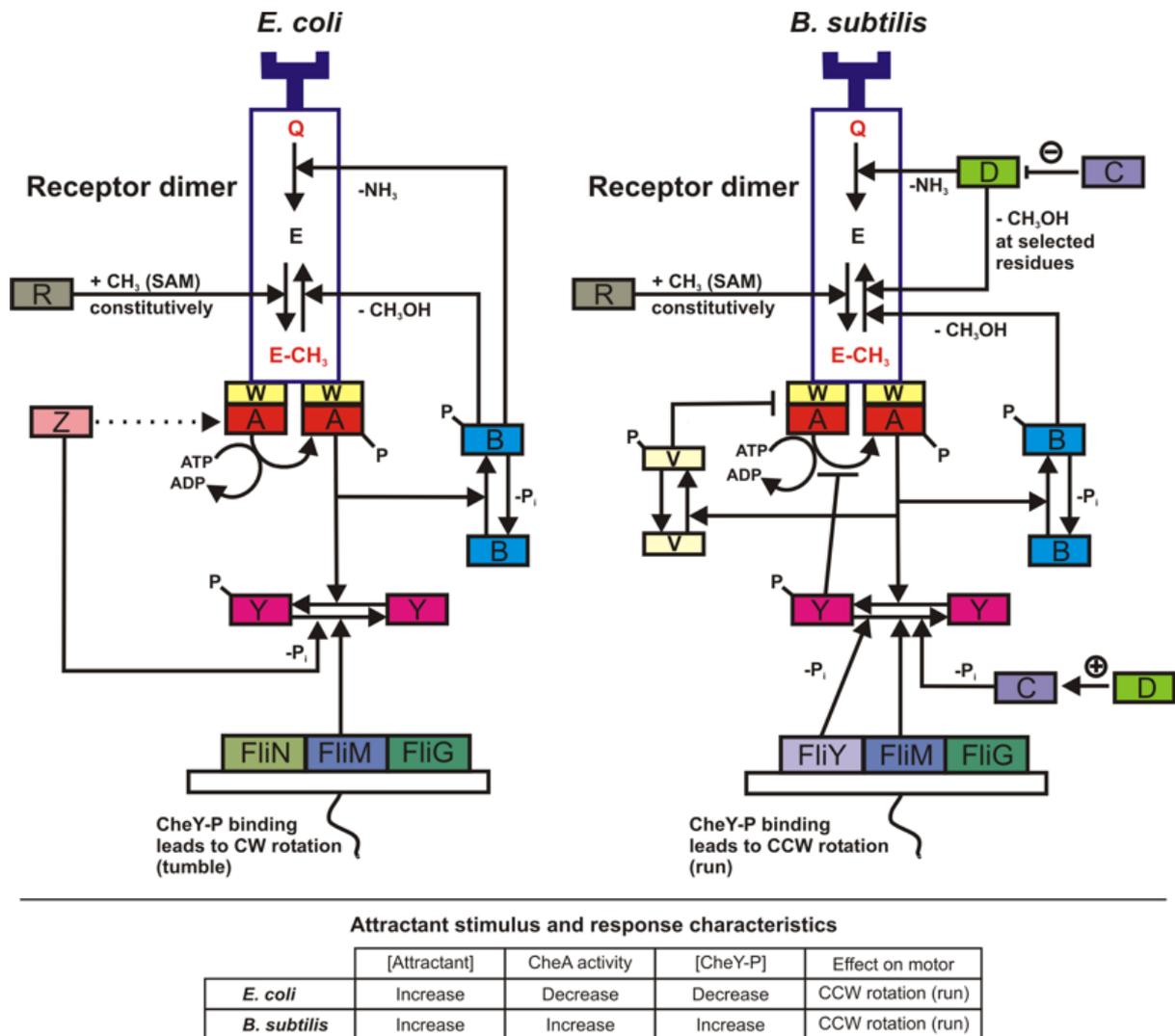
**Figure 2.10: Comparison of *E. coli* and *B. subtilis* chemotaxis.** The figure summarizes the known functions of the proteins involved in chemotaxis of *E. coli* and *B. subtilis* and compares the attractant stimulus and response characteristics. For simplicity, in the *B. subtilis* system, adaptation by selective methylation and the putative involvement of CheY-P as a switch is replaced by a simple negative feedback loop on CheA activity.

## 2.3.6 Chemo- and phototaxis of *H. salinarum* shares similarities with *E. coli* and *B. subtilis* chemotaxis

**Excitation and signal termination**

*H. salinarum* is the best-studied model organism for archaeal chemo- and phototaxis. It is able to respond to various environmental stimuli by changing its swimming behavior. The spectrum of stimuli that are known to be sensed by the function of specific transducers to date comprises light, oxygen, amino acids, compatible osmolytes and membrane potential (for more details see 2.3.9). Responses to further stimuli like phenol, temperature and pH were described, but could not be functionally linked to a transducer. Analysis of lysates from *in vivo* [$^3$H]methyl labeled *H. salinarum* cells revealed the presence of proteins with apparent MWs between 90 - 135 kDa. Repellent and attractant stimulation of the labeled cells resulted in intensity changes of specific bands, indicating a changed level of methylation of these proteins (Alam et al., 1989). This was a first indication that the *h*alobacterial *tr*ansducer proteins (Htrs) are MCPs.

Like *B. subtilis*, *H. salinarum* has an extended set of chemotaxis proteins, but lacks a CheZ homolog. Besides homologs to the *E. coli* chemotaxis proteins CheA, CheY, CheB and CheR, *H. salinarum* has two CheW, one CheD and three CheC homologs (for genomic arrangement of *che* genes see Fig. 3.21, p. 83). *In vitro* phosphorylation assays showed that the halobacterial wild type CheA autophosphorylates while a CheA$^{\text{H44Q}}$ mutant with mutated putative phosphorylation site does not. Detection of phosphorylated CheY by SDS-PAGE and autoradiography was not possible, which led to the estimation that phosphorylated halobacterial CheY has a half life $< 5$ s. It was speculated that due to this short half-life, the presence of a phosphatase CheZ is not necessary. Phosphorylation of CheY could be shown indirectly, though. In presence of CheY, but not CheY$^{\text{D53A}}$, in which the putative phosphate accepting Asp is mutated, CheA is dephosphorylated (Rudolph et al., 1995). Phosphorylation of CheB was not investigated.

Deletion of either *cheA* or *cheY* abolishes both chemo- and phototaxis. The mutations affect swimming in two ways. Wild type cells spontaneously reverse their swimming direction by switching the rotational sense of the flagella from CW to CCW and vice versa and spend equal times in either mode (see 2.1.5 and associated Fig. 2.3). By contrast, even upon a negative stimulus the *cheA* and *cheY* mutants never reverse and 99% of the cells rotate their flagella CW (Rudolph and Oesterhelt, 1995; Rudolph et al., 1996). Based on these phenotypes it was concluded that like in *E. coli* CheY gets phosphorylated by repellent stimulation and that CheY-P is the signal that makes the motor switch its rotational sense, independent of its current rotational state. The effect on the rotational bias remained obscure.

**Adaptation**

Deletion of *cheB* abolishes chemotaxis and results in cells that very frequently switch, but the rotational bias is unaffected. Deletion of the previously unknown *cheJ*[5] results in cells that switch slightly more frequently than wild type and show reduced chemo- and

---

[5]CheJ was later renamed to CheC1 due its homology to *B. subtilis* CheC.

phototactic efficiency. The rotational bias of this mutant is shifted to 88% CW (Rudolph and Oesterhelt, 1996). The phenotype of a *cheR* mutant was never explicitly reported, but a mutant Pho72 that was generated by chemical mutagenesis and lacks methylated Htr bands was reported to hardly switch (Sundberg et al., 1990). Thus, at least with respect to their switching frequencies, the *cheB* and putative *cheR* mutants behave in analogy to the corresponding *E. coli* mutants. The analogies to *E. coli* chemotaxis are contrasted by the fact that like in *B. subtilis* repellent and attractant stimulation both lead to increased methanol release (Nordmann et al., 1994). As observed in *B. subtilis*, deletion of *cheY* leads to the asymmetric methanol release pattern that is known for *E. coli*. Thus, like in the case of *B. subtilis* a CheY-dependent negative feedback was proposed. The same study showed that in *H. salinarum* adaptation does not require that the stimulated Htr is methylatable. In such a case, methanol release upon stimulation is still observed. Obviously the remaining methylatable Htrs are involved in this process, indicating that CheR and CheB act on all Htrs to achieve adaptation (Perazzona and Spudich, 1999).

### 2.3.7 Phototaxis in *H. salinarum*

Light plays a dominant role in the bioenergetics of *H. salinarum* (see 2.1.4). It is therefore not surprising that *H. salinarum* has photosensors tailored to direct the cells into regions that meet the light requirements of the two light-driven ion pumps BR and HR. On the other hand the cells have to avoid harmful UV irradiation. *H. salinarum* has a three-color vision system. Light is sensed by the retinal proteins SRI and SRII. Like the other two retinal proteins BR and HR, SRI and SRII run through a photocycle upon illumination of the appropriate wavelength (Fig 2.11). However, instead of pumping ions, SRI and SRII transmit signals to their cognate transducers HtrI and HtrII, respectively. SRI is a photochromic receptor that detects orange- and uv-light and SRII detects blue light. Orange-light induced photoconversion of the $SRI_{587}$ ground state light produces the photointermediate $SRI_{373}$ that itself transmits a positive signal to HtrI and at the same time is a receptor for uv-light. $SRI_{373}$ has two ways to return to the ground state $SRI_{587}$. It can either return by thermal conversion or - upon uv-light illumination - about 10-fold faster via the photointermediate $SRI_{510}$. $SRI_{510}$ transmits a negative signal to HtrI. In case of SRII, blue light illumination of the $SRII_{487}$ ground state produces the photointermediates $SRII_{360}$ and $SRI_{540}$ that transmit a negative signal to HtrII. Avoidance of blue light makes sense as blue light is inefficient for ion-pumping by BR and HR. The photosensory system of *H. salinarum* is very sensitive. It was shown that in principle a single photon is sufficient to produce a response (Marwan et al., 1988). Negative and positive light stimuli were found to be integrated (Spudich and Stoeckenius, 1979).

Light activation of SRI and SRII was found to induce release of membrane bound fumarate (Marwan et al., 1990; Montrone et al., 1993). In *H. salinarum* fumarate was identified as additional switch factor besides CheY-P due to its ability to complement a non-switching mutant M415. Fumarate was then also found to affect switching behavior of *E. coli* (Barak and Eisenbach, 1992; Montrone et al., 1996; Prasad et al., 1998).

Compared to HR and BR, SRI and SRII are slow cycling molecules that are bleached at high light intensities. However, in such a case *H. salinarum* is still able to indirectly
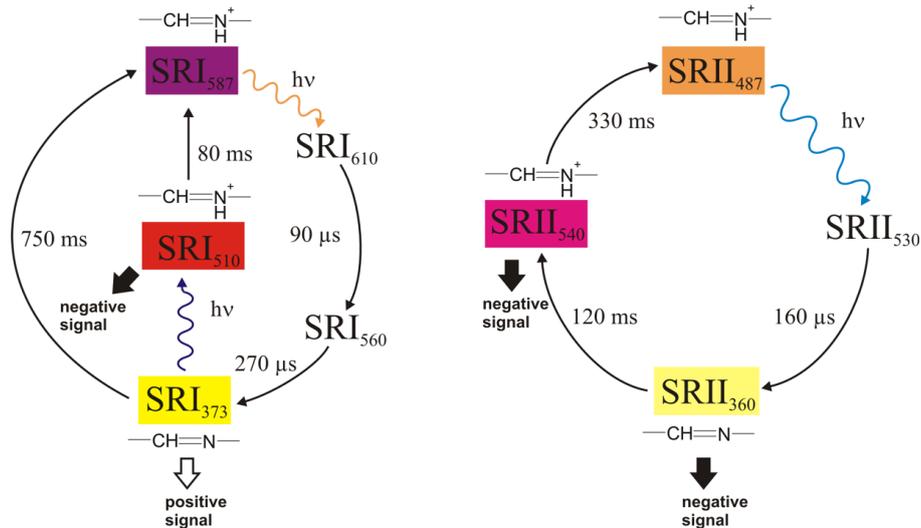
**Figure 2.11: Photocycles of SRI and SRII**. Photoconversion steps are depicted by wavy, colored arrows. The color of the arrow indicates the color of the excitation light. Regular arrows indicate thermal conversion with half-lifes of the intermediates according to (Hoff et al., 1997). Absorption maxima of the states are given as subscripts and the protonation state of the Schiff base is indicated. Ground and signaling states are boxed. The color of the boxes reflect the color of the protein in the respective state. Open arrows indicate signaling to the transducers.

detect differences in light intensity by the actions of BR and HR (Bibikov et al., 1991, 1993). When the light intensity decreases, BR and HR pump less ions, which leads to a transient drop in the membrane potential that is detected by the transducer MpcT (Htr14) (Koch and Oesterhelt, 2005).

The gene coding for the SRI apo-protein, *sopI* overlaps with *htrI* and *sopII* is separated from *htrII* only by a few bases, suggesting coexpression of the *sop* genes with their respective *htr* genes and in fact HtrII dimers are found to be surrounded by two SRII molecules. While SRII is constitutively expressed, the SRI content increases with growth of the cells, probably due to dropping oxygen tension as observed in the case of BR and HR. After 2 days of growth the copy numbers of SRI and SRII were determined to be approx. 5000 and 500 molecules per cell (Otomo et al., 1989). Approximate copy numbers of BR and HR are 300.000 and 30.000 per cell (Oesterhelt and Tittor, 1989). Illumination of various regions of elongated *H. salinarum* cells indicated that sensory rhodopsins mainly localize to the poles (Oesterhelt and Marwan, 1987) (for localization of Htrs see also 2.3.11).

## 2.3.8 A model for the *H. salinarum* motor switch and its photosensory control

Over the years, it has become clear that biosynthesis, assembly and composition of the halobacterial flagellar apparatus is distinct from its bacterial counterpart. Analysis of data for spontaneous and light controlled motor switching that had accumulated over the last 30 years resulted in a model for the *H. salinarum* flagellar motor and its photosensory control that was able to explain most of the data. As none of the existing models of *E. coli* motor switching could reproduce the data, a new, clearly distinct model was developed (Nutsch et al., 2005). Thus, it seems that indeed the archaeal flagellar motor is not only made up by different components, but also differs in the way in which its switching is regulated by CheY-P. The model is mainly based on the following observations:

1. The flagellar motor(s) act as a unit, i.e. they act synchronously and are all either in CW or CCW rotational mode (Marwan et al., 1991).

2. Without being stimulated, the cells on average spend equal times in CW and CCW rotational modes (Hildebrand and Schimz, 1985; Schimz and Hildebrand, 1985).

3. Cells are equally responsive to attractant and repellent stimuli in CW and CCW rotational mode (Schimz and Hildebrand, 1985).

4. The run-length of a given interval does not depend on the run-length of the preceding one (McCain et al., 1987; Hildebrand and Schimz, 1985).

5. After a stop, regardless if spontaneous or induced, the cells do not respond to a repellent stimulus for approx. 2 s or respond only with a delay. For up to 6 s after a stop an attractant stimulus surprisingly is inducing reversals instead of suppressing them (McCain et al., 1987).

6. Even after a saturating stimulus, a minimal time elapses before the cells respond (Marwan and Oesterhelt, 1987).

7. The motor passes through an irreversible cyclic process, i.e. after a stop, the motor always continues to spin in the opposite direction.

From the swimming behavior of *H. salinarum* (see section 2.1.5) directly two states or phases, Stop and Run can be deduced. Observations 1 - 3 lead to a doubling of the phases (Run and Stop phases in both CW and CCW mode) and suggests that the probability for the transitions from Stop to Run are identical in both rotational modes, which results in a symmetric model. Observation 5 required a refinement of the Run phases into the phases Refractory and Competent and observation 6 led to the additional introduction of an Active phase. Thus the model consists of $2 \times 4$ phases. In the model, CheY-P retards the transition from Refractory to Competent phases (due the counterintuitive response of cells to stimuli in the Refractory phase, observation 5) but accelerates the transitions from Competent to Active phases. At steady state CheY-P levels (adapted cells) the motor(s) spend most of the time in the Competent phase. Observation 6 implies that there must be an input of energy somewhere in the cycle, probably by hydrolysis of CheY-P. A Petri Net representation of the model is shown in Fig. 2.12.
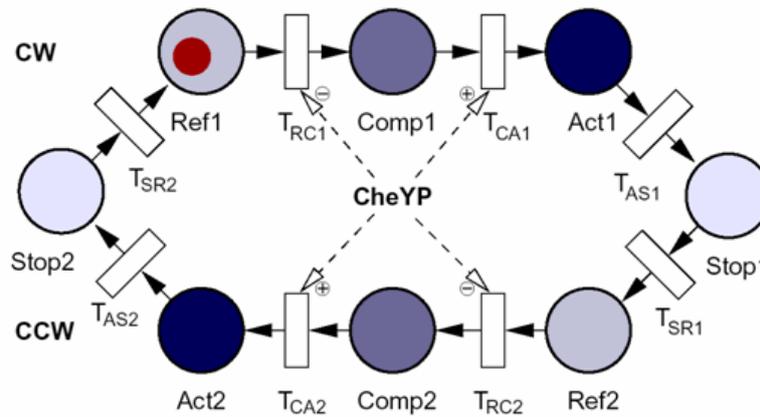
**Figure 2.12: Petri Net representation of the *H. salinarum* flagellar motor switch cycle**. Circles ("places") represent phases, rectangles represent transitions and filled red circles ("tokens") in places indicate the current state of the flagellar motor. Stop: Stop phases, Comp: Competent phases; Ref: Refractory phases; Act: Active phases; 1: CW rotation; 2: CCW rotation; T: Transitions. While the probability of the transitions $T_{RC1/2}$ are decreased, the probabilities of the transitions $T_{CA1/2}$ are increased by CheY-P. Modified from Oesterhelt and Marwan (2005).

## 2.3.9 Bacterial and Archaeal Chemoreceptors

### *E. coli* chemotaxis receptors

*E. coli* possesses 5 transducers, two "high-abundance" transducers Tsr and Tar and 3 "low abundance" transducers Trg, Tap and Aer. They mediate responses to Ser (Tsr), Asp and maltose (Tar), ribose and galactose (Trg), dipeptides (Tap) and oxygen (Tsr and Aer). Sensing of maltose, ribose, galactose and dipeptides requires the periplasmic binding proteins MalE, RbsB, MglB and DppA, respectively. In the case of Aer, regulation of transducer activity is methylation independent. The high-abundance receptors possess a C-terminal pentapeptide NWETF/NWESF motif that constitutes a high affinity binding site for CheR and a low affinity binding site for CheB that is distinct from their actual catalytic sites. The NWETF motif is required for efficient methylation, demethylation and deamidation. The low abundance receptors require the high-abundance receptors for adaptational assistance, because they lack the NWETF motif. Addition of the NWETF motif to a low-abundance receptor enhances adaptation even in absence of high-abundance receptors (Feng et al., 1999; Li and Hazelbauer, 2005).

### *B. subtilis* chemoreceptors

*B. subtilis* has 10 putative receptors (Kunst et al., 1997), the chemoreceptors McpA, McpB and McpC (Hanlon and Ordal, 1994; Müller et al., 1997), the previously identified transducer-like proteins TlpA, TlpB and TlpC (Hanlon et al., 1994; Hanlon and Ordal, 1994), the aerotaxis receptor HemAT (Hou et al., 2000), and three proteins of unknown function: YfmS, YoaH and YvaQ (Kunst et al., 1997). McpB is the sole receptor for asparagine and McpC is the sole receptor for proline and carbohydrate attractants (Garrity et al., 1998; Kristich et al., 2003).

### H. salinarum chemo- and photoreceptors

In the genome of *H. salinarum* a total of 18 genes coding for putative transducer proteins (Htrs) were identified due to homology to the highly conserved signaling domain of MCPs. Until now, functional assignment was only possible for 8 Htrs. The Htrs can be classified based on their putative topology, reflecting their probable cellular localization, and the mode by which they sense stimuli.

Sequence analyses and TM predictions revealed five groups (Koch, 2005): Htrs 9, 10, 11, 12, 13 and 15 (group 1) lack TM helices; Htr1 and 14 (group 2) contain 2 TM helices connected by a short hairpin loop; Htr2, 3, 4, 5, 6, 16 and 18 (group 3) contain 2 TM helices with an extensive extracellular domain in between; Htr7 and 17 (group 4) contain 3 TM helices and lack an extracellular domain; Htr8 (group 5) contains 6 TM helices and also lacks an extracellular domain.

Htrs either act as stand-alone modules in the sense that they act as receptors and transducers in one or they detect environmental signal with the help of separate receptor modules. The membrane bound Htr8 and soluble HemAT (Htr10) mediate attractive and phobic response to oxygen, respectively (Brooun et al., 1998; Hou et al., 2000). They both contain putative heme binding sites. Arginine sensing by Car (Htr11) requires the uptake of arginine by the arginine:ornithine exchanger due to the cytoplasmic nature of this transducer (Storch et al., 1999). BasT (Htr3) is responsible for chemotaxis to the **b**ranched **a**nd **s**ulfur containing amino acids Leu, Ile, Val, Met, Cys and CosT (Htr5) mediates signaling to **c**ompatible **os**molytes of the betaine family (Kokoeva and Oesterhelt, 2000; Kokoeva et al., 2002). They both belong to the group of Htrs that require binding proteins to transduce environmental stimuli. In contrast to the binding proteins known from *E. coli*, BasB and CosB, the cognate binding proteins of BasT and CosT, contain a putative lipid anchor motif and are therefore thought to be membrane associated. The *cosB* open reading frame (orf) is located upstream of the *cosT* orf and ends only 4 bases in front it and the *basB* orf overlaps with the *basT* orf, suggesting co-transcription of these orfs. A similar situation is found in further cases, in which however, functional assignment has not yet been achieved. Phototaxis is mediated by the photoreceptors SRI and SRII that transmit signals to their cognate transducers HtrI and HtrII (Htr1 and Htr2). When overexpressed, HtrII, in addition to its involvement in phototaxis, was reported to mediate taxis to Ser, probably via its extracellular loop (Hou et al., 1998). MpcT (Htr14) is involved in detection of membrane potential changes that occur e.g. when BR and HR reduce their $H^+$ and $Cl^-$ pumping activity due to decreased orange light illumination (Koch and Oesterhelt, 2005). In addition, *H. salinarum* was reported to respond to Asp, Glu and His by the action of a transducer HtrXI from strain Flx15 (Brooun et al., 1997), that surprisingly differs in sequence from Car (from strains S9 or R1, respectively) in only 9 residues. An overview of the stimulus spectrum and number of TM domains of *H. salinarum* transducers is given in Figure 2.13.
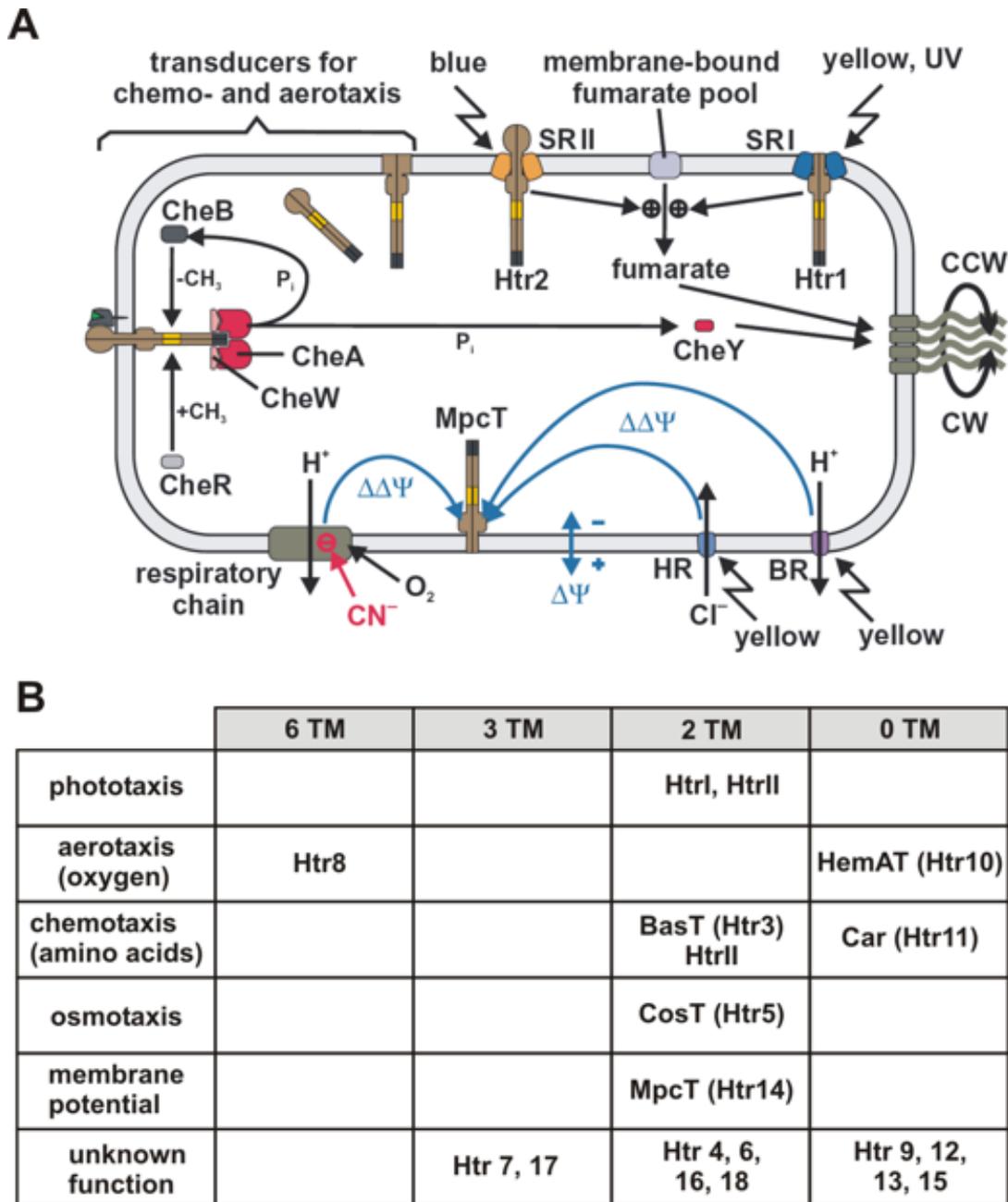
**Figure 2.13: (A) Htrs and their involvement in halobacterial taxis**. Htrs are depicted as dimers (brown) and are shown in their expected topology. The Htr regions involved in adaptation (yellow) and in signal relay (dark grey) to the flagellar motor via Che proteins are indicated. The actions of the Che-protein machinery, described in the text, are only illustrated for the Htr on the left, for which an interaction with a substrate-loaded, membrane-anchored binding protein is indicated. CheD and CheC proteins are omitted for clarity. Figure and part of the caption are from Koch and Oesterhelt (2005). **(B) Classification of Htrs according to the number of TM domains and stimulus spectrum**.

**Comparison of bacterial and archaeal transducers**

Based on multiple sequence alignments of the C-terminal cytoplasmic domains of transducers from different organism, Le Moual and Koshland (1996) concluded that eubacterial and archaeal transducers constitute a protein superfamily. They proposed that these transducers differ in the presence or absence of two pairs of insertion/deletion regions (indels) of 14 residues within both the signaling and the methylation regions of the cytoplasmic domain (see Fig. 2.14). Class III transducers contain both indel pairs, class II transducers lack the indel pairs within the signaling region and class I transducers lack both indel pairs. It was hypothesized that class III receptors represent the evolutionary ancestor of the other two classes.

*B. subtilis* McpB and *H. salinarum* transducers are class III transducers, those of *E. coli* are class I transducers. Originally, it was thought that all class I transducers release methanol upon application of negative stimuli and that class III transducers release methanol to all stimuli, but class I receptors of *Rhodobacter sphaeroides* release methanol upon addition of attractant (Martin et al., 2001a). Both *B. subtilis* McpB and all *H. salinarum* receptors lack the NWETF motif which raises the question how efficient adaptation is achieved. A recent study suggests that organisms which contain only transducers without NWETF motif possess slightly different CheR proteins that do not require tethering at the receptor (Perez and Stock, 2006). In fact analysis of MCP C-terminal ends showed that only approx. 10% out of 1121 analyzed MCPs contain a putative C-terminal binding motif, the majority of which are restricted to the different proteobacteria classes ($\alpha$, $\beta$, $\gamma$, $\delta$). The authors suggest that CheR-tethering by a NWETF motif has evolved relatively late (Perez and Stock, 2006).

## 2.3.10 Structure of transducers and transmembrane signaling

Signaling by eukaryotic receptors like receptor tyrosine kinases often relies on dimerization upon ligand binding. A prominent case is the epidermal growth factor receptor EGFR (Ullrich and Schlessinger, 1990). This principle cannot apply to prokaryotic chemoreceptors as they form stable dimers even in the absence of ligand (Milligan and Koshland, 1988). Thus the question arises how the signal is transferred from the periplasmic sensing domain across the membrane to the distant cytoplasmic signaling domain.

Crystal structures of periplasmic fragments showed that the ligand binding domain of each monomer of the aspartate receptor Tar is a four helix bundle (Milburn et al., 1991; Chi et al., 1997). The structure of the membrane spanning regions is unknown. The membrane spanning domain TM2 and the cytoplasmic portion of the receptor are connected by a linker or HAMP domain (Aravind and Ponting, 1999). The HAMP domain consists of two amphipathic sequences (AS-1 and AS-2), that were predicted to form two $\alpha$-helices (Appleman and Stewart, 2003) and indeed a recently published NMR-structure of an archaeal HAMP domain shows that the dimer forms a parallel, four helical coiled coil (Hulko et al., 2006). Crystal structures of the cytoplasmic fragments of bacterial MCPs revealed an extended coiled-coil of two antiparallel helices connected by a "U-turn". Two of these domains form an up to 225 Å long, supercoiled, four-helical bundle in the cytoplasmic portion of the receptor (Kim et al., 1999; Park et al., 2006a).
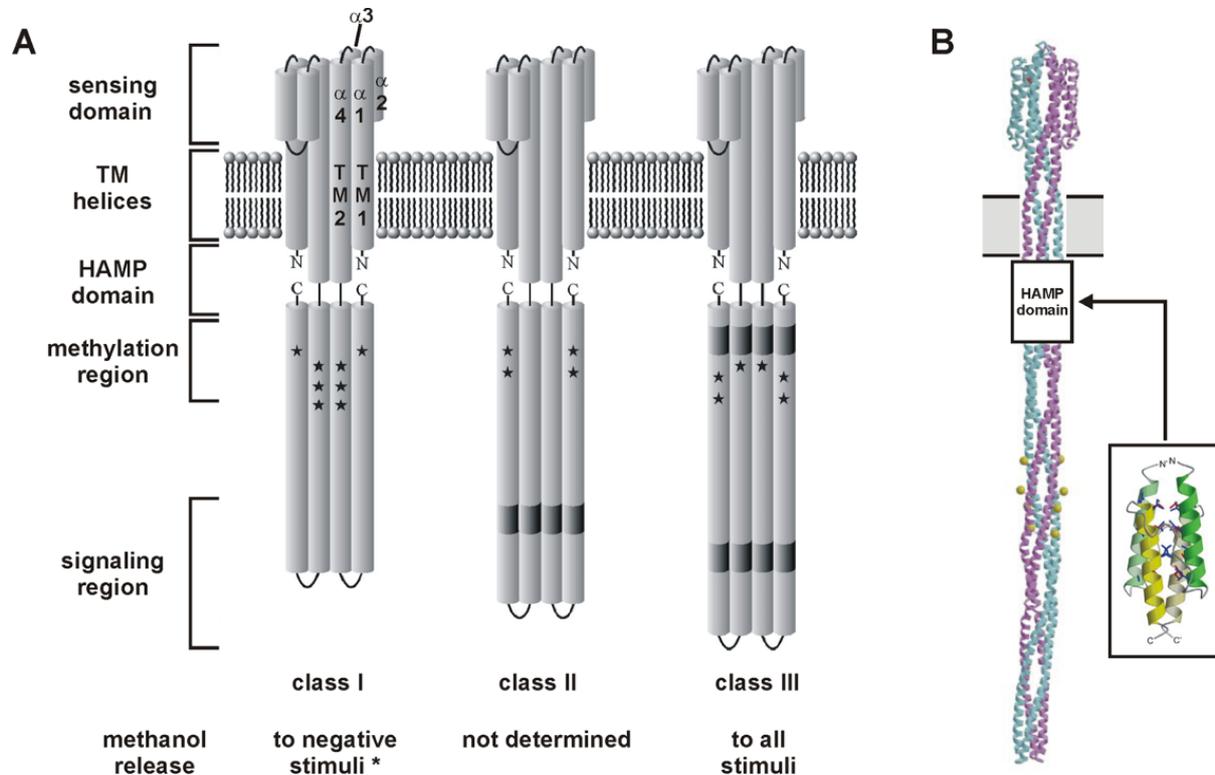
**Figure 2.14: Schematic of the three transducer classes and structure of a class I transducer (A) Schematic of the three classes of transducers, according to Le Moual and Koshland (1996).** Shown is a representative dimer for each class of chemotaxis receptors. Insertion/deletion regions (indels) are shaded in dark gray. Stars indicate sites of methylation for (from left to right) *E. coli* Tar, *M. xanthus* FrzCD, and *B. subtilis* McpB. * With respect to methanol release class I receptors of *Rhodobacter sphaeroides* are a notable exception, because they release methanol to positive stimuli (Martin et al., 2001b). Figure and caption were modified from Szurmant and Ordal (2004). **(B) Model of an intact *E. coli* Tsr receptor dimer**. The intact Tsr model was built by combining the crystal structure of a cytoplasmic portion of Tsr (cTsrQ) and a model of the ligand domain of Tsr based on the crystal structure of the ligand domain of an *E. coli* aspartate chemotaxis receptor, Tar (Chi et al., 1997). Shown is the ribbon diagram of the intact Tsr dimer model viewed perpendicularly to the noncrystallographic two-fold symmetry axis. One monomer is in purple, and the other in cyan. Methylation sites are marked by yellow balls in one monomer and orange balls in the other, and the ligand serine is drawn as a red ball partially hidden at upper left corner. Note that for the membrane-spanning regions and the C-terminal CheR-binding region no structural data are available. Inset: ribbon diagram of a recently published NMR structure of an archaeal HAMP domain (Hulko et al., 2006). Figure and caption are modified from Kim et al. (1999).

Fig 2.14 shows a model for Tar and the HAMP domain based on crystallographic and NMR data.

In principle the transmembrane signal could be carried by helix sliding, tilting or rotation, or altered helix dynamics (Falke and Hazelbauer, 2001). However, most experimental data support the so-called "swinging-piston" model (Chervitz and Falke, 1996). In the model ligand binding induces a piston-like 1.6 Å downward movement of the periplasmic and transmembrane $\alpha 4$/TM1 domain against the $\alpha 2$/TM2 domain of the same monomer subunit accompanied by a 5° tilt. This displacement is propagated all the way to the tip of the four helix bundle, where the signaling domain resides. Based on their NMR structure of the HAMP domain and activity measurements of HAMP-adenylate cyclase and HAMP-Tsr fusions, Hulko et al. (2006) concluded that the HAMP domain transduces signals by a concerted, reversible 26° rotation of all four $\alpha$-helices like cogwheels in a gearbox. In their model, the HAMP domain reverses the direction of rotation induced by ligand binding. In this context it is notable that the transducers of *H. salinarum* contain two HAMP domains that are connected by an additional linker (Aravind and Ponting, 1999). According to the "cogwheel/gearbox" model, this would lead to a twofold rotational inversion in signal propagation.

Similar to *H. salinarum*, the haloalkalophilic archaeon *Natronomonas pharaonis* senses blue light by a sensory rhodopsin (NpSRII) and its associated transducer (NpHtrII) (for phototaxis of *H. salinarum* see section 2.3.7). Light-induced isomerization of the retinal triggers outward movement of the NpSRII helix F. This outward movement leads to a tangential collision with the NpHtrII TM2 helix that results in a 15° clockwise rotation accompanied by a 0.9 Å displacement of this helix at the cytoplasmic surface (Gordeliy et al., 2002; Klare et al., 2004; Moukhametzianov et al., 2006). However, a small piston like downward movement of about 1 Å cannot be excluded.

## 2.3.11 Receptor clustering and the sensitivity paradox

In the beginning of research on bacterial chemotaxis, it was assumed that the ternary signaling complexes act as isolated units and that an equal distribution of the complexes over the cell surface would be most beneficial. However, it turned out that receptors form clusters mainly at the cell poles and to a lesser extent at lateral, potential cell division sites (Maddock and Shapiro, 1993; Sourjik and Berg, 2000). It soon became clear that clustering is not restricted to *E. coli* but is found in various bacteria and also in the archaeon *H. salinarum* (Gestwicki et al., 2000; Kirby et al., 2000). In the case of cytosolic receptors two phenomena were observed. In *Pseudomonas aeruginosa* a cytosolic receptor was found to cluster with TM receptors (Bardy and Maddock, 2005), but in *Rhodobacter sphaeroides* cytosolic receptors were found to form a cytoplasmic cluster. This organism has three *che* operons and the Che proteins almost exclusively localize to either the polar or the cytosolic receptor clusters (Wadhams et al., 2003).

In the crystal structure of cytoplasmic Tar fragments Kim et al. (1999) found trimers of receptor dimers that interact via their signaling tips. Trimers of dimers could be the smallest unit of a cluster and via contacts of the periplasmic receptor domains an extended receptor array could be built. However, trimer formation of isolated cytosolic fragments could well be an artifact and in a recent study rather a "hedgerow of dimers" was found

(Park et al., 2006a). Thus, there is an ongoing discussion about the arrangement of the receptors in the cluster and the importance of CheA and CheW for cluster formation. Latest results suggest that main determinants for cluster formation are receptor interactions themselves and that the important interactions are found in the cytoplasmic portion above the signaling tip. CheA and CheW are thought to enhance efficiency and specificity of the pathway (reviewed by Kentner and Sourjik (2006)). Various models of cluster formation are depicted in Fig. 2.15.
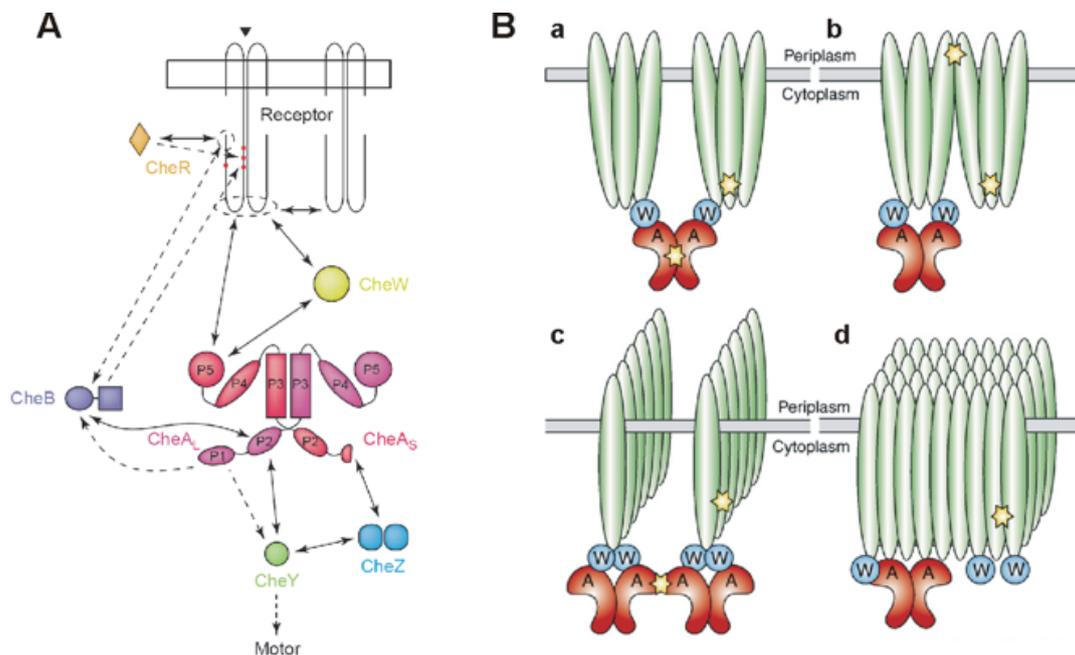


**Figure 2.15: Transducer clustering in prokaryotic chemotaxis. (A) Protein interactions involved in the assembly and function of the sensory complex**. Solid arrows show interactions important for receptor cluster formation and protein localization; dashed arrows show interactions that are not involved in protein localization but rather in the function of the sensory complex. Receptors, CheA and CheZ are each present in dimeric form, whereas CheW, CheY, CheR and CheB are monomeric. CheR and CheB bind to the pentapeptide sequence (NWETF/NWESF) at the C-terminus of the major receptors, although CheB binding is not sufficiently strong to localize the full-length CheB to the clusters. Binding to the pentapeptide sequence tethers CheR, and perhaps also CheB, close to four specific glutamyl residues (red dots; two of the residues are originally incorporated as glutamines), which are methylated by CheR and demethylated or deamidated by CheB. Figure and part of the caption are from Sourjik (2004). **(B) Models of cluster organization**. Crucial interactions are marked with a yellow star. **(a)** Trimers of receptor dimers, formed by interactions at the cytoplasmic receptor tip, bind CheA through CheW and are connected by CheA dimerization. **(b)** Trimers-of-dimers interact at the periplasmic side. **(c)** Receptors form one-dimensional hedgerows through lateral interactions between their cytoplasmic domains. CheA dimers bind receptors via CheW and connect adjacent hedgerows through interactions between the P5 domains. **(d)** Receptors self-organize into a two-dimensional lattice through lateral interactions between their cytoplasmic domains. CheW and CheA bind with a variable stoichiometry and stabilize clustering. Figure and caption are from Kentner and Sourjik (2006).

Sensory responses in the prokaryotic signal transduction pathway are extremely sensitive. *E. coli* is able to respond to increases in Asp concentrations that correspond to less than 10 molecules in the volume of an *E. coli* cell (Mao et al., 2003; Sourjik and Berg, 2002a) and *H. salinarum* was reported to respond to single photons (Marwan et al., 1988). Signal amplification was calculated to be in the range of approx. 100-fold (Segall et al., 1986). On the other hand these organisms respond and continuously adapt to stimuli that range over five orders of magnitude. It is hard to imagine that this is possible with just 5 methylatable residues to achieve adaptation and indeed early two state models of the receptor complex, in which only isolated signaling complexes were considered, failed in this respect. This obvious conflict was termed "sensitivity paradox" (Sourjik, 2004). The solution to the problem might be to consider that allosteric interactions between the receptors play the major role in signal integration, amplification and adaptation.

## 2.4 Objectives of the thesis

This thesis dealt with two closely related topics: biogenesis and motility of the flagellar system of *Halobacterium salinarum* and the photo- and chemotactic system that governs the response of this motility system. The combination of these two systems allows the cells to find those regions of their habitat that offer optimal growth conditions.

Before this study, it was known that archaeal flagellar biogenesis and the components that generate flagellar rotation are different from the bacterial flagellar systems. In the genome of *H. salinarum* a so-called *fla* gene cluster had been identified and one of the proteins, FlaI was shown to be involved in flagellar biogenesis. Proteins with homology to bacterial systems were not identified. In order to study the function of the other Fla proteins, single in-frame deletions of the corresponding *fla* genes were generated. A major aim was to distinguish whether these Fla proteins are involved in flagellar biogenesis or motility. To this end, the mutants were investigated with phase contrast- and dark-field microscopy, swarm plate assay, computerized cell tracking and electron microscopy.

Despite the differences in their flagellar systems, the chemotaxis systems of bacteria and archaea that relay sensory signals to the flagellar motor consist of homologous proteins. Before this study, several main components of the halobacterial phototaxis/chemotaxis system had already been investigated. However, analysis of the complete *H. salinarum* genome revealed the presence of further chemotaxis proteins with unknown function, but homology to the extended chemotaxis protein set of *B. subtilis*. In order to study the function of these proteins, single in-frame deletions were generated. Using swarm plates, computerized cell tracking and dark-field microscopy, the mutants were analyzed with respect to phototactic- and chemotactic efficiency and flagellar rotational bias. In two of the mutants, receptor methylation and deamidation which is a major feature of sensory adaptation were analyzed. The analysis yielded important information about the function of the corresponding chemotaxis proteins.

A detailed description of the objectives concerning the two related topics will be given in sections 3.2.1 and 3.4.2.

# 3 Results and Discussion

## 3.1 Gene deletion as an approach to elucidate protein function in *H. salinarum*

*H. salinarum* is an extremely halophilic organism, that employs a "salt-in" strategy (see 2.1.3). This circumstance severely limits available techniques that can be used to elucidate gene/protein function.

At the beginning of these studies, the sequenced and annotated genome of *H. salinarum* was available. Therefore, a gene deletion approach was chosen to obtain information about the function of several genes that are putatively involved in motility and signal transduction.

Heterologous expression even of cytosolic *H. salinarum* proteins usually results in the formation of inclusion bodies (Rudolph et al., 1995). Thus, renaturation in high salt is a prerequisite for biochemical studies and structural elucidation. Methods for monitoring the refolding success are not precise. Neither the homogeneity of the protein sample nor the degree of refolding of the protein can be well determined. Only partially refolded proteins may not be functional.

Fortunately, the development of transformation methods for halophilic archaea made *H. salinarum* accessible to genetic manipulation. However, the halophilic nature of *H. salinarum* limits the possibilities for genetic manipulation. For example, yeast two hybrid assays proved to be inapplicable. On the one hand, the functional expression of halophilic proteins in yeast is not guaranteed, on the other hand, due to the acidic nature of halophilic proteins, a high degree of $\beta$-galactosidase auto-induction is observed (M. Schlesner, unpublished). *In vivo* protein interaction- and localization studies using fusions of GFP and its variants are hampered by the fact that the GFP portion requires proper folding in high salt. Another drawback is that to date no established inducible promoter is available.

### 3.1.1 General strategy to create in-frame deletions with subsequent complementation

In-frame deletion of specific genes and complementation of the resulting gene deletion strains was achieved by use of "suicide plasmids", which can only replicate upon recombinational integration into the genome. Plasmids used for deletion contained the fused upstream (US) and downstream (DS) regions with omission of the target gene. In two successive crossover events, the target gene bounded by US and DS regions was eliminated and replaced by the direct US/DS fusion as present on the plasmid. Similarly, plasmids used for complementation contained the target gene bounded by its US and DS regions.

In two successive crossover events, the directly fused US/DS sequences were replaced by the target gene bounded by its US and DS regions. Thus, the gene was reintroduced into its original site and was under control of its native promoter. This method allows the deletion of genes from polycistronic operons without polar effects.

The DNA fragments needed for the crossover events were produced by PCR (see subsection below and the associated Fig. 3.1). As recipient pMKK100, a *E. coli/H. salinarum* shuttle plasmid was used. For cloning purposes and propagation pMKK100 contains a multiple cloning site, an ampicillin resistance gene and origin of replication for *E. coli*. For primary selection of *H. salinarum* transformants, pMKK100 contains a mevinolin resistance gene and as additional marker a halophilic $\beta$-galactosidase from *Haloferax alicantei* (Holmes and Dyall-Smith, 2000; Patenge et al., 2000), that is suitable for blue-red screening in *H. salinarum* (Koch and Oesterhelt, 2005).

Throughout this study, S9$_{mot}$ (Storch et al., 1999; Patenge et al., 2001), a highly motile single colony isolate of the bacteriorhodopsin overproducing *H. salinarum* strain S9 (Wagner et al., 1981) with an intact chemotaxis signal transduction cascade was used as parental strain for the generation of knockout strains.

The first crossover is achieved by transformation of *H. salinarum*. To allow cells of the first crossover to undergo the desired second crossover, they are grown for several generations without selection pressure by mevinolin.

## Fusion of upstream and downstream regions by means of overlap extension PCR

The US and DS regions of the target genes were fused by means of an overlap extension PCR technique (Fig. 3.1). First, in two separate PCR reactions, the US and DS regions that were $\approx 400$ base pairs long were produced. The forward- and reverse primers of the US and DS regions (P1 and P4), respectively, contained a restriction site at their 5´ ends to facilitate subsequent cloning. The reverse primer for the US region (P2) contained an extension of $\approx 14$ base pairs at its 5´end that originated from the DS region. Similarly, the forward primer for the DS region (P3) contained an extension at its 5´ end that originated from the US region. The US and DS products were then fused in a two-step PCR reaction. In the first step the plus strand of the US- and the minus strand of the DS region hybridize by their extensions and mutually serve as primers. In the second step, the double stranded product which contains the DS and US regions directly fused is amplified by means of the forward and reverse primers of the US and DS regions (P1 and P4), respectively.

Most of the genes that were deleted in this study were part of an operon and in many cases genes overlap by a few bases. Therefore, in order to make sure that the downstream genes are in frame after deletion of the target gene and in order not to delete a start or a stop codon of a directly adjacent gene, special attention had to be paid to the thorough construction of the primers that define the deleted regions (i.e. primers P2 and P3 in Fig. 3.1).
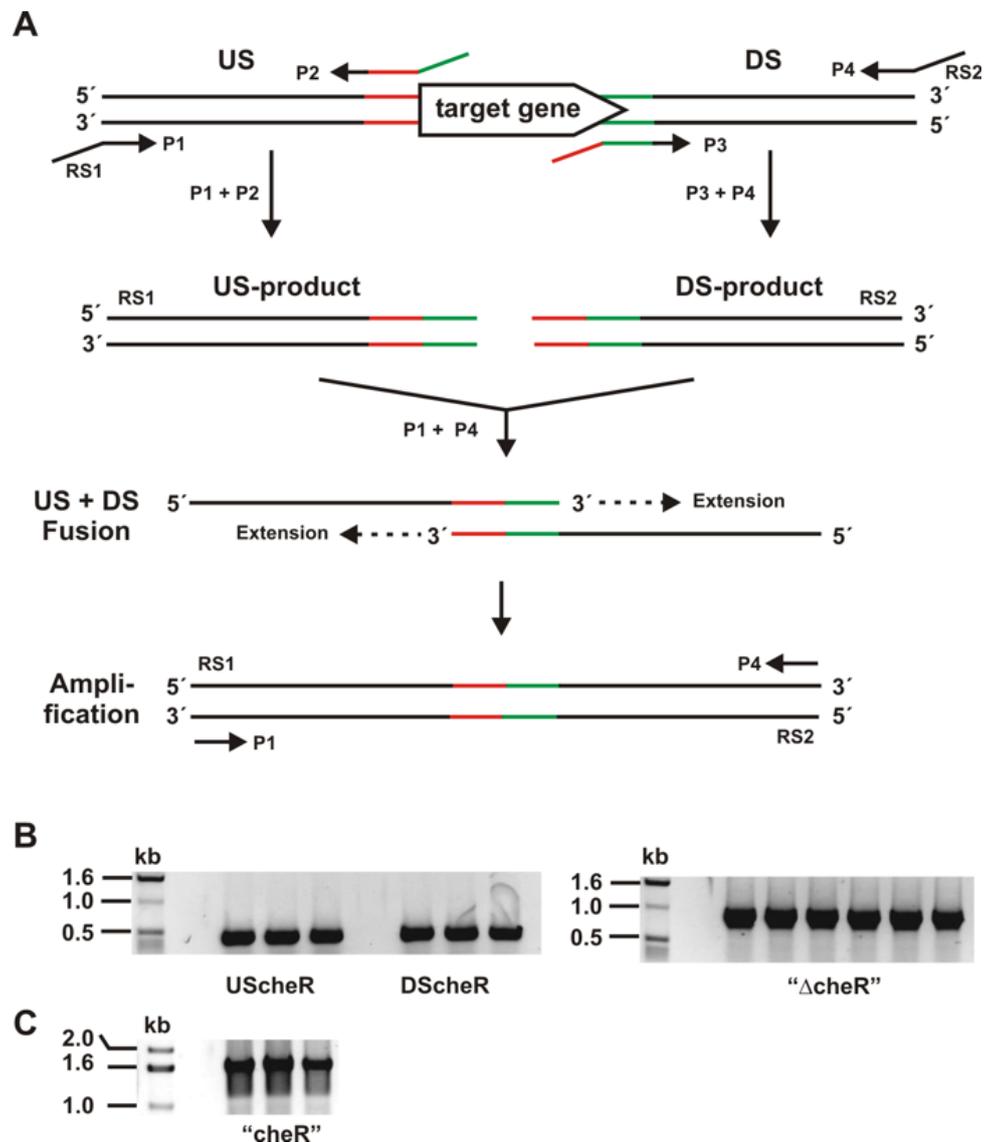
**Figure 3.1:** **(A) Principle of the overlap extension PCR as described in the text.** US: *up*stream region, DS: *down*stream region of the target gene; filled arrows denote primers and the bent part of the primer indicates artificially introduced extensions that allows for the fusion of the US- and DS regions and to introduce restriction sites, respectively; RS: restriction site; The primers are drawn next to the strand to which they anneal. **(B) Example of an overlap-extension PCR as performed in this study.** Left: 1% agarose gel of separately amplified US- (UScheR) and DS (DScheR) regions of *cheR*. UScheR was produced with primers UScheR-1.seq and DScheR-1.rev corresponding to primers P1 and P2 in (A). DScheR was produced with primers DScheR-1.seq and DScheR-1.rev corresponding to primers P3 and P4 in (A). Right: 1% agarose gel with the amplified fused US and DS regions with omission of the *cheR* gene ("ΔcheR"). **(C) Example of a PCR-amplified DNA-fragment that was cloned into pMKK100 to achieve complementation of the respective knockout strain.** Shown is a 1% agarose gel of the *cheR* gene enclosed by its US- and DS regions ("cheR"). "cheR" was produced with primers UScheR-1.seq and DScheR-1.rev corresponding to primers P1 and P4 in (A).

## Blue-red colony screening

After two successive crossover events with the suicide plasmid, either the target gene is deleted or the genotype of the parental strain is restored (Fig. 3.2). To identify cells that have undergone a second crossover event, a recently established, time-saving blue-red screening method was employed (Koch and Oesterhelt, 2005).

During the first crossover, the complete plasmid is integrated into the genome via homologous recombination between either the US or the DS regions contained on the plasmid and in the genome. Thus, positive transformants are resistant to mevinolin and develop a blue color on X-Gal containing plates. In the genome of transformants, the US- and DS regions are now contained twice in close proximity, which increases the probability for another recombination event between these regions. During the second crossover, the plasmid together with its mevinolin-resistance and $\beta$-galactosidase genes is excised from the genome. As a consequence, a second crossover can only be achieved by growth in absence of mevinolin. Nevertheless, even after several rounds of growth a second crossover only occurs in a small fraction of the cells (approx. 5% in total). On X-Gal containing plates without mevinolin, cells that have undergone a second crossover can readily be identified based on their red color (due to bacteriorhodopsin and bacterioruberin) in contrast to blue colonies that still contain the plasmid.

However, as the second crossover can occur in two ways, deletion of the target gene only occurs in $\leq 50\%$ of the red colonies. While two successive crossover events between the same homologous regions (i.e. two US- or two DS crossover events) lead to restoration of the genotype of the parental strain, an US crossover followed by a DS crossover or vice versa leads to deletion of the target gene. Thus, deletion of the target gene finally had to be verified via Southern Blot or PCR analysis.

## Nomenclature of mutants

The following strain designation will be used throughout this study. First, the name of the parental strain is given, followed by a "$\Delta gene$", indicating that the gene in question was deleted. In case of complemented strains "$/gene^+$" is added, indicating that the gene is present again. Thus, e.g. S9$\Delta flaJ$ means that $flaJ$ was deleted from the parental strain S9 and S9$\Delta flaJ/flaJ^+$ means that strain S9$\Delta flaJ$ was complemented with $flaJ$ according to 3.1.1. For convenience the abbreviations "$\Delta gene$" and "$gene^+$" will be used to indicate the genotype of deletion- and complemented strains.
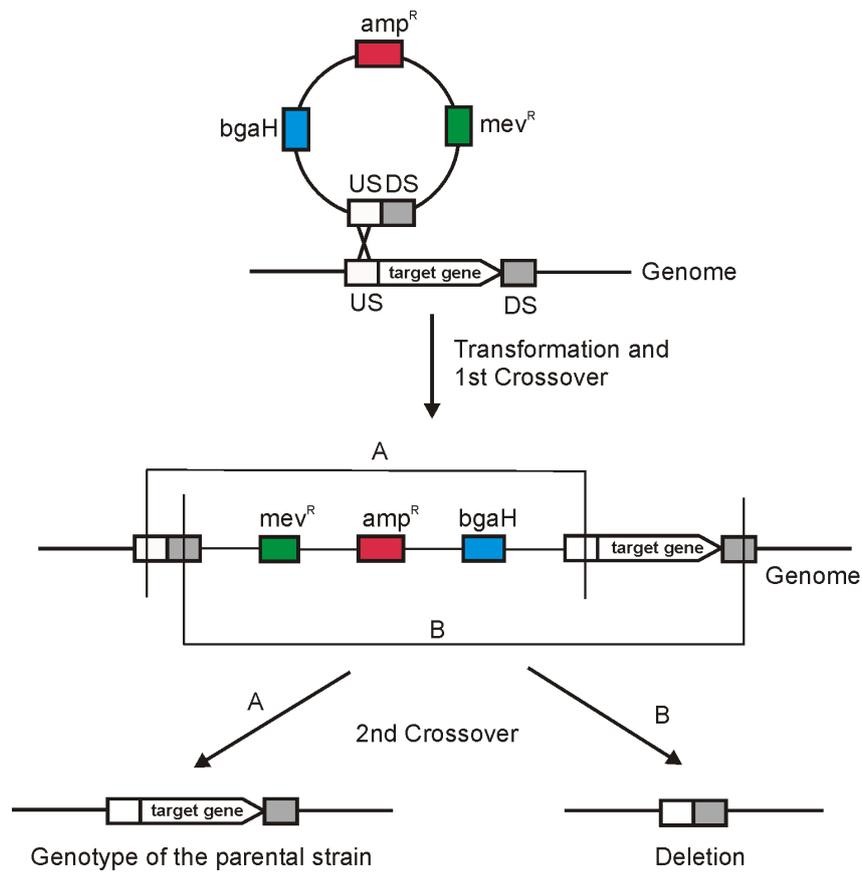
**Figure 3.2: Schematic diagram of the first and second crossover events with a suicide plasmid derived from pMKK100.** The suicide plasmid contains the fused US- and DS regions of the target gene. The first crossover is exemplified by a crossover of the US regions contained on the plasmid and in the genome, but might as well happen between the DS regions. If the second crossover occurs between the US region again (A), the genotype of the parent strain is restored. If the second crossover occurs between the DS regions (B), the target gene is deleted.

## 3.2 Investigations on flagellar biogenesis and motility of *H. salinarum*

### 3.2.1 Objectives

In bacteria, flagellar biogenesis and structure and function of the flagellar motor have been extensively studied. However, little is known about the archaeal flagellar apparatus. Current knowledge is mainly restricted to the composition and structure of the filament and the swimming behavior of halophilic archaea. Only few details are known about archaeal flagellar biogenesis and the constituents of the flagellar motor remain to be discovered. Because both bacterial and archaeal flagella are driven by rotatory motors that switch between clockwise (CW) and counterclockwise (CCW) rotation, it has been assumed that both flagellar motility systems are quite similar. In fact, this kind of rotatory principle requires that in both systems rotor, stator and switch are present. However, it turned out that structure, composition and biogenesis of bacterial and archaeal flagellar filaments are fundamentally different. Subtle differences in the swimming behaviors of bacteria and archaea suggest that the differences extend to the flagellar motor. A detailed description of the bacterial and archaeal motility systems is given in sections 2.1.5 and 2.2.

At the beginning of this study, it was known that so-called *fla* gene clusters of e.g. *H. salinarum* and *M. voltae* encode genes that are involved in archaeal flagellar biogenesis. Despite considerable effort homologs to the bacterial rotor/switch proteins of the C-ring (FliG, FliM, FliN) and the stator proteins MotA and MotB could not be identified in the complete genomes of archaea. This and a bioinformatic analysis presented in this study suggested that some of the Fla proteins may be part of the flagellar motor rather than part of the flagellar assembly machinery. In order to test this hypothesis, mutants bearing single deletions of the *fla* genes $flaD$, $flaCE$, $flaF$, $flaG$, $flaH$ and $flaJ$ were analyzed in a joint project for the presence of flagella and motility. In a simplified view, deletion of genes involved in flagellar biogenesis should result in non-flagellated mutants (Fla$^-$ mutant class), whereas deletion of genes that code for motor proteins are expected to result in flagellated mutants that have either impaired motility or are completely immotile (Mot$^-$ mutant class)[1]. Table 3.1 gives an overview of the *fla* gene mutants that are now available and classifies them as Fla$^-$ or Mot$^-$ mutants where applicable.

In the genome of *H. salinarum*, $flgXXX$ was identified as gene coding for a putative flagellin protein in addition to those that were shown to be components of the filament. There was a chance that FlgXXX like before the *M. voltae* flagellar hook component FlaB3 has escaped detection due to its low abundance. To address this question, the swimming efficiency of a $flgXXX$ deletion mutant was analyzed.

---

[1] For the use in archaea the definition of the Fla$^-$/Mot$^-$ mutant classes were modified as described in section 3.2.5.

| Strain | Genotype | Parental strain | Reference | Mutant class[†] |
|---|---|---|---|---|
| MKK215 | *htr15* deleted in frame | S9$_{mot}$ | Koch (2005) | no phenotype observed |
| S9Δ*flaD* | *flaD* deleted in frame | S9$_{mot}$ | this study | Mot⁻ |
| S9Δ*flaCE* | *flaCE* deleted in frame | | | |
| R1M1Δ*flaF* | (*flaF* deleted in frame)[‡] | R1M1 | V.Y. Tarasov | (Mot⁻)[‡] |
| R1M1Δ*flaG* | (*flaG* deleted in frame)[‡] | | | |
| S9Δ*flaH* | *flaH* deleted in frame | S9$_{mot}$ | N. Patenge, results reported in this study | Fla⁻ |
| S9Δ*flaI* | *flaI* deleted in frame | S9$_{mot}$ | Patenge et al. (2001) | |
| S9Δ*flaJ* | *flaJ* deleted in frame | S9$_{mot}$ | this study | |
| S9Δ*parA1* | *parA1* deleted in frame | S9$_{mot}$ | Staudinger (2001) | possibly involved in chemotaxis |
| S9Δ*flgXXX* | *flgXXX* deleted in frame | S9$_{mot}$ | this study | no phenotype observed |

**Table 3.1: Overview of *H. salinarum fla* gene cluster knockout mutants**.
[†] The definition of mutant classes for *H. salinarum* is: Fla⁻: mutant has no flagella; Mot⁻: mutant has flagella, but is immotile or has impaired motility; For details regarding the definition of the mutant classes of bacteria and *H. salinarum* see section 3.2.5. [‡] The use of the $\beta$-gyrase-inhibitor novobiocin as antibiotic specifically in strain R1M1 resulted in the loss of large gene regions including the flagellin B operon (*flgB1-flgB3*) in addition to the desired deletions of *flaF* and *flaG*. Therefore the phenotype of these mutants has to be taken with care. *flgXXX* is not part of the *fla* gene cluster, but codes for a protein with high homology to the known flagellin genes of *H. salinarum*. A detailed description of the phenotypes is given in Table 3.7 on page 76.

## 3.2.2 The *fla* gene cluster of *H. salinarum*

The *fla* gene cluster of *H. salinarum* contains 9 open reading frames: *htr15*, *flaD* - *flaJ* and *parA1*. In contrast to *M. voltae*, in *H. salinarum* the *fla* genes are transcribed in opposite direction to the adjacent filament structural genes *flgB1* - *flgB3* (Fig. 3.3). RT-PCR and Northern Blot analysis of the *H. salinarum fla* gene cluster revealed that *htr15*, which codes for one of the 18 halobacterial transducer proteins and *flaD* form one transcription unit and *flaE* - *parA1* are transcribed into another, separate polycistronic message (Patenge et al., 2001).

Insertional inactivation of *flaH* in *M. voltae* and in frame deletion of *flaI* in *H. salinarum* resulted in non-flagellated cells (Thomas et al., 2001c; Patenge et al., 2001). In case of the *M. voltae flaH* mutant a polar effect on downstream genes could not be ruled out and thus the loss of flagella could not be directly assigned to the inactivation of *flaH*. In case of the *H. salinarum* mutant however, the loss of flagella could be clearly assigned to the deletion of *flaI*. FlaI is homologous to the NTP binding proteins PilB and PilT of the type IV pili (T4P) mediating twitching motility (Whitchurch et al., 1991; Merz et al., 2000). PilT is involved in retraction of the pilus by depolymerization of the
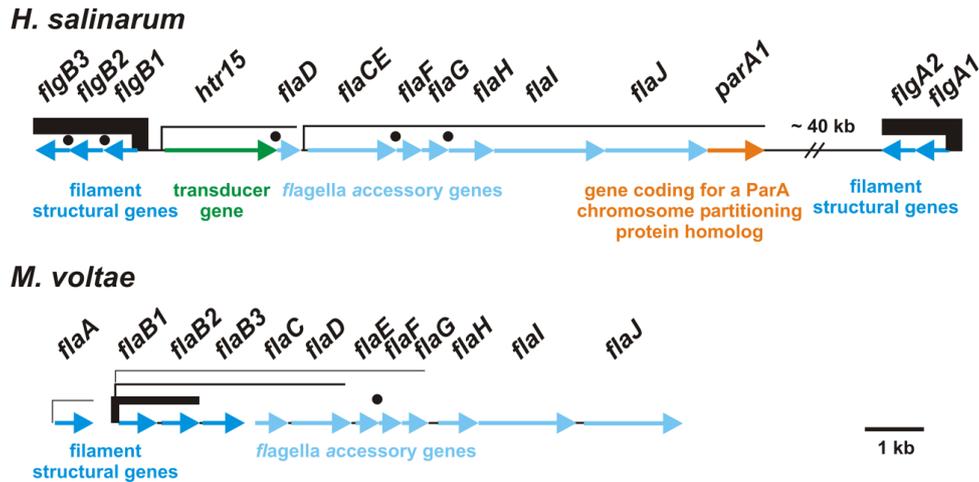
**Figure 3.3: Schematic comparison of the organization of flagella-related protein genes in *H. salinarum* and *M. voltae* with updated gene names.** Note that since the *H. salinarum fla* gene cluster was published first (Patenge et al., 2001), *flaE* was renamed to *flaCE* and *flaK* was renamed to *parA1* in the HaloLex database (http://www.halolex.mpg.de). The reason for this will be discussed in 3.2.3. Rectangular bars indicate known transcription units (Gerl and Sumper, 1988; Patenge et al., 2001; Thomas et al., 2001c). The thickness of the bars indicates the approximate relative abundances of the transcripts within the given organism according to Thomas et al. (2001a). Black dots indicate an overlap of two adjacent genes. Note, that in *H. salinarum*, filament structural genes have the prefix "*flg*" and flagella accessory genes have the suffix "*fla*". In contrast, in *M. voltae* both, the flagellar accessory genes as well as the filament structural genes have the prefix "*fla*".

filament structural protein PilA and *pilT* mutants still possess T4P, but lack twitching motility (Wu et al., 1997; Wolfgang et al., 1998). On the other hand, PilB is required for T4P formation most probably by polymerization of PilA (Turner et al., 1993; Wall and Kaiser, 1999). Thus, PilB in a way has a dual function as it is required for pilus biogenesis as such and at the same time serves as a motor protein by extension of the pilus. Further FlaI homologs are found in the type II secretory pathway. These proteins are all involved in protein secretion or pseudopilus formation, but do not serve as motor proteins. Regarding the differences between the pilus retraction mechanism of twitching motility and the rotatory principle of the *H. salinarum* flagellar motor and the phenotype of the *flaI* mutant, it was concluded that FlaI is not a motor protein, but rather involved in flagellar biosynthesis (Patenge et al., 2001).

ParA1 is a putative ATPase that is not encoded in *fla* gene clusters of other archaea (see below). Its influence on the motility of *H. salinarum* was investigated by in frame deletion of the *parA1* gene (Staudinger, 2001). Deletion of *parA1* had no obvious effect on motility in liquid medium as observed by phase contrast microscopy and electron microscopy did not reveal any deviation concerning flagella number or morphology compared to the parental strain. However, in the "swarm plate assay", which is a motility/chemotaxis assay based on the migration of the cells through semi-solid agar, a significantly reduced diameter of the "swarm ring" was observed. The complemented mutant produced swarm rings that had the same size as wild type. These findings suggest an influence of ParA1 on chemotaxis rather than on motility. In *Rhodobacter sphaeroides* the ParA1 homolog PpfA is required for proper localization and clustering of cytoplasmic transducers (Thompson

et al., 2006). Like the *H. salinarum parA1* mutant, a *ppfA* knockout mutant exhibited reduced swarming (Porter et al., 2002). Thus, ParA1 might play a similar role. A more detailed discussion of this issue is given in section 3.4.12.

### 3.2.3 Bioinformatic analysis of the proteins encoded in the *fla* gene cluster

In order to obtain an insight into the putative function of the proteins encoded in the *fla* gene cluster, a SMART database search with the protein sequences of the *H. salinarum* and *M. voltae* Fla proteins was performed. The SMART database allows the identification of conserved domains within a protein (Schultz et al., 1998; Letunic et al., 2006). The results of the SMART database search are summarized in Table 3.2. For completeness, where available, additional information about protein localization and characteristics as published by Thomas et al. (2001a) were added (labeled with an asterisk).

It was often stated, that FlaF as found e.g. in *M. voltae* is limited to methanococcal *fla* gene families (Thomas et al., 2001a; Thomas and Jarrell, 2001) and indeed a pairwise alignment of FlaF from *M. voltae* and *H. salinarum* reveals only poor homology of the two proteins. However, the SMART analysis indicated that both proteins belong to the family of archaeal FlaF proteins. To unravel this apparent contradiction, BLAST searches with the two FlaF sequences were performed. While the best hits (lowest e-value) for *M. voltae* FlaF were proteins from *Methanococci*, the best hits for *H. salinarum* FlaF were proteins from halophilic and thermophilic organisms. However, FlaF (gi 55378884) from *Haloarcula marismortui* ATCC 43049 was a shared hit (e-values were 2.2 for *M. voltae* FlaF and $2e^{-20}$ for *H. salinarum* FlaF). Thus, it seems that the archaeal FlaF family comprises two subgroups (methanococcal and halophilic/thermophilic FlaF proteins) that are, albeit very distantly, related.

In the *H. salinarum fla* cluster, FlaC seems to be missing. In addition, while in *M. voltae* FlaD is longer than FlaE, the opposite is true for the correspondingly named *H. salinarum* proteins. The SMART analysis showed, that (i) FlaD and FlaE proteins both have an archaeal FlaDE domain and (ii) that the halobacterial FlaE is a fusion protein with a N-terminal FlaC domain and an C-terminal FlaDE domain. Therefore, the published protein name (Patenge et al., 2001) was changed from FlaE to FlaCE in the HaloLex database (`http://www.halolex.mpg.de`).

An alignment performed with "Blast 2 sequences" (Tatusova and Madden, 1999) with the *H. salinarum* FlaF and FlaG sequences using the program´s default settings gave a score of 33% identities, 46% positives and 11% gaps. Both proteins have an N-terminal hydrophobic region with homology to the N-terminus of mature archaeal flagellins (FlaG) or at least a similar hydropathy profile (FlaF). The hydrophobic N-termini of the flagellins and the FlaF and FlaG proteins might act as "polymerizations domain" or might - at least transiently - anchor the protein to the cell membrane as suggested by Falb et al. (2005).

ParA1 is a putative ATPase that is only present in the *fla* gene cluster of *H. salinarum*. It belongs to a family of ATPases that are involved e.g. in active partitioning of diverse bacterial plasmids (Motallebi-Veshareh et al., 1990; Koonin, 1993). Homologs to this protein are found in most archaea, often as multiple copies. The homology of ParA1

| Protein | Characteristics of *M. voltae* protein | Characteristics of *H. salinarum* protein |
|---|---|---|
| FlaC | length: 188<br>52 - 173: Pfam:FlaC_arch<br>high-charged-amino-acid content (34%)*<br>membrane associated* | not present as separate protein,<br>however a FlaC domain is present<br>in FlaCE (see below) |
| FlaD | length: 341<br>C-terminal region exhibits sequence<br>similarity to FlaE*<br>membrane associated* | length: 156<br>49 - 156: Pfam:Arch_fla_DE |
| FlaE/FlaCE | length: 135<br>1 - 109: Pfam:Arch_fla_DE<br>Sequence similarity to the C-terminal<br>region and short version of FlaD*<br>membrane associated* | length: 504<br>1 - 24: putative signal peptide<br>77 -138: coiled coil region<br>82 - 147: Pfam:FlaC_arch<br>375 - 485: Pfam:FlaDE_arch |
| FlaF | length: 132<br>1 - 132: Pfam:FlaF_arch | length: 145<br>1 - 145: Pfam:FlaF_arch |
| | N-terminal hydrophobic region with hydropathy profile similar to that of flagellins* | |
| FlaG | length: 150<br>1 - 150: Pfam:FlaG_arch | length: 151<br>1 - 150: Pfam:FlaG_arch |
| | N-terminal hydrophobic region with weak sequence similarity to flagellins* | |
| FlaH | length: 230<br>31 - 38: putative Walker Box A motif<br>membrane associated* | length: 256<br>35 - 42: putative Walker Box A motif<br>96 - 103: putative Walker Box A motif |
| | found in all flagellated archaea where sequence data are available* | |
| FlaI | length: 552<br>156 - 446: Pfam:GSPII_E<br>306 - 312: putative Walker Box A motif<br>376 - 381: unusual Walker Box B motif[†]<br>membrane associated* | length: 629<br>232 - 514: Pfam:GSPII_E<br>378-385: putative Walker Box A motif<br>449 - 454: unusual Walker Box B motif[†] |
| | found in all flagellated archaea where sequence data are available* | |
| FlaJ | length: 558<br>1 - 60: putative signal peptide<br>80 - 210: Pfam:GSPII_F<br>335 - 466: Pfam:GSPII_F<br>5 TMs: 220 - 242; 268 - 290;<br>300 - 318; 493 - 515; 527 - 549 | length: 581<br>107 - 236: Pfam:GSPII_F<br>8 TMs: 42 - 64; 69 - 91; 252 - 274;<br>294 - 316; 326 - 345 ; 470 - 492;<br>523 - 540; 553 - 575 |
| | found in all flagellated archaea where sequence data are available* | |
| FlaK | length: 233<br>5 - 130: Pfam:Peptidase_A24<br>145 - 226: Pfam:Arc_PepC_II | length: 314<br>12 - 143: Pfam:Peptidase_A24<br>216 - 310: Pfam:Arc_PepC_II |
| | not present in the *fla* gene cluster | |
| ParA1 | not present in the *fla* gene cluster<br>of *M. voltae* | length: 323<br>11 - 209: Pfam:CbiA (contains a putative<br>deviant walker A Box motif)<br>117 - 121: putative Walker Box B motif[†]<br>homologous to *R. sphaeroides* PpfA |

**Table 3.2: Properties of flagella accessory proteins from *M. voltae* and *H. salinarum*.**
Domains were retrieved by search in the SMART database (`http://smart.embl-heidelberg.de/`) (Schultz et al., 1998; Letunic et al., 2006). Numbers denote the start and end amino acids of the domain, respectively. TMs: transmembrane domains as predicted by a HMMER algorithm. A detailed description of the Pfam protein family domains detected by the SMART search, their properties and examples for further proteins that belong to those protein families may be found in the Pfam database (e.g. `http://pfam.janelia.org`). Additional information about the *M. voltae* Fla proteins and their localization were adopted from Thomas and Jarrell (2001) and are labeled with an asterisk; [†]: manually assigned; Walker Box A motif: a nucleotide binding characterized by the amino acid sequence $[AG](X)_4GK[TS]$; deviant Walker Box A motif: $K(G)_2K(X)_2K[ST]$ (Koonin, 1993), alternative residues are written in brackets. Walker Box B motif: $(h)_4[DE]$, h stands for hydrophobic.

to the *R. sphaeroides* PpfA protein was discussed in the previous section. Originally, the *H. salinarum parA1* was named *flaK*, because it follows *flaJ* and is cotranscribed with the other *fla* genes (Patenge et al., 2001). However, when later a gene coding for an archaeal preflagellin peptidase was identified in the genome of *M. jannaschii* directly downstream of the corresponding *flaJ* gene, it was also named *flaK* and this annotation was applied also to the preflagellin peptidases of the other methanogens (Bardy and Jarrell, 2002; Bardy et al., 2003a). Therefore, the original *flaK* in *H. salinarum* was renamed into *parA1* and the name *flaK* was reassigned to the putative *H. salinarum* preflagellin peptidase OE4201R (`http://www.halolex.mpg.de`).

According to Thomas and Jarrell (2001) FlaH, FlaI and FlaJ are found in the *fla* gene clusters of all flagellated archaea, where sequence data are available. However, unambiguous information about which archaeal organisms are flagellated and motile or not is sparse. In order to find out if it is possible to generate a phylogenetic profile that can distinguish between motile and non-motile archaea, BLAST searches with the Fla- and the archaeal flagellin protein sequences were performed (Klein, 2005). The BLAST analysis comprised bacterial and 16 euryarchaeal genomes. Indicator proteins for archaeal motility had to satisfy the following criteria:

- No homologs must be found in bacterial genomes.

- No homologs must be found in the non-motile archaeon *Haloquadratum walsbyi*.

- Homologs must be found in the motile archaea *Halobacterium salinarum*, *Natronomonas pharaonis* and *Haloarcula quadrata*

The analysis revealed that a combination of FlaH, FlaJ, an archaea-specific portion of FlaI and a consensus flagellin sequence strictly met these criteria and thus may be used as an indicator for archaeal motility. In doing so, 12 of the 16 euryarchaea were classified as motile. Starting from this analysis a phylogenetic profile was defined that was expected to allow for the identification of central components of the flagellar motor. The following criteria should apply to such components:

- They must occur in all 12 Euryarchaeota that were considered motile.

- They must not occur in the 4 Euryarchaeota that were considered non-motile.

- They must not be present in bacteria.

The constituents of the archaeal flagellar apparatus can be coarsely classified into two groups, proteins involved in assembly and/or export of the apparatus and "operational" proteins that are in the broadest sense involved in the function of the flagellar apparatus. Nothing is known about the structure of the archaeal flagellar apparatus beyond its external structure, the flagellum, but from what is known about its function the presence of certain structures must be postulated. Every rotating motor consists of a rotating part called rotor and a fixed, resting part, the stator. The stator proteins must be anchored in the membrane either directly (like MotA and MotB in the bacterial flagellar motor) or indirectly by interaction with other membrane-anchored proteins. The motor switches

between CW and CCW rotation and switching is controlled by CheY-P which means that there must be a switch.

Application of the phylogenetic profile revealed that FlaJ and FlaH are perfect hits, which suggests that FlaJ and FlaH are components of the archaeal flagellar apparatus. FlaJ is a membrane-spanning multi-TM protein and FlaI is a putative ATPase. Both proteins have homologs in the bacterial type II secretion pathway (T2SS) and the biogenesis of type IV pili (T4P) (see section 2.2.4). Thus, FlaI and FlaJ are most likely involved in flagellin export/flagellar assembly. Two additional gene pairs coding for FlaI- and FlaJ homologs are found in the genome of *H. salinarum* itself: OE2215R (GspE, GSPII_E motif)/OE2212R (GSPII_F motif) and OE1347R (GspE1, GSPII_E motif, not found by SMART search)/OE1342R (GSPII_F motif). The phenotype of the *flaI* knockout mutant shows that the FlaI-homologs cannot compensate for the loss of FlaI (Patenge et al., 2001) and - as will be shown in the following sections - the same is true for FlaJ and its homologs. This suggests that FlaI and FlaJ homologs belong to general or unknown protein export/assembly systems and that FlaI and FlaJ themselves are further specialized for the export/assembly of flagellins.

FlaH is a putative ATPase that does not occur in the T2SS and T4P systems and therefore might be a good candidate for a motor protein, implying that archaea use ATP to drive the flagellar motor. Interestingly Ng et al. (2006) found, that in the archaea *Methanococcoides burtonii*, *Methanosarcina mazei* and *Methanosarcina barkeri* genes that code for FlaH/FlaI/FlaJ homologs are present at two different loci. In the case of *M. mazei* and *M. barkeri* it seems that a complete second *fla* gene cluster is present. Unfortunately, experimental data about the function of these two separate *fla* gene homology clusters are currently not available.

The bioinformatic analysis suggests that while FlaI and FlaJ are most likely involved in flagellar biogenesis, the putative ATPase FlaH is a candidate for a flagellar motor protein. This implies that the archaeal flagellar motor may be driven by ATP instead of a proton gradient. In case of FlaD, FlaCE, FlaF and FlaG the analysis did not allow to draw conclusions if these proteins are involved in biogenesis of the flagellar apparatus or if they are part of the flagellar motor.

## 3.2.4 Construction and genotypic analysis of *fla* gene knockout mutants

Single deletions of *flaD*, *flaCE* and *flaJ* and complementations of the resulting knockout strains were generated according to the general outline in section 3.1.1. As mentioned there, deletion is achieved by two crossover events with a suicide plasmid. Only $\leq 50\%$ of those cells that have undergone a second crossover event contain the desired deletion, in the other $> 50\%$, the genotype of the parental strain is restored. Therefore, the desired deletion had to be confirmed by Southern Blot or at least PCR. To this end, DIG-11-dUTP labeled probes hybridizing to the upstream region ("PRE" probe) and to a region within the gene ("CORE" probe), respectively, were produced by PCR.

Figure 3.4 (A) shows a schematic view of the loci of the *fla* genes based on the sequence of the *H. salinarum* strain R1 as retrieved from the HaloLex database

(`http://www.halolex.mpg.de`) and Figure 3.4 (B) shows typical results of the deletion/complementation experiments. Southern Blot analysis with genomic DNA of the respective colonies confirmed successful deletion of $flaD$ and $flaCE$ and successful complementation of the $flaJ$ knockout mutant, respectively.

## 3.2.5  *FlaH*⁻ and *flaJ*⁻ mutants are devoid of flagella while *flaD*⁻ and *flaCE*⁻ mutants have less flagella

**Classification of bacterial mutants altered in flagellar biosynthesis, motility or swimming behavior**

Regarding flagellar biosynthesis, motility and swimming behavior, bacterial mutants can be subdivided into three phenotypic classes (Macnab, 1996).

The **Fla⁻** (nonflagellate or partially flagellate) phenotype is defined as "any substantial diminution of the flagellar apparatus". This is a quite far reaching definition and thus phenotypes range from total lack of any flagellar structure to partial basal structures to defective external structures, e.g. the filament.

**Mot⁻** (paralyzed) mutants possess a flagellar apparatus including flagella. However, the flagellar apparatus is unable to rotate. Depending on the importance of a gene product for flagellar assembly, this may occur either upon its complete absence (e.g. $motA$ and $motB$) or its partial functional loss (e.g. in case of the *E. coli* motor/switch genes $fliG$, $fliM$, $fliN$). Complete absence of the latter gene product class prevents flagellar assembly.

**Che⁻[CW]** or **Che⁻[CCW]** (switch defective) mutants are characterized by the presence of rotating flagella but unusual switching behavior caused by a deviation from the wild type CW/CCW flagellar rotational distribution. This phenotype class mainly contains mutants that have defects in chemotaxis, but mutations in motor/switch genes may also produce a switch defect.

**Redefinition of the terms Fla⁻ and Mot⁻ for the use in *H. salinarum***

Given the lack of detailed knowledge about biosynthesis and function of the flagellar motor of *H. salinarum*, we redefine the terms Fla⁻ and Mot⁻ for the use in *H. salinarum* in the following way:

- **Fla⁻** mutants shall be defined as mutants that do not possess flagella.

- **Mot⁻** mutants shall be defined as mutants that possess flagella, but are defective in motility.
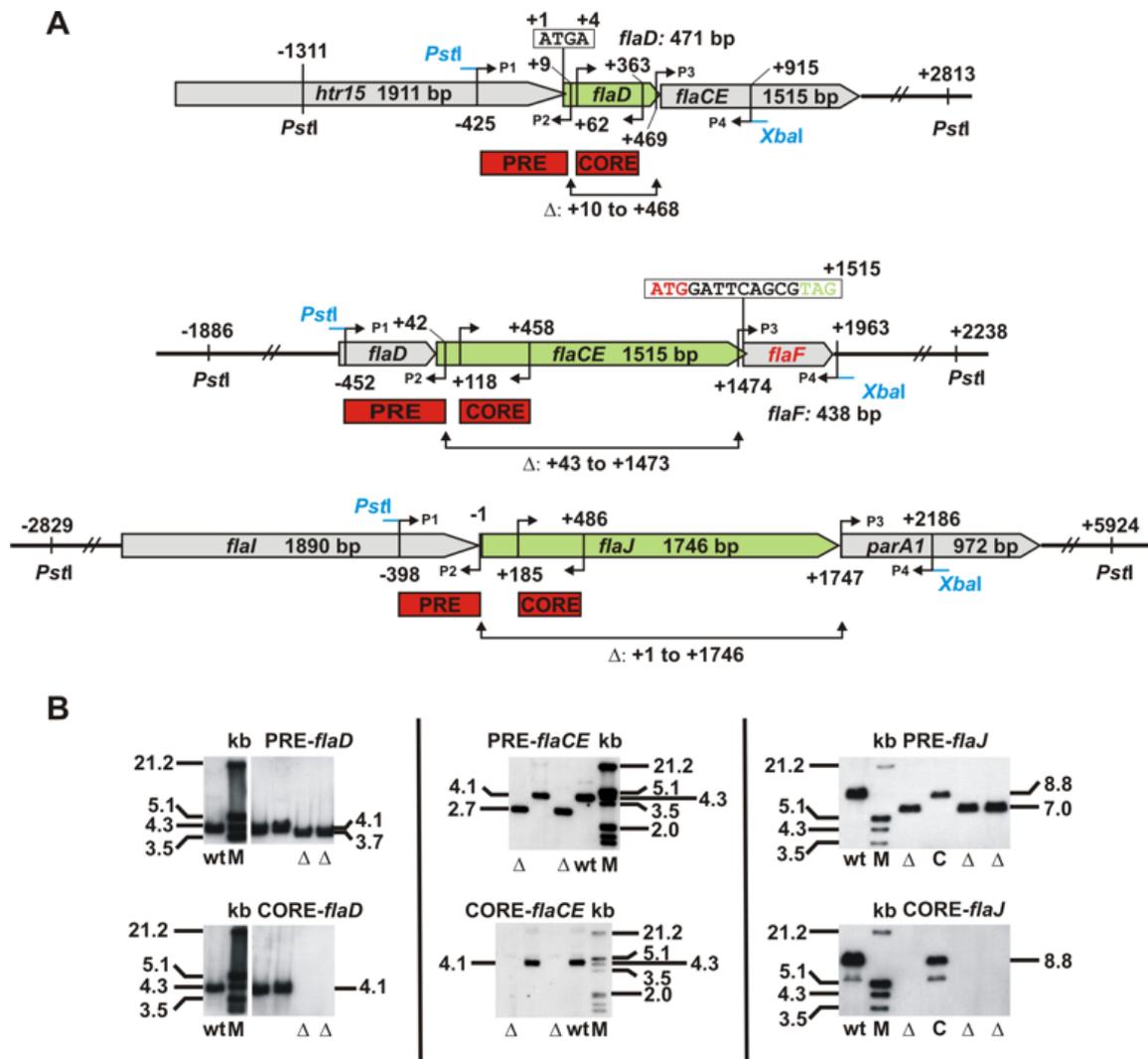
**Figure 3.4: Genotypic analysis of *fla* gene knockout strains. (A) Schematic of the loci of the *fla* genes that were deleted in this study**. Numbers indicate nucleotide positions relative to the target gene (in light green color) with the following convention: +1 is the position of the first base of the target gene, -1 is the position of the preceding base. Primers are indicated as bent arrows. Primers P1 - P4 were used to create the US- and DS fragments of the target gene and are named according to Fig. 3.1. Red boxes indicate the hybridization positions of DIG-11-dUTP-labeled probes in front (PRE) or within (CORE) the target gene that were produced with the other primers. In case of overlapping genes, the start and stop nucleotides are given in boxes. Numbers following "Δ:" denote start- and end position of the deleted region **(B) Southern Blot analysis with genomic DNA of the *fla* gene knockout strains.** Genomic DNA was digested with *Pst*I. M: marker lane; Δ: lane with hybridization signal that is in accordance with deletion of the target gene; C: lane with hybridization signal that is in accordance with a complementation; wt: lane with hybridization signal obtained with wild type DNA. Lanes that are shown for blots obtained with the PRE- and CORE probes for the respective target gene correspond to each other. White vertical lines indicate that the lanes shown were not directly adjacent in the blot.

**Light microscopy**

Motile *H. salinarum* cells swim back and forth by rotation of a right handed helical flagellar bundle consisting of 5 - 10 flagella (Alam and Oesterhelt, 1984). Swimming phases are spontaneously interrupted by short stop phases followed by a reversal of swimming direction (Marwan et al., 1991) (for a detailed description see section 2.1.5).

The easiest, most straightforward methods to study motility of *H. salinarum* cells are phase contrast- and high-intensity dark-field microscopy. Phase contrast microscopy allows a first qualitative estimation of cell motility. While motile cells perform a directed movement that can be recognized as a track when following the cells for several minutes, immotile cells perform a Brownian motion that manifests as a twitching movement without noteworthy net displacement on the minute time scale (Fig. 3.5 (B)). Using these criteria, it is usually easy to discriminate between motile and immotile cells, but whenever motility falls below a certain threshold, this is a very challenging task, especially in case of mutants which have defects in either the flagellar biosynthesis or in structural elements of the motility apparatus. In such cases atypical patterns of movement can be expected that may be misinterpreted as Brownian motion.



**(A)** Motile *H. salinarum* cells      **(B)** Cells treated with formaldehyde
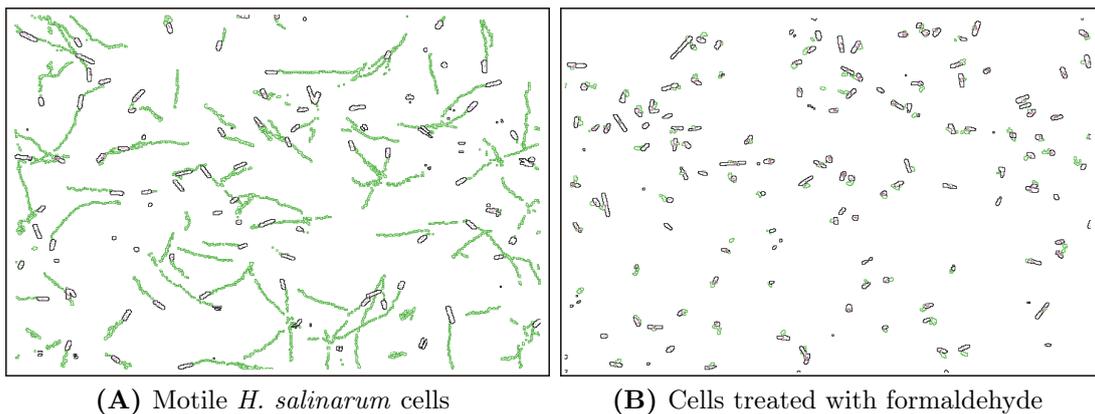
**Figure 3.5: Swimming tracks of motile and immotile *H. salinarum* cells**. Screenshots of 10 s swimming intervals are shown for (A) motile S9$_{mot}$ cells and (B) immotile cells that were generated by formaldehyde treatment. The original pictures were generated and edited as described in Fig. 3.7. Black dotted circles represent cells, green colored dots represent the cells´ positions during the course of the 10 s interval.

In case of immotile cells, phase contrast microscopy does not allow to discriminate between a Fla$^-$ or a Mot$^-$ phenotype. However, unstained bacterial and *H. salinarum* flagella can in principle be visualized by high-intensity dark-field microscopy due to a light scattering effect (Macnab, 1976; Alam et al., 1984). The visibility of the flagella depends among other factors on the motility of the cells and the efficiency of the flagella to form a compact bundle. It has to be noted that frequently flagella even of a highly motile cell cannot be visualized. It can be expected that non-rotating flagella attached to cells are hard to visualize, but it is known that detached flagella can aggregate into thick spiral bundles called "super-flagella" that can be easily visualized with dark-field microscopy. Typical examples of flagella attached to swimming cells and super-flagella

visualized by dark-field microscopy are given in Figure 3.6.



**(A)** Monopolarly flagellated   **(B)** Bipolarly flagellated   **(C)** Laterally flagellated



**(D)** Super-flagella                    **(E)** Super-flagella
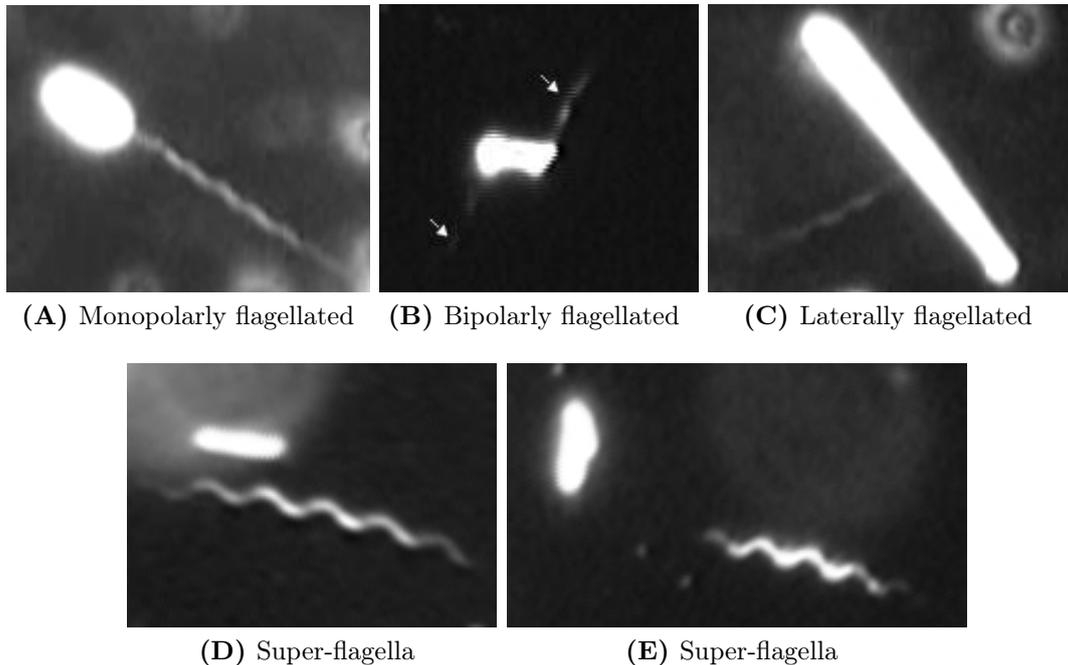
**Figure 3.6: Dark-field microscopic snapshots of swimming *H. salinarum* cells and super-flagella**. (A) - (C) Snapshots were extracted from dark-field microscopic videos that were recorded from wild type cells and chemotaxis mutants during the course of this study. (D) - (E) Super-flagella were found in stationary cultures of the complemented strains S9$\Delta flaD/flaD^+$ and S9$\Delta flaD/flaCE^+$, respectively. Note that the super-flagella are not attached to the cells above them. The cells may serve as size markers.

Super-flagella are mostly found in stationary wild type cell cultures or in all growth phases of flagella overproducing mutants like M-175 (Alam and Oesterhelt, 1984; Alam et al., 1984). Thus, by visualization of rotating flagella, dark-field microscopy facilitates the discrimination between inefficiently swimming and immotile cells and, provided that non-rotating flagella attached to cells can be visualized, it helps to discriminate between mutants of the Fla$^-$ or Mot$^-$ phenotype. Increased formation of super-flagella indicates either overproduction or increased shearing of flagella.

Motility of the $\Delta flaH$, $\Delta flaJ$, $\Delta flaD$ and $\Delta flaCE$ deletion- and the corresponding complemented mutants was first inspected visually by phase contrast microscopy and compared to the parental strain. While single deletions of $flaH$, $flaJ$ and $flaCE$ resulted in immotile cells, a small fraction of motile cells was observed reproducibly in cultures of the $\Delta flaD$ mutant. In all cases, cultures of the complemented mutants were clearly motile. However, restoration of wild type motility seemed to be somewhat incomplete. At closer inspection, a relatively large fraction of cells that stick to the glass surface of the microscopic slides or coverslips was observed, which explains why the complemented mutants appeared to be less motile than the parental strain. Cells that completely stick accumulate in planes where they have contact with glass and do not even perform Brownian motion. This phenomenon was described very early and seems to

occur spontaneously, i.e. sometimes single colonies stick, even if the parental strain does not (Spudich and Stoeckenius, 1979).

Dark-field microscopy with the $\Delta flaH$, $\Delta flaJ$ and $\Delta flaCE$ mutants confirmed that these cells were immotile. In addition, despite repeated inspection of samples under the microscope, no indications for the presence of flagella were found. In contrast, in samples of the $flaD$ mutant, reproducibly a small percentage of swimming cells was found and in some cases flagella were visible. Usually, when flagella were detected, their visibility was worse compared to flagella from wild type cells. Reduced visibility of flagella could be caused by a reduced efficiency to form a bundle or by a reduced number of flagella. This again, could be caused by an increased loss of flagella. In such a case an increased abundance of super-flagella even in exponentially growing cultures would be expected. However, this was not observed. Inspection of the complemented mutants $flaJ^+$, $flaD^+$ and $flaCE^+$ confirmed restoration of wild type swimming behavior. Flagella were readily observed and their visibility was comparable to that of wild type cells. The results are summarized in Table 3.3.

| *Strain* | *Motility (phase contrast and dark-field)* | *flagella (dark-field)* |
|---|---|---|
| $\Delta flaH$ | indistinguishable from Brownian motion | not observed |
| $\Delta flaJ$ | indistinguishable from Brownian motion | not observed |
| $flaJ^+$ | reduced in comparison to S9$_{mot}$, "sticky" | present |
| $\Delta flaD$ | reproducibly, a small percentage of motile cells was observed | observed on motile cells, reduced visibility |
| $flaD^+$ | slightly reduced in comparison S9$_{mot}$, slightly "sticky" | present |
| $\Delta flaCE$ | indistinguishable from Brownian motion | not observed |
| $flaCE^+$ | reduced in comparison to S9$_{mot}$, "sticky" | present |

**Table 3.3: Motility of *fla* deletion mutants and presence of flagella as judged by phase contrast microscopy**.

As mentioned above, visibility of flagella in dark-field microscopy depends on several factors. Therefore, in order to find out whether the $\Delta flaH$ and $\Delta flaJ$ mutants possess flagella and in order to find out why the visibility of the $\Delta flaD$ mutant flagella is reduced, electron microscopy was performed (see below).

### Computerized cell tracking

Another light microscopy based, however more quantitative way to determine halobacterial motility is computer-aided two-dimensional cell tracking (motion analysis) (Marwan and Oesterhelt, 1990). The system was originally designed to determine spontaneous and stimulus induced reversal frequencies and this application will be discussed in more detail in section 3.4.8, but it may also be used to measure swimming velocities (Bibikov et al., 1991). In brief, the system consists of a phase contrast microscope equipped with a CCD camera that transmits grey scale pictures with a defined frame rate to an image processor. Based on the grey-scale value, the computer system identifies the cells, calculates the centroids of the cells and assigns $x$-$y$ values in a coordinate plane to these

centroids. From the $x$-$y$ values of the cells in a series of successive frames a cell track can be reconstructed and from the changes in the $x$-$y$ values ($\Delta x \Delta y$) per frame, swimming velocities can be calculated. Figure 3.5 on page 57 shows tracks of *H. salinarum* cells that were obtained with an advanced motion analysis system developed by Streif et al. (2007).

Cell velocities of S9$_{mot}$, S9$\Delta flaJ$, S9$\Delta flaD$, S9$\Delta flaCE$ and the complemented strains were determined in 60 single measurements from 3 microscopic specimens for each strain. To this end, the cells were diluted to equal optical densities (OD$_{600}$ = 0.31) in complex medium supplemented with arginine as described in section 4.5.2. Each specimen was prepared right before it was measured and was preincubated on the microscopic stage for 10 min at 25°C. To guarantee optimal energization of the cells, the specimen was continuously illuminated with orange light (580 ± 50 nm, 290 W/m$^2$).

A first qualitative impression of cell motility was obtained by activating the "locate cells" function of the system, that allows to display cell tracks on-line. Screenshots of cell tracks of the mutants and the complemented mutants from swimming intervals of 10 s are shown in Figure 3.7. For comparison, cell tracks of S9$_{mot}$ wild type cells and formaldehyde treated, dead cells are shown in Figure 3.5, page 57. On screenshots of the S9$_{mot}$ cells and the complemented mutants a large number of cell tracks were found. In contrast, only few cell tracks were found on screenshots of the $\Delta flaD$ mutant and no cell tracks were found on screenshots of the $\Delta flaJ$ and $\Delta flaCE$ mutants. This confirmed the previous observation that while the $\Delta flaJ$ and $\Delta flaCE$ mutants were immotile, some residual motility was present in cultures of the $\Delta flaD$ mutant.

For quantitative measurements, from each specimen 20 single measurements of 5 s duration were recorded and for every single measurement a new section of the specimen was selected to obtain a better average velocity value of the specimen. Cell velocities of the various strains are summarized in Table 3.4. The output values of the measurements are among others the number of detected cells, the number of motile cells and the mean velocity. Detected cells are objects that are recognized as cells due to their grey level value and size. Cells that perform Brownian motion lead to a high rate of changes in $\Delta x \Delta y$ values of the cell centroids, which for the tracking algorithm simulates motility. Therefore, a minimal move radius that is defined as a radius around the center of the whole cell track, was introduced as a threshold for moving cells. This threshold was determined experimentally on dead cells as described in section 4.5.2 to be 2.5 µm at 25°C. Motile cells are the number of detected cells that cross the minimal move radius. The error for false positive classification of immotile as motile cells is $\approx 2\%$. The mean velocity is defined as the average velocity of all motile cells in a single measurement. A simple average of the mean velocities could in an extreme case lead to a velocity value that is determined by a single motile cell. Therefore, a more robust value for the average velocity of the whole cell population ("average velocity" $\bar{v}$ in Table 3.4) from the 60 single measurements was calculated as follows:

$$\bar{v} = \frac{\sum_{i=1}^{60} \text{motile cells}_i \cdot \text{mean velocity}_i}{\sum_{i=1}^{60} \text{detected cells}_i} \tag{3.1}$$
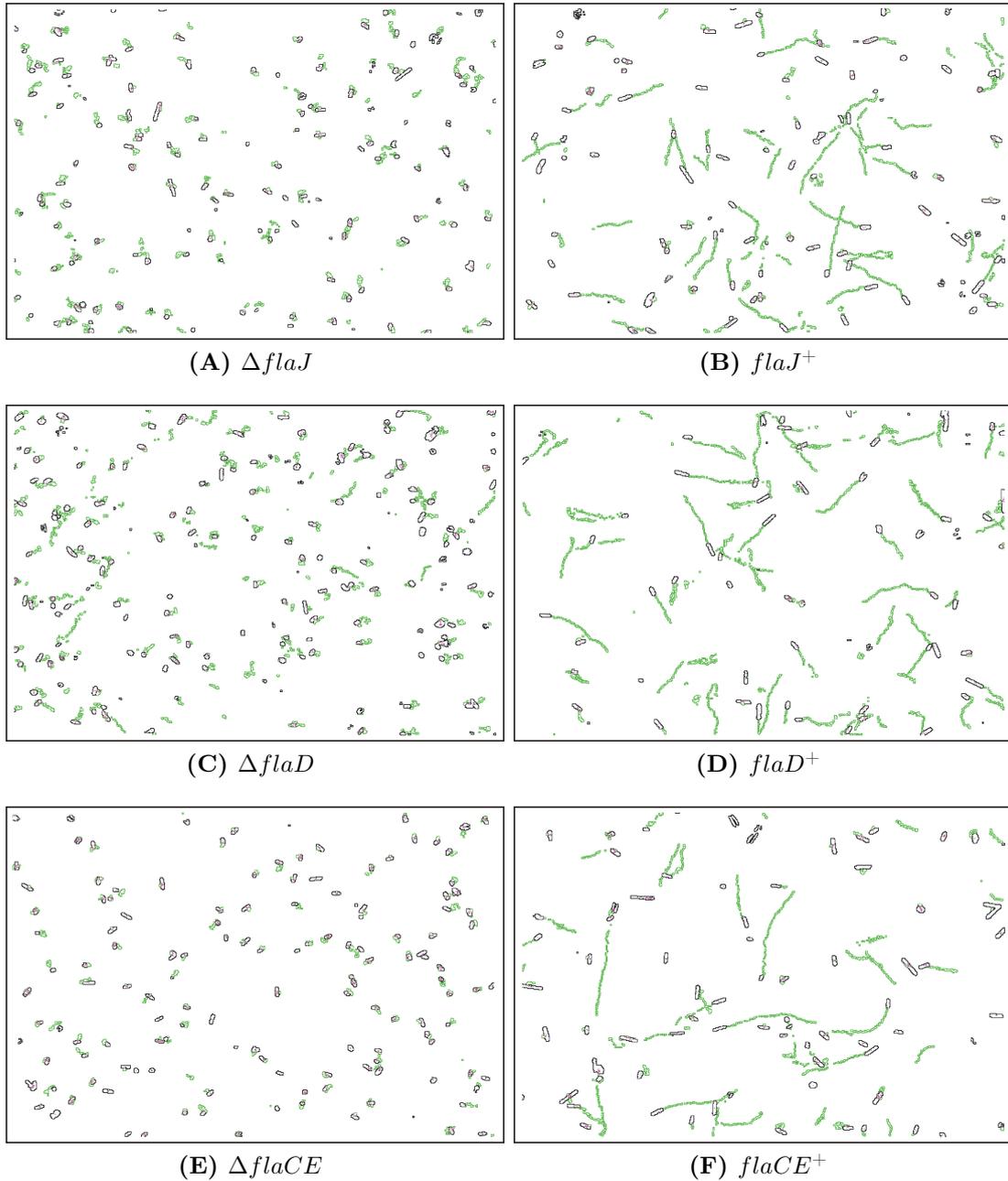
**Figure 3.7: Swimming tracks of *H. salinarum fla* knockout- and complemented mutants**. Screenshots of 10 s swimming intervals are shown. They were generated by activating the "locate cells" function of the computerized cell tracking system (Streif et al., 2007) and taking a screenshot after 10 s. For better visibility of the tracks, the original pictures were edited with Corel Photo Paint (menu "effects", submenus "contour", "vectorialization contour", "plain" value: 90). Black dotted circles represent cells, green colored dots represent cell positions during the course of the 10s interval. For comparison cell tracks of S9$_{mot}$ that were generated in the same experiment are shown in Fig. 3.5.

| Mutant | $\bar{v}$ [$\mu m/s$] | Detected cells (d) | Motile cells (m) | Ratio m/d |
|---|---|---|---|---|
| S9$_{mot}$ | 3.4 | 1740 | 1325 | 0.76 |
| $\Delta flaJ$(F) | 0$^\dagger$ | 2559 | 20 | 0.00$^\dagger$ |
| $flaJ^+$ | 1.1 | 2495 | 699 | 0.28 |
| $\Delta flaD$(2) | 0.3 | 2728 | 239 | 0.08 |
| $flaD^+$ (1) | 2.7 | 1785 | 1084 | 0.61 |
| $\Delta flaCE$(2) | 0$^\dagger$ | 2754 | 2 | 0.00$^\dagger$ |
| $flaCE^+$(1) | 1.1 | 2019 | 520 | 0.26 |

**Table 3.4: Motility of *fla* gene knockout- and complemented mutants determined by computerized cell tracking**. $\bar{v}$: average velocity as defined by equation 3.1; $^\dagger$ The ratio of motile cells to detected cells is below the measurement error for discrimination between detected and motile cells. Therefore, the value for the average velocity $\bar{v}$ was set to zero. Numbers/letters in parentheses in strain designations denote which clone was investigated.

The cell velocities determined by computerized cell tracking once again convincingly showed that the $\Delta flaJ$ and $\Delta flaCE$ mutants were immotile and that a certain percentage of motile cells was present in the $\Delta flaD$ mutant. In the cultures of the $\Delta flaJ$ and $\Delta flaCE$ mutants only 20 out of 2559 and 2 out of 2754 detected cells were classified as motile. This is well below the 2% measurement error and visual inspection of the videos indicated that these cells were false positives. By contrast, measurement of the complemented mutants showed that these cells were clearly motile. However, except for $flaD^+$, the percentage of motile cells and the average velocity of the whole cell population of the complemented mutants was clearly diminished. This may at least partially be explained by the observation that in the complemented strains a certain percentage of cells stick to the glass surface. "Sticky" cells are included as detected but not as motile cells in the calculation of the average velocity according to equation 3.1 and thus lower the average velocity. In addition, it has to be noted that while the parental strain was selected as a motile single colony, this was not done in case of the mutants and complemented mutants to avoid enrichment of cells with altered genotype e.g. suppressor mutants. Diminished motility was previously reported for the complemented $\Delta flaI$ mutant, albeit in this case, the $flaI$ gene was under control of the *bop* promoter instead of its original promoter (Patenge et al., 2001).

## Swarm plate assay

The swarm plate assay is a widespread assay to study motility and chemotactic ability of flagellated microorganisms. It is also employed to select highly motile cells. In the case of *H. salinarum* cells the assay has the advantage that the motility of cells that stick to glass surfaces is not impaired (Spudich and Stoeckenius, 1979). Thus, this assay was regarded especially suitable to check the motility of the sticky complemented mutants.

In the swarm plate assay a small volume of liquid culture is stabbed underneath the surface of a soft-agar plate containing either a specific nutrient or - as in the case of this study - complex medium. The concentration of the agar is such that it allows the cells to swim. After inoculation, the cells begin to propagate and consume the nutrients. In doing

so they produce a gradient of nutrients and chemotactically active substances. Motile, chemotactic cells follow up the gradient and form a continuously expanding "swarm ring" of relatively low cell density whereas cells with impaired motility or chemotaxis fall behind and form a solid disc of higher cell density. The diameter of the "swarm ring" is therefore a measure of cell motility and chemotactic efficiency. Compared to microscopic inspection of cell motility, it is much easier in the swarm plate assay to trace minimal motility of cells and relative differences in swimming speed can be quantified simply by measuring diameters of "swarm rings". The major disadvantage of the assay is that the relative contributions of motility and chemotactic ability on the diameter of the "swarm ring" cannot be discriminated. Therefore, in order to be able to draw valid conclusions about the chemotactic efficiency of a mutant, its motility has to be checked in the microscope before the assay is conducted.

Representative swarm plates for S9$_{\text{mot}}$, $\Delta flaJ$, $\Delta flaD$, $\Delta flaCE$ and the complemented mutants are shown in Figures 3.8 - 3.10. Table 3.5 summarizes the swarm ring diameters relative to S9$_{\text{mot}}$. In order to allow a direct visual comparison of relative swarm ring diameters, two swarm plates that were inoculated with the $\Delta flaH$, $\Delta flaJ$, $\Delta flaD$, $\Delta flaCE$ and $\Delta parA1$ mutants are shown in Figure 3.11.

While the swarm ring diameter of the $\Delta flaJ$ and $\Delta flaCE$ mutants was in the same range, the swarm ring diameters of the $\Delta flaD$ mutant were only slightly, however reproducibly larger. The difference in motility between the $\Delta flaJ/\Delta flaCE$ and $\Delta flaD$ mutants was more apparent in plates that were incubated for a longer time (see Fig. 3.11). In some plates of the $\Delta flaJ$ and $\Delta flaCE$ mutants a small zone of lower cell density was observed. This could be misinterpreted as residual motility, but is an artifact that sometimes occurs due to displacement of the soft-agar caused by the injection of the liquid culture. This artifact is also seen in swarm plates of the non-flagellated $\Delta flaI$ mutant (Patenge et al., 2001). From the inspection of many swarm plates of the $\Delta flaD$ mutant, I concluded that in this case, there was really swarming. All complemented mutants produced swarm rings with diameters that were well within the range of colonies that were not selected for their motility (Patenge et al., 2001). Thus, in contrast to the velocity measurements by computer-aided cell tracking that may have been tampered by sticky cells, the swarm plate assay indicated that wild type motility was quite well restored in the complemented mutants. On the other hand, the assay clearly demonstrated, that the immobility and reduced motility of the *fla* knockout mutants as observed in the other assays was not caused by sticking of the cells. In principle, the reduced swarming ability of the *fla* gene knockout mutants investigated in this study could also caused by a reduced chemotactic efficiency. However, the results obtained with light microscopy clearly indicate that the absence and reduced swarming of the *fla* mutants at least mainly reflects the absence of or reduced motility, respectively. Also, given that the *fla* genes are not involved in signal transduction, the reduced swarming ability was not caused by an unrelated additional mutation because (i) the results were comparable for several single clones that bore the same deletion and were derived from different single clones of the first crossover and (ii) complementation was successful. The situation may be different in case of deletion of *parA1*, which is the last gene in the *flaE - parA1* transcription unit (Fig. 3.3). In this mutant, reduced swarming ability (Fig. 3.11), but no obvious

impairment of motility in liquid medium was observed and the mutant had a wild type number of filaments (Staudinger, 2001). Thus, in this case, an involvement of *parA1* in signal transduction is likely.

Altogether, the results obtained with the swarm plate assay were in good agreement with the results obtained with the light microscopic observations and computer-aided cell tracking and provide independent confirmation, especially they are based on a radically different experimental principle.

| *Mutant* | *% Diameter relative to wild type* |
|---|:---:|
| wild type | 100 (internal reference) |
| $\Delta flaJ$ (B) | 17 |
| $\Delta flaJ$ (D) | 18 |
| $\Delta flaJ$ (E) | 19 |
| $\Delta flaJ$ (F) | 11 |
| $\Delta flaJ$ (G) | 13 |
| $\Delta flaJ$ (F)/$flaJ^+$ (2) | 93 |
| $\Delta flaJ$ (F)/$flaJ^+$ (3) | 93 |
| $\Delta flaJ$ (F)/$flaJ^+$ (4) | 96 |
| $\Delta flaD$ (1) | 24 |
| $\Delta flaD$ (2) | 25 |
| $\Delta flaD$ (3) | 26 |
| $\Delta flaD$ (4) | 26 |
| $\Delta flaD$ (5) | 24 |
| $\Delta flaD$ (1)/$flaD^+$ (1) | 88 |
| $\Delta flaD$ (1)/$flaD^+$ (2) | 92 |
| $\Delta flaCE$ (1) | 15 |
| $\Delta flaCE$ (2) | 13 |
| $\Delta flaCE$ (3) | 24 |
| $\Delta flaCE$ (1)/$flaCE^+$ (1) | 91 |
| $\Delta flaCE$ (1)/$flaCE^+$ (2) | 111 |
| $\Delta flaCE$ (1)/$flaCE^+$ (3) | 111 |
| $\Delta flaCE$ (1)/$flaCE^+$ (4) | 114 |

**Table 3.5: Quantitative estimation of motility by comparison of wild type and *fla* mutant swarm ring diameter**. Equal amounts of wild type cells and mutant cells ($6 - 8 \cdot 10^6$, depending on the experiment) were injected underneath the surface of semi-solid soft-agar peptone plates (0.25% agar (w/v)). The diameter was measured after incubation for 4 (in case of deletion mutants) or 3 days (in case of complemented mutants) at 37°C in the dark. Numbers/letters in parentheses denote the respective clone that was investigated.
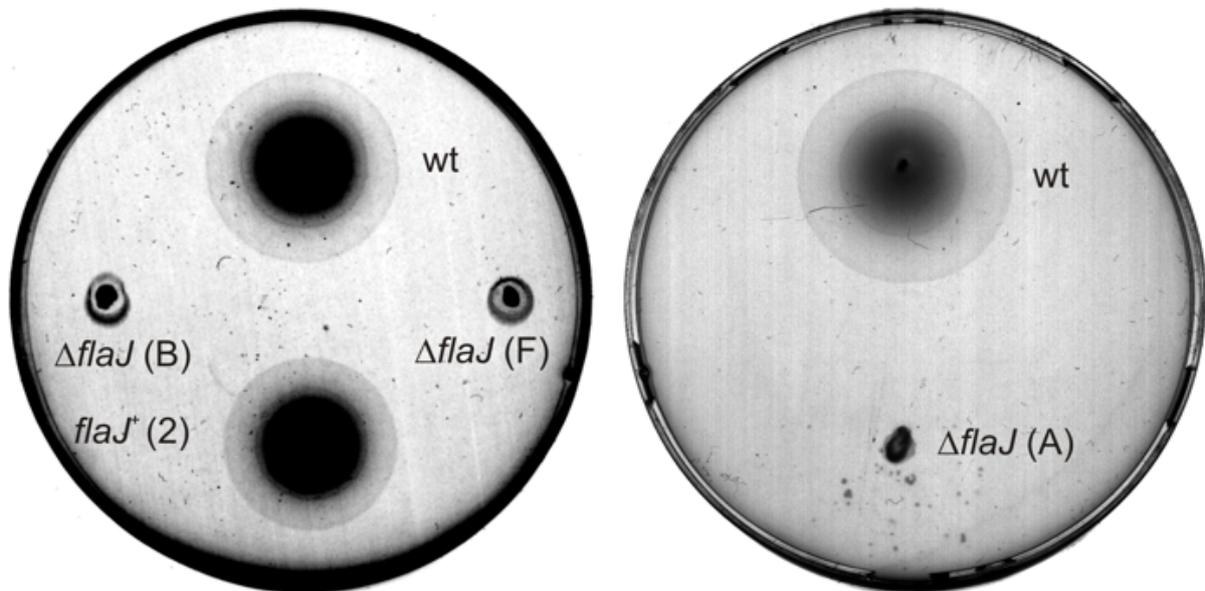
**Figure 3.8: Swarm plates with deletions and complementations of *flaJ*.**
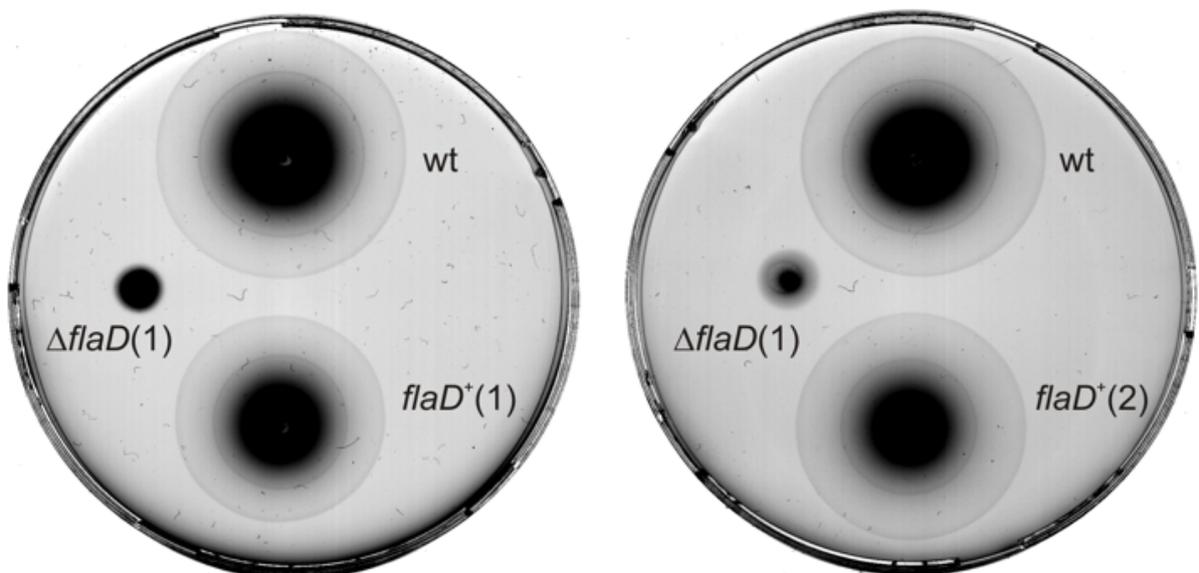


**Figure 3.9: Swarm plate assay with mutants deleted for *flaD*.**
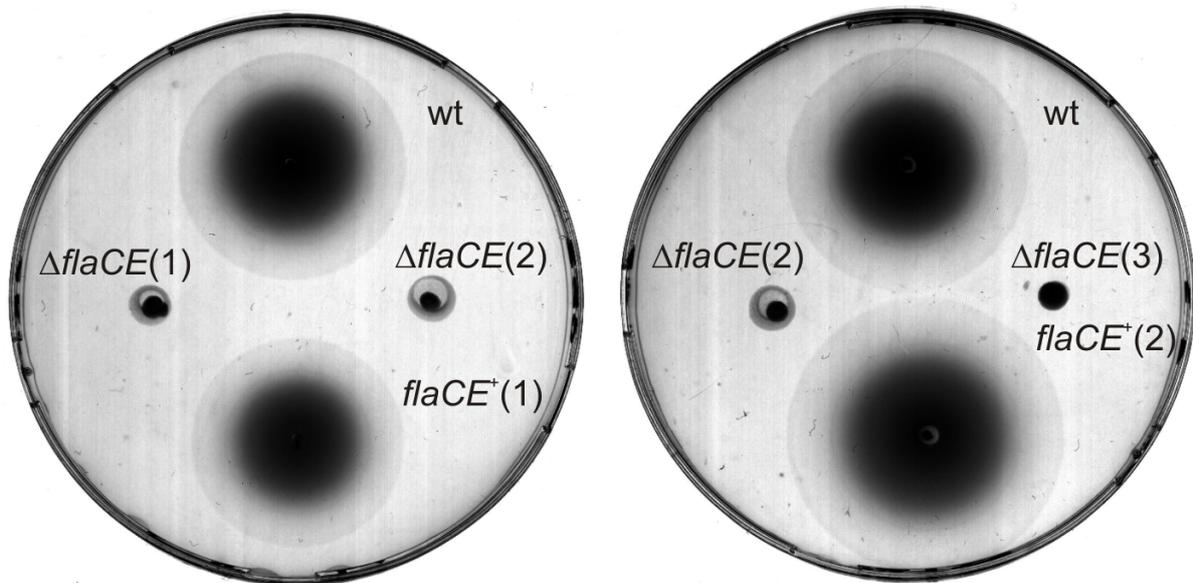
**Figure 3.10:** Swarm plates with deletions and complementations of *flaCE*.
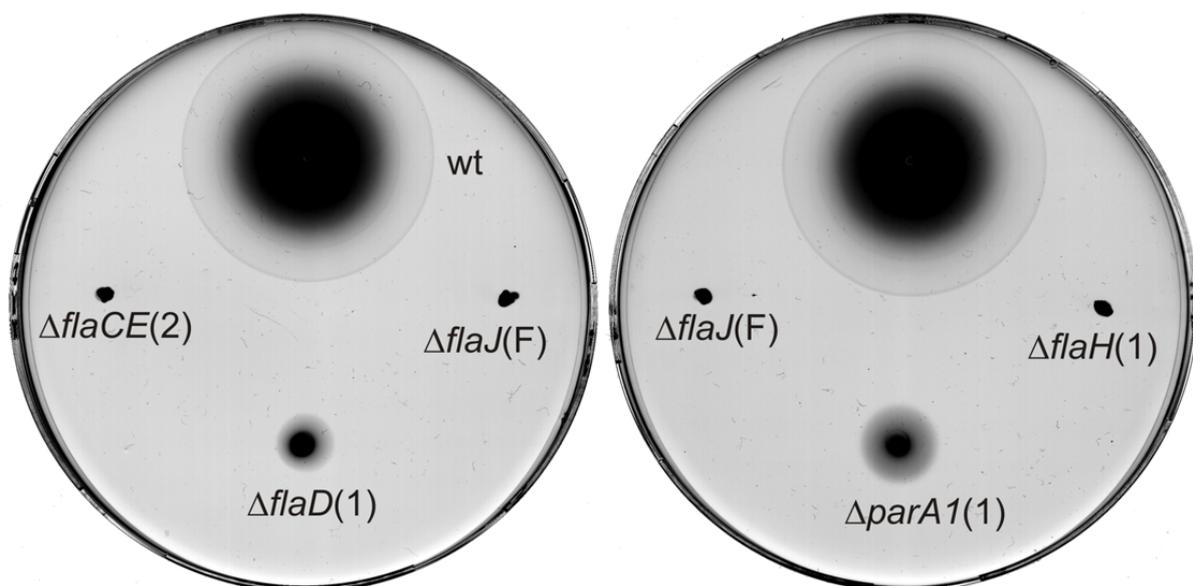


**Figure 3.11:** Swarm plates of *fla* knockout strains in comparison to wild type.

## Electron microscopy

Dark-field microscopic observation had shown that at least a part of the $\Delta flaD$ mutant cells possess flagella. In contrast, no flagella could be visualized in cultures of the $\Delta flaH$, $\Delta flaJ$ and $\Delta flaCE$ mutants. However, visibility of flagella in dark-field microscopy strongly depends on motility of the cells and efficient bundle formation. Thus, it could not be completely excluded that these mutants still possess flagella. To address this question, electron microscopy was performed.

Electron micrographs of the $\Delta flaH$ (done by Nadja Patenge and Harald Engelhardt) and $\Delta flaJ$ mutants showed that they were completely devoid of flagella. Complementation of both mutants was successful (Fig. 3.12 and Fig. 3.13). In contrast, in electron micrographs of the $\Delta flaD$ and $\Delta flaCE$ mutants frequently a single filament was observed (Fig. 3.14 and Fig. 3.15). Usually on *H. salinarum* cells 5-10 flagella are seen like e.g. in case of the $flaJ^+$ complemented mutant, which has the same genotype as the parental strain S9$_{mot}$. Thus both, the $\Delta flaD$ and $\Delta flaCE$ mutants were in principle able to synthesize and assemble filaments, but the number of filaments was drastically reduced. This observation could also be an artifact that occurred during sample preparation. One could e.g. imagine that compared to wild type in the mutants the flagella are only loosely anchored in the cell membrane and are therefore prone to shearing during sample preparation. However, in such a case most likely an increased formation of super-flagella would have been observed in dark-field microscopy (see section 3.2.5 and Fig. 3.6 (D) - (E)).



(A) $\Delta flaH$, magnification: 13.500 $\times$     (B) $flaH^+$, magnification: 36.000 $\times$
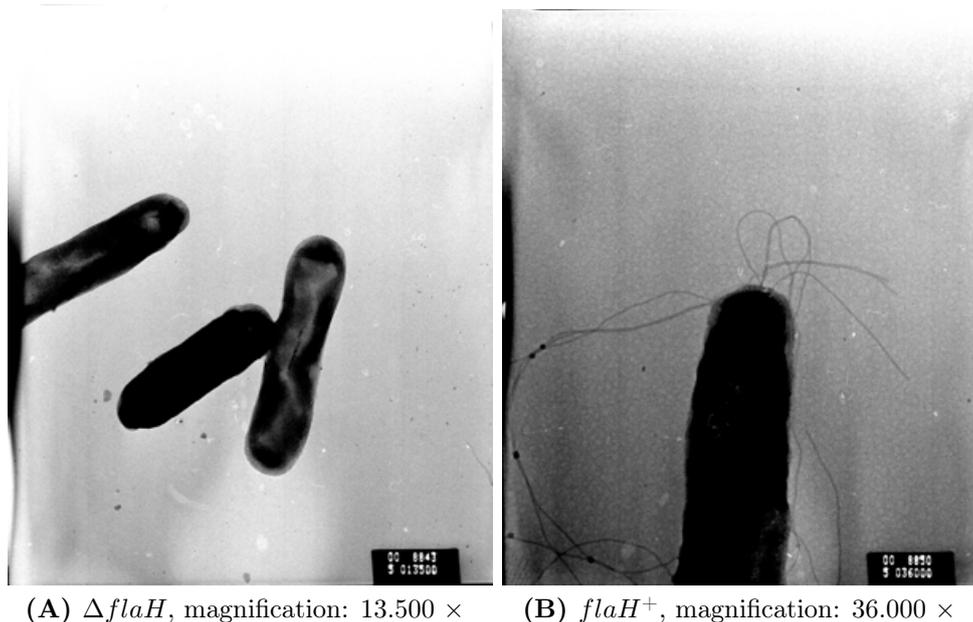
**Figure 3.12: Electron micrographs of uranyl acetate negatively stained *H. salinarum* S9$\Delta$*flaH* cells.**

**(A)** $\Delta flaJ$(F)



**(B)** $\Delta flaJ$(F)



**(C)** $flaJ^+$
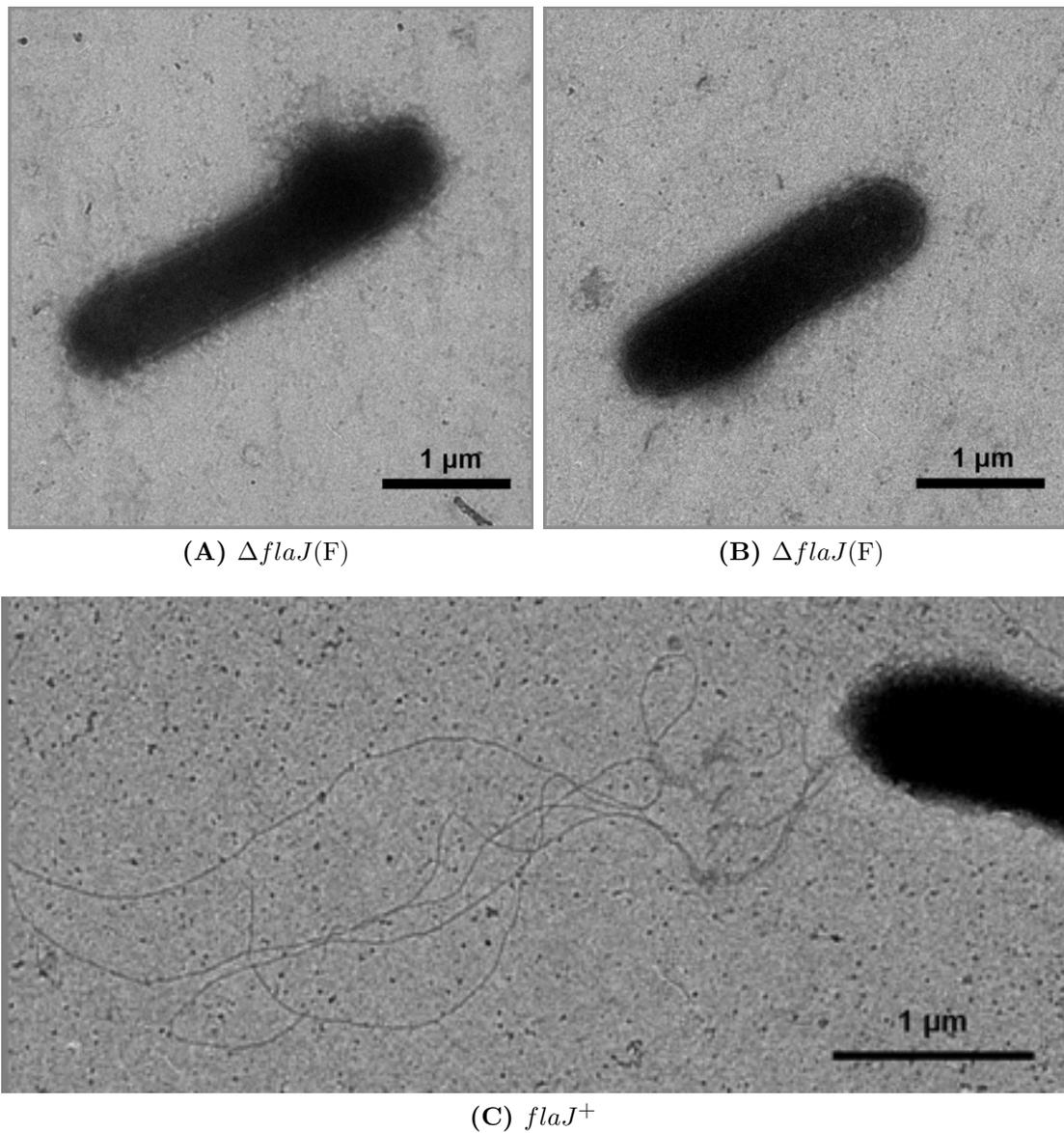
**Figure 3.13:** **Electron micrographs of uranyl acetate negatively stained *H. salinarum* S9$\Delta$*flaJ* and S9$\Delta$*flaJ*/*flaJ*$^+$ cells.**

**(A)** $\Delta flaD(1)$             **(B)** $\Delta flaD(1)$
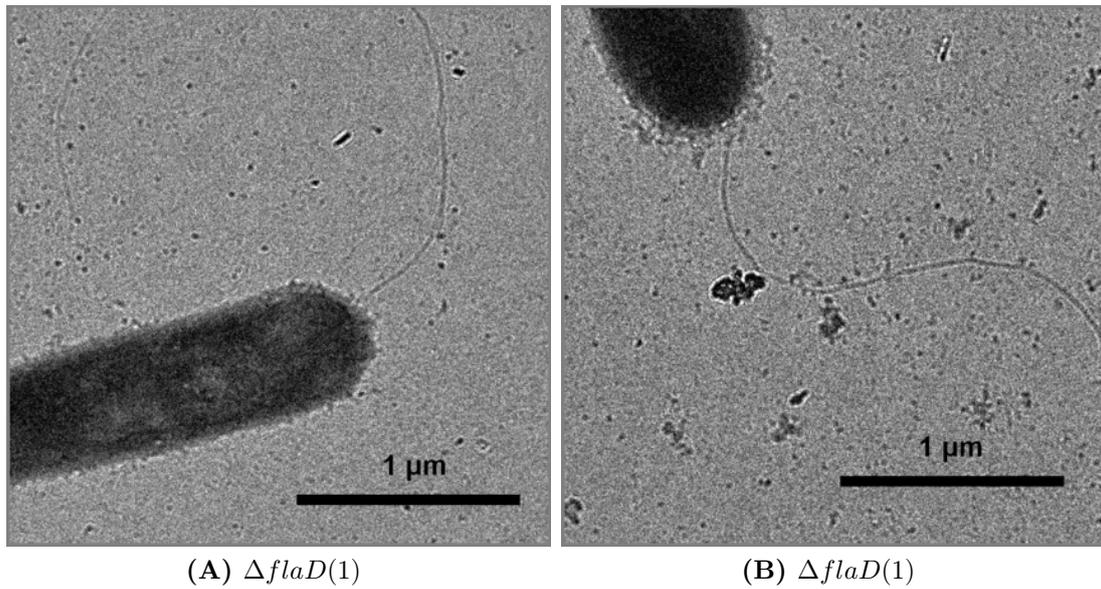
**Figure 3.14: Electron micrographs of uranyl acetate negatively stained *H. salinarum* S9Δ*flaD* cells.**



**(A)** $\Delta flaCE(1)$             **(B)** $\Delta flaCE(1)$
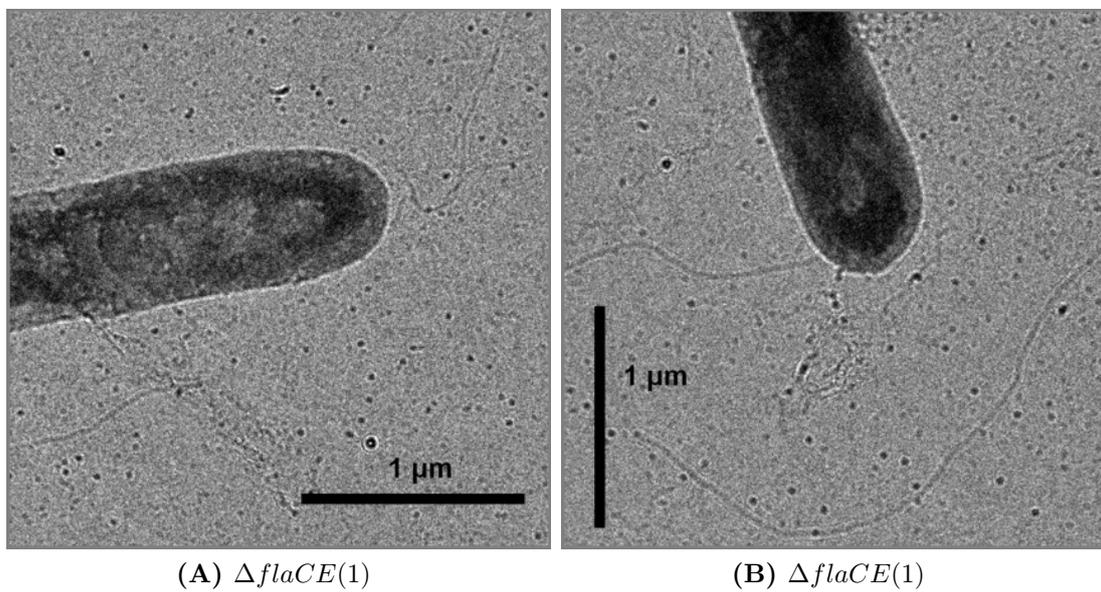
**Figure 3.15: Electron micrographs of uranyl acetate negatively stained *H. salinarum* S9Δ*flaCE* cells.**

## 3.2.6 Deletion of *flgXXX* has neither an effect on flagellar biosynthesis nor on motility

**FlgXXX is highly homologous to the *H. salinarum* flagellins**

Purified *H. salinarum* flagella preparations run on an SDS PAGE as multiple, somewhat diffuse bands with three centers of intensity that were referred to as Fla I, Fla II and Fla III (Alam and Oesterhelt, 1987). It turned out that actually, five different but highly homologous flagellin proteins are contained in these bands (Gerl and Sumper, 1988; Gerl et al., 1989). The corresponding flagellin genes are tandemly arranged in two operons that are separated by $\approx$ 40 kb (see Fig. 3.3). Analysis of the complete genome of the *H. salinarum* strain R1 revealed the presence of an orf that may encode and additional flagellin, FlgXXX that was not identified in the flagellin bands (OE2695F, `http://www.halolex.mpg.de`). This is reminiscent of the situation in *M voltae*. Four flagellin genes were cloned and sequenced, but two of them, the less abundant FlaA and FlaB3, were at first not detected in the filament (Kalmokoff and Jarrell, 1991; Kalmokoff et al., 1988). FlaA was later found to be indeed part of the filament and FlaB3 could be identified after enrichment of a curved region of the filament (Bardy et al., 2002). The authors concluded that FlgB3 could perform the role of a bacterial hook protein.

A sequence alignment of the confirmed *H. salinarum* flagellin proteins and the putative flagellin FlgXXX reveals that FlgXXX is highly homologous to the other flagellins (3.16. The sequence around the putative cleavage site of FlgXXX is in good agreement with the published consensus sequence (Thomas et al., 2001b):

- Invariant Gly residues at positions -1 (corresponding to the last amino acid of the signal peptide) and +3 (corresponding to the 3rd amino acid of the mature flagellin.)

- A positively charged amino acid at position -2.

- A charged amino acid at position -3.

Three deviations from the invariant residues of the published consensus sequence are found in the sequence of FlgXXX: (1) Ile instead of Val at position +8, (2) Met instead of Val at position +11 and (3) Thr instead of Val at position +23. The sequence alignment also reveals that the halobacterial flagellins can be grouped into two subclasses. One subclass contains FlgA2, FlgB1 and FlgB3 and the other contains FlgA1 and FlgB2.

The most prominent differences between the FlgA2/FlgB1/FlgB3 and FlgA1/FlgB2 subclasses are that:

- FlgA1/FlgB2 have some additional amino acids at alignment positions 73 - 80 which introduces gaps in the alignment

- FlgA1/FlgB2 have a Thr at alignment position 114 while FlgA2/FlgB1/FlgB3 have a Lys.

- FlgA2/FlgB1/FlgB3 have 2 - 3 additional residues at alignment positions 122 - 124.

**Figure 3.16: ClustalW sequence alignment of the known *H. salinarum* flagellins and the putative flagellin FlgXXX.** The alignment was generated with the BioEdit Sequence Alignment Editor software using the Blosum62 matrix (Hall, 1999). Shading of the amino acid residue was done with a threshold of 66%. The vertical arrow indicates the site at which cleavage is predicted to occur based on the demonstrated cleavage of leader peptides in methanogens (Thomas et al., 2001b). Numbers above the alignment denote "alignment positions" including gaps. Numbers to the right of the sequences denote the actual amino acid position in the sequence of each protein. Numbers above the alignment in bold denote amino acid positions relative to the cleavage site. Consensus: consensus sequence around the cleavage site as determined by Thomas et al. (2001b). The amino acids in the consensus sequence were found in at least 70% of all 41 archaeal flagellin sequences analyzed, except for position +2 (denoted by an asterisk). At five positions (-2, -3, +22, +28 and +30), an approximately equal frequency of 2 or 3 amino acids was found as shown. Invariant amino acids are shown in bold.

- FlgA1/FlgB2 have Asp-Ala at alignment positions 129 - 130 while FlgA2/FlgB1/FlgB3 have Leu-Gly.

- FlgA1/FlgB2 have an Asp residue at alignment position 158, but FlgA2/FlgB1/FlgB3 have a Tyr.

FlgXXX belongs to neither subclass. It is considerably longer and thereby introduces a large gap at alignment positions 167 - 178. The highest homology to the flagellins is found in the N- and the very C-terminal portion of the protein, in the middle portion of the protein, the homology is comparably low. The putative leader peptide of FlgXXX is shorter than that of the other flagellins, but its length is still in the range of leader peptides from other archaea. This is again reminiscent of *M. voltae* FlaB3, which is, compared to the other *M. voltae* flagellins significantly longer and has a shorter leader peptide. This raises the possibility that FlgXXX could have a similar role as FlaB3 in *M. voltae* and like FlaB3 has escaped previous detection. In order to find out if this is the case, $flgXXX$ was deleted in frame and the phenotype of the mutant was analyzed with respect to motility.

## Generation and genotypic analysis of the *flgXXX* deletion mutant

The $flgXXX$ knockout mutant was generated according to the general strategy outlined in section 3.1.1. The desired deletion was confirmed by Southern Blots using DIG-11-dUTP labeled probes that were produced by PCR and hybridize to the upstream region ("PRE" probe) and to a region within $flgXXX$ ("CORE" probe), respectively.

Fig. 3.17 (A) shows a schematic of view the $flgXXX$ locus based on the sequence of the *H. salinarum* strain R1 as retrieved from the HaloLex database (`http://www.halolex.mpg.de`) and Fig. 3.17 (B) shows the Southern Blot analysis that confirmed successful deletion of $flgXXX$ in some of the colonies that had undergone two successive crossover events.
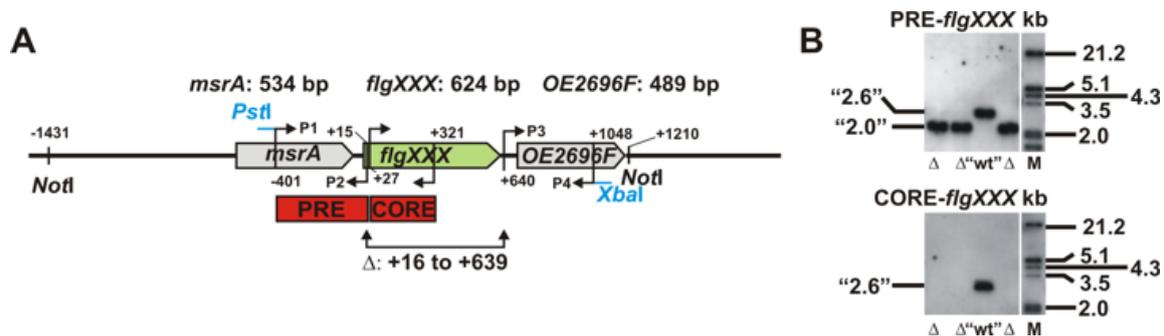


**Figure 3.17: Genotypic analysis of *flgXXX* knockout strain. (A) Schematic view of the *flgXXX* locus**. Numbers indicate nucleotide positions relative to the target gene (in light green color) with the following convention: +1 is the position of the first base of the target gene, -1 is the position of the preceding base. Primers are indicated as bent arrows. Primers P1 - P4 were used to create the US- and DS fragments of the target gene and are named according to Fig. 3.1. Red boxes indicate the hybridization positions of DIG-11-dUTP-labeled probes in front (PRE) or within (CORE) the target gene that were produced with the other primers. Numbers following "Δ:" denote start- and end position of the deleted region **(B) Southern Blot analysis with genomic DNA of the *flgXXX* gene knockout strain.** Genomic DNA was digested with *Not*I. M: marker lane; Δ: lane with hybridization signal that is in accordance with deletion of the target gene; "wt": lane with hybridization signal as obtained with wild type DNA. Lanes that are shown for blots obtained with the PRE- and CORE probes for the respective target gene correspond to each other. The white vertical line indicates that the lanes shown were not directly adjacent in the blot. The blots clearly show that flgXXX was deleted. However, the size of the bands for both wild type and deletion were approx. 500 bp larger than expected. This may be due the presence of the insertion element ISH2 (521 bp) in strain S9 either in the upstream or the downstream region of $flgXXX$.

## Swarm plate assay with *flgXXX* knockout mutants

In archaea, flagella are built from multiple flagellins. Mutants in which single or several flagellins are deleted usually are not completely devoid of flagella, but possess flagella with altered shape and/or reduced functionality, i.e. the mutants are less motile (Jarrell et al., 1996; Tarasov et al., 2000). In order to check if deletion of $flgXXX$ has an effect on flagella biogenesis or motility, swarm plate assays were performed with all single clones that were identified as $\Delta flgXXX$ mutants. Figure 3.18 on page 74 shows two representative swarm plates with $flgXXX$ knockout mutants in comparison with wild

type and Table 3.6 summarizes the results that were obtained for five different single $\Delta flgXXX$ mutant clones. While in the case of clones (2), (4) and (5) clearly a reduction of motility was observed, clone (3) showed motility close to wild type and motility of clone (1) was indistinguishable from wild type. As in the case of the complemented *fla* gene mutants, no further selection for motile single colonies was done after identification of the $\Delta flgXXX$ mutant clones. The apparently reduced motility of some of the mutant clones is still in the range of what can be expected if no motility selection is performed. From these data, it cannot be ultimately excluded that FlgXXX is a minor component flagellar filament. However, all flagellin mutants that were reported so far, had very severe defects in motility. Unfortunately, a phenotype for a *M. voltae flaB*3 was not reported. But, if *H. salinarum* FlgXXX like *M. voltae* FlaB3 would have a function of a hook protein that flexibly connects the membrane-anchored part of the filament with the external filament structure, a $\Delta flgXXX$ mutant would be expected to be devoid of flagella. This is definitely not the case. Deletion of $flgXXX$ has neither a significant effect on motility nor does it impair flagellar assembly.
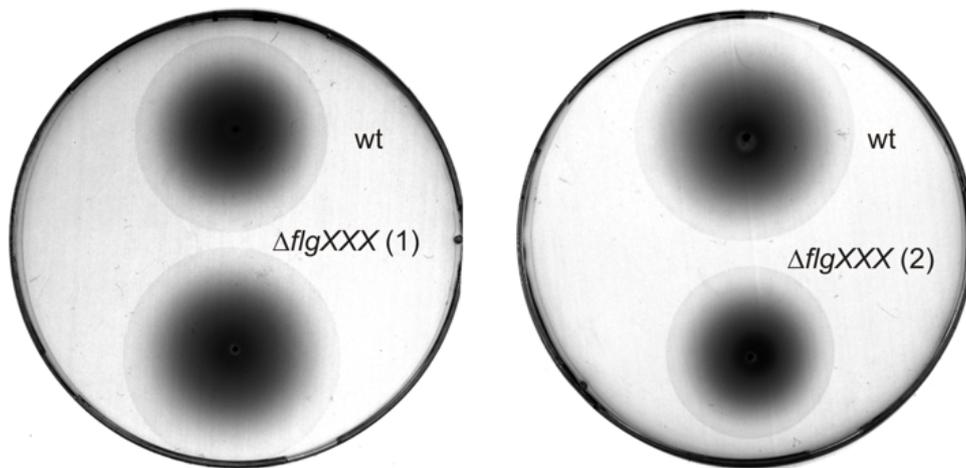


**Figure 3.18: Swarm plate assay with *flgXXX* knockout mutants**

| Mutant | % Diameter relative to wild type |
|---|---|
| wild type | 100 (internal standard) |
| $\Delta flgXXX$ (1) | 102 |
| $\Delta flgXXX$ (2) | 80 |
| $\Delta flgXXX$ (3) | 89 |
| $\Delta flgXXX$ (4) | 74 |
| $\Delta flgXXX$ (5) | 77 |

**Table 3.6: Quantitative estimation of motility by comparison of wild type and mutant *flgXXX* swarm ring diameter**. Equal amounts of wild type cells and mutant cells ($6 - 8 \cdot 10^6$, depending on the experiment) were injected underneath the surface of semi-solid soft-agar peptone plates (0.25% agar (w/v)). The diameter was measured after incubation for 6 days at 37°C in the dark. Numbers in parentheses denote the respective clone that was investigated.

### 3.2.7 Summary

Mutational studies of the archaeal *fla* gene cluster in both methanogens and the halophilic *H. salinarum* showed the importance of these genes for flagellar biosynthesis (Ng et al., 2006; Patenge et al., 2001). The strictly anaerobic nature of methanogens requires *in vivo* motility assays to be performed in an anaerobic chamber. This may explain why in most studies the analysis of motility was confined to electron microscopy, which merely allows a comparison of flagella number and shape in wild type and mutants. Sometimes the results were supported by swarm plate assays (Jarrell et al., 1996). However, to my knowledge, rotation of flagella of e.g. *M. voltae* was never reported. In contrast, a variety of methods that allow a closer inspection of motility of mutants can be routinely applied to living *H. salinarum* cells. These methods were extensively used to study the phenotypes of the in-frame deletion mutants $\Delta flaH$, $\Delta flaJ$, $\Delta flaD$ and $\Delta flaCE$. Phase contrast microscopy revealed that the $\Delta flaH$, $\Delta flaJ$ and $\Delta flaCE$ mutants were immotile. In contrast, residual motility was seen in cultures of the $\Delta flaD$ mutant. This subjective impression was confirmed by cell velocities that were determined with the help of computer-aided two-dimensional cell tracking and swarm plates. In cell tracking experiments, restoration of wild type motility seemed to be incomplete in the complemented strains. This could be explained by the "sticky" nature of these cells, and indeed, the swarm plate assay, which is not influenced by sticking cells, indicated restoration of wild type swimming. Dark-field microscopy allowed the observation of a small number of flagellated $\Delta flaD$ mutant cells. In case of the other mutants neither flagella attached to cells nor super-flagella were observed. Electron microscopy showed that the $\Delta flaH$ and $\Delta flaJ$ mutants were devoid of flagella and that the $\Delta flaD$ and $\Delta flaCE$ mutants possess a single filament. Based on the definition of motility/flagellar biosynthesis mutant classes for *H. salinarum* (see section 3.2.5), the $\Delta flaH$ and $\Delta flaJ$ mutants belong to Fla$^-$ mutant class and the $\Delta flaD$ and $\Delta flaCE$ mutants belong to the Mot$^-$ mutant class. Table 3.7 gives a short summary of the phenotypes of the *H. salinarum fla* gene knockout mutants that were investigated so far.

It is currently not clear if a single filament is sufficient to propel a *H. salinarum* cell. The phenotype of the $\Delta flaD$ mutant suggests that this is the case. However, it could well be that the small fraction of motile cells in the culture of the $\Delta flaD$ mutant possess more than one filament. Due to the low abundance of these cells, they might have escaped observation with electron microscopy. Thus, it is very likely, but not ultimately clear that the single filament seen on the $\Delta flaCE$ mutant is paralyzed. Alternatively, rotation of the single filament might simple be inefficient to propel the cells.

For completeness, it should be mentioned that mutants with single deletions of $flaF$ and $flaG$ were analyzed by a colleague. These mutants had a reduced number of shortened filaments and were immotile. Based on this phenotype, they belong to the Mot$^-$ mutant class. However, it turned out that in these two mutants in addition to $flaF$ or $flaG$ large gene regions including the flagellin B operon (*flgB1-flgB3*) were deleted. It seems that the use of the $\beta$-gyrase inhibitor novobiocin as antibiotic for selection caused these events specifically in strain R1M1. Whatever the true phenotype of *H. salinarum* $flaF$ and $flaG$ knockout mutants may be, the loss of additional genes should rather aggravate than rescue the defects caused by the loss of $flaF$ or $flaG$. It is therefore unlikely

| *Mutant* | *Phenotype* | *Mutant Class* |
|---|---|---|
| $\Delta flaD$ | reduced number of filaments, reduced motility | Mot$^-$ |
| $\Delta flaCE$ | reduced number of filaments, immotile | |
| $\Delta flaF$ | (reduced number of shortened | (Mot$^-$)$^\dagger$ |
| $\Delta flaG$ | filaments, immotile)$^\dagger$ | |
| $\Delta flaH$ | | |
| $\Delta flaI$ | no flagella | Fla$^-$ |
| $\Delta flaJ$ | | |
| $\Delta parA1$ | reduced swarming | possibly involved in chemotaxis |
| $\Delta flgXXX$ | no flagellar biogenesis or motility related phenotype observed | not applicable |

**Table 3.7: Phenotypes and classification of *fla* knockout mutants.**$^\dagger$ The use of the $\beta$-gyrase-inhibitor novobiocin as antibiotic for selection specifically in strain R1M1 resulted in the loss of large gene regions including the flagellin B operon (*flgB1-flgB3*) in addition to the desired deletions of *flaF* and *flaG*. Therefore the phenotype of these mutants has to be taken with care. *flgXXX* is not part of the *fla* gene cluster, but codes for a protein with high homology to the known flagellin genes of *H. salinarum*.

that *flaF* or *flaG* knockout mutants belong to the Fla$^-$ mutant class. By contrast, data from the *Sulfolobus solfataricus* strain P2 suggest that a *flaG* knockout mutant is Fla$^-$. This strain, in which *flaG* is disrupted by a transposon, is non-flagellated (Szabó et al., 2007), although the transposon does not interfere with transcription of the downstream *fla* genes (Albers and Driessen, 2005).

### 3.2.8 Conclusions and outlook

This is the first time that phenotypes for halobacterial *flaD* and a *flaCE* mutants were reported. It has to be noted, that FlaD and FlaCE belong to the proteins encoded in the *fla* gene cluster that are less conserved than FlaH, FlaI and FlaJ. FlaD and FlaE/FlaCE in *M. voltae* and *H. salinarum* have different sizes and *H. salinarum* FlaCE is really a FlaC/FlaE or FlaC/FlaD fusion protein (see Fig. 3.3 and Table 3.2). This means that the phenotypes of the *H. salinarum* $\Delta flaCE$ and probably also of the $\Delta flaD$ mutant can be expected to be different from those of the corresponding *M. voltae* *flaD* and *flaE* mutants.

Both FlaD and FlaCE possess an archaeal FlaDE motif and both the $\Delta flaD$ and the $\Delta flaCE$ mutant had only one filament. Thus, it can be speculated that the reduced number of flagella is caused by loss of the FlaDE domain. On the other hand, in each of the two mutants one protein with FlaDE domain is still produced, which may alleviate the effect that would be seen if no protein with FlaDE motif were present at all. In this case, concomitant deletion of both *flaD* and *flaCE* should result in non-flagellated cells. Proteins with similar domains often interact via these domains and this may apply to FlaD and FlaCE. This notion is supported by the fact, that in some archaea a single protein with fused archaeal FlaDE- and FlaC domains is found (Ng et al., 2006).

In principle, a reduced filament number could be due to inefficient transcription of

the flagellin genes. However, a role of FlaD and FlaCE or a FlaD:FlaCE complex in transcription enhancement of the flagellins is unlikely since FlaD and FlaCE are neither homologous to the archaeal TATA box-binding protein (TBP) nor to the transcription factors B (TFB) or E (TFE) or any of the known positive regulators of transcription. An auxiliary function of the FlaD and FlaCE in flagellar assembly or perhaps anchoring of the filaments is more likely. In case of the $\Delta flaCE$ mutant it seems that in addition to a reduction of filament number, which is also seen in the $\Delta flaD$ mutant, the remaining filament is paralyzed. This additional phenotype may be due to lack of the archaeal FlaC domain. Thus, this protein domain may be somehow involved in rotation or the transfer of rotational motion to the filaments, which raises the possibility that membrane anchored FlaD/FlaCE complexes may form a link that connects the rotatory unit and the filaments.

FlaH, FlaI and FlaJ are to my best knowledge found in all genomes of flagellated archaea (see section 3.2.3), which means that phenotypes that occur due to mutations in any of the corresponding genes can be expected to be applicable to all other flagellated archaea. In *M. voltae* a $flaH$ insertional mutant was shown to be devoid of flagella, but polar effects on transcription of the downstream $flaI$ and $flaJ$ genes were anticipated (Thomas et al., 2001c). Indeed, deletion of $flaI$ was shown to be sufficient to produce such a phenotype (Patenge et al., 2001). Thus, the phenotype of the *H. salinarum* $\Delta flaH$ mutant generated by N. Patenge shows for the first time, that a single deletion of $flaH$ results in non-flagellated cells. During the course of this study, it was published that in *M. voltae* a non-polar $flaJ$ insertion mutant has no flagella (Thomas et al., 2002). This is in agreement with the phenotype of the *H. salinarum* $\Delta flaJ$ mutant reported here. In contrast to FlaH, both FlaI and FlaJ have homologs in the type II secretory pathway and the type IV pili system which is best compatible with a role in flagellin secretion and/or flagellin assembly into the filament. FlaJ is predicted to be a multi-TM protein and as a putative NTPase FlaI could provide energy for transport/assembly. The phenotype of the $\Delta flaH$ and the putative function of FlaH as NTPase is consistent with a role as additional protein that provides energy for another step in transport/assembly. An alternative explanation is that FlaH is a motor component that drives the motor. This implies that in contrast to previous assumption, ATP instead of protons is the driving force of the archaeal flagellar motor. The absence of flagella can be easily explained assuming that FlaH is at the same time an important structural component of the motor complex. Two types of experiments that allow to test these hypotheses are currently under way. First, a point mutation in FlaH that abolishes its ATPase function but otherwise leaves the overall structure of the protein unaltered should result in either of two phenotypes: either the point mutant is non-flagellate like the knockout mutant or, in contrast to the knockout mutant, it has flagella but is immotile. The latter phenotype would clearly indicate a role of FlaH in energization of the flagellar motor. Second, photokinesis measurements with cells in which the ATP synthase is inhibited will possibly allow to exclude either protons or ATP as the driving force of the flagellar motor. While in the first case inactivation of the ATPase is not expected to influence swimming velocity, in the latter case cells are expected to lose their motility as soon as the ATP level falls below a certain threshold value.

## 3.3 Studies on phototaxis of *H. salinarum* wild type cells

### 3.3.1 The response of *H. salinarum* cells to blue light pulses obeys the Bunsen Roscoe law of reciprocity

**Application of Poisson statistics to the photophobic response of *H. salinarum***

Marwan and Oesterhelt (1987) found that within a certain range of relatively high light intensities the response time of *H. salinarum* cells to single or double blue light pulses can be calculated by a "flash equation". The response time of the cells to blue light pulses is inversely proportional to the light intensity of the blue light pulses. At saturating light intensity a minimal response time $t_{min}$ is reached. Upon lowering light intensity a maximal response time $t_{max}$ is reached that is still approx. 5 to 10-fold below average spontaneous swimming intervals. When the light intensity is further lowered another phenomenon is observed. Light stimuli of the same intensity sometimes elicit a response and sometimes they do not. In this range of light intensities the probability of a cell to respond increases with increasing light intensity. The reason is that the intensities are so low that absorption of a photon by a receptor molecule becomes a stochastic process. Marwan et al. (1988) applied Poisson statistics to dose response curves of *H. salinarum* cells. Equation 3.2 gives the probability $\widehat{P}_n$ that $n$ or less photons elicit a response. $\alpha$ is the average number of photons contributing to a response and is proportional to the photon exposure $F$, the number of photoreceptors $R$, the absorption cross-section $\sigma$, the quantum yield $\phi$ and a constant $c$ that contains the efficiency of the transduction chain and other processes that influence the efficiency of the whole process (Marwan et al., 1988).

$$\widehat{P}_n(\alpha) = 1 - \sum_{k=0}^{n-1} \frac{\alpha^k \cdot e^{-\alpha}}{k!} \tag{3.2}$$

A plot of $\widehat{P}_n$ *versus* the common logarithm of $\alpha$ or the photon exposure $F$ will be termed "Poisson curve" in this study. The minimal number of photons $n$ required to elicit a response determines the shape or steepness of the curve. The steepness of the curves increases with increasing $n$. Experimental dose-response curves can be fit by theoretical Poisson curves by shifting the theoretical curves along the abscissa. By comparing the shape of theoretical Poisson curves for various numbers of $n$ with the shape of experimental dose-response curves, the best value for the minimal photon requirement $n$ can be deduced. In measurements of dose-response curves for the SRII/HtrII mediated response of *H. salinarum* to blue light flashes, Marwan et al. (1988) found that found that the best fit was obtained with $n = 1$. Their interpretation was that in principle one photon is sufficient to elicit a response. However, from the experimentally applied photon exposure at which according to Poisson statistics on average one photon elicits a response ($\log \alpha = 0$, $\alpha = 1$) the number of excited receptors $R$ was calculated to be 13. The authors concluded that "out of 10 to 20 photoreceptor molecules only one causes the

motor to stop. All other signal chains started by excited photoreceptors vanish without success".

### The Bunsen-Roscoe law of reciprocity and its relevance in biological systems

In 1859 Robert Bunsen and Henry Roscoe discovered that the degree of blackening of photographic films is a product of light intensity and exposure time i.e. the photon exposure, a relationship that is now known as the Bunsen-Roscoe law of reciprocity. Many plant seedlings show a phenomenon called phototropism, i.e. certain parts of the seedling bend towards or away from light. The strength of the response is a product of intensity and exposure time. The Bunsen-Roscoe law also seems to apply to the human eye (Brindley, 1952).

### Blue light dose-response curves of *H. salinarum* cells measured with two different exposure times

In order to find out if the photophobic response of *H. salinarum* towards blue light pulses satisfies the Bunsen-Roscoe law, two dose-response curves were measured in which the exposure times of 8 ms and 503 ms, respectively, were kept constant and the light intensities were varied. The photon exposure $F$ is the product of exposure time and light intensity. Therefore, if the Bunsen-Roscoe law applies to the SRII mediated response to blue light pulses, the dose-responses curves obtained with the 8 and 503 ms pulses should be identical when the fraction of reversing cells is plotted *versus* $\log F$.

The response of the cells was measured with a computerized cell tracking system as described in section 4.5.2. In brief, the percentage of cells that reversed within 4 s after application of blue light pulse was measured. In the measurements of Marwan et al. (1988) single cells were stimulated 2 s after a spontaneous reversal. Therefore, the flagellar motors of these cells were all in comparable states. In contrast, here a population of cells was measured. As a consequence, the cells were unsynchronized with respect to the state of their flagellar motors. It is clear that a certain percentage of the cells has just switched and is in the non-responsive Refractory phase (for an explanation see section 2.3.8). The maximal percentage of reversing cells $R_{max}$ in the measurements was 86%. On the other hand it is clear that a certain percentage of cells switch spontaneously within the 4 s observation interval. The percentage of spontaneously reversing cells $R_{min}$ in the measurements was 8%. The normalized fraction of responding cells $R'$ for each light intensity was calculated from the measured percentage of reversals $R_{app}$ as follows:

$$R' = \frac{R_{app} - R_{min}}{R_{max} - R_{min}} \tag{3.3}$$

The photon exposures that were required to elicit responses were in a range comparable to the experiments of Marwan et al. (1988) (approx. $4 \times 10^{-6}$ - $32 \times 10^{-6}$ mol/m$^2$ in this study compared to approx. $1 \times 10^{-6}$ - $32 \times 10^{-6}$ mol/m$^2$).

In Figure 3.19 on page 81 the normalized fraction of reversing cells $R'$ is plotted *versus* the log of the light intensity $I$. As expected for the measurements with 8 ms exposure

time, higher light intensities were required to elicit responses equivalent to those achieved with the 503 ms pulses. To check the validity of the Bunsen-Roscoe law, in Figure 3.20 on page 82, $R'$ is plotted *versus* $\log F$. The two curves that were obtained with 8 ms and 503 ms align very well. The main difference between the curves is their different shape, i.e. the optimal value for $n$ is 4.8 for the 8 ms pulses, but 3.7 for the 503 ms pulses (Fig. 3.19 (B) and (C)). However, the error bars indicate that this difference is not significant. Thus, it seems that the Bunsen-Roscoe law of reciprocity applies for exposure times ranging at least from 8 ms to 503 ms.

This means that in the investigated range of exposure times from 8 ms to 503 ms and the given light intensities *H. salinarum* linearly integrates over all absorbed photons such that the response only depends on the number of absorbed photons. In other words, within 503 ms the last photons that are absorbed have the same efficiency as photons that are absorbed at the onset of the stimulus. Obviously, processes that could render the input-output behavior of the SRII/HtrII signaling pathway non-linear in a time-dependent manner such as changes in cooperativity between receptors or changed sensitivity due to the onset of adaptation do not play a significant role.

Another issue is that both curves had an optimal value for $n$ clearly above 1. This was observed in several independent experiments. The reason is not clear at the moment and efforts to model Poisson curves with values for $n > 1$ did not succeed so far (Nutsch, 2006).
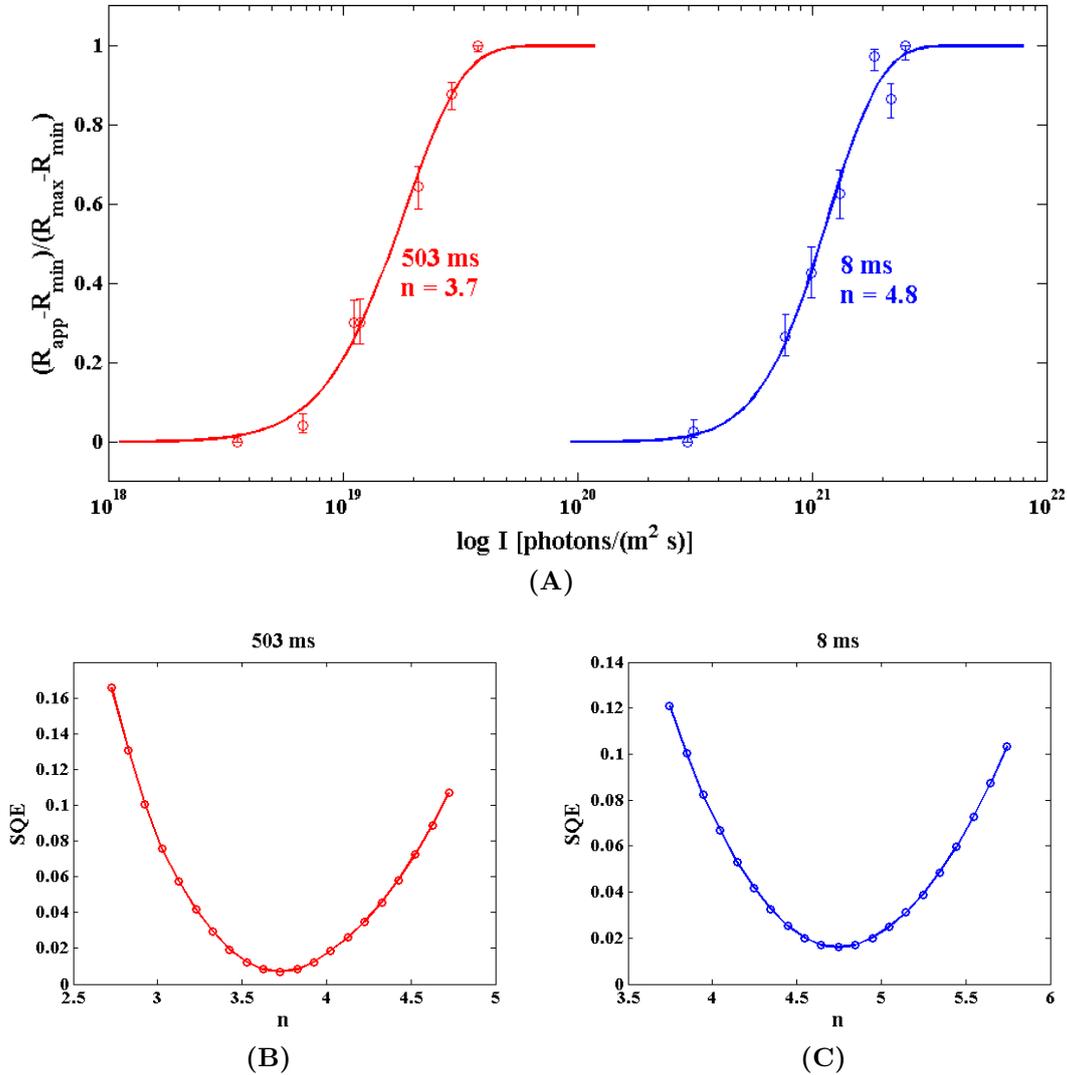
**Figure 3.19: (A) Dose-response curves of *H. salinarum* obtained with blue light pulses of 8 and 503 ms duration.** The fraction of responding cells is plotted *versus* the common log of the light intensity $I$. Cells of *H. salinarum* strain D1 ($BR^-$, $HR^-$, $SRI^-$, $SRII^+$, $HtrII^+$) (Scharf et al., 1992) were stimulated with either 8 ms or 503 ms blue light pulses ($480 \pm 15$ nm) of varying intensities and the fraction of cells that reversed within an interval of 4 s was measured with a computerized cell tracking system (Marwan and Oesterhelt, 1990). $R_{app}$: absolute percentage of reversing cells; $R_{min}$: percentage of spontaneously reversing cells; $R_{max}$: maximal percentage of reversing cells. Open circles: measured data points. Solid lines: Poisson curves ($\widehat{P}_n$ plotted versus $\log I$) that yielded the best fit to the measured data points with the corresponding value of $n$ given in the plot. The fits were performed with a least square method. Error bars were calculated according to Hald (1952) with a confidence interval of 95% for the upper and lower limits (see eqn. 4.2, p. 141). **(B) - (C) Plot of the least square deviations (SQE) versus various values of $n$ as obtained by fitting the Poisson curves in (A) to the measured data points.**
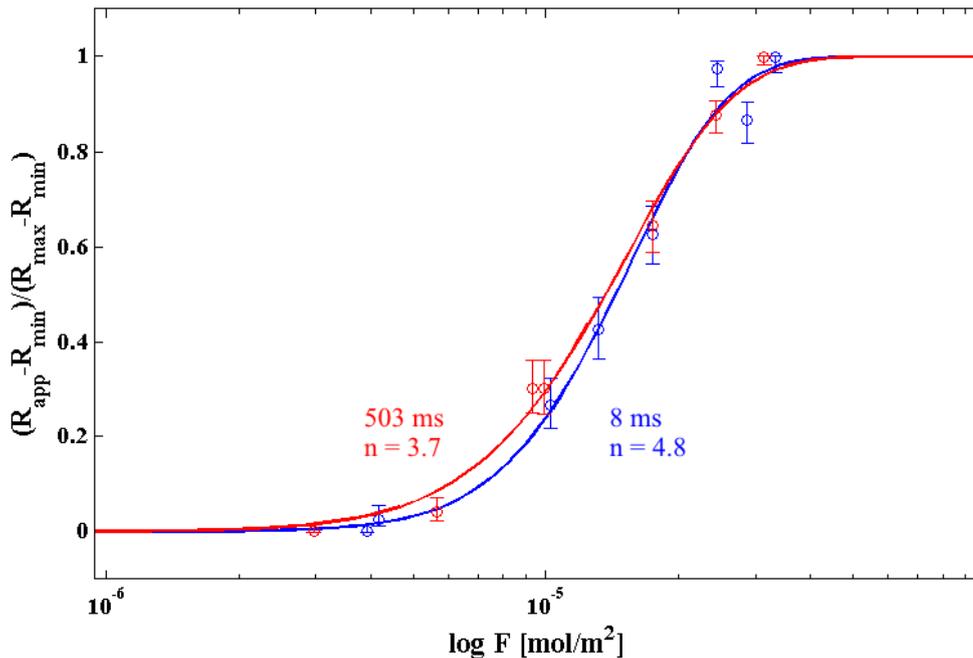
**Figure 3.20: Validity of the Bunsen-Roscoe law for the response of *H. salinarum* cells to blue light pulses.** Shown are dose-response curves of halobacterial cells in which the fraction of responding cells is plotted versus the common log of the photon exposure $F$. Solid lines: Poisson curves ($\widehat{P}_n$ plotted versus $\log F$) that yielded the best fit to the measured data points with the corresponding value of $n$ given in the plot.

## 3.4 Behavioral studies of *H. salinarum* cells deleted for chemotaxis genes

### 3.4.1 The *H. salinarum che* operon

*H. salinarum* has many signal transduction components with homology to components of the *E. coli* chemotaxis system. Due to the high conservation of the signaling domain, 18 putative halobacterial transducer proteins (Htrs) with homology to *E. coli* receptors (MCPs) were identified in the genome of *H. salinarum* strain R1 (for details about MCPs and Htrs see section 2.3.9). Even before the genome sequence of *H. salinarum* was completed, a so-called *che* operon encoding homologs to the *E. coli* chemotaxis proteins was identified and experimental data showed that the *H. salinarum* CheA, CheY, CheB homologs and an orf coding for a previously unknown protein called CheJ[2] are involved in chemo- and phototaxis of *H. salinarum* (see section 2.3.6 and references therein).

Analysis of the complete genome revealed that the *che* operon of *H. salinarum* is in close proximity to the *fla* gene cluster and the *flgB* operon (Fig. 3.21). This region is also referred to as motility and signal transduction (MO-ST) cluster (Falb et al., 2005) and harbors most of the known and putative chemotaxis genes of *H. salinarum*.

---

[2]CheJ was later renamed in CheC1 due to its homology to *B. subtilis* CheC
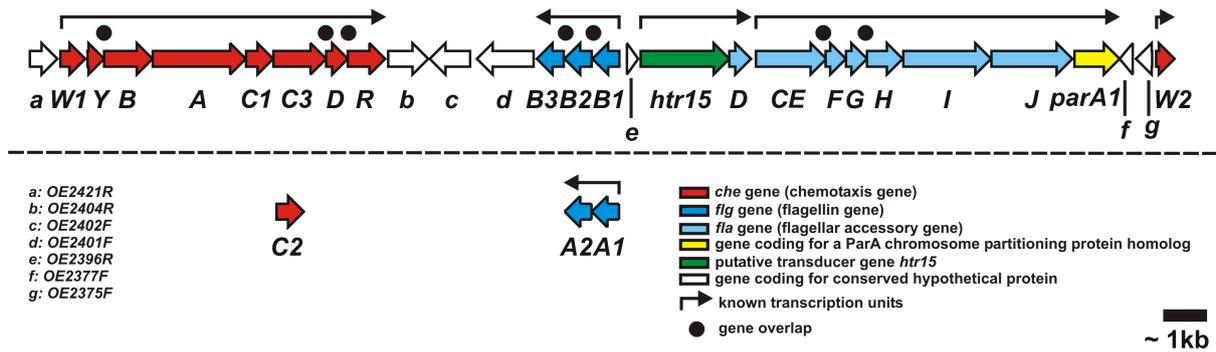
**Figure 3.21: Schematic view of the *H. salinarum* motility and signal transduction (MO-ST) gene cluster.** Note that the *cheJ* gene published by Rudolph and Oesterhelt (1996) was renamed to *cheC1* and *flaK* was renamed to *parA1*. Additional genes which are found outside the MO-ST gene cluster are indicated below the dashed line.

The *che* operon itself encodes the proteins CheW1, CheY, CheB, CheA, CheC1, CheC3, CheB and CheR which are homologous to their bacterial namesakes. RT-PCR analysis revealed that *cheW1 - cheR* are transcribed into a polycistronic mRNA. An orf coding for a second CheW homolog, CheW2, is located upstream of the *fla* gene cluster and is transcribed into a monocistronic mRNA (Aregger, 2003). Finally, an orf, coding for a third CheC homolog, CheC2, was identified outside the MO-ST gene cluster. Altogether, the genome data indicate that *H. salinarum* like *B. subtilis* and many other archaea has an extended set of chemotaxis proteins compared to *E. coli*. Except for the missing CheZ homolog, *H. salinarum* has a full complement of homologs to the *E. coli* Che proteins, but in addition has two CheW homologs, three CheC and one CheD homolog. On the other hand, *B. subtilis* has only one CheW and one CheC protein, but has in addition has the CheW/CheY two-domain protein CheV. Thus, the network structure of the *H. salinarum* chemotaxis system is different from that of both *E. coli* and *B. subtilis* which means that data from *B. subtilis* can merely serve as a clue for the function of the *H. salinarum* proteins.

## 3.4.2 Objectives

Rudolph et al. (1995) showed that similar to CheA and CheY in *E. coli* chemotaxis, phosphorylation of the *H. salinarum* CheA and CheY homologs plays a central role in photo- and chemotaxis of this archaeon (Rudolph et al., 1995). Thereafter, mutants with deletions of several of the halobacterial chemotaxis genes were generated and characterized. Table 3.8 gives a summary of the chemotaxis gene knockout mutants that were available in our lab at the beginning of this study.

In order to elucidate the function of the other previously ignored chemotaxis proteins, single in frame deletions of *cheR*, *cheD* and *cheC3* were generated in strain S9$_{mot}$ and the mutants were analyzed with respect to their swimming behavior and their capability to perform photo- and chemotaxis. As shown in Table 3.8, *cheB* and *cheC1* knockout mutants generated from strain Flx15ΔΔ were previously analyzed (Rudolph and Oesterhelt, 1996). Nevertheless, in this study, *cheB* and *cheC1* single deletion mutants from

| Strain | Description of the genotype | Parental strain | Reference |
|---|---|---|---|
| E4 | central part of *cheA* replaced by a mevinolin resistance cassette | S9 | Rudolph and Oesterhelt (1995) |
| Flx15$\Delta\Delta$ ($\Delta\Delta$) | largest portion of *che* operon deleted, $nov^R$ (see Fig. 3.22 (A)) | Flx15 | Rudolph and Oesterhelt (1996) |
| Flx15$\Delta cheA$ ($\Delta$A) | $cheA^-$, $nov^R$, $mev^R$ [†] | Flx15$\Delta\Delta$ | Rudolph and Oesterhelt (1996) |
| Flx15$\Delta cheY$ ($\Delta$Y) | $cheY^-$, $nov^R$, $mev^R$ [†] | Flx15$\Delta\Delta$ | Rudolph and Oesterhelt (1996) |
| Flx15$\Delta cheB$ ($\Delta$B) | $cheB^-$, $nov^R$, $mev^R$ (see Fig. 3.22 (B)) [†] | Flx15$\Delta\Delta$ | Rudolph and Oesterhelt (1996) |
| Flx15$\Delta cheJ$ ($\Delta$J) | $cheC1^-$, $nov^R$, $mev^R$ [†] | Flx15$\Delta\Delta$ | Rudolph and Oesterhelt (1996) |
| Flx15$\Omega$ ($\Omega$) | deleted portion of *che* operon reintroduced, $nov^R$, $mev^R$ [†] | Flx15$\Delta\Delta$ | Rudolph and Oesterhelt (1996) |
| H. s.-$\Delta cheW1$ | $cheW1^-$ [‡] | S9 | Aregger (2003) |
| H. s.-$\Delta cheW2$ | $cheW2^-$ [‡] | S9 | Aregger (2003) |
| H. s.-$\Delta\Delta cheW1/cheW2$ | $cheW1^-$, $cheW2^-$ [‡] | S9 | Aregger (2003) |
| H. s.-$\Omega cheW2$ | $cheW2^-/cheW2^+$ [‡] | H. s.-$\Delta cheW2$ | Aregger (2003) |

**Table 3.8: Chemotaxis gene knockout mutants that were available in our lab at the beginning of this study**. The *che* locus of Flx15$\Delta\Delta$ is depicted schematically in Fig. 3.22; [†]: these deletions were generated by a single crossover with plasmids that contained basically the portion of the *che* operon that was deleted in Flx15$\Delta\Delta$ with omission of the gene to be deleted. Such a plasmid and the resulting genotype of the single crossover between the *che* operon contained in Flx15$\Delta\Delta$ and the plasmid is exemplified in Fig. 3.22 for the Flx15$\Delta cheB$ mutant; [‡]: these deletion mutants/complemented mutants were generated employing a strategy comparable to that employed in this study.

strain $S9_{mot}$ were generated and investigated, because it is reasonable to analyze and compare mutants that have an identical genetic background and - more importantly - my analysis of the Flx15 mutants revealed that the genotype of these mutants is ambiguous (see subsequent section 3.4.3).

In the Flx15$\Delta cheY$ (Rudolph and Oesterhelt, 1996) deletion mutant two phenomena are observed. The mutant shows neither spontaneous nor induced reversals and the CW/CCW rotational bias of the flagellar motor is 99% as compared to 50% in case of wild type cells. This result was recently confirmed for a $S9_{mot}$ *cheY* deletion mutant (Weidinger, 2007). The non-switching phenotype is in agreement with the notion that the concentration of phosphorylated CheY (CheY-P) is the output signal of the chemotaxis/phototaxis signaling cascade and serves as a switching signal at the flagellar motor of *H. salinarum* and can be readily explained with an existing quantitative model for *H. salinarum* motor switching and its sensory control (Nutsch et al., 2005). The CW bias of the mutant, however, cannot be explained without further assumptions. This prompted me to search for the possibility to generate a hyperactive CheY *in vivo* which should produce a quasi opposite situation compared to a knockout of *cheY* and should therefore provide an interesting insight into the operating mode of the *H. salinarum* flagellar motor. The *E. coli* CheY$^{D13K, Y106W}$ (CheY**) protein is such a hyperactive mutant *in vitro* and *in vivo*. In *E. coli*, CheY-P causes tumbling of the cells by inducing CW rotation of the flagellar motor. CheY** causes a strong tumbling phenotype of the cells (Scharf et al., 1998). It can be phosphorylated to some extent, but is active without

phosphorylation (Turner et al., 1999). The binding affinity of CheY$^{**}$ to its target, the N-terminal 16 amino acid long peptide of the flagellar switch protein FliM (FliM$_{16}$), is about 10-fold enhanced compared to CheY (Schuster et al., 2000). In a crystal structure of CheY$^{**}$ in presence of FliM$_{16}$ the asymmetric unit contained four CheY$^{**}$- and four FliM$_{16}$ molecules (Dyer et al., 2004). Two of the CheY$^{**}$ molecules had FliM$_{16}$ bound while the other two were unbound. The FliM$_{16}$-bound CheY$^{**}$ molecules adopted a conformation similar to CheY-BF$_3^-$, which is a non-dephosphorylatable, active CheY-P analog, and had FliM$_{16}$ bound in an almost identical manner (Lee et al., 2001). The unbound CheY$^{**}$ had a conformation similar to unphosphorylated wild type CheY. The authors concluded that the hyperactive phenotype of CheY$^{**}$ is due to facilitated transition between active and inactive conformation. Conservation of the D13 and Y106 residues suggested that the corresponding *H. salinarum* CheY$^{D10K, Y100W}$ mutant may have the same properties. This includes the speculative assumption that the *H. salinarum* CheY$^{**}$ has an enhanced binding affinity to its as yet unidentified interaction partner in the halobacterial flagellar motor, like *E. coli* CheY$^{**}$ has to FliM. One of the difficulties in the identification of the *H. salinarum* CheY interaction partner at the flagellar apparatus is that CheY-P is very sensitive to hydrolysis and thus the interaction is short-lived.

In order to investigate the phototactic, chemotactic and swimming behavior of CheY$^{**}$ containing *H. salinarum* cells, the wild type *cheY* allele was replaced by the mutated version and in order to identify the *H. salinarum* switch protein, Matthias Schlesner introduced *cheY$^{**}$* alleles coding for CheY$^{**}$ proteins that are either C-terminally or N-terminally tagged with a cellulose binding domain.

In *E. coli*, all stimuli sensed by MCPs are processed by the same set of Che proteins, which means that deletion of *cheW*, *cheA*, *cheY*, *cheZ*, *cheB* or *cheR* always has the same effect on sensing by these different MCPs. In contrast, in *B. subtilis* single deletions of *cheD* and *cheC* both strongly affect McpC-mediated proline sensing, but have comparably mild effects on McpB-mediated asparagine sensing (for details and references see section 2.3.5). Another partially related aspect is the presence of several Che paralogs in *H. salinarum*, e.g. three CheC homologs. In *Rhodobacter sphaeroides*, multiple paralogous Che proteins are encoded in three *che* operons, two of which (*che*Op$_2$ and *che*Op$_3$) are required for chemotaxis under laboratory conditions. Except the CheB homologs which freely diffuse in the cytoplasm and the CheY homologs that could not be located, the other Che proteins exclusively localize to either a polar or a cytoplasmic receptor cluster (Wadhams et al., 2003). This means that paralogous Che proteins may not only have distinct functions, but may also be involved in separate signaling pathways. Therefore, the *che* mutants were investigated for both their ability to perform SRI/HtrI and SRII/HtrII mediated phototaxis as well as chemotaxis, however in this case without stimulation of specific receptors.

### 3.4.3 Analysis of already available *H. salinarum che* mutants

In the Flx15ΔΔ mutant, which is the parental strain of all Flx15 *che* gene knockout mutants, *cheY*, *cheB*, *cheA* and *cheC1* are deleted, but *cheW1* and *cheW2* are still present and are transcribed (see Fig. 3.22 (A)). In addition, a truncated *cheC3* and complete *cheD* and *cheR* genes are present, but are probably not transcribed, because transcrip-

tion may be interrupted by a novobiocin resistance cassette positioned between *cheW1* and the truncated *cheC3*. The Flx15ΔΔ derived knockout mutants were generated by a single crossover between Flx15ΔΔ and plasmids that basically contain the part of the *che* operon that is deleted in Flx15ΔΔ plus a truncated *cheW1* and complete *cheC3*, *cheD* and *cheR* genes, minus the gene to be deleted. The natural promoter of the *che* operon which was found to be upstream of *cheW1* is not contained on these plasmids. A typical example for such a plasmid is given in the lower part of Fig. 3.22 (A).
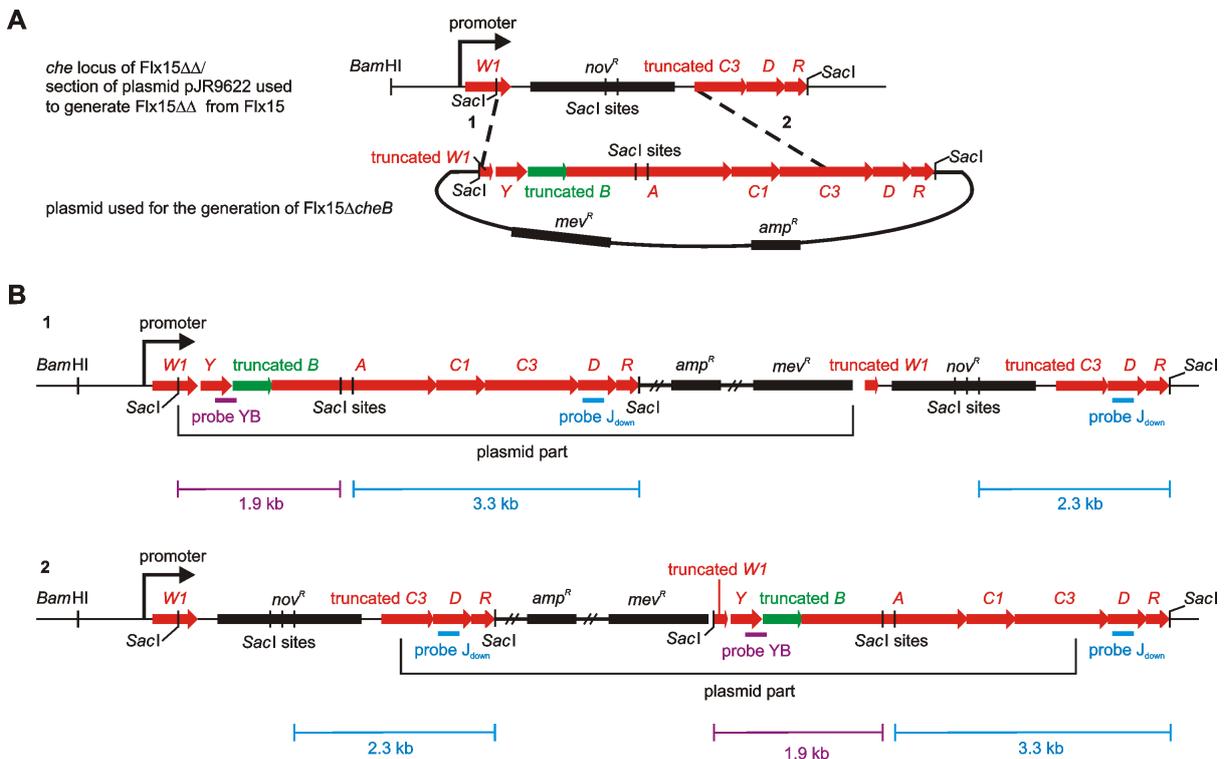


**Figure 3.22: Alternative potential genotypes of strain Flx15Δ*cheB*. (A) Schematic view of the *che* locus of strain Flx15ΔΔ and the plasmid used to generate strain Flx15Δ*cheB*.** Top: Schematic view of the *che* locus of strain Flx15ΔΔ/section of plasmid pJR9622 used to generate strain Flx15ΔΔ from strain Flx15 (Rudolph and Oesterhelt, 1996). By two successive crossover events between Flx15 and pJR9622 the *che* locus of wild type strain Flx15 (see Fig. 3.21) was replaced by the *che* locus contained on pJR9622. Bottom: *che* locus contained on the plasmid used to generate strain Flx15Δ*cheB* (Rudolph and Oesterhelt, 1996). Flx15Δ*cheB* was generated by a single crossover between Flx15ΔΔ and the plasmid. The plasmid still contains a large portion of *cheB* corresponding to the C-terminus of CheB. Dashed lines numbered 1 and 2 indicate potential crossover sites between genomic DNA of Flx15ΔΔ and plasmid. **(B) Schematic views of the two potential genotypes of strain Flx15Δ*cheB*.** 1: Genotype after a single crossover at site 1 as indicated in (A). 2: Genotype after a single crossover at site 2 as indicated in (A). Purple and light blue bars indicate sites to which probes YB and J$_{down}$ hybridize. The size of DNA fragments detected by the probes in Southern Blot analysis using *Sac*I digested genomic DNA is indicated below in corresponding color. Note that the Southern Blot analysis does not allow to discriminate between crossover at site 1 or site 2, because hybridization signals of identical sizes are obtained in both cases.

As indicated in Fig. 3.22, the single crossover between the *che* operon contained on the plasmid and the residual *che* operon of Flx15ΔΔ can occur at two sites, either between the *cheW1* sequences (*cheW1* site) or - with higher probability - the *cheC3* or

*cheC3* upstream sequences (*cheC3* site). The gene arrangements resulting from these possibilities are exemplified in Fig. 3.22 (B) for the Flx15Δ*cheB* mutant. Integration of the plasmids into the *cheW1* is expected to produce clear results. In this case all *che* genes except for the gene to be deleted are transcribed from their natural promoter. However, it is not clear if the truncated *cheC3* and second complete *cheR* and *cheD* genes downstream of the mevinolin resistance cassette are transcribed. In case of integration into the *cheC3* site, the expected result is less clear. While *cheW1* will be transcribed from its natural promoter, transcription of the largest part of the *che* operon which is downstream of the mevinolin resistance cassette is uncertain since the natural promoter is missing. Unfortunately, the Southern Blot analyses performed by Rudolph and Oesterhelt (1996) do not allow to conclude at which site integration of the respective plasmids has occurred, because in both cases identical hybridization signals are obtained. In case of the Flx15Δ*cheB* mutant it has to be added that almost half of the gene corresponding to the C-terminal portion of CheB is still present.

### 3.4.4 Bioinformatic analysis of the *H. salinarum* CheC proteins

The chemotaxis proteins CheC and CheX belong to a widespread family of homologous CheY-P phosphatases (for details see section 2.3.5 and associated Fig. 2.9). While CheX forms a homodimer, CheC achieves similar phosphatase activity only by complex formation with CheD (Szurmant et al., 2004; Park et al., 2004; Chao et al., 2006). Park et al. (2004) noted that CheX is currently found in 20+ genomes often in multiple versions, however so far has not been found in archaea.

The crystal structures of CheC and the CheX dimer revealed that both proteins are characterized by an internal 2-fold pseudosymmetry (Fig. 3.23). However, CheX is different from CheC in the following structural aspects:

1. the $\alpha3´$ helix is missing

2. the $\alpha1$ helix is shorter

3. the $\alpha2$ and $\alpha2´$ helices are replaced by two $\beta$ strands $\beta_x$ and $\beta_x´$

The $\beta_x´$ strand of CheX is important for dimerization by making four main chain hydrogen bonds with $\beta1$ of the adjacent CheX subunit while the $\alpha2´$ helix of CheC interacts with CheD. Park et al. identified a conserved Gly 121 (or rarely a Ser, *T. maritima* numbering) in CheX proteins in contrast to two nonglycine-residues Asp 143 and Met 144 in CheC proteins at the end of the $\beta1$ strands of both proteins as the residues that decide whether a $\beta_x´$ sheet or rather a $\alpha2´$ helices is formed. Based on these sequence markers, they concluded that in the NCBI database numerous CheX sequences are annotated incorrectly as CheC.

In the genome of *H. salinarum* three CheC homologs have been annotated, two of which (CheC1 and CheC3) are encoded in the *che* operon (Fig. 3.21, p. 83). In order to check the annotation of the halobacterial CheC homologs as "CheC" proteins and thereby identify or exclude them as putative interactors of halobacterial CheD, the sequences of the halobacterial CheC homologs were analyzed in more detail. A SMART database
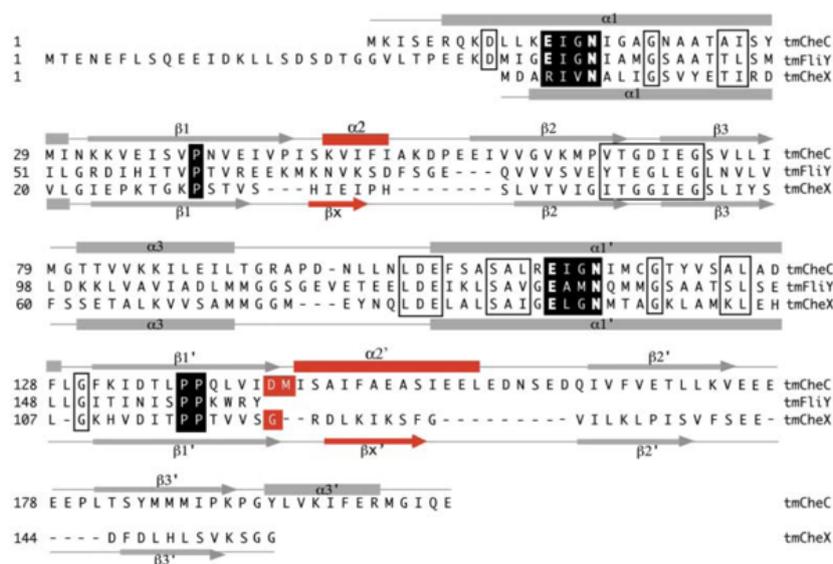
**Figure 3.23: Sequence alignments of *T. maritima* CheC, FliY, and CheX.** Secondary structure elements of CheC (above) and CheX (below) are similar except for the regions (in red) that form helices in CheC ($\alpha2$ and $\alpha2'$) and $\beta$ strands ($\beta_x$ and $\beta_x'$) in the dimer interface of CheX. Residue conservation (boxes) clusters in the regions of $\alpha1$ ($\alpha1'$) and $\beta1$ ($\beta1'$). Black boxes highlight conserved residues in the active site regions, and red boxes encircle residues that are markers for the CheX family *versus* CheC family. Figure and figure captions are from Park et al. (2004).

search revealed that CheC1 and CheC2 each possess one CheC domain at amino acid position 105 - 142 and 103 - 140, respectively. The longer CheC3 protein has two CheC domains at amino acid positions 90 - 127 and 277 - 314. ClustalW alignments of the halobacterial CheC proteins and *T. maritima* CheC and CheX identified Asp 141 Ser 142 in CheC2 at the crucial positions. In case of CheC3 Asp 129 Glu 130 are found in the first CheC domain and Asp 315 Ala 316 in the second CheC domain at the corresponding positions. Thus, although the Met at the second position is missing, it seems to be clear that CheC2 and the two CheC domains of CheC3 are of the CheC type. However, in case of CheC1, the situation is different. Here, the alignment identified Ala 143 Ser 144 at the crucial positions and as both Ala and Ser are rather small residues compared to Asp and Met formation of the $\beta_x'$ could not be excluded. This prompted me to run a secondary structure prediction with the halobacterial CheC proteins using the PSIPRED protein structure prediction server (Jones, 1999; McGuffin et al., 2000; Bryson et al., 2005). However, in order to test if the PSIPRED algorithm could yield a reliable result for CheC and CheX proteins, the prediction was first run with the *T. maritima* CheC and CheX sequences. The secondary structure prediction of CheC yielded a good result with just minor deviations from the X-ray structure e.g. $\beta1$, $\beta1'$ and $\alpha2'$ were torn into two strands and helices, respectively and the exact positions of the strands and helices were not always correct (Fig. 3.24). However the features that characterize CheC were predicted. The prediction for CheX was less successful. The program failed to identify $\beta_x$ and $\beta_x'$, but at least it did not predict $\alpha$ helices at these positions. These results lead to the conclusion that the secondary structure prediction can be used to distinguish between CheC and

CheX proteins. The secondary structure prediction for the halobacterial proteins yielded the following result for CheC1, CheC2 and the C-terminal CheC domain of CheC3 (3.25 and 3.26):

1. long $\alpha 1$ helices

2. $\alpha 2$ and $\alpha 2'$ helices instead of $\beta_{\mathrm{x}}$ and $\beta_{\mathrm{x}}'$ strands

3. $\alpha 3'$ helices present

In case of the N-terminal CheC motif of CheC3, the $\alpha 3$ and $\alpha 1'$ helices (N$\alpha 3$ and N$\alpha 1'$) seem to be fused to a single $\alpha$ helix and at the position where $\beta 3'$ is expected, instead a $\alpha$ helix is predicted (indicated by a red exclamation mark in Fig. 3.26).

Based on the secondary structure predictions, it can be concluded that all three halobacterial proteins are correctly annotated as CheC proteins and thus in principle all three proteins could interact with CheD.

*T. maritima* CheC has two sites with dephosphorylating activity that are located in the $\alpha 1$ and $\alpha 1'$ helices, respectively and show different activities (Park et al., 2004). Mutant studies identified Glu13 and Asn16 in the $\alpha 1$ helix and Glu112 and Asn115 in the $\alpha 1'$ helix as the crucial residues and suggested that the active site in the $\alpha 1'$ helix has the higher activity. Table 3.9 shows which amino acids are found in the *H. salinarum* CheC homologs at positions corresponding to Glu13, Asn16, Glu112 and Asn115 when ClustalW alignments are done. It is striking that in all four CheC domains of the three CheC proteins a Glu-Asn signature is only found in the putative $\alpha 1'$ helices. In CheC1 and CheC2 Glu residues are found in the $\alpha 1$ helices, but the Asn is missing. Thus, sites with putative CheY-P dephosphorylating activity corresponding to the more active site in *T. maritima* CheC are conserved in all *H. salinarum* CheC homologs.

| Residue (Helix) — Protein | $\mathbf{E13_{Tm}}$ ($\alpha 1$) | $\mathbf{N16_{Tm}}$ ($\alpha 1$) | $\mathbf{E112_{Tm}}$ ($\alpha 1'$) | $\mathbf{N115_{Tm}}$ ($\alpha 1'$) |
|---|---|---|---|---|
| CheC1$_{\mathrm{Hsal}}$ | **E15** | R18 | **E112** | **N115** |
| CheC2$_{\mathrm{Hsal}}$ | **E15** | D18 | **E110** | **N113** |
| CheC3$_{\mathrm{Hsal}}$ (N$\alpha 1$, N$\alpha 1'$) | R13 | D16 | **E97** | **N100** |
| CheC3$_{\mathrm{Hsal}}$ (C$\alpha 1$, C$\alpha 1'$) | Q191 | S194 | **E284** | **N287** |

**Table 3.9: Conservation of amino acid residues important for dephosphorylating activity of *T. maritima* (Tm) CheC in the *H. salinarum* (Hsal) homologs CheC1, CheC2 and CheC3.** Numbering of residues in the headline refers to *T. maritima* CheC, numbering of the others refers to the *H. salinarum* proteins. N$\alpha 1$/N$\alpha 1'$, C$\alpha 1$/C$\alpha 1'$: N-terminal/C-terminal $\alpha 1$/$\alpha 1'$ helices corresponding to Fig. 3.25 and Fig. 3.26. Matching residues are in bold.

**(A)** CheC_Tm

**(B)** CheX_Tm
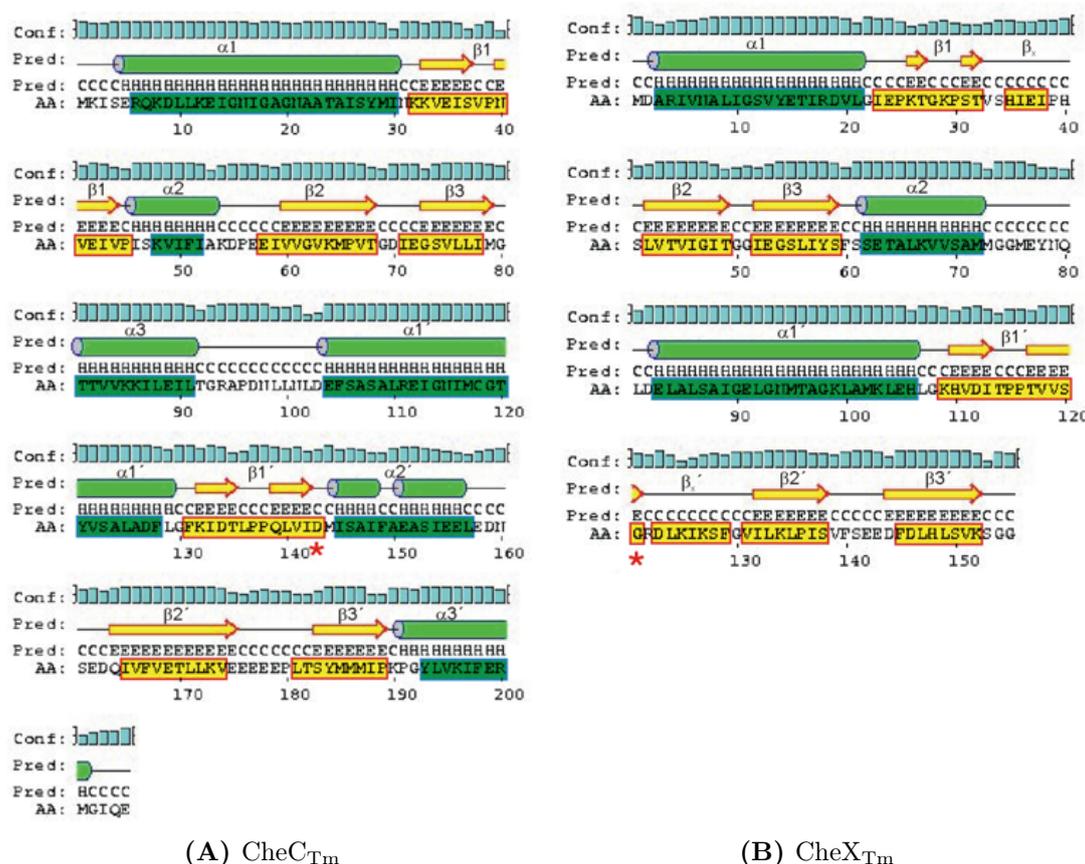
**Figure 3.24: Secondary protein structure prediction for *T. maritima* CheC and CheX performed with PSIPRED** (http://bioinf.cs.ucl.ac.uk/psipred/psiform.html). Pred: "H" and green bars: predicted $\alpha$ helices; Pred: "C" and yellow arrows: predicted $\beta$ sheets; blue columns represent the confidence level of the prediction in arbitrary units; AA: amino acid sequence; green and yellow bars printed over the amino acid sequence represent $\alpha$ helices and $\beta$ sheets, respectively, that were found in the X-ray structure; red asterisks mark amino acids that are sequence markers for a successive $\alpha$ helix or $\beta$ sheet according to Park et al. (2004)

**(A)** CheC1$_{Hsal}$

**(B)** CheC2$_{Hsal}$
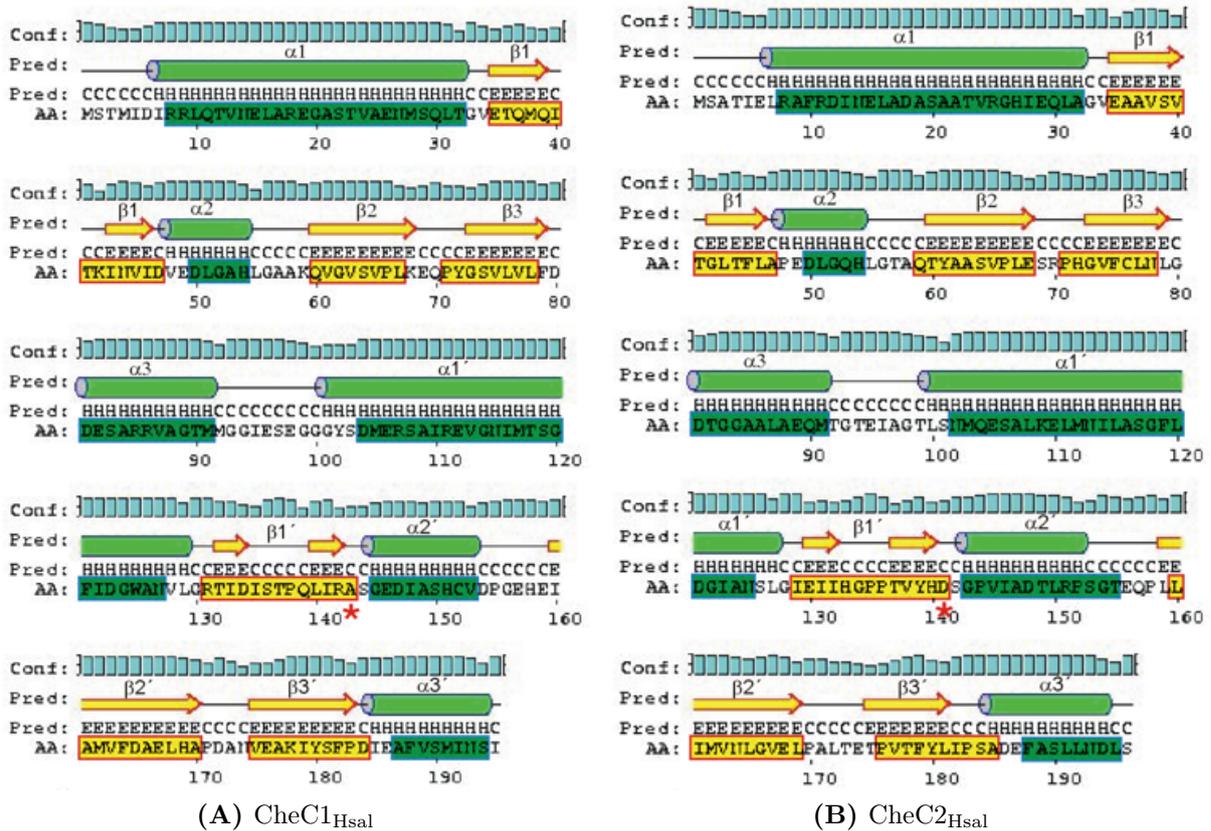
**Figure 3.25: Secondary protein structure prediction for the *H. salinarum* proteins CheC1 and CheC2 performed with PSIPRED** (http://bioinf.cs.ucl.ac.uk/psipred/psiform.html). Pred: "H" and green bars: predicted $\alpha$ helices; Pred: "C" and yellow arrows: predicted $\beta$ sheets; blue columns represent the confidence level of the prediction in arbitrary units; AA: amino acid sequence; green and yellow bars printed over the amino acid sequence represent $\alpha$ helices and $\beta$ sheets, respectively, that are expected at the indicated amino acid positions based on a ClustalW alignment (Blosum62 matrix) with CheC and CheX from *T. maritima*; red asterisks mark amino acids that are sequence markers for a successive $\alpha$ helix or $\beta$ sheet according to Park et al. (2004).
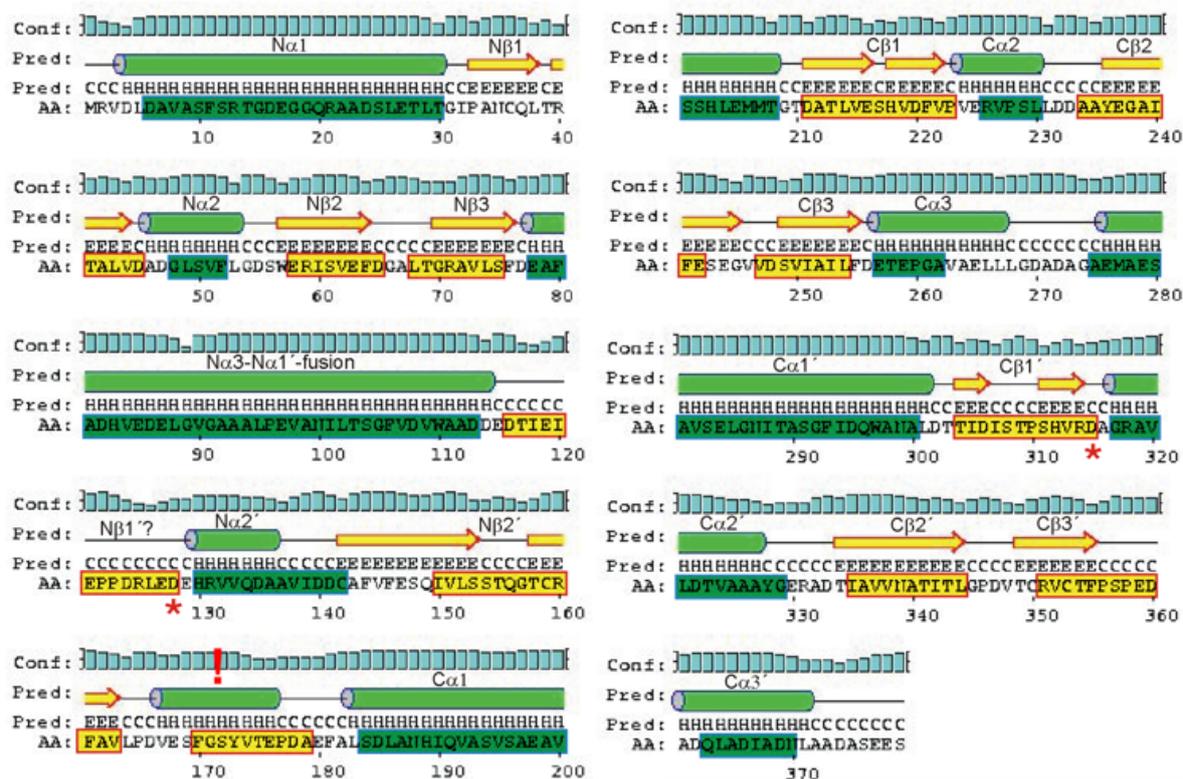
**Figure 3.26:** **Secondary protein structure for *H. salinarum* CheC3 performed with PSIPRED** (http://bioinf.cs.ucl.ac.uk/psipred/psiform.html). Pred: "H" and green bars: predicted $\alpha$ helices; Pred: "C" and yellow arrows: predicted $\beta$ sheets; blue columns represent the confidence level of the prediction in arbitrary units; AA: amino acid sequence; green and yellow bars printed over the amino acid sequence represent $\alpha$ helices and $\beta$ sheets, respectively, that are expected at the indicated amino acid positions based on a ClustalW alignment (Blosum62 matrix) with CheC and CheX from *T. maritima*; red exclamation mark: at this position $\beta3'$ is expected, but a $\alpha$ helix is predicted; red asterisks mark amino acids that are sequence markers for a successive $\alpha$ helix or $\beta$ sheet according to Park et al. (2004).

### 3.4.5 Generation and genotypic analysis of *che* gene knockout mutants

Single in frame deletions of *cheR*, *cheB*, *cheD*, *cheC1* and *cheC3* and complementations of the *cheR* and *cheB* knockout strains were generated according to the general outline in section 3.1.1. Fig. 3.27 shows a schematic view of the relevant *che* gene loci based on the sequence of the *H. salinarum* strain R1 as retrieved from the HaloLex database (`http://www.halolex.mpg.de`). Southern Blot or PCR analyses were carried out as described in Fig. 3.28 and confirmed the desired genotype.

### 3.4.6 Generation and genotypic analysis of a *cheY*$^{D10K,Y100W}$ double mutant

A 1167 bp *Pst*I/*Xba*I PCR fragment containing the wild type *H. salinarum cheY* gene flanked by its upstream and downstream regions was cloned into pUC19. CheY D10K and Y100W mutations were introduced by mutagenic primers in two successive steps using the QuikChange$^{®}$ site-directed mutagenesis kit (Stratagene, La Jolla, CA, USA). Presence of the respective mutations was confirmed by DNA sequencing of the resulting plasmids. The *Pst*I/*Xba*I fragment bearing both *cheY* mutations was then ligated with *Pst*I/*Xba* digested pANX (V. Tarasov, unpublished) to yield suicide vector pMS7 (M. Schlesner, unpublished). pANX is a shuttle vector bearing a selection marker and origin of replication for cloning purposes in *E. coli* and a novobiocin selection marker and halophilic β-galactosidase for genetic manipulation of *H. salinarum*. Thus, pANX has the same basic features as pMKK100 (Koch and Oesterhelt, 2005). *H. salinarum* strain S9$_{mot}$ was transformed with pMS7 as described in section 4.3.5. In two consecutive crossover events between the genomic upstream and downstream regions of *cheY* and their plasmid-borne counterparts, wild type *cheY* was replaced by the mutated *cheY* allele (*cheY*$^{D10K,Y100W}$ or *cheY*$^{**}$). For selection of single colonies that had undergone the first and the second crossover events, respectively, a blue-red screening method was employed as described for the generation of deletion mutants (see section 3.1.1). Replacement of *cheY* by *cheY*$^{**}$ in single colonies of the second crossover event was verified by sequencing of PCR fragments produced from genomic DNA of the respective colonies.

### 3.4.7 Chemotaxis proteins influence the rotational bias of the *H. salinarum* flagellar motor

**CW biases and spontaneous reversal frequencies of the *che* mutants**

Several methods have been used to determine the rotational bias[3] of the flagellar motor of *H. salinarum*. Hildebrand and Schimz (1985) measured the duration of successive swimming intervals of single cells and compared the durations of even and odd swimming intervals. This allowed them to conclude that the flagellar motors of *H. salinarum* cells on average spend equal times in CW and CCW modes. High-intensity dark-field

---

[3]Rotational bias: the fraction of time the flagellar motor spends in CW or CCW mode.
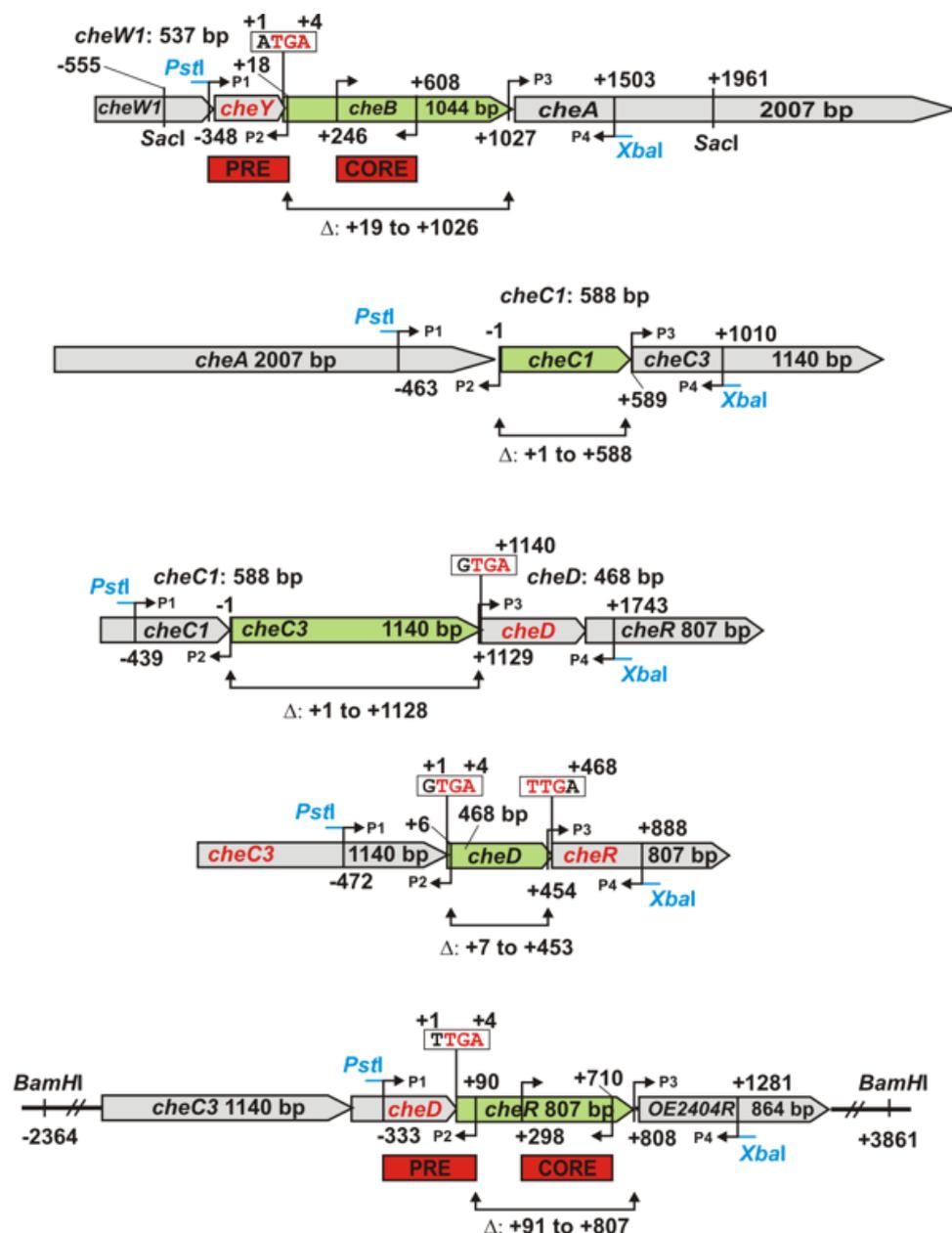
**Figure 3.27: Schematic view of the loci of the *che* genes that were deleted in this study.**
Numbers indicate nucleotide positions relative to the target gene (in light green color) with the following convention: +1 is the position of the first base of the target gene, -1 is the position of the preceding base. Primers are indicated as bent arrows. Primers P1 and P2 were used to generate the US fragments and primers P3 and P4 to generate the DS fragments of the target gene and are named according to Fig. 3.1. Red boxes indicate the hybridization positions of DIG-11-dUTP-labeled probes in front (PRE) or within (CORE) the target gene. In case of overlapping genes, the stop and start codons are given in boxes. Stop and start codons of the genes that precede and follow the target gene, respectively, are in red. Numbers following "Δ:" denote start- and end position of the deleted region.
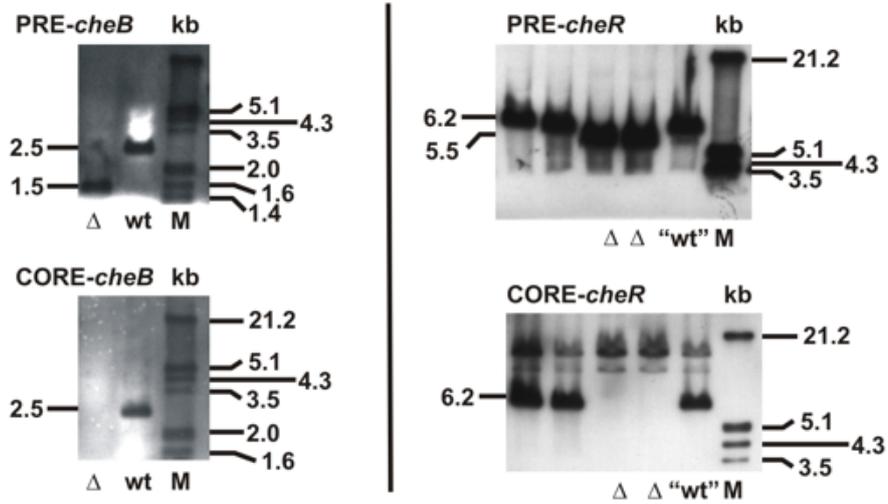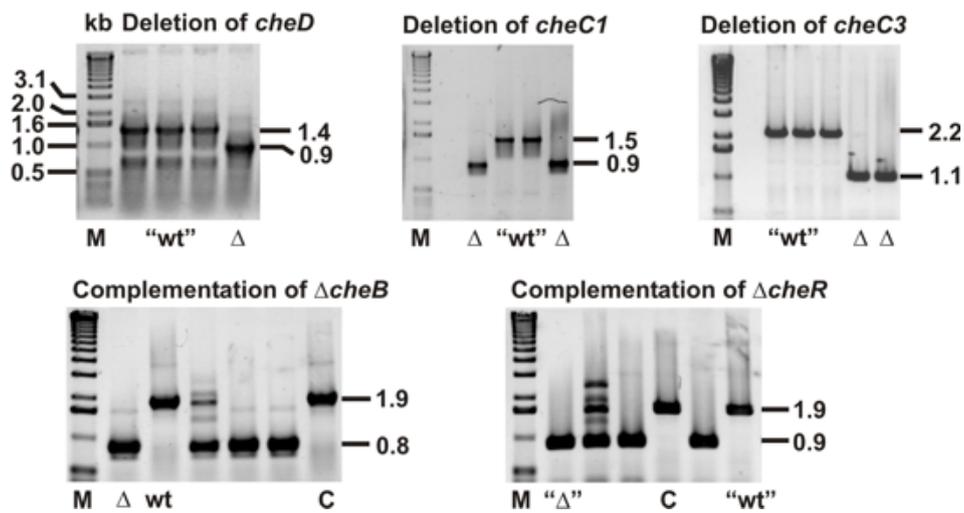
**Figure 3.28: Genotypic analysis of *che* gene knockout strains. (A) Southern Blot analysis.** Genomic DNA of putative $\Delta cheB$ and $\Delta cheR$ deletion mutants was digested with *Sac*I and *BamH*I, respectively. Positions of restriction sites and hybridizing regions of the "PRE" and "CORE" probes are given in Fig. 3.27. M: marker lane; $\Delta$: lane with hybridization signal that is in accordance with deletion of the target gene; wt: lane with hybridization signal obtained with wild type DNA. Lanes that are shown for blots obtained with the PRE- and CORE probes for the respective target gene correspond to each other. **(B) PCR analysis.** PCR reactions were carried out with primers P1 and P4, with annealing positions given in Fig. 3.27. In all cases control reactions with DNA of the parental strain $S9_{mot}$ were performed. In case of complementations, in addition, control reactions with DNA of the starting deletion mutant were performed. M: marker lane; wt: lane with PCR products obtained with wild type DNA; "wt": lane with DNA pattern that corresponds to a band pattern as obtained with wild type DNA; C: lane with PCR product that is expected for a complemented mutant; $\Delta$: lane with PCR products that were obtained with DNA from a deletion mutant; "$\Delta$": lane with DNA band pattern that corresponds to a band pattern as obtained with DNA of a deletion mutant.

microscopy cannot only be used to visualize halobacterial flagella, but also to determine their rotational mode. In *H. salinarum*, CW and CCW modes are defined as proposed by Macnab and Ornston (1977). From a practical point of view this means that when a free-swimming cell is pulled by the flagellar bundle, the bundle rotates CCW and when the cell is pushed, the flagellar bundle rotates CW (see Fig. 2.3). Marwan et al. (1987) determined the initial rotational mode of single cells by high-intensity dark-field microscopy and then determined the duration of subsequent swimming phases. A histogram in which the durations of CW and CCW swimming phases are displayed separately showed that the durations of swimming intervals are equally distributed in CW and CCW mode and thus the reversing probability in both modes is equal. In other words, both studies showed that *H. salinarum* wild type cells have a 50% CW bias.

Mutations in chemotaxis genes are known to influence the flagellar rotational bias in *E. coli* and *B. subtilis* (Parkinson, 1976; Fuhrer and Ordal, 1991). Using dark-field microscopy, deviations from the wild type 50% CW distribution were also found in some chemotaxis mutants of *H. salinarum* (Rudolph and Oesterhelt, 1996). In this study the flagellar rotational bias was determined, as by Rudolph and Oesterhelt (1996), i.e. by counting the number of free-swimming cells that were found to be pushed (CW) or pulled (CCW) by the flagellar bundle. The ratio of the number of cells swimming in CW and CCW mode should reflect the average percentage of time the cells spend in each mode. In addition, the spontaneous reversal/switching frequency was judged by visual inspection of the cells. It has to be noted that the reversal frequencies given in table 3.10 may be somewhat subjective as they were not results of sophisticated measurements, but reflect an impression that was gained by following single cells and looking at the whole cell population.

The CW biases and the spontaneous reversal frequencies of the wild type and the *che* mutants are summarized in Table 3.10.

| *Mutant* | *Spont. reversals* | *Tot. CW* | *Tot. CCW* | *Av % CW* |
|---|---|---|---|---|
| wild type | + | 455 | 405 | 53 |
| $\Delta cheB$ | + | 541 | 1193 | 31 |
| $\Delta cheB/cheB^+$ | + | 281 | 449 | 38 |
| $\Delta cheR$ | very rare | 1111 | 648 | 63 |
| $\Delta cheR/cheR^+$ | + | 162 | 121 | 57 |
| $\Delta cheC1$ | rare | 158 | 147 | 52 |
| $\Delta cheC3$ | rare | 707 | 277 | 72 |
| $\Delta cheD$ | very rare | 605 | 98 | 86 |
| $cheY^{**}$ | extremely rare | 1357 | 13 | 99 |

**Table 3.10: Flagellar rotational bias and swimming behavior of *H. salinarum che* mutants as observed by high intensity dark-field microscopy.** Spont. reversals: spontaneous reversals; +: approx. wild type switching behavior; Tot. CW, Tot. CCW: sum of cells of all single experiments with their flagella rotating in CW and CCW mode, respectively; Av % CW: average percentage of cells swimming in CW mode. In most cases, the data were composed from several experiments and in some cases from more than one clone of the respective mutant. The raw data from which the values were composed are given in table 5.4. Cells were grown to an $OD_{600}$ of $\approx 0.6$ and diluted to an $OD_{600} = 0.1$ with fresh complex medium containing arginine in a final concentration of 0.1% (w/v).

Except the $\Delta cheB$ mutant, all other deletion mutants had reduced reversal frequencies compared to wild type. This was especially marked in case of the $cheY^{**}$ mutant, followed by the $\Delta cheR$ and $\Delta cheD$ mutants. The Flx15$\Delta cheB$ mutant was reported to switch every 2 - 3 s on average (Rudolph and Oesterhelt, 1996). However, this was not observed for the $\Delta cheB$ mutant reported here, which showed wild type switching behavior. Likewise the switching behavior of the complemented mutant $\Delta cheR/cheR^+$ was indistinguishable from wild type.

The observation that all of the mutants reversed, albeit significantly less frequent than wild type cells, is important for the interpretation of the CW biases. It directly shows that the CW bias determined for e.g. the $\Delta cheD$ mutant is 86%, because the cells on average spend 86% of the time in CW mode and not because 86% of the cells´ motors were built such that they rotate CW. It can be assumed that during the two days of growth before measurement, the cells have switched sufficiently often to adopt the observed CW bias, whatever their initial CW bias was directly after assembly of the flagellar motor.

As expected, the wild type showed a close to 50% CW bias. All mutants apart from the $\Delta cheC1$ mutant (52% CW), showed significant deviations from the 53% CW bias determined for wild type. The rotational biases of the mutants gradually covered a range from 30% to 99% CW. Compared to the results of Rudolph and Oesterhelt (1996) two deviations were observed: the $\Delta cheB$ mutant reported here had a CW bias of 30% instead of 50% and the $\Delta cheC1$ mutant had a 52% CW bias instead of 88%. These deviations may be attributed to polar effects in the previously described mutants (see 3.4.3). With a CW bias of 57% compared to 63% of the $\Delta cheR$ mutant, the complemented mutant $\Delta cheR/cheR^+$ approached the wild type value, but due to the small number of cells from which the CW bias was determined, restoration of the wild type CW bias cannot be concluded with absolute certainty. Complementation of the $\Delta cheB$ mutant, lead to a 38% CW bias. This is closer to the wild type CW bias than the 31% found in the $\Delta cheB$ mutant, but is still very close to the bias of the $\Delta cheB$ parental strain. The reason for this is unclear at the moment.

A plausible model that is at least partially able to explain the deviations from the wild type 50% CW rotational bias and the low reversal frequencies observed in most of the mutants will be discussed later in section 3.4.13 in context with the results obtained in chemotaxis and phototaxis assays.

## Validity of the method used to determine the rotational biases

Counting of cells in CW and CCW seems to be a straightforward approach, however there are some drawbacks that one should keep in mind. Flagella can be observed only on a fraction of cells and the visibility of halobacterial flagella is better in CW than in CCW mode (Marwan et al., 1991). This may to lead to a systematic error that shifts the result to an excessive percentage of CW mode, especially under conditions where the visibility of the flagella is suboptimal (e.g. when cells have a bad motility). The severeness of such a systematic error is difficult to predict.

Another problem, once again, arises from bipolarly flagellated cells. In this case both flagellar bundles may contribute to the overall movement of the cell. Because each flagellar bundle can rotate independently either in CW or CCW mode or stop, six situations occur,

where net movement of the cells is observed and three in which the cells stop (Fig. 2.3, p. 10). If both flagellar bundles rotate in opposite mode (one in CCW mode, the other in CCW mode), the cell moves from right to left or the other way round, depending on the positions of the CW and CCW rotating flagellar bundles. If one of the flagellar bundles is not visible, the swimming direction may be misinterpreted in terms of CW *versus* CCW rotational mode. As bipolarly flagellated cells mainly occur in stationary cultures, this problem was partially circumvented by using early to late logarithmic instead of late stationary cultures. Another possibility to avoid the problem is to follow the cell until it switches. In most cases this gives a clue if a cell is mono- or bipolarly flagellated. However, this is a very tedious procedure which was - due to the low switching frequency of the mutants - not practicable. The values for wild type in both this study and the study by Rudolph and Oesterhelt (1996) were close to and exactly 50% CW, respectively (see Table 3.10).

The "tethered cell assay" is an alternative, widespread method to determine the flagellar rotational bias. In this assay, the cells are tethered to the microscopic slide or coverslip via their flagella. The flagellar rotation is converted into CW or CCW rotation of the cell body, depending on the rotational mode of the tethered filament. This is the classical evidence for the rotary mechanism of the bacterial flagellar motor (Silverman and Simon, 1974). In case of tethered cells the rotational bias can be determined by measuring the time the cells spend in each rotational direction. However, tethering resulted in the incorrect observation that the rotational bias of the *H. salinarum cheA* mutant E4 corresponds to wild type, i.e. 50% CW (Rudolph and Oesterhelt, 1995). Analysis of free-swimming cells revealed, that in fact 99% of the mutant cells swim by CW direction of their flagella (Rudolph and Oesterhelt, 1996). The original misinterpretation was most likely due to the frequent bipolar flagellation of *H. salinarum* cells that is especially observed in stationary cultures (Alam and Oesterhelt, 1984). Rudolph and Oesterhelt suggested that a cell could be tethered via a truncated filament on one pole while another still somewhat intact filament at the other pole could cause rotation of the cell. Rotations caused by both the tethered and the free filament could then mimic a wild type rotational bias. Therefore, I preferred to determine the rotational biases on free-swimming cells.

As mentioned above Hildebrand and Schimz (1985) and Marwan and Oesterhelt (1987) applied methods to determine the rotational bias that exclude tampering of values by unequal visibility of flagella in CW and CCW rotational mode and both found that the rotational bias of wild type cells is 50% CW. This suggests that the method of counting free-swimming cells in CW and CCW mode yields plausible, significant values of the rotational bias.

### 3.4.8 Phototaxis and spontaneous motor switching of *H. salinarum che* mutants

In order to analyze the swimming behavior of the *che* gene deletion mutants and their ability to perform phototaxis, the percentage of cells that reversed in a given time interval after application of either no stimulus (spontaneous reversals) or phobic light stimuli (light-induced reversals) were measured with the computerized cell tracking system de-

scribed in section 4.5.2. As attractant light stimuli suppress reversals, the phototactic efficiency of the cells could also be determined by measuring the decrease of reversals after application of an attractant light stimulus. However, the numerical difference between the percentage of spontaneously reversing cells and the percentage of stimulation-induced reversals is larger and thus yields results of higher significance.

Fig. 3.29 (A) schematically shows the course of the measurements and the stimulation patterns that were applied to determine spontaneous and light-induced reversals. SRII/HtrII mediated phototaxis towards blue light was measured by application of a blue light pulse to dark-adapted cells. SRI/HtrI mediated phototaxis to orange light was measured by application of a step down in orange light to cells that were adapted to orange light. The results for wild type, the $\Delta cheB$, $\Delta cheR$, $\Delta cheC1$, $\Delta cheC3$, $\Delta cheD$, $cheY^{**}$ mutants and the complemented mutant $\Delta cheB/cheB^+$ are shown in Fig. 3.29 (B).

Unfortunately in this series of measurements, the response to a step down in orange light of the $\Delta cheD$ mutant and the complemented $\Delta cheB/cheB^+$ mutant failed. However, Figure 3.30 shows the results of another measurement series that contains these data and in addition results for the complemented mutant $\Delta cheR/cheR^+$. It has to be noted that the absolute values of these measurements cannot be compared with those in Figure 3.29, as the measurements were obtained with a slightly different setup and different measurement conditions (compare Figs. 3.29 (A) and 3.30 (A)). Therefore, to allow a better comparison of results, measurements for wild type and the $\Delta cheB$ and $\Delta cheR$ mutants are included in Figure 3.30.

## Spontaneous reversals

Visual inspection of video sequences that were evaluated for reversals by the computerized system revealed that the system detects a rate of approx. 10 to 15% false positive reversals (indicated by a horizontal line in the bar diagrams). Without stimulus, 20 - 30% of the wild type cells reversed within the evaluated time interval. This was clearly above the background levels and the occurrence of true reversals could be confirmed by visual inspection of the recorded videos. The $\Delta cheB$ mutant reached values comparable to the wild type and again, true reversal could be confirmed by visual inspection. In contrast, values of the other deletion mutants and the $cheY^{**}$ mutant were below the threshold. Visual inspection of videos of these mutants revealed that sometimes, albeit very rarely, true reversals occurred. This agrees with the qualitative observations made with dark-field microscopy (see Table 3.10), although reversals appeared to occur more frequently when the cells were observed with dark-field microscopy. In contrast to the $\Delta cheR$ mutant, the complemented mutant $\Delta cheR/cheR^+$ reached wild type levels of spontaneous reversals, indicating that the rare reversal events seen in the $\Delta cheR$ mutant are really due to a lack of $cheR$. Finally it has to be noted that in contrast to the results presented here, Rudolph and Oesterhelt (1996) found in similar measurements that 100% of $\Delta$B mutant cells spontaneously reversed.

**(A)** Stimulation patterns.

**(B)** Bar diagram of the average percentage of reversing cells.
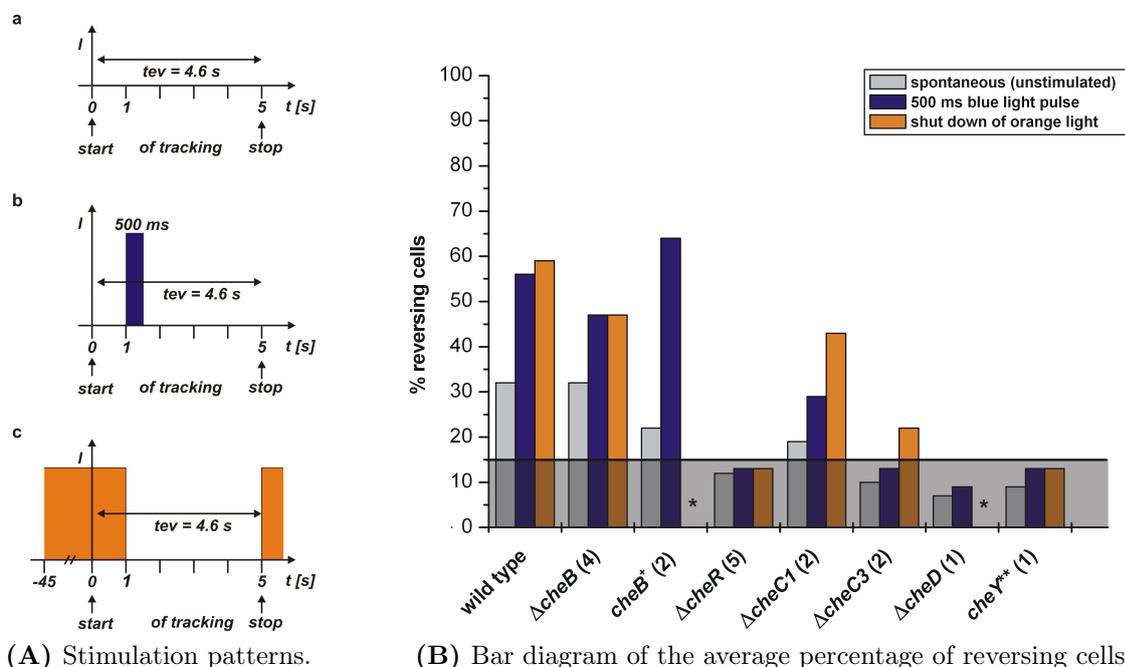
**Figure 3.29: Analysis of spontaneous reversal frequencies and phototactic responses of *H. salinarum che* mutants determined by computerized cell tracking. (A) Schematic diagram of the stimulation patterns used to determine the percentage of spontaneous and light-stimulus induced cell reversals.** In all measurements cells were tracked for 5 s and evaluated for reversals in a time interval of tev = 4.6 s. I: light intensity; start/stop: Onset/end of tracking; Stimuli were applied 1 s after the onset of tracking. **(a)** For measurement of spontaneous reversals dark-adapted cells were measured without applying a stimulus. **(b)** For measurement of SRII/HtrII mediated phototaxis, dark-adapted cells were stimulated by a 500 ms blue light pulse ($480 \pm 50$ nm, 24 W/m$^2$). Between measurements the position of the sample slide was shifted to avoid stimulation of the same individual cells. **(c)** For measurement of SRI/HtrI mediated phototaxis, orange-light adapted cells were stimulated by a step down in orange light (from $580 \pm 50$ nm, 390 W/m$^2$ to zero). Between measurements the cells were allowed to readapt to orange light for 45 s. **(B) Average percentage of reversing wild type and *che* deletion mutant cells.** Grey bars: spontaneous reversals; blue bars: reversals after a blue light pulse; orange bars: reversals after a step down in orange light; *: measurement failed due to a defect of the light source. Shaded region bounded by a horizontal line: false positive rate of the computerized cell tracking system. The raw data including the number of evaluated cells are given in Table 5.2, p. 147.

**(A)** Stimulation patterns.

**(B)** Bar diagram of the average percentage of reversing cells.
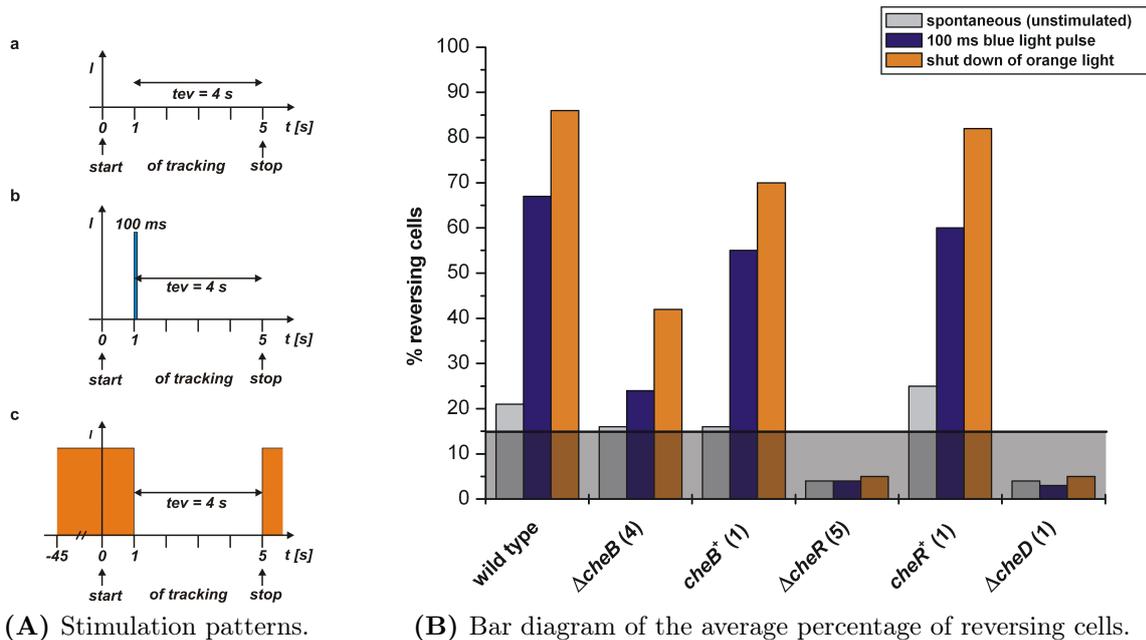
**Figure 3.30: Supplemental measurements of spontaneous reversal frequencies and phototactic responses of *H. salinarum che* mutants by computerized cell tracking. (A) Schematic diagram of the stimulation patterns used to determine the percentage of spontaneous and light-stimulus induced cell reversals.** Differences compared to Fig 3.29 (A): 1) time interval evaluated for reversals $t_{ev} = 4$ s. 2) Stimulus for measurement of SRII/HtrII mediated phototaxis: 100 ms blue light pulse ($480 \pm 50$ nm, 24 W/m$^2$). **(B) Average percentage of reversing wild type and *che* deletion mutant cells.** Grey bars: spontaneous reversals; blue bars: reversals after a blue light pulse; orange bars: reversals after a step down in orange light; Shaded region bounded by a horizontal line: false positive rate of the computerized cell tracking system. The raw data including the number of evaluated cells are given in Table 5.3, p. 148.

## Photophobic responses

Wild type cells showed a clear increase in reversals in response to both a blue light pulse and a step down in orange light intensity, indicating that both the SRI/HtrI and the SRII/HtrII signaling pathways were intact. Admittedly, the responses in measurements for Figure 3.29 were considerably worse than in measurements for Figure 3.30. The reason for this difference is not clear at the moment. Direct comparison of stimulus-induced reversal frequencies of the $\Delta cheB$ mutant with wild type response and response of the complemented $\Delta cheB/cheB^+$ mutant show that deletion of the putative methylesterase gene *cheB* still allowed, albeit reduced responses of the cells. In contrast, no stimulus-induced increases in reversal frequencies were seen in case of the $\Delta cheR$ mutant. Thus, while deletion of the putative methylesterase gene *cheB* still allowed phototaxis, deletion of the putative methyltransferase gene *cheR* did not. The validity of this result is confirmed by the fact that the $\Delta cheR/cheR^+$ mutant showed wild type responses (see Fig. 3.30). The $\Delta cheC1$ mutant responded to photostimuli, but less efficiently than the $\Delta cheB$ mutant. At first sight, it seems that in this mutant the response to blue light

was worse than the response to orange light, but this is due to averaging of values from two measurements. In the first measurement, the response to blue light was worse than that to the step down in orange light, but this could not be confirmed in a second measurement. In contrast, the $\Delta che$C3 mutant repeatedly showed a small, but significant increase in reversals in response to a step down in orange light, but not to a blue light pulse. The $\Delta cheD$ and $cheY^{**}$ mutants did not respond to either stimulus.

### 3.4.9 Chemotaxis of *H. salinarum che* mutants

The capability of the *che* gene deletion mutants to perform chemotaxis was investigated with the swarm plate assay, which is a widespread assay to investigate the motility and chemotactic efficiency of prokaryotic microorganisms. The principle of the swarm plate assay is described in section 3.2.5. In this study, the swarm plates contained complex medium, i.e. the main component of the medium besides a number of salts was peptone. Thus, the response of the cells seen in the assay as performed in this study, reflects the integrated response to all chemotactically active substances contained in the peptone. Provided that the inoculated cells have the same growth rate, the diameter of the concentric ring emerging around the inoculation site (swarm ring) is a measure of both cellular motility and the capability of the cells to perform chemotaxis. A major drawback of the assay is that the contributions to the ring size of motility on the one hand and chemotactic efficiency on the other hand cannot be discriminated. In order to avoid distortion of the results by impaired motility of the cells, their motility was qualitatively checked in the microscope. Clones and cultures that were obviously immotile or impaired in motility were excluded from further analysis.

In *E. coli*, it was found that non-chemotactic cells are able to migrate through semi-solid agar. The rotational bias of mutants has a large influence on the size of swarm rings (Wolfe and Berg, 1989). Non-chemotactic mutants that tumble frequently by CW rotation of their flagella form larger rings than mutants that solely run. The reason is that tumbling allows the cells to back away from obstructions in the agar while cells that only run tend to get trapped. *H. salinarum* cells do not tumble but swim back and forth. Therefore, in *H. salinarum* an increased reversal frequency rather than a certain CW bias might positively influence the size of the swarm ring diameter. This means that spreading of cells in swarm plates per se is not a sign of chemotaxis. Fig. 3.31 shows two representative swarm plates on which clones of all *che* gene deletion mutants generated in this study were inoculated.

In all cases except the $cheY^{**}$ double point mutant, besides a dark, massive inner disc of high cell density that can be attributed to cell migration followed by propagation, a light outer concentric zone of lower cell density was observed like in chemotactic wild type cells. One might argue that in Fig. 3.31 also for the $cheY^{**}$ a light zone is seen, but in this case the light zone is an artifact that sometimes occurs due to displacement of the softagar caused by the injection of the liquid culture. Such a light zone is neither seen in flagella-less *H. salinarum* cells like the $\Delta flaJ$ mutant (see Fig. 3.8) nor in a flagellated, motile *cheY* knockout mutant Weidinger (2007), which indicates that neither diffusion of non-motile nor of motile cells produces such a zone. As the *cheY* knockout mutant can be expected to be non-chemotactic, my conclusion is that the light ring
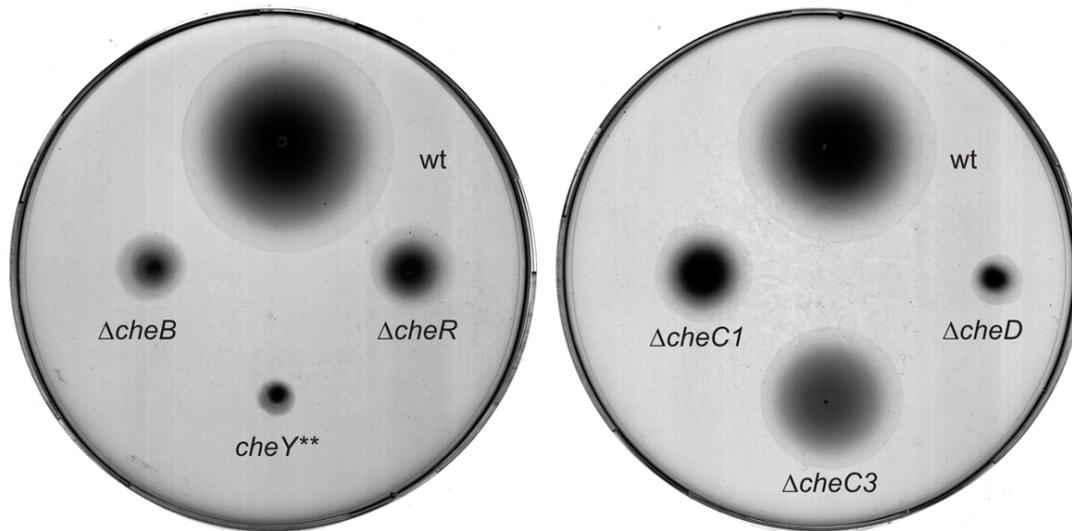
**Figure 3.31: Overview of the chemotactic behavior of specific chemotaxis gene deletion mutants.** The parental strain S9 (wt) and specific *che* gene deletion mutants were compared for their ability to perform chemotaxis on semisolid peptone swarm plates (0.3% (w/v) agar). $8 \cdot 10^6$ cells were inoculated beneath the surface and allowed to grow and swarm for 7 days at 37°C.

results from chemotactic cells that actively follow the emerging attractant gradient and thus is a chemotactic zone. In other words, the swarm plate assay suggests, that all mutants except the *cheY*** mutant were capable of some residual chemotaxis, which implies straight away that under the conditions of the swarm plate assay, the mutants were able to reverse. The latter result is consistent with results obtained with dark-field microscopy and computerized cell tracking. However, considering the weak to nonexistent phototactic responses of the mutants, their ability to perform chemotaxis is unexpected. The consequences of this observation will be discussed in section 3.4.11. The averaged results of the swarm ring diameters of the *che* mutants relative to wild type are given in Table 3.11.

The results suggest that the chemotactic efficiency is best in the $\Delta cheC3$ mutant, followed by $\Delta cheC1$, then $\Delta cheR/\Delta cheB$ and finally the $\Delta cheD$ mutant. While in case of the complemented $\Delta cheR/cheR^+$ strain the wild type swarm diameter was perfectly restored, the averaged diameter of clones of the complemented $\Delta cheB/cheB^+$ strain reached only 75% of the wild type. This is somewhere in between the chemotactic efficiencies seen in the $\Delta cheC1$ and $\Delta cheC3$ mutants. The best clone out of 6 of the $\Delta cheB/cheB^+$ strain reached an average value of 86% of the wild type. In contrast to the wild type strain which was originally selected as a motile, chemotactic, single colony, this procedure was not repeated after generation of the *che* mutants and the respective complemented mutants. Therefore, a certain clone to clone variation and general decrease of chemotactic efficiency can be expected in the mutant and above all in the complemented strains. It is not clear if the decreased chemotactic efficiency of the complemented $\Delta cheB/cheB^+$ mutant is due to clone variability or due to incomplete restoration of chemotaxis and/or motility.

In contrast to the $\Delta cheB$ deletion mutant described here, Rudolph and Oesterhelt

| Mutant | Number of clones examined | % average diameter relative to wild type | Chemotactic zone |
|---|---|---|---|
| wild type | 1 | 100 | + |
| $\Delta cheB$ | 4 | $35 \pm 5$ | + |
| $\Delta cheB$ (4)/$cheB^+$ | 6 | $75 \pm 9$ | + |
| $\Delta cheR$ | 3 | $35 \pm 5$ | + |
| $\Delta cheR$ (5)/$cheR^+$ | 3 | $94 \pm 12$ | + |
| $\Delta cheC1$ | 5 | $66 \pm 8$ | + |
| $\Delta cheC3$ | 3 | $81 \pm 8$ | + |
| $\Delta cheD$ | 1 | 23 | + |
| $cheY^{**}$ | 2 | $17 \pm 2$ | - |

**Table 3.11: Quantitative estimation of chemotactic efficiency by comparison of wild type and *che* mutant swarm ring diameter**. To allow direct comparison of the chemotactic efficiency, equal amounts of wild type and mutant cells ($6 - 8 \cdot 10^6$, depending on the experiment) were injected underneath the surface of the same semi-solid soft-agar peptone plate (0.3% agar (w/v)). The diameters were measured after incubation for 4 to 7 days at 37°C in the dark. Where reasonable, standard deviations are given. Numbers in parentheses in strain designation of complemented strains denote which clone was complemented.

(1996) found that "although not forming a true swarm, the $\Delta$B strain showed a slightly expanded and fuzzy swarm compared to the non-swarming [$\Delta$A and $\Delta$Y] mutants". The difference may be due to technical differences of gene deletion. While the cloning strategy described here attempts to produce minimal side effects on neighboring genes, the $\Delta$B mutant described earlier is only a partial gene deletion that might have additional polar effects (for a detailed explanation see section 3.4.3). Both the *cheC1* mutant described here and the *cheC1* mutant described by Rudolph and Oesterhelt (1996) were found to be able to perform albeit impaired chemotaxis.

## 3.4.10 *H. salinarum* CheR is a methyltransferase and CheB is a methylesterase and glutamine deamidase

The homology of *H. salinarum* CheR and CheB proteins to their bacterial namesakes is a strong indication for *H. salinarum* CheR and CheB to act as methyltransferase and methylesterase, respectively. In *E. coli*, CheB has an additional deamidase activity that converts certain Gln residues in the adaptation region of the MCPs into Glu to render them methylatable (Kehry et al., 1983b,a). However, in *B. subtilis*, CheD rather than CheB is the transducer Gln deamidase at least in case of the McpA transducer (Kristich and Ordal, 2002). As *H. salinarum* has both CheB and CheD, the question arises which of the two proteins is responsible for deamidation of *H. salinarum* transducers. The results obtained in this study clearly show an involvement of CheR, CheB and CheD in photo and chemotaxis, but the phenotypes of the $\Delta cheR$, $\Delta cheB$ and $\Delta cheD$ mutants are not sufficient to allow unambiguous functional assignment. To address this question, the transducer methylation states in the $\Delta cheR$ and $\Delta cheB$ mutants were studied.

The first experimental hint toward a function of *H. salinarum* CheR as methyltransferase and CheB as methylesterase came from Western Blot analysis of membrane fractions from S9 (wild type) and the Δ*cheR* and Δ*cheB* mutants (Koch and Oesterhelt, 2005).
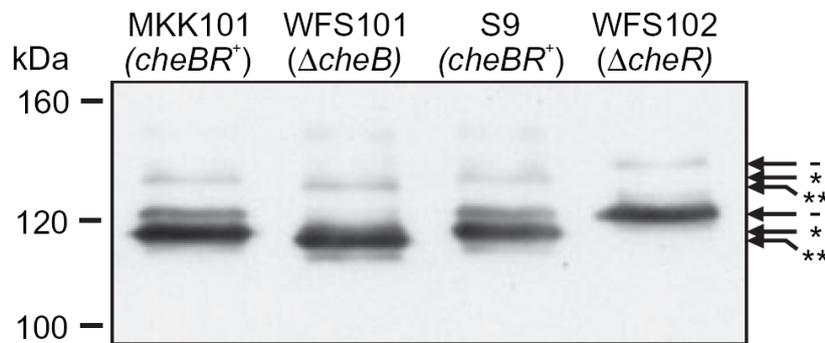


**Figure 3.32: Western Blot of S9, Δ*cheR* and Δ*cheB* membrane fractions showing different mobilities of Htr14 species caused by different degrees of methylation.** Arrows mark the band positions attributed to putatively unmethylated (–), moderately methylated (*) and highly methylated (**) species of MpcT, which are the most prominent (or the only) species in the Δ*cheR*, *cheBR*⁺ and Δ*cheB* strains respectively. Strains WFS101 and WFS102 are the Δ*cheR* and Δ*cheB* mutants, respectively, that were generated during this study. Taken from Koch and Oesterhelt (2005).

Altogether, two groups of triplet bands were detected by an MpcT specific antibody (see Fig. 3.32). While the two groups of bands may be attributed to two majorly different conformations of MpcT with the dominant species at a lower apparent MW of approx. 120 kDa, the occurrence of the triplets was attributed to MpcT species that have different degrees of methylation. It is known from *E. coli* that the methylation state influences the migration behavior of MCPs in SDS gels (Boyd and Simon, 1980; Kehry and Dahlquist, 1982). An increase in methylation increases the electrophoretic mobility of MCPs in SDS gels. In case of the *H. salinarum* Δ*cheB* mutant, the lowest band of the triplet was most abundant, in wild type the intermediate band was most abundant, and in case of the Δ*cheR* mutant only the upper band was seen. This observation is consistent with the putative roles of *H. salinarum* CheR and CheB as methyltransferase and methylesterase, respectively. A lack of CheR should result in unmethylated, slow migrating MpcT and a lack of CheB should result in highly methylated, fast migrating MpcT. The assignment of the triplet bands as differentially methylated MpcT species was later confirmed by mass spectrometry (see below). Interestingly, the use of the HC23 antibody (Zhang et al., 1996) that recognizes the signaling domain of Htrs revealed that methylation-dependent shifts are only seen for MpcT.

In order to identify the *in vivo* methylation and deamidation sites of Htrs, a mass spectrometric approach was chosen (Koch, 2005; Koch et al., 2007). To this end membrane fractions of wild type, Δ*cheR* and Δ*cheB* were separated in SDS gels. The protein bands were cut out, the proteins in-gel digested with the protease Asp-N and the resulting peptides were analyzed by liquid chromatography electro-spray ionization tandem mass spectrometry (LC ESI MS/MS). This technique allows to discriminate between methylated and unmethylated peptides and may ideally unambiguously identify the methylation

site within the peptide. In addition, it allows to detect deamidation of Gln residues to Glu and their subsequent methylation. In the Htr4 peptide DEMSATIEEVAASA from wild type indications for double methylation of the underlined Glu pair were found. Due to its higher abundance, the doubly methylated form of the peptide was unambiguously identified in preparations from $\Delta cheB$. For the aforementioned Htr4 peptide from S9 approximate ratios of unmethylated to singly methylated to doubly methylated were 47% : 52% : < 1% and for the Htr5 peptide DLSAAIEEVAASA from S9 similar ratios were found. In contrast, ratios for the Htr4 peptide from the $\Delta cheB$ mutant were $\approx$ 0% : 36% : 64%. Thus, virtually no unmethylated peptide was found in the $\Delta cheB$ mutant, which strongly suggests a methylesterase activity CheB as methylesterase. However, there was a considerable amount of the singly methylated species. Several reasons may account for this. Either CheR did not have access to all methylation sites e.g. due the conformational state of the transducer or due to receptor clustering or there is a certain rate of spontaneous, CheB independent hydrolysis. Alternatively, CheD might act as additional methylesterase. In *T. maritima* both CheB and CheD act as methylesterases that recognize different substrate sites with some overlap in specificity (Chao et al., 2006). In case of the $\Delta cheR$ mutant, no methylated peptides were found. This means that in comparison to wild type the methylation state of transducers in the $\Delta cheR$ mutant is changed more drastically than in the $\Delta cheB$ mutant.

Transducer deamidation was also analysed by LC ESI MS/MS. In wild type, deamidations were identified in Htr2, Htr4, Htr15, Htr6 and in addition indications for deamidation were found in Htr13. In contrast, deamidations of Htr4 and Htr2 were not found in the $\Delta cheB$ mutant, which indicates that CheB rather than CheD is the deamidase at least for Htr4 and Htr2. Thus, *H. salinarum* is similar to *E. coli*, but differs from *B. subtilis* with respect to receptor deamidation. The effect of the *cheD* deletion has not yet been determined. Therefore it is still possible that both CheB and CheD are deamidases that recognize different substrate sites. In *T. maritima* CheD is the receoptor deamidase, but in addition is a methylesterases that recognizes different substrate sites than CheB with some overlap of specificity. Although so far not reported, it may be that *T. maritima* CheB is also a receptor deamidase that recognizes different substrate sites than CheD and the same may apply to *H. salinarum* CheB.

## 3.4.11 Comparison of the phototactic and chemotactic responses of the *che* mutants suggests the existence of alternative Htr-mediated signaling pathways

The phototactic and chemotactic efficiencies of the *che* gene deletion mutants and the $cheY^{**}$ mutant were analyzed by two complementary assays: computerized cell tracking and the swarm plate assay. Results are summarized in Table 3.12.

The first remarkable observation is that there are obvious discrepancies between the chemotactic and phototactic efficiencies of the mutants. Except the $cheY^{**}$ mutant, all other mutants formed a chemotactic zone, which indicates that these mutants were still capable to perform at least residual chemotaxis. In contrast, the $\Delta cheR$ and the $\Delta cheD$ mutants did not respond to light stimuli. From the phototactic behavior of the $\Delta cheB$

mutant, one would expect that this mutant swarms best of all mutants. However, the swarms of this mutant are comparable to that of the non-phototactic $\Delta cheR$ mutant. On the other hand, the $\Delta cheC3$ mutant that showed weaker phototactic responses than the $\Delta cheB$ and $\Delta cheC1$ mutants swarmed more efficiently than all other mutants.

| Mutant | Phobic Phototaxis: computerized cell tracking | | | Chemotaxis: Swarm plates |
|---|---|---|---|---|
|  | Spontaneous | Blue (HtrII) | Orange (HtrI) |  |
| wild type | + + + | + + + | + + + | + + + |
| $\Delta cheB$ | + + + | + + | + + | + (+) |
| $\Delta cheR$ | + | - | - | + (+) |
| $\Delta cheC1$ | + + | + + | + + | + + |
| $\Delta cheC3$ | + | - | + | + + (+) |
| $\Delta cheD$ | + | - | - | + |
| $cheY^{**}$ | + | - | - | - |

**Table 3.12: Comparison of the swimming behavior and chemotactic and phototactic responses of the *che* mutants.** Given is a qualitative rating of the reversal frequencies/responses based on the data from Figs. 3.29 and 3.30 and table 3.11. Reversals/responses increase with increasing number of + symbols. (+) equal 0.5 +. + + +: wild type reversal frequency/response; + +: reduced reversal frequency/response; +: strongly reduced reversal frequency/response; -: response absent.

These data raise the question whether the observed differential effects of the single deletions on chemo- and phototaxis are indicative of alternative signal transduction pathways or caused by differences in the setup of the assays.

As for the principle ability to perform chemotaxis or phototaxis, it has to be noted that there is a difference in the temporal course of the phototaxis assay and the swarm plate assay. In the phototaxis assay, stimuli act on the cells only for a very short time. In contrast, the swarm plate assays were performed over a period of at least three days. Thus, in principle, the cells have more time to respond. However, to my knowledge, in *E. coli* differences in the tethered cell assay, in which the response of the cells to relatively short-lived stimuli are measured and the swarm plate assay are not observed.

Another aspect that should not be underestimated, is the difference in stimulus strengths in the two assays. The stimuli in the phototaxis assay were at least close to saturating. In contrast, in swarm plates rather shallow gradients may be expected. In *B. subtilis* the presence of a methylation-independent adaptation system was hypothesized among other things, because a *cheB* mutant was able to respond and adapt to low attractant concentrations but largely impaired in response and adaptation to high attractant concentrations (see section 2.3.5). To apply this hypothesis to *H. salinarum* one has to assume an intermediate stimulus strength in the swarm plate assay which already partially requires the action of the methylation-dependent system. Otherwise, analogous to *B. subtilis*, at sufficiently low concentrations a very close to wild type response would be expected. Given such an intermediate stimulus strength, the presence of a methylation-independent adaptation in *H. salinarum* would explain why deletion of the methyltransferase gene *cheR* abolished response to highly intense light stimuli but still allowed residual swarming, but it does not explain why deletion of the methylesterase gene *cheB* allowed both responses. The answer may lie in the observation that in case of the

$\Delta cheB$ mutant besides doubly methylated transducer peptides also a significant amount of singly methylated peptides were found, which means that in the $\Delta cheB$ mutant steady state methylation of the transducers was closer to the wild type situation than in case of the $\Delta cheR$ mutant (see above). It also allows the speculation that there is an additional methyl group hydrolyzing activity e.g. that of a second methylesterase like CheD that partially counterbalances methylation of transducers by CheR and thus allows some degree of methylation-dependent adaptation. However, in this case one would expect that the $\Delta cheB$ mutant swarms more efficiently than the $\Delta cheR$ mutant, which is not the case.

As for the swarming efficiency, it may be that cells that have a higher CW bias are able to migrate through the soft agar more efficiently as long as they are in principle able to reverse, for it is known that cells swim more efficiently in CW mode than in CCW mode (Marwan et al., 1991). Therefore it might be easier for such cells to traverse obstructions in the agar.

In *E. coli*, each of the Che proteins plays the same role in each of the MCP-mediated signaling pathways. On the other hand, differential effects of Che proteins on signaling mediated by different transducers were indeed reported. In *B. subtilis* deletions of *cheD* and *cheC* have severe effects on McpC mediated signaling, but have rather mild effects on McpB mediated signaling (see section 2.3.5). It was concluded that although CheC and CheD are known to interact, they may also be involved in separate signaling pathways. As explained in section 2.3.6, *H. salinarum* shares considerable similarity with *B. subtilis* chemotaxis. Like *B. subtilis*, *H. salinarum* has an extended set of chemotaxis genes including CheD and CheC homologs and exhibits a very similar methanol release pattern, indicating that the methylation system works in a similar way. Thus, it is possible that e.g. CheC1 and CheC3 are both phosphatases but act in different signaling pathways or alternatively differently contribute to different signaling pathways. Application of this hypothesis to the data presented here indicates that CheC3 may be more important for the HtrII mediated negative phototaxis than for HtrI mediated negative phototaxis.

Unfortunately, the data presented here cannot reveal potential differential effects that may be present in the chemotaxis pathways of *H. salinarum* as in the swarm plate assay the integrated response of an unknown number of transducers is seen.

## 3.4.12 Is *H. salinarum* ParA1 involved in partitioning and localization of cytoplasmic transducer clusters?

The phototactic purple, non-sulfur bacterium *Rhodobacter sphaeroides* has three *che* operons, two of which ($che$Op$_2$ and $che$Op$_3$) are required for chemotaxis under laboratory conditions. Except the CheB homologs which freely diffuse in the cytoplasm and the CheY homologs that could not be localized, the other Che proteins exclusively localize to either a polar or a cytoplasmic receptor cluster (Wadhams et al., 2003). The $che$Op$_3$ operon encodes a protein called PpfA (**p**rotein **p**ositioning **f**actor A, previously called Slp). PpfA is a deviant Walker type ATPase protein (Koonin, 1993) with homology to DNA partitioning factors of the ParA family and the cell-division protein MinD. A *ppfA* deletion mutant ($\Delta ppfA$) showed reduced swarming (Porter et al., 2002).

It turned out that PpfA has a similar role in localization and partitioning of the cytoplasmic, cluster-forming transducers in dividing cells like ParA has in localization and partitioning of plasmids (Thompson et al., 2006). In wild type cells either one midcell localized cytoplasmic receptor cluster or two cytoplasmic clusters localized at one-fourth and three-fourths of the cell length was found. By contrast, $\Delta ppfA$ cells had only one cluster located at the one-fourth position and it seems that upon division only one daughter cell receives a cluster which has a higher than usual protein content. It is assumed that the other daughter cell has to synthesize the cytoplasmic cluster *de novo* before it regains its ability to respond chemotactically. The reduced chemotactic efficiency might therefore be explained by the presence of a certain percentage of cells that have recently divided and do not yet possess a cytoplasmic receptor cluster.

These observations are reminiscent to the situation in *H. salinarum* with respect to the following aspects. In the genome of *H. salinarum* the gene coding for a ParA/MinD homolog, ParA1 (previously named FlaK or MinD1), is cotranscribed with genes of the *fla* gene cluster (see Fig. 3.21, p. 83 and Table 3.2, p. 52). The *fla* gene cluster itself is located in close proximity to the *che* gene cluster. Like in *R. sphaeroides*, no ParB homolog is encoded in proximity to the *parA1* locus. Deletion of the *H. salinarum parA1* resulted in significantly reduced swarming (see Fig. 3.11), however had no influence on the response to a step down in orange light (Staudinger, 2001). This observation is consistent with an involvement of *H. salinarum* ParA1 in partitioning and localization of cytoplasmic transducer cluster(s) analogous to PpfA in *R. spharoides*. In case of motile *H. salinarum* cells the swarm plate assay reflects the integrated response to all chemotactically active substances contained in peptone. Some of these substances may be sensed by cytoplasmic Htrs that may require ParA1 for partitioning and localization in a cluster. In the genome of *H. salinarum*, 6 putatively cytoplasmic transducers were identified (see Fig. 2.13 (B)). Only for two them a function was assigned. One of them is HemAT, which mediates the phobic response to oxygen (Hou et al., 2000), the other is Car, which senses arginine (Storch et al., 1999). A phobic response to oxygen is unlikely to occur in swarm plates, but arginine is surely contained in swarm plates. Thus, in case of swarm plates, deletion of *parA1* can be expected to influence chemotaxis. On the other hand HtrI and HtrII are membrane proteins and expected to be part of the polar clusters. Therefore it is not surprising that deletion of *parA1* had no effect on phototaxis. Unfortunately, it is not known if the putatively cytoplasmic Htrs really form a cytoplasmic cluster. Alternatively, they might colocalize and interact with polarly located transmembrane Htrs as it was observed in case of the soluble *Pseudomonas aeruginosa* receptor McpS (Bardy and Maddock, 2005). Gestwicki et al. (2000) reported only polar localization of Htrs.

The putative presence of cytoplasmic and polar receptor clusters in *H. salinarum* seems to offer a reasonable explanation why *H. salinarum* has three CheC paralogs and two CheW paralogs. At the same time, it would potentially offer an explanation for differential influences of Che proteins on signaling pathways mediated by different Htrs. Like in *R. sphaeroides* some of the paralogs could be involved in signaling of the polar clusters while the others could be involved in signaling of the cytoplasmic clusters. Important Che proteins that constitute the core of the Che machinery i.e. CheA, CheY, CheB and CheR

could be involved in signaling of both clusters. However, this does not seem to be the case for CheC1 and CheC3. The data presented here suggest that both CheC1 and CheC3 are involved in phototaxis mediated by the membrane spanning transducers HtrI and HtrII that are expected to be part of the polar clusters. Similarly, CheW2 is involved in both BasT (2 TM) and Car (soluble) mediated signaling (Aregger, 2003). Thus, assuming that separate signaling pathways exist, they are not separated by localization of transducers in polar and cytoplasmic clusters.

## 3.4.13 Interpretation of the switching frequencies and rotational biases and introduction of a modified motor model

*E. coli* cells swim when their flagellar motors rotate CCW and tumble when they rotate CW. Tumbling leads to a random reorientation of the cells. Without CheY-P the motors rotate CCW and CheY-P binding to the motor switch induces CW rotation. A biased random walk which directs the cells to most favorable conditions is achieved by modulating the ratio of CW (swimming) and CCW (tumbling) events in a CheY-P concentration dependent manner. In other words CheY-P influences the CW bias. An *E. coli* $\Delta cheB$ mutant which has a high steady state CheY-P concentration has a high CW bias and a $\Delta cheR$ mutant which has a low steady state CheY-P concentration has a low CW bias compared to wild type.

In contrast to *E. coli*, *H. salinarum* cells swim forward by CW and back by CCW rotation of the flagellar bundle. Repellent stimuli induce switching events between the two swimming directions and attractant stimuli suppress switching. Orientation toward favorable conditions is achieved by modulating the length of swimming intervals in either direction. Due to the non-switching phenotype of the $\Delta cheY$ mutant, CheY-P was postulated as switch factor in *H. salinarum* taxis that upon stimulation increases in concentration and thereby increases the switching probability of the cells (Rudolph and Oesterhelt, 1996). When the effect of CheY-P on the *E. coli* motor is transferred to the different mode of operation of the *H. salinarum* flagellar motor, one expects that *H. salinarum* mutants with increased steady state concentrations of CheY-P switch more frequently. Deviations of the wild type 50% CW rotational bias due to changed steady state CheY-P concentrations are not expected. However, in this study two unexpected phenomena were observed. All mutants, even those with presumably elevated CheY-P steady state concentrations, exhibited either decreased or wild type switching frequencies and most of the mutants had CW biases that deviate from 50%.

### Interpretation of switching frequencies

Examples of *H. salinarum* mutants with presumably elevated and quasi elevated steady state concentrations of CheY, respectively are e.g. the $\Delta cheB$ and the $cheY^{**}$ mutant. CheY-P levels should be elevated in $\Delta cheB$ for two reasons. First, transducers are higher methylated than in wild type (see section 3.4.10) which should result in higher transducer activity and second, there is no competition between CheY and CheB for phosphate groups from CheA. The assumption that the $cheY^{**}$ mutant has a quasi elevated "CheY-P" concentration is based on the observation that in *E. coli* non-phosphorylated CheY$^{**}$

preferably adopts a CheY-P like conformation and causes increased tumbling of the cells (see section 3.4.2, p. 83 ff. and references therein.). Except $\Delta cheB$, the *che* mutants that were investigated in this study exhibited significantly reduced switching frequencies. In an earlier study, *H. salinarum* cells were subjected to chemical mutagenesis followed by selection for cells with impaired tactic behavior. Notably, only mutants with either wild type like switching behavior or reduced switching, but no mutants with increased switching frequencies were mentioned (Sundberg et al., 1990). This gives rise to the idea that while temporary elevated CheY-P concentrations increase the switching probability, permanently elevated CheY-P concentrations do not.

In section 2.3.8 the main features of a model for the *H. salinarum* motor switch and its photosensory control developed by Nutsch et al. (2005) are illustrated. The motor model is symmetric with respect to CW and CCW rotation and includes $2 \times 4$ motor phases (4 phases for each rotational mode, see Fig. 2.12). In the model, sensory input via CheY-P influences the switch cycle at only two transitions per rotational mode. CheY-P decreases the probability for transition from Refractory to Competent phase but increases the probability for transition from Competent to Active phase.

The model is able to explain why both a $\Delta cheY$ mutant and the $cheY^{**}$ mutant have extremely low switching frequencies and also explains why the $\Delta cheB$ mutant does not exhibit increased switching frequency. At wild type steady state concentrations of CheY-P probabilities are highest for the motor to be in the Competent phase. Without CheY-P the probability for transition from Competent to Active phase is very low. Thus the motor gets "stuck" in the Competent phase for most of the time. In contrast, at very high steady state CheY-P concentrations as presumably mimicked by $CheY^{**}$, the probability for transition from Refractory to Competent phase becomes very low and the motor is "stuck" in the Refractory phase for most of the time. In either situation the probability for motor switching becomes very low and the cells are unable to respond to light stimuli. However, it has to be noted that in both cases the switching probability is not zero, which is consistent with the observation that not only $cheY^{**}$, but also $\Delta cheY$ mutant cells occasionally switch (Weidinger, 2007). From a thermodynamic point of view, the motor continuously and irreversibly runs through a cycle which means that there must be an energy input to drive the cycle. It was suggested that hydrolysis of CheY-P could supply this energy (Nutsch et al., 2005). Switching of the CheY-P deficient $\Delta cheY$ and $cheY^{**}$ mutants suggests, that CheY-P hydrolysis is not this energy source. Thermal energy may be sufficient to drive the cycle. According to the model, CheY-P dependent increased switching probability occurs when stimulation produces a pulse-shaped increase of CheY-P concentrations while steady state CheY-P concentrations that are deviant from that of wild-type lead to reduced switching probability. However, this does not mean that increased switching frequencies cannot occur in unstimulated cells. The high switching frequency that Rudolph and Oesterhelt (1996) reported for their $\Delta cheB$ mutant was not found for the $\Delta cheB$ mutant generated in this study. Therefore it may not have resulted from deletion of *cheB*. However, the observation of the high switching frequency of this mutant as such is well documented. During this study, I occasionally observed wild type cells that switched more than usually observed. Hildebrand and Schimz (1987) reported different switching frequencies in different strains. They were able to further select for

single colonies with either extraordinarily high or low switching frequencies. Upon further cultivation of these cultures switching frequencies became heterogeneous again. One explanation for higher switching frequencies are fluctuations in CheY-P concentration. Another clue comes from the model. Any change of parameters in the model that will enhance transitions between the phases will speed up cycling between CW and CCW and therefore increase switching frequencies.

### Interpretation of rotational biases and introduction of a modified motor model

The observation that the rotational biases of the *che* mutants gradually covered a range from 30% to 99% CW gives an important clue about how the rotational bias is regulated. A possible explanation is that there is a factor that in principle is able to dynamically regulate the bias, but in adapted wild type cells and the mutants has different, however fixed steady state concentrations. An obvious candidate for such a factor is CheY-P. Due to its symmetric nature with respect to CW and CCW rotational modes, the motor model by Nutsch et al. (2005) cannot explain why *che* mutants deviate in their rotational biases from the wild type 50% CW bias. This prompted us to investigate whether it is possible to introduce an asymmetry in the model that results in a CheY-P dependent change of CW biases. This seems to be trivial at first sight, because any parameter that prolongs or shortens the duration of either rotational mode in dependence of the CheY-P concentration will produce such an effect if changed only for CW or CCW mode. However, to be valid, the asymmetric model is still required to explain all phenomena of spontaneous and light-induced motor switching that the original model could explain. And the model has to behave "pseudosymmetric", i.e. at wild type steady state CheY-P concentrations, the model has to reproduce the 50% CW bias of wild type cells.

It was reported by Rudolph and Oesterhelt (1996) and later confirmed by Weidinger (2007) that deletion of *cheY* like the *cheY*$^{**}$ mutation produces a 99% CW bias. Deletion of *cheY* does not only alter the function of CheY but abolishes the molecular function. This may produce additional unexpected effects like reduced instead of increased methanol release upon positive stimulation with orange light (Perazzona and Spudich, 1999). Therefore, we decided to model the *cheY*$^{**}$ mutant.

The model by Nutsch et al. consists of a considerable number of differential equations and associated parameters. In order to identify those parameters for which the model is most sensitive to perturbation with respect to CW bias, we performed a sensitivity analysis (del Rosario et al., 2007). The two most sensitive parameters were $C$ and $R$ with $C$ about two orders of magnitude more sensitive than the other parameters. $R$ and $C$ influence the cooperative transition of the motor switch subunits from Refractory to Competent phase ($R$) and from Competent to Active phase ($C$), respectively. Numerical calculations showed that at high steady state CheY-P concentrations ([CheYP]/[CheYP$_{SS}$] values $> 1$) an increase of 10% in $R$ in the CW mode compared to $R$ in the CCW mode is sufficient to shift the bias to $> 50\%$ CW (Fig. 3.33). Conversely, CheY-P levels below wild type level ([CheYP]/[CheYP$_{SS}$] values $< 1$) lead to a bias $< 50\%$. At the same time at wild type steady state CheY-P concentrations ([CheYP]/[CheYP$_{SS}$] = 1) the CW bias remains close to 50%. The changes in $R$ did not affect reproduction of wild type behavior e.g. the frequency distributions of switching events of unstimulated and light-stimulated

cells. Thus, the modified asymmetric model still explains all experimental data that were considered in the previous model and in addition is able to explain the behavior of the $cheY^{**}$ mutant. It also shows that the symmetric behavior of the motor as observed in wild type cells is probably not an intrinsic property of the motor, but may be caused by the steady state CheY-P concentrations that are found in such cells.
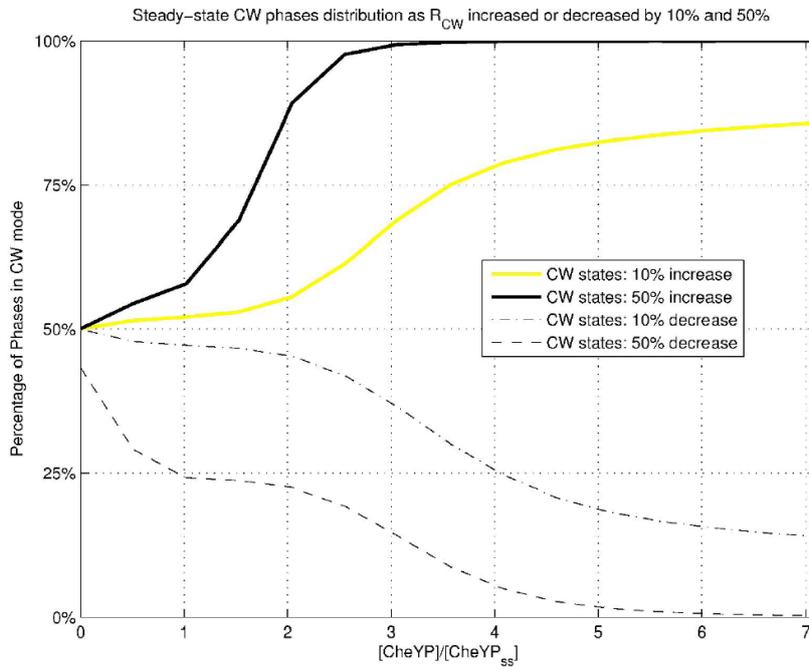


**Figure 3.33: Influence of an asymmetric change in parameter $R$ on the rotational bias at various steady state concentrations of CheY-P.** [CheYP] is the steady state CheY-P level e.g. of mutants. [CheYP$_{SS}$] is the steady state CheY-P level of wild type cells. A 10% increase of parameter $R$ in the CW direction is sufficient to shift the CW/CCW steady-state distribution to CW at high CheY-P levels (yellow plot), but at normal CheY-P levels this is not apparent (52% CW). The shift is towards the counterclockwise mode if $R$ in CW direction is decreased (dash-dot plot). A 50% increase (thick black plot) yields 100% CW rotation at high CheY-P levels while only slightly affecting the distribution at normal CheY-P levels (57% CW). However, a 50% decrease (dashed plot) already causes 25% CW at normal CheY-P levels. Figure and caption are taken from del Rosario et al. (2007).

Most changes in the chemotaxis network e.g. deletion of *che* genes or point mutation of Che proteins result in altered steady state CheY-P levels. Using the asymmetric model and the known or putative functions of the deleted or mutated *che* gene products, CW biases can be predicted. Table 3.13 shows a comparison of the expected steady state CheY-P concentrations in the *che* mutants, the resulting expected CW ratios according to the asymmetric model and the observed CW ratios. In the $\Delta cheR$ mutant a low CheY-P steady state concentration is expected as the transducers are undermethylated and therefore have a very low activity. Deletion of the putative CheY-P phosphatase genes *cheC1* and *cheC3* should result in elevated CheY-P concentrations. In addition, in the *B. subtilis cheC* mutant transducers are overmethylated and the cells swim smooth, which is consistent with a high CheY-P level [4]. In the *B. subtilis cheD* mutant receptors

---

[4] Note that CheY-P has contrary effects on the swimming behavior of *E. coli* and *B. subtilis* (Fig. 2.10,

are undermethylated and the cells tumble frequently which argues for a low CheY-P level in this mutant. The expected CheY-P levels of the $\Delta cheB$ and the $cheY^{**}$ mutant were discussed above.

| *Mutant* | *expected CheY-P conc.* | *expected CW bias* | *observed CW bias* |
|---|---|---|---|
| wild type | intermediate | 50% | 53% |
| $cheY^{**}$ | mimics: very high | very high | 99% |
| $\Delta cheY$ | 0 | very low | 99%[¶] |
| $\Delta cheA$ | very low | very low | 99%[§] |
| $\Delta cheB$ | high | high | 31% |
| $\Delta cheR$ | low | low | 63% |
| $\Delta cheC1$ | high | high | 52% |
| $\Delta cheC3$ | high[†] | high | 72% |
| $\Delta cheD$ | low[‡] | low | 86% |

**Table 3.13: Comparison of expected CheY-P steady state concentrations and expected CW biases with observed CW biases in *che* mutants.** The expected CW bias is based on the modified model of the *H. salinarum* flagellar motor and its sensory control (del Rosario et al., 2007). [¶]: data are from Weidinger (2007); [§]: data are from (Rudolph and Oesterhelt, 1996); [†]: based on the smooth swimming behavior of the *B. subtilis cheC* mutant and the twofold overmethylation of transducers in this mutant (Rosario et al., 1995); [‡]: based on the tumbly swimming behavior of the *B. subtilis cheD* mutant and the undermethylation of transducers in this mutant (Rosario et al., 1995).

Unfortunately predicted and observed CW biases do not fit very well. Two discrepancies are especially apparent. For the $\Delta cheY$ and the $\Delta cheA$ mutants very low CW biases are predicted, but in fact 99% CW are observed (Rudolph and Oesterhelt, 1996; Weidinger, 2007). In the $\Delta cheY$ mutant in addition to CheY-P the unphosphorylated CheY species is missing. It was already mentioned that the lack of unphosphorylated CheY may have unexpected effects (see above). One possible effect is that lack of unphosphorylated CheY may lead to a construction artifact of the motor such that 99% of the motors rotate CW. However there are two arguments that speak against this idea. First, switching events of $\Delta cheY$ mutant cells were occasionally observed (Weidinger, 2007). These switching events should randomize the rotational modes over time. Second, in the $\Delta cheA$ mutant which has also a 99% bias, CheY is present (Rudolph and Oesterhelt, 1996). This points to the lack of CheY-P rather than CheY as cause of the observed 99% CW bias. Discrepancies are also seen in case of the $\Delta cheR$ and $\Delta cheB$ mutants. In case of the $\Delta cheD$, $\Delta cheC1$ and $\Delta cheC3$ mutants, it has to be pointed out that estimation of CheY-P steady state concentrations is quite speculative. Due to the presence of multiple CheC proteins that may or may not interact with CheD, a simple extrapolation based on the *B. subtilis* mutants may be misleading.

Finally, some critical points with respect to the physiological function of the *H. salinarum* CheY$^{**}$ mutant protein have to be discussed. For modeling we assumed that unphosphorylated CheY$^{**}$ mimics a CheY-P species that cannot be deactivated by dephosphorylation. This assumption was based on *in vitro* and *in vivo* data of the corresponding *E. coli* mutant protein and due to the conservation of the mutated amino acid

residues. In *E. coli* CheY-P interacts with FliM to induce CW rotation of the flagellar motor. However, in *H. salinarum* there is no FliM homolog and the protein that interacts with CheY at the flagellar motor is unknown (see section 2.2.4). This means that in *H. salinarum* CheY-P and the motor switch protein may use different interaction sites. In this case the effects of the point mutations are different from the effects in *E. coli*. The *E. coli* CheY is already activated by the DK mutation and the YW mutation enhances the effect (Bourret et al., 1990; Zhu et al., 1996). However, in the bacteria *B. subtilis* and *R. sphaeroides* the respective DK mutations do not result in phenotypes that argue for the presence of an activated CheY species (Bischoff et al., 1993; Porter et al., 2006). Another question is whether the CheY$^{**}$ protein is expressed and correctly folded in *H. salinarum*. Matthias Schlesner found by mass spectrometry that a cellulose-binding domain tagged version of the protein that is expressed from the natural promoter is present, but the quantity and the folding state is currently unknown.

We also tried to model the 99% CW bias of the $\Delta cheY$ mutant. To obtain a high CW bias for zero CheY-P concentration, now parameter $C$ in CW direction had to be changed. Numerical calculations showed that a 65% CW bias can be achieve by a 50% increase of $C$ in CW direction. This shows that no matter whether *H. salinarum* CheY$^{**}$ really mimics hyperactive CheY or whether the $\Delta cheY$ mutant would have been the better choice for modeling, the basic idea behind the modified model, namely that the behavior of wild type cells may disguise the asymmetric nature of the flagellar motor, remains valid.

## 3.4.14 Outlook

Given the lack of data, the current models of the flagellar motor and its sensory control implement adaptation in a very simplified form that only considers methylation by CheR and demethylation by CheB. In the model, CheR methylates transducers at a constant rate and CheB-P demethylates transducers at a rate that is proportional to the CheB-P concentration. However, the data presented here clearly show that CheD, CheC1 and CheC3 are indeed involved in chemo and phototaxis of *H. salinarum* and more specifically in adaptation as suggested by their homologies to the *B. subtilis* proteins. In order to include these proteins in the model, further data are required that either directly or indirectly point to their function.

Using the MpcT antibody, Western Blots of the membrane fractions of the *che* mutants could yield a first indication of the transducer methylation states in these mutants. In *B. subtilis* such analyses revealed large deviations in the methylation states of the transducers from *cheD* and *cheC* mutants (Rosario et al., 1995; Kirby et al., 2001; Kristich and Ordal, 2002). It would be interesting to compare the effects of the $\Delta cheC1$, $\Delta cheC3$ mutation and the $\Delta cheC2$ mutation that was recently generated by Elisabeth Weidinger (2007). Mass spectrometric analysis of transducer methylation states in mutants has proved to yield a deeper insight into the functions of *H. salinarum* CheR and especially CheB. So far, the data point to CheB as the transducer Gln deamidase in *H. salinarum*, but the analysis has not been done with the $\Delta cheD$ mutant and the cytosolic fraction containing the soluble Htrs was excluded from the analysis.

The classical way to show CheY-P phosphatase activities of the *H. salinarum* CheC

homologs would be *in vitro* phosphorylation assays. In these assays CheY is phosphorylated with $^{32}$P and the loss of the label over time is followed in autoradiograhps. A comparison of the kinetics of label loss in absence and presence of the putative phosphatases allows to conclude phosphatase activity. In addition, the phosphatase activities of the CheC homologs could be assayed in presence of CheD to see if CheD activates phosphatase activities of the CheC homologs. Such an approach was successfully applied with the *Thermotoga maritima* proteins that were heterologously expressed in *E. coli* (Chao et al., 2006). The thermophilic nature of these proteins facilitates their separation from the mesophilic *E. coli* proteins. However, in case of *H. salinarum* the situation is different. Heterologous expression of functional halophilic proteins in *E. coli* is not trivial. CheA and CheY had to be purified from inclusion bodies followed by refolding. Another even more serious problem is that the half-life of *H. salinarum* CheY-P seems to be extraordinarily short in the first place. Dephosphorylation of CheA by CheY could only be shown by loss of the label on CheA, the phosphorylated CheY species was not seen on autoradiographs (Rudolph et al., 1995). Given that the CheY preparation was not contaminated with one of the CheC homologs, this means that it will not be possible to study dephosphorylation the classical way and at the same time raises the question whether a CheY-P phosphatase is required in *H. salinarum* at all.

In this study, the effects of specific single deletions of chemotaxis genes were investigated. Surprisingly, in some of the mutants phototaxis and chemotaxis were affected to different degrees e.g. deletion of *cheC3* had severe effects on phototaxis but comparably mild effects on chemotaxis. This observation suggests that alternative Htr-mediated signaling pathways exist. In the case of phototaxis, it was possible to link the effects to the receptors/transducers SRI/HtrI and SRII/HtrII, respectively by investigating the effect of blue light and orange light stimuli. By contrast, the swarm plate assay that was used to study chemotaxis in general does not allow such differentiations. To address the question whether the deletions have differential effects on different Htrs involved in chemotaxis, assays have to be applied that allow the specific stimulation of these Htrs and at the same time allow the analysis of the cells´ response. The analysis is restricted to those Htrs with assigned function (see Fig. 2.13). In the capillary assay chemotactic efficiency is determined by counting the number of cells that swim into capillaries filled with specific chemicals. The tethered cell assay is a microscopic assay in which the cells are tethered via their flagella to the coverslip of a laminar-flow chamber. Depending on the rotational mode of the flagellar motor the cell bodies rotate either CW or CCW. The response of the cells is analyzed by inspection of changes of the rotational direction caused by a laminar flow of chemicals that passes the cells. One advantage of the assay is that it allows a dissection of excitation and adaptation efficiency. In addition, the response to attractant stimuli e.g. by addition of attractant and repellent stimuli e.g. by subsequent removal of the attractant can be analyzed in one setup.

For *B. subtilis*, the existence of a methylation-independent adaptation system that works at low stimulus concentrations was proposed (Kirsch et al., 1993a; Zimmer et al., 2002). In order to study if a methylation-independent adaptation system exists in *H. salinarum*, the response of the *che* mutants to a variety of stimulus strengths has to be analyzed. It may be that some of the *H. salinarum che* mutants are able to respond

and adapt to light intensities that are lower than those applied in this study. This could be done by measuring stimulus-response curves for the mutants. Another approach is to study the response of strains in which transducers lack methylation sites. Ideally, the response and adaptation of a mutant strain that posses only one transducer with its methylation sites removed (e.g. with the respective Glu residues mutated to Ala) could be studied. This could be achieved by reintroducing the gene coding for such a mutated transducer in a transducer-less strain. However, a strain that lacks all 18 or at least a large number of transducers is currently not available. It was shown that replacement of a single transducer species by a non-methylatable variant is not sufficient. In such cases methylation-dependent adaptational assistance by the remaining transducers is observed in both *H. salinarum* and *B. subtilis* (Perazzona and Spudich, 1999; Zimmer et al., 2002). Perazzona and Spudich (1999) expressed HtrI and HtrII variants that were supposed to be non-methylatable in a strain devoid of these transducers and still observed methanol release upon their stimulation. Our studies on transducer methylation sites revealed that in the HtrII variant one methylation site was left that was not mutated, which would explain the methanol release. However, our data indicate that in case of the HtrI variant, all methylation sites were eliminated and thus methanol release must origin from other transducers.

The elucidation of the function of the *R. sphaeroides* PpfA protein may allow to predict the function of *H. salinarum* ParA1. The phenotype of the *H. salinarum* Δ*parA1* mutant and the location of *parA1* near the *che* gene cluster indicates that ParA1 like PpfA may be involved in targeting of soluble transducers to cytoplasmic clusters. Two aspects have to be studied to prove this hypothesis. First of all, the existence of cytoplasmic transducer clusters in *H. salinarum* has to be shown. In case cytoplasmic transducer clusters exist, the growth-stage-dependent localization and number of these clusters in wild type and the *parA1* mutant has to be compared. One possibility is to generate fusions of soluble Htrs e.g. of Car with GFP and study the localization of these Htrs with fluorescence microscopy. As mentioned in section 3.1 this technique is not yet established for *H. salinarum* mostly due to inhibition of GFP fluorescence under halophilic growth conditions. However, in the meantime a salt-tolerant GFP variant was used in another halophilic organism, *Haloferax volcanii* (Reuter and Maupin-Furlow, 2004). This GFP variant may also work in *H. salinarum*. Alternative methods are immunogold labeling, immunofluorescence labeling or cryo EM. Unfortunately, all of these methods require at some stage that the cells are treated with low salt buffer, which usually destroys the cells.

The second aspect is to study more specifically and in more detail the influence of the *parA1* deletion on cytoplasmic *versus* TM transducers. This can be done with the aforementioned capillary and tethered cell assays.

In this study, the CW biases of the mutants were determined by counting the number of cells that were found with their flagellar bundle rotating in either direction. This allows a conclusion about the relative durations of CW and CCW swimming phases, but it does not tell anything about the absolute durations of CW and CCW swimming phases. Deviations from the wild type 50% CW ratio as such are already an interesting phenomenon, but the study of absolute distributions of CW and CCW swimming phases could reveal further deviations from wild type behavior even in the Δ*cheC*1 mutant that

showed a 50% CW bias. A *B. subtilis cheB* mutant has a close to wild type CW bias. However, analysis of the durations of CW and CCW swimming intervals revealed that the wild type bias is due to an almost equivalent decrease of both CW and CCW interval durations (Saulmon et al., 2004). Analysis of absolute CW and CCW durations requires the analysis of the behavior of single cells which could either be done by tethering cells or by single cell tracking. As mentioned in section 3.4.7 tethering of *H. salinarum* cells led to misinterpretations of the rotational bias. Therefore, single cell tracking seems to be the more suitable method.

Another interesting question is what a decreased percentage of responding cells exactly means. It could either mean that a certain percentage of cells never responds while the other cells respond or it could mean that in all cells the signaling efficiency is decreased. In *B. subtilis* it was found in at least two cases that in certain mutants subpopulations with distinct characteristics exist (Kirsch et al., 1993b; Kirby et al., 2001). To study such phenomena single cells have to be studied either in tethered cell assays or by single cell tracking.

# 4 Materials and Methods

## 4.1 Chemicals

All chemicals used in this study were purchased from Sigma-Aldrich (St. Louis, MO, USA) or Merck (Darmstadt, Germany) at the highest purity grade available. Exceptions are indicated within the methods chapters or are listed below:

| | |
|---|---|
| Bacto™ agar | Difco, Detroit, MI, USA |
| Bacto™ tryptone | Difco, Detroit, MI, USA |
| Bacto™ yeast extract | Difco, Detroit, MI, USA |
| BMA Seakem™ LE agarose | Biozym, Hess. Oldendorf, Germany |
| Bromophenolblue | Difco, Detroit, MI, USA |
| CSPD | Roche Diagnostics, Mannheim Germany |
| DIG-11-dUTP | Roche Diagnostics, Mannheim Germany |
| DNA ladder 1 kb | Invitrogen, Karlsruhe, Germany |
| DNA ladder 100 bp | Peqlab, Erlangen, Germany |
| Neutralized bacteriological peptone L34 | Oxoid, Basingstoke, Hampshire, UK |
| Paraffin wax white, pastilles, congealing point 50 - 61°C | Riedel de Haen, Seelze, Germany |
| $PEG_{600}$ | Sigma Aldrich, St. Louis, USA |
| Tris | Riedel de Haen, Seelze, Germany |
| Vaseline white | Riedel de Haen, Seelze, Germany |

## 4.2 Kits and Enzymes

All restriction enzymes were purchased from New England Biolabs, Beverly, MI, USA. Other enzymes or kits used in this study are listed below (in alphabetical order):

| | |
|---|---|
| ABI Prism Big Dye™ Cycle Sequencing Ready Reaction Kit | Applied Biosystems, Foster City, CA, USA |
| Anti Digoxigenin AP $F_{ab}$ fragments | Roche Diagnostics, Mannheim Germany |
| Pfu Turbo™ DNA polymerase | Stratagene, La Jolla, CA, USA |
| Phusion™ DNA polymerase | Finnzymes OY, Espoo, Finland |
| QIAprep™ Spin Miniprep Kit | Qiagen, Hilden, Germany |
| QIAquick™ Gel Extraction Kit | Qiagen, Hilden, Germany |
| Sawady Taq DNA polymerase | Peqlab Biotechnologie GmbH, Erlangen, Germany |
| T4 DNA ligase | Gibco BRL, Karlsruhe, Germany |

# 4.3 Microbiological materials and methods

## 4.3.1 Strains and culture conditions

### Overview of strains

The *E. coli* and *H. salinarum* strains that were used or generated in the course of this study are listed in Table 4.1, p. 121.

### Culturing of *E. coli*

*E. coli* cells were grown in LB medium, supplemented with ampicillin if indicated, at 37°C with constant shaking at 250 rpm. To isolate single colonies, cells were plated onto LB agar plates containing ampicillin if indicated.

### Culturing and storage of *H. salinarum*

Unless stated otherwise, cultures were grown aerobically in the dark in *H. salinarum* complex medium under constant shaking at 100 rpm and 40°C. Typically 35 ml of complex medium in a 100 ml Erlenmeyer flask were inoculated with 500 µl (1.4% (v/v)) of a 5 day old starter culture. For long term storage 17 ml of a culture that was grown freshly for 5 days were transferred to a sterile 20 ml polyethylene vial. The vial was tightly closed and stored at room temperature in the dark. Starter cultures for chemotactic and phototactic assays were generated in the same manner but stored at 4°C in the dark for at most two years. Cell growth was monitored by measuring the optical density at 600 nm ($OD_{600}$) in a spectrophotometer (Ultrospec 3000, Pharmacia Biotech, Uppsala, Sweden). As a rule of thumb 1 ml of culture of an $OD_{600} = 1.0$ contains $1.34 \cdot 10^9$ cells.

### Selection of motile halobacterial cells

To generate highly motile cultures, 10 µl of a freshly grown culture ($OD_{600} = 0.4 - 0.8$) were injected underneath the surface of a soft agar plate (swarm plate), which contained 0.3% (w/v) agar in complex medium. Preparation of swarm plates is described in section 4.5.1. The plates were incubated at 37°C in the dark, until the emerging "swarm ring" had a diameter of 7.5 cm. The procedure was then repeated twice with 10 µl of cell-agar mixture isolated from the outer ring. From the final swarm plate 5 times 10 µl of cell-agar mixture were isolated from the outmost ring, inoculated in 35 ml complex medium and grown under standard conditions. If not indicated otherwise, the culture was plated to isolate single colonies that were then tested for motility and functional phototactic behavior. A detailed description of the process underlying swarm ring formation is given in section 3.2.5, page 62.

None of the strains generated in this study by recombinant techniques was subjected to swarm plate selection, in order to avoid unwanted alterations in the genotype.

## 4.3.2 Plasmids

All plasmids used in this study were generated by cloning restriction digested PCR frag-

| strain (published name) | relevant phenotype/genotype $^{a,b,c}$ [source or reference] |
|---|---|
| **_E. coli_** | |
| DH5$\alpha$ | F$^-$ $\phi$80d$lacZ\Delta$M15 $\Delta(lacZYA-argF)$ U169 $recA1$ $endA1$ $hsdR17$(r$_k$$^-$, m$_k$$^+$) $phoA$ $suppE44$ $\lambda^-$ $thi$-1 $gyrA96$ $relA1$ [Invitrogen, Karlsruhe, Germany] |
| TOP10 | F$^-$ $mcrA$ $\Delta(mrr-hsdRMS-mcrBC)$ $\phi$80$lacZ\Delta$M15 $\Delta lacX74$ $recA1$ $ara\Delta139$ $\Delta(ara-leu)7697$ $galU$ $galK$ $rpsL$ (Str$^R$) $endA1$ $nupG$ [Invitrogen, Karlsruhe, Germany] |
| **_H. salinarum_** | |
| S9 | BR$^{++}$, HR$^+$, SRI$^+$, Htr1$^+$, SRII$^+$, Htr2$^+$, Htr11$^+$ [(Wagner et al., 1981) ] |
| S9$_{\rm mot}$ | Genotype of S9, except for $htr11^{+/-}$. A highly motile single colony isolate of the S9 strain collected from expanding rings on a swarm plate [(Storch et al., 1999)] |
| D1 | BR$^-$, HR$^-$, SRI$^-$, SRII$^+$ [(Scharf et al., 1992; Ferrando-May et al., 1993)] |
| S9$\Delta flaD$ | Like S9, except $\Delta flaD$. Generated from S9$_{\rm mot}$ by deletion of $flaD$ using plasmid pWS$\beta\Delta flaD$ [this study] |
| S9$\Delta flaD/flaD^+$ | S9$\Delta flaD$ complemented with $flaD$ using plasmid pWS$\beta flaD$ [this study] |
| S9$\Delta flaCE$ | Generated from S9$_{\rm mot}$ by deletion of $flaCE$ using plasmid pWS$\beta\Delta flaCE$ [this study] |
| S9$\Delta flaCE/flaCE^+$ | S9$\Delta flaCE$ complemented with $flaCE$ using plasmid pWS$\beta flaCE$ [this study] |
| S9$\Delta flaJ$ | Generated from S9$_{\rm mot}$ by deletion of $flaJ$ using plasmid pWS$\beta\Delta flaJ$ [this study] |
| S9$\Delta flaJ/flaJ^+$ | S9$\Delta flaJ$ complemented with $flaJ$ using plasmid pWS$\beta flaJ$ [this study] |
| S9$\Delta flgXXX$ | Generated from S9$_{\rm mot}$ by deletion of $flgXXX$ using plasmid pWS$\beta\Delta flgXXX$ [this study] |
| S9$\Delta cheB$ (WFS101) | Generated from S9$_{\rm mot}$ by deletion of $cheB$ using plasmid pWS$\beta\Delta cheB$ [this study, (Koch and Oesterhelt, 2005)] |
| S9$\Delta cheB/cheB^+$ | S9$\Delta cheB$ complemented with $cheB$ using plasmid pWS$\beta cheB$ [this study] |
| S9$\Delta cheR$ (WFS102) | Generated from S9$_{\rm mot}$ by deletion of $cheR$ using plasmid pWS$\beta\Delta cheR$ [this study, (Koch and Oesterhelt, 2005)] |
| S9$\Delta cheR/cheR^+$ | S9$\Delta cheR$ complemented with $cheR$ using plasmid pWS$\beta cheR$ [this study] |
| S9$\Delta cheC1$ | Generated from S9$_{\rm mot}$ by deletion of $cheC1$ using plasmid pWS$\beta\Delta cheC1$ [this study] |
| S9$\Delta cheC3$ | Like S9, except $\Delta cheC3$. Generated from S9$_{\rm mot}$ by deletion of $cheC3$ using plasmid pWS$\beta\Delta cheC3$ [this study] |
| S9$\Delta cheD$ | Generated from S9$_{\rm mot}$ by deletion of $cheD$ using plasmid pWS$\beta\Delta cheD$ [this study] |
| S9$cheY^{\rm D10K,Y100W}$ | Like S9, except $cheY^{\rm D10K,Y100W}$. Generated from S9$_{\rm mot}$ by exchange of $cheY$ for $cheY^{\rm D10K,Y100W}$ using plasmid pMS7 [this study] |

**a:** Information about all mentioned halobacterial genes, their sequences and additional names is available from the HaloLex database `http://www.halolex.mpg.de`.
**b:** Information about the exact position of the deleted nucleotides is given in Table 4.2, p. 123.
**c:** +: present (in typical amounts), ++: overexpressed, $htr11^{+/-}$: in a subpopulation of S9$_{\rm mot}$ $htr11$ is missing [(Matthias Koch, unpublished)].

**Table 4.1:** Overview of strains

ments into the multiple cloning site of pMKK100 (Koch and Oesterhelt, 2005) with one exception: pMS7 was constructed by Matthias Schlesner in a joint project from plasmid pANX (Valery Tarasov, unpublished). A list of all plasmids and their features is given in Table 4.2: Overview of plasmids, p. 123.

### 4.3.3 Media and antibiotics

#### Media for *E. coli*

| **LB medium** | | | |
|---|---|---|---|
| 1% | tryptone | 10 g | tryptone |
| 0.5% | yeast extract | 5 g | yeast extract |
| 0.5% | NaCl | 5 g | NaCl |
| | | ad 1 l | $H_2O$ |

| **SOC medium** | | | |
|---|---|---|---|
| 2% | tryptone | 20 g | tryptone |
| 0.5% | yeast extract | 5 g | yeast extract |
| 8.6 mM | NaCl | 0.5 g | NaCl |
| 2.5 mM | KCl | 10 ml | 0.25 M KCl |
| 10 mM | $MgCl_2$ | 5 ml | 2 M $MgCl_2$ |
| 20 mM | glucose | 20 ml | 1 M glucose |
| | | ad 1 l | $H_2O$ |

The filter-sterilized solutions of $MgCl_2$ and glucose are added after autoclaving and cooling to approx. 60°C.

#### Complex medium for *H. salinarum*

| **H. salinarum complex medium** (Oesterhelt and Krippahl, 1983) | | | |
|---|---|---|---|
| 81 mM | $MgSO_4$ | 20 g | $MgSO_4$·$7H_2O$ |
| 10 mM | $Na_3$citrate | 3 g | $Na_3$citrate·$2H_2O$ |
| 27 mM | KCl | 2 g | KCl |
| 4.3 M | NaCl | 250 g | NaCl |
| 1% (w/v) | peptone (L34, Oxoid) | 10 g | peptone (L34, Oxoid) |
| | | ad 1 l | $H_2O$ |
| pH is adjusted to 7.0 with NaOH | | | |

#### Antibiotics

The following antibiotics were used in the course of this study:

| *Antibiotic* | *stock solution* | *final concentration* |
|---|---|---|
| ampicillin | 100 mg/ml in water (filter sterilized) | 100 µg/ml |
| mevinolin (lovastatin) | 10 mg/ml in ethanol | 10 µg/ml |
| novobiocin | 0.5 mg/ml | 0.15 - 0.2 µg/ml |

The mevinolin (monacolin K, lovastatin, 404.5 g/mol) stock solution was prepared by ethanol extraction of Mevinacor™-tablets (MSD Sharp & Dohme, Haar, Germany). 10 tablets of 20 mg lovastatin each were ground up in a mortar and suspended in 20 ml of ethanol p.A.. The suspension was shaken in a Falcon tube at room temperature for

| plasmid name | description of the plasmid [reference] |
|---|---|
| pMKK100 | 7213 bp *E. coli*/*H. salinarum* shuttle vector with the following features:<br>1. *E. coli* origin of replication for plasmid propagation in *E. coli*<br>2. ampicillin resistance marker for selection of *E. coli* transformants<br>3. mevinolin resistance marker for selection of *H. salinarum* transformants<br>4. halophilic $\beta$-galactosidase gene *bgaH* as additional selection marker for<br>   *H. salinarum* (see red-blue clone screening, p. 126)<br>5. multiple cloning site (MCS) [(Koch and Oesterhelt, 2005)] |
| pWS$\beta\Delta flaD$ | 8058 bp suicide vector, containing a *Pst*I/*Xba*I digested $\Delta flaD$ fragment:<br>-425 to +915 present, but lacking +10 to +468 (*flaD*: 471 bp) [this study] |
| pWS$\beta flaD$ | 8517 bp suicide vector, containing a *Pst*I/*Xba*I digested *flaD* fragment:<br>-425 to +915 [this study] |
| pWS$\beta\Delta flaCE$ | 8160 bp suicide vector, containing a *Pst*I/*Xba*I digested $\Delta flaCE$ fragment:<br>-452 to +1963 present, but lacking +43 to +1473 (*flaCE*: 1515 bp) [this study] |
| pWS$\beta flaCE$ | 9591 bp suicide vector, containing a *Pst*I/*Xba*I digested *flaCE* fragment:<br>-452 to +1963 [this study] |
| pWS$\beta\Delta flaJ$ | 8015 bp suicide vector, containing a *Pst*I/*Xba*I digested $\Delta flaJ$ fragment:<br>-398 to +2186 present, but lacking +1 to +1746 (*flaJ*: 1746 bp) [this study] |
| pWS$\beta flaJ$ | 9761 bp suicide vector, containing a *Pst*I/*Xba*I digested $\Delta flaJ$ fragment:<br>-398 to +2186 [this study] |
| pWS$\beta\Delta flgXXX$ | 8002 bp suicide vector, containing a *Pst*I/*Xba*I digested $\Delta flgXXX$ fragment:<br>-401 to +1048 present, but lacking +16 to +639 (*flgXXX*: 624 bp) [this study] |
| pWS$\beta\Delta cheB$ | 8020 bp suicide vector, containing a *Pst*I/*Xba*I digested $\Delta cheB$ fragment:<br>-348 to +1503 present, but lacking +19 to +1026. (*cheB*: 1044 bp) [this study] |
| pWS$\beta cheB$ | 9028 bp suicide vector, containing a *Pst*I/*Xba*I digested *cheB* fragment:<br>-348 to +1445 [this study] |
| pWS$\beta\Delta cheR$ | 8074 bp suicide vector, containing a *Pst*I/*Xba*I digested *cheR* fragment:<br>-333 to +1281 present, but lacking +91 to +807 (*cheR*: 807 bp) [this study] |
| pWS$\beta cheR$ | 8791 bp suicide vector, containing a *Pst*I/*Xba*I digested *cheR* fragment:<br>-333 to +1281 [this study] |
| pWS$\beta\Delta cheC1$ | 8062 bp suicide vector, containing a *Pst*I/*Xba*I digested *cheC1* fragment:<br>-463 to +1010 present, but lacking +1 to +588. (*cheC1*: 588 bp) [this study] |
| pWS$\beta\Delta cheC3$ | 8231 bp suicide vector, containing a *Pst*I/*Xba*I digested *cheC3* fragment:<br>-439 to +1743 present, but lacking +1 to +1128 (*cheC3*: 1140 bp) [this study] |
| pWS$\beta\Delta cheD$ | 8090 bp suicide vector, containing a *Pst*I/*Xba*I digested *cheD* fragment:<br>-472 to +888 present, but lacking +7 to +453. (*cheD*: 468 bp) [this study] |
| pANX | 9401 bp *E. coli*/*H. salinarum* shuttle vector with the same basic features as<br>pMKK100, except that it contains a novobiocin selection marker instead<br>of a mevinolin marker and a MCS is missing [(Valery Tarasov, unpublished)]. |
| pMS7 | 9960 bp suicide vector derived from pANX by replacing a *flgA1* fragment<br>between *Pst*I and *Xba*I with a *Pst*I/*Xba*I digested *cheY*$^{\mathrm{D10K,Y100W}}$ fragment:<br>-416 to +751 (*cheY*: 468 bp). Mutations are: 1. CGAC beginning at +27 to<br>TAAA, destroying a *Sal*I site and introducing mutation D10K. 2. T at +288<br>mutated to C, introducing a *Nae*I site and 3. AC beginning at +299 mutated<br>to GG, introducing mutation Y100W. [(Matthias Schlesner, unpublished)] |

**Table 4.2:** Overview of plasmids

1 h and centrifuged at $5000 \cdot g$ for 5 min. The supernatant was filtered through a sterile 0.22 µm PVDF-filter. All antibiotics were stored at - 20°C.

## 4.3.4 Transformation of *E. coli*

### Preparation of electrocompetent cells

500 ml LB medium were inoculated with 5 ml of an overnight culture of DH5$\alpha$ cells (35 ml LB medium, inoculated from a plate, shaken at 37°C, 250 rpm). The cells were grown at 37°C and 250 rpm to a density of $OD_{600} = 0.5 - 0.7$, cooled down to 4°C and pelleted by centrifugation (GS3 rotor, 3000·g, 20 min, 4°C). All steps were performed at 0 - 4°C using sterile equipment and solutions. The cells were gently resuspended and washed 3 times in decreasing volumes of 10% glycerol (500 ml, 250 ml and 50 ml). The final pellet was resuspended in 800 µl of 10% glycerol. Aliquots of 70 µl were frozen in liquid $N_2$ and stored at $-70$°C.

### Electroporation of *E. coli*

*E. coli* cell were transformed employing the electroporation method. Electrocompetent cells were thawed and kept on ice for all subsequent steps. For each transformation 35 - 50 µl of cells were incubated for 5 min with an appropriate amount of DNA (in the case of ligation reactions 1 - 2 µl, in the case of plasmid propagation the amount of DNA depended on the electrocompetence of the cells) and transferred into electroporation cuvettes (0.2 cm electrode gap, Biorad, München, Germany). The mixture was electro-porated in a Gene Pulser™ (Biorad, München, Germany) with the following settings: 400 $\Omega$, 2.5 kV and 25 µF. Typical values of time constants were between 8 - 9 s. Immediately after electroporation the cells were diluted with 500 µl SOC medium and incubated for 30 – 60 min in a test tube at 37°C and 250 rpm to allow for their regeneration and the expression of the $\beta$-lactamase. Finally, the cells were plated onto ampicillin-containing LB agar plates and incubated at 37°C overnight.

## 4.3.5 Transformation of *H. salinarum*

### PEG transformation

Transformation of *H. salinarum* was performed according to the PEG method (Cline et al., 1989) with minor modifications.

To increase the competence of halobacterial cells, they were cultured two to three times under standard conditions (see section 4.3.1, p. 120) to an $OD_{600} = 0.3 - 0.5$ and finally once more to an $OD_{600} = 0.4 - 0.8$.

2 ml of the final culture were spun down (8000·g, 2 min, RT) and the supernatant removed. After an additional short spinning step, residual medium was removed with a pipette tip to get rid of the largest amount of magnesium. The cell pellet was then gently resuspended in 200 µl spheroplasting solution (SPH). To produce spheroplasts, 10 µl 0.5 M EDTA in SPH were added and the whole mixture incubated at RT until > 99% of the cells were round (typically 10 min incubation was sufficient). Formation of

spheroplasts was checked in the microscope at 400-fold magnification. The spheroplasts were transferred to a 2 ml centrifuge tube containing 2 - 3 µl (approx. 1 µg) plasmid DNA, gently mixed with the DNA and incubated for 5 min at RT. 220 µl of 60% $PEG_{600}$ were filled into the lid of the centrifuge tube and rapidly mixed with the spheroplasts by closing the lid and vigorous shaking of the centrifuge tube to avoid cell lysis due to high local concentrations of $PEG_{600}$. After incubation for 20 min at RT the largest amount of $PEG_{600}$ was removed by addition of 1.6 ml of spheroplast dilution solution (SVL), followed by centrifugation (8000·g, 2 min, RT) and careful decanting of the supernatant. The pellet was gently resuspended in 800 µl complex medium and the cell suspension shaken for 16 to 24 h (250 rpm, 37°C) to allow the cells to restore their S-layer. For selection of transformants 5 aliquots of 80 µl cell suspension each were plated on complex medium plates containing the appropriate antibiotic. The remaining 400 µl of cell suspension were concentrated to 100 µl and plated in the same manner. In this study all plasmids used for transformation carried the gene coding for the halophilic galactosidase gene *bgaH* from *H. volcanii* (Holmes and Dyall-Smith, 2000; Patenge et al., 2000). Therefore, before plating the cells, the plates were supplied with X-Gal (Roth, Karlsruhe, Germany): equal volumes of X-Gal stock solution (40 mg/ml X-Gal in DMF) and sterile, bidistilled $H_2O$ were freshly mixed. Of this mixture 80 µl were spread on each plate. After the X-Gal solution had sufficiently dried, the cells were plated. The plates were placed in a closed transparent plastic box that contained a petri dish filled with BSH to prevent the plates from drying out and incubated at 40°C. Usually, first transformants became visible after 10 to 14 days. As soon as the colonies had grown to a reasonable size, the plastic box containing the plates was placed onto a light box at room temperature until the colonies had developed an unambiguous color.

## Solutions for transformation of *H. salinarum*

| **SPH solution** | | | |
|---|---|---|---|
| 2 M | NaCl | 11.7 g | NaCl |
| 25 mM | KCl | 2.5 ml | 1 M KCl |
| 15% (w/v) | sucrose | 15 g | sucrose |
| | | ad 100 ml | $H_2O$ |

| **0.5 M EDTA in SPH solution** | | | |
|---|---|---|---|
| 0.5 M | EDTA | 9.3 g | $Na_2EDTA \cdot 2H_2O$ |
| 2 M | NaCl | 5.85 g | NaCl |
| 25 mM | KCl | 1.25 ml | 1 M KCl |
| 15% (w/v) | sucrose | 7.5 g | sucrose |
| 50 mM | Tris/HCl, pH 8.75 | 2.5 ml | 1 M Tris/HCl, pH 8.75 |
| | | ad 50 ml | $H_2O$ |
| To dissolve the EDTA, the pH is adjusted to 8.75 with 10 M NaOH. | | | |

| **60% (w/v) $PEG_{600}$ in SPH solution** |
|---|
| Like SPH solution, but additionally containing 60% (w/v) $PEG_{600}$ (Merck, Darmstadt, Germany) |

| SVL solution | | | |
|---|---|---|---|
| 4.3 M | NaCl | 25.1 g | NaCl |
| 80 mM | $MgCl_2$ | 8 ml | 1 M $MgCl_2$ |
| 10 mM | $Na_3$citrate | 1 ml | 1 M $Na_3$citrate |
| 1.4 mM | $CaCl_2$ | 140 µl | 1 M $CaCl_2$ |
| 15% (w/v) | sucrose | 15 g | sucrose |
| 50 mM | Tris/HCl, pH 7.4 | 5 ml | 1 M Tris/HCl, pH 7.4 |
| | | ad 100 ml | $H_2O$ |

All solutions were sterilized by filtration through a 0.22 µm filter (Rotilabo™ syringe filter, Roth, Karlsruhe, Germany) and kept at 4°C until use. They were brought to RT directly before use.

## Blue-red colony screening

For selection of single colonies of the desired genotype a recently established, time saving red-blue selection method was employed (Koch and Oesterhelt, 2005). All plasmids used in this study to transform halobacterial cells were suicide plasmids containing either a mevinolin or a novobiocin resistance gene and the gene coding for the halophilic galactosidase gene *bgaH* from *H. volcanii* (Holmes and Dyall-Smith, 2000; Patenge et al., 2000). In a first homologous recombination event the plasmid is integrated into the genome. Positive transformants were therefore resistant against the respective antibiotic and developed a blue color on X-Gal containing plates. Blue, antibiotic resistant single colonies were then picked and cultured 2 to 4 times in antibiotic-free complex medium to allow for a second homologous recombination event in which the plasmid together with its antibiotic resistance and *bgaH* genes is lost again. Thus, after plating the cells on X-Gal containing complex medium plates without antibiotic, colonies that had undergone the desired second recombination event (approx. 5% in total) could be easily identified on the basis of their purple/red color caused by bacteriorhodopsin and bacterioruberin. In $\leq 50\%$ of the red colonies the genotype of the parental strain was restored, whereas the rest had the desired genotype, which was finally verified via Southern Blot analysis.

# 4.4 Molecularbiological Methods

## 4.4.1 Preparation of unpurified ("crude") DNA from *H. salinarum*

Halobacterial DNA for PCR and Southern Blot analysis was prepared by water lysis of cells without further purification. 1.2 ODml of a fresh halobacterial culture were spun down ($10,600 \cdot$ g, 2 min) and the supernatant removed. After an additional short spinning step, residual liquid was removed with a pipette tip to get rid of the largest amount of salt. The pellet was then lysed by adding 400 µl of sterile deionized water and immediate rapid up- and down pipetting until all lumps were dissolved and a uniform solution was obtained. 1 µl of this DNA contained approx. 10 ng of DNA from $4 \cdot 10^6$ cells. The DNA preparation was stored at 4°C and was used as a template in PCRs for approx. 3 months. DNA for Southern Blot analysis was used within 5 days.

## 4.4.2 Preparation of plasmid DNA from *E. coli*

Plasmid DNA was isolated from *E. coli* cells using the QIAprep Miniprep kit. In brief, a clone of transformed cells was selected on an ampicillin-containing agar plate and the cells were grown overnight (37°C, 250 rpm) in 5 ml of LB medium supplied with ampicillin. Cells from 4 ml of this culture were pelleted and treated according to the manufacturer's protocol. The final elution from the QIAprep column with 2 mM Tris/HCl at pH 8.5 usually yielded 50 µl of plasmid DNA (200 - 600 ng/µl).

## 4.4.3 Isolation of DNA fragments from agarose gels

Electrophoretic separation of DNA fragments was done in gels of 1 - 2% agarose in 1 x TAE buffer at 5 V/cm. The samples were applied to the gels dissolved in 1 x DNA sample buffer. The DNA was visualized by staining the gel for 20 min in ethidium bromide solution ($c_f = 10^{-4}\%$ (w/v)) followed by washing for 20 min in $H_2O$ and exposing it to uv light at 302 nm. For documentation purposes a uv-cabinet equipped with a uv table, a CCD camera connected to a PC and a gel documentation software was used (cabinet: TFPM/WL, Vilber Lourmat, Torcy Z.I. Sud, France; software: BioCapt 11.03). To isolate specific DNA fragments from agarose gels, the QIAquick Gel Extraction kit was used. In brief, a gel slice containing only the desired fragment was excised from the gel and treated according to the manufacturer's protocol.

| *50 x TAE buffer* | | | |
|---|---|---|---|
| 2 M | Tris/acetate, pH 8.5 | 242 g | Tris base |
| | | 57.1 ml | glacial acetic acid |
| 100 mM | EDTA | 37.2 g | Na$_2$EDTA·2H$_2$O |
| | | ad 1 l | H$_2$O |
| The final 1 x TAE electrophoresis buffer is 40 mM Tris/acetate, pH 8.3 and 2 mM EDTA | | | |

| *6 x DNA sample buffer* | | | |
|---|---|---|---|
| 47% (v/v) | glycerol | 5.4 ml | 87% glycerol |
| 10 mM | Tris HCl pH 7.0 | 100 µl | 1 M Tris/HCl, pH 7.0 |
| 0.025% | bromophenolblue | 125 µl | 2% (w/v) bromophenolblue in 20% ethanol |
| 0.025% | xylene cyanol FF | 125 µl | 2% (w/v) xylene cyanol FF in 20% ethanol |
| | | ad 10 ml | $H_2O$ |

## 4.4.4 Determination of DNA concentration

The concentrations of solutions of plasmid DNA or PCR products after purification via agarose gels were determined with a Gene Quant II spectrophotometer (Pharmacia Biotech, Uppsala, Sweden) by measuring the absorption at 260 nm. For a pathlength of 1 cm an absorption of 1.0 corresponds to a concentration of double stranded DNA of 50 µg/ml. For a rough estimation, PCR fragments or digested plasmid were applied on an agarose gel that was stained with ethidium bromide. The brightness of the UV signals of the corresponding bands was then compared to that of the 1.6 kb band of the 1 kb DNA ladder assuming a linear relationship between brightness and amount of DNA. The 1 kb DNA ladder was prepared such that the 1.6 kb band contained 50 ng DNA per 10 µl DNA marker.

## 4.4.5 Sequencing of DNA

Sequencing of DNA templates present in the generated plasmids was done using the method of Sanger. In this study the ABI PRISM BigDye Terminator Cycle Sequencing kit (Applied Biosciences, Foster City, CA, USA) was used. The Terminator Ready Reaction Mix contained the dyelabeled ddNTPs (BigDye terminators), dNTPs (dATP, dCTP, dGTP and dUTP), AmpliTaq DNA polymerase and $MgCl_2$ in Tris/HCl buffer at pH 9.0. The DNA fragments were generated from the template DNA by subjecting the sequencing reaction mix to thermocycling as described below. The product of the sequencing reaction was purified via MicroSpin G-50 columns according to the manufacturer's protocol (Amersham Biosciences, Freiburg, Germany) to remove excessive dNTPs and BigDye terminators. The eluates were dried in a Speedvac for 30 min. Sequencing was performed by gel electrophoresis in an ABI PRISM 377 DNA sequencer (Applied Biosystems, Foster City, CA, USA). For analysis of the electropherograms and to check the generated sequences via alignment to the expected sequences the computer program BioEdit (Hall, 1999) was used.

| *Sequencing reaction mix* | | | |
|---|---|---|---|
| 100 - 200 fmol | plasmid DNA | 1.5 µl | plasmid solution produced by a QIAprep miniprep (200 - 600 ng/µl) |
| 15 pmol | primer | 1.5 µl | 10 pmol/µl primer solution |
| | Terminator Ready Reaction mix | 3 µl | Terminator Ready Reaction mix, Version 2 |
| 1.07 M | betaine | 3 µl | 5 M betaine |
| | | ad 14 µl | $H_2O$ |

| description | temperature | time | number of cycles |
|---|---|---|---|
| DNA melting | 94°C | 20 s | |
| annealing and elongation | 60°C | 4 min | 30 |
| storage | 4°C | $\infty$ | |

## 4.4.6 Generation of PCR fragments and plasmid construction

### Polymerase chain reaction with Phusion™ DNA polymerase

**PCR reaction mixture**

| | |
|---|---|
| forward primer | 20 pmol |
| reverse primer | 20 pmol |
| "crude" DNA | 1 µl (10 ng) |
| DMSO | 1.5 µl |
| Phusion HF buffer (5 x) | 10 µl |
| dNTPs (2.5 mM each) | 4 µl |
| Phusion™ DNA polymerase | 1 U |
| H$_2$O | ad 50 µl |

**Thermocycling conditions**

| description | temperature | time | number of cycles |
|---|---|---|---|
| DNA melting | 98°C | 30 s | 1 |
| DNA melting | 98°C | 10 s | |
| annealing | T$_m$ + 3°C | 30 s | 30 |
| elongation | 72°C | 15 - 30 s/kb | |
| elongation | 72°C | 10 min | 1 |
| storage | 4°C | $\infty$ | |

Calculation of the melting temperature T$_m$ according to the nearest neighbor method was done essentially as described by Breslauer et al. (1986) but using the values published by Sugimoto et al. (1996). For this purpose the Oligonucleotide Properties Calculator OligoCalc by Kibbe (2007) available online at `http://www.basic.northwestern.edu/biotools/oligocalc.html` was used.

### Polymerase chain reaction with Pfu Turbo™ DNA polymerase

**PCR reaction mixture**

| | |
|---|---|
| forward primer | 20 pmol |
| reverse primer | 20 pmol |
| "crude" DNA | 1 µl (10 ng) |
| DMSO | 3 µl |
| Pfu buffer (10 x) | 5 µl |
| dNTPs (2.5 mM each) | 3 µl |
| Pfu Turbo™ DNA polymerase | 1.25 U |
| H$_2$O | ad 50 µl |

### Thermocycling conditions

| description | temperature | time | number of cycles |
|---|---|---|---|
| DNA melting | 96°C | 2 min | 1 |
| DNA melting | 96°C | 15 s | |
| annealing | $T_a = T_m$ - 5°C | 30 s | 30 |
| elongation | 72°C | 1 min/0.5 -0.7 kb | |
| storage | 4°C | $\infty$ | |

Calculation of the melting temperature $T_m$ was done using the formula $T_m = 4(N_G + N_C) + 2(N_A + N_T)$, where $N_X$ is the number of X = G, C, T and A contained in the primer that anneal with the target sequence.

## Polymerase chain reaction with Sawady Taq DNA polymerase

### PCR reaction mixture

| | |
|---|---|
| forward primer | 20 pmol |
| reverse primer | 20 pmol |
| "crude" DNA | 1 µl (10 ng) |
| DMSO | 3 µl |
| reaction buffer Y (10 x) | 5 µl |
| dNTPs (2.5 mM each) | 3 µl |
| Sawady Taq DNA polymerase | 1.25 U |
| H$_2$O | ad 50 µl |

### Thermocycling conditions

| description | temperature | time | number of cycles |
|---|---|---|---|
| DNA melting | 94°C | 2 min | 1 |
| DNA melting | 94°C | 15 s | |
| annealing | $T_a = T_m$ - 3°C | 30 s | 30 |
| elongation | 72°C | 1 min/kb | |
| storage | 4°C | $\infty$ | |

Calculation of the melting temperature $T_m$ was done as for Pfu Turbo™ DNA polymerase.

## Restriction digest

Restriction digests were performed mainly for cloning purposes or to produce DNA fragments from genomic halobacterial DNA suitable for Southern Blot analysis. Digests were done as recommended by the enzyme manufacturer. In case of double digests the buffer was chosen such that the highest possible activity for the combination of both enzymes was achieved. Whenever indicated, BSA was included in the reaction mixture.

| Reaction mixtures for restriction digest | | | |
|---|---|---|---|
| *type of DNA* | *purified PCR product* | *purified plasmid* | *genomic "crude DNA"* |
| NE-buffer (10 x) | 10 µl | 5 µl | 6 µl |
| BSA solution (10 x) | 10 µl | 5 µl | 6 µl |
| DNA fragment | 50 µl | 25 µl | 30 µl |
| endonuclease 1 | 1 µl | 1 µl | 1 µl |
| endonuclease 2 | 1 µl | 1 µl | – |
| H$_2$O | ad 100 µl | ad 50 µl | ad 60 µl |
| incubation conditions | 37°C, 2 - 14 h | 37°C, 2 - 14 h | 37°C, 16 - 24 h |

**Ligation**

Ligation of restriction digested plasmids and PCR fragments was done with T4 DNA ligase (Gibco BRL, Berlin, Germany). Standard reaction mixtures contained plasmid and PCR fragment (insert) in a molar ration of 1:5. Usually 25 ng of plasmid were used. The mass of insert to be used was calculated according to equation 4.1. The corresponding volume of insert solution was calculated from its concentration which was determined photometrically and counterchecked on an ethidium bromide stained agarose gel using the 1.6 kb band of the 1 kb DNA ladder as a reference.

$$mass\,(insert) = 5 \cdot mass\,(plasmid) \cdot \frac{number\ of\ bp\,(insert)}{number\ of\ bp\,(plasmid)} \qquad (4.1)$$

| Reaction mixtures for T4 DNA ligase | |
|---|---|
| reaction buffer (5x) | 2 µl |
| plasmid | 25 ng |
| insert | 5-fold molar amount of plasmid |
| T4 DNA ligase | 1 µl |
| H$_2$O | ad 10 µl |

## 4.4.7 Southern Blot analysis

After two recombination events, the red blue screening method used to generate deletion mutants yielded red single colonies in which either the genotype of the parental strain was restored or the desired deletion was introduced (for an explanation see section 3.1.1 and associated Figure 3.2). To discriminate between these two possibilities, Southern Blot analysis was performed.

Probes for hybridization were digoxigenin labeled PCR products that were generated by incorporation of digoxigenin-labeled dUTP (DIG-11-dUTP) in a PCR. In all cases two probes hybridizing to the upstream region ("PRE" probe) and a region inside of the corresponding gene ("CORE" probe), respectively, were generated. The desired DNA fragment was first amplified from genomic DNA in a standard PCR (see p. 129). Approx. 50 ng of

the purified DNA fragment then served as template for a second PCR reaction in which 1 µl of 1 mM DIG-dUTP in addition to the unlabeled dNTPs was contained. In these PCRs Sawady Taq or Pfu Turbo™ DNA polymerase had to be used since Phusion™ DNA polymerase does not tolerate dUTP as a substrate.

To analyze the genotypes of single colonies, "crude" DNA was prepared and digested with a suitable restriction endonuclease (see restriction digest, p. 130) such that the genomic DNA was cut upstream of the region hybridizing with the PRE probe and downstream of the gene whose presence had to be checked, and created hybridizing DNA fragments that had sizes of 2 - 8kb. Using this strategy, the genotype was verified twice. In cases where the desired deletion had taken place, the PRE probe detected a DNA fragment that, in comparison the to the DNA fragment of the parental strain, was reduced in size by the number of deleted basepairs, whereas the CORE probe did not detect any DNA fragment.

The DNA fragments were separated in a 1% agarose gel and vacuumblotted on a Hybond N nylon membrane (Amersham Biosciences, Freiburg, Germany). Approximately 70 ng of digested genomic DNA were applied per lane. For size determination of the DNA fragments, in at least one of the lanes 8 - 10 µl of digoxigenin labeled DNA molecular weight marker III (Roche Diagnostics, Mannheim, Germany) were included. All gel pretreatment steps like depurination, denaturation and equilibration were done *in situ* on a custom made vacuum blotting apparatus (Olszewska and Jones, 1988). After UV-crosslinking the DNA to the nylon membrane ($2 \times 120{,}000 \ \mu J/cm^2$ with UV Stratalinker™ 2400, Stratagene, La Jolla, USA) all further steps including prehybridization, hybridization, washing and chemiluminescent detection with CSPD solution were performed according to the manufacturer´s recommendations (Roche Diagnostics, Mannheim, Germany).

## Additional materials and solutions

| | |
|---|---|
| vacuumblot apparatus | custom made, MPI of Biochemistry |
| 3 MM Chr cellulose chromatographic paper | Whatman Biometra, Göttingen, Germany |
| hybridization tubes | Boekel Scientific, Feasterville, PA, USA |
| hybridization oven OV 5 | Whatman Biometra, Göttingen, Germany |
| Plastibrand ® polypropylene disposal bags | Brand, Wertheim, Germany |
| heating block | BT3 Science Services, München, Germany |
| x-ray film | Hyperfilm ECL RPN 2103, Amersham Biosciences, Freiburg, Germany |
| x-ray film cassette X-OMATIC™ | Kodak, Stuttgart-Wangen, Germany |
| x-ray developer X-OMAT™ | Kodak, Stuttgart-Wangen, Germany |

**_HCl wash_**

| | | | |
|---|---|---|---|
| 0.25 M | HCl | 21 ml | HCl |
| | | ad 1 l | $H_2O$ |

**_NaOH wash_**

| | | | |
|---|---|---|---|
| 0.5 M | NaOH | 20 g | NaOH |
| 1.5 M | NaCl | 87.6 g | NaCl |
| | | ad 1 l | $H_2O$ |

**_Tris wash_**

| | | | |
|---|---|---|---|
| 0.5 M | Tris/HCl, pH 7.5 | 60.5 g | Tris |
| 1.5 M | NaCl | 87.6 g | NaCl |
| | | ad 1 l | $H_2O$ |

**_20 x SSC_**

| | | | |
|---|---|---|---|
| 3 M | NaCl | 175.2 g | NaCl |
| 0.3 M | $Na_3$citrate | 88.2 g | $Na_3$citrate·$2H_2O$ |
| | | ad 1 l | $H_2O$ |

**_buffer 1_**

| | | | |
|---|---|---|---|
| 0.1 M | maleic acid | 11.7 g | maleic acid |
| 0.15 M | NaCl | 8.8 g | NaCl |
| pH adjusted to 7.5 with NaOH (solid) | | | |
| | | ad 1 l | $H_2O$ |
| autoclaved | | | |

**_buffer 2_**

| | | | |
|---|---|---|---|
| 1% (v/v) | blocking reagent | 10 ml | 10% blocking reagent (w/v) |
| | | ad 100 ml | buffer 1 |
| autoclaved | | | |

**_buffer 3_**

| | | | |
|---|---|---|---|
| 0.1 M | Tris/HCl, pH 9.5 | 12.1 g | Tris |
| 0.1 M | NaCl | 5.8 g | NaCl |
| 50 mM | $MgCl_2$ | 10.2 g | $MgCl_2$·$6H_2O$ |
| | | ad 1 l | $H_2O$ |

| *10% (w/v) blocking reagent* | | | |
|---|---|---|---|
| 10% (w/v) | blocking reagent | 25 g | blocking reagent |
| | buffer 1 | ad 250 ml | buffer 1 |
| autoclaved and stored at 4°C | | | |

| *10% (w/v) N-laurylsarcosine* | | | |
|---|---|---|---|
| 10% (w/v) | N-laurylsarcosine | 40 g | N-laurylsarcosine, sodium salt |
| | ad 400 ml | $H_2O$ | |

| *prehybridization buffer* | | | |
|---|---|---|---|
| 50% (v/v) | formamide | 50 ml | formamide |
| 5 x | SSC | 25 ml | 20 x SSC |
| 2% | blocking reagent | 20 ml | 10% blocking reagent (w/v) |
| 0.1% (v/v) | N-laurylsarcosine | 1 ml | 10% N-Laurylsarcosine (w/v) |
| 0.02% | SDS | 200 µl | 10% SDS (w/v) |
| | | ad 100 ml | $H_2O$ |
| stored at -20°C | | | |

| *hybridization buffer* | |
|---|---|
| formamide | 10 µl |
| DIG PCR probe | 5 µl |
| prehybridization buffer | 30 ml |

10 µl formamide and 5 µl of the DIG labeled probe are mixed and heated for 5 min at 95°C. This mixture is added to the preheated (42°C) hybridization buffer.

| *10% SDS* | | | |
|---|---|---|---|
| 10% (w/v) | SDS | 40 g | sodiumdodecylsulfate |
| | | ad 400 ml | $H_2O$ |

| *hyb wash 1* | | | |
|---|---|---|---|
| 2 x | SSC | 100 ml | 20 x SSC |
| 0.1% (v/v) | SDS | 10 ml | 10% SDS (w/v) |
| | | ad 1 l | $H_2O$ |

| *hyb wash 2* | | | |
|---|---|---|---|
| 0.1 x | SSC | 5 ml | 20 x SSC |
| 0.1% (v/v) | SDS | 10 ml | 10% SDS (w/v) |
| | | ad 1 l | $H_2O$ |

| *wash buffer* | | | |
|---|---|---|---|
| 0.3% (v/v) | Tween 20 | 3 ml | Tween 20 |
| | | ad 1 l | buffer 1 |

Tween 20 is added to autoclaved buffer 1 as autoclaving may destroy Tween 20.

| *CSPD solution* | | | |
|---|---|---|---|
| 0.25 mM | CSPD | 10 µl | CSPD stock solution |
| | | ad 1 ml | buffer 3 |

| *methylene blue staining solution* | | | |
|---|---|---|---|
| 0.03% | methylene blue | 30 mg | methylene blue |
| 3 M | sodium acetate | 24.6 g | sodium acetate |
| pH is adjusted to 5.2 with acetic acid | | | |
| | | ad 100 ml | $H_2O$ |

# 4.5 Behavioral studies

## 4.5.1 Swarm plate assay

### Preparation of swarm plates

Swarm plates consisted of *H. salinarum* complex medium supplemented with 0.25% and 0.3% agar (w/v), respectively. Autoclaving of complex medium together with the agar frequently resulted in soft agar that did not solidify. Therefore, the agar was added to sterile complex medium and was boiled under stirring until the agar was dissolved. After cooling to 80°C, the soft agar was poured into plastic petri dishes (94 mm × 16 mm or 154 mm × 22 mm, both with vents, Greiner Bio-one GmbH, Frickenhausen, Germany). After solidification of the soft agar, the plates were stored upright in plastic boxes at 4°C and brought to RT directly before use. The plates were used within 2 months as longer storage seems to negatively influence the diameter of swarm rings.

### Procedure

Wild type and mutant cultures were grown to an $OD_{600}$ = 0.6 - 0.8 and reinoculated twice with equal amounts of cells to achieve equal cell densities in the final cultures used in the assays. 10 µl of undiluted culture with an $OD_{600}$ = 0.6 - 0.8 were injected with a pipette tip underneath the surface of the soft agar. To guarantee best comparability of swarm ring diameters, mutants and wild type cells were inoculated in the same plate. The plates were incubated for 3 - 6 days at 37°C in the dark. The plates were scanned with a flat bed scanner (e.g. Agfa SnapScan 600) in transparent mode/gray scale with a resolution of at least 300 dpi and edited with Corel Photo-Paint 11 (menu "picture", submenu "contrast enhancement") to highlight the boundaries of the outer swarm ring.

## 4.5.2 Computerized cell tracking (Motion Analysis)

Spontaneous reversal frequencies and phototactic responses of *H. salinarum* cells were measured with a computerized cell tracking system equipped with two light sources for specific stimulation of the cells (Streif et al., in preparation). The central component of the system is the cell tracking system. It consists of a phase contrast microscope that uses non-actinic infrared light for stimulus-free observation of the cells and a CCD camera that transmits greyscale pictures via a an analog/digital transducer (digitizer) to a data processing computer. The basic principle of cell tracking is described in section 3.2.5, page 59. In brief, the system is capable to detect cell centroids in a series of video frames and to connect them to a time-resolved cell track. For detection of cell reversals the double-arrow algorithm by Marwan and Oesterhelt (1990) was applied: the cell track was scanned continuously frame by frame by two arrows that touch each other

and extend 6 frames forward and backward, respectively, from where they touch. If the angle $\beta$ enclosed between the two arrows is smaller than or equal to 66.4° (or more precisely $\cos\beta \geq 0.4$), a reversal is detected (Fig. 4.1).
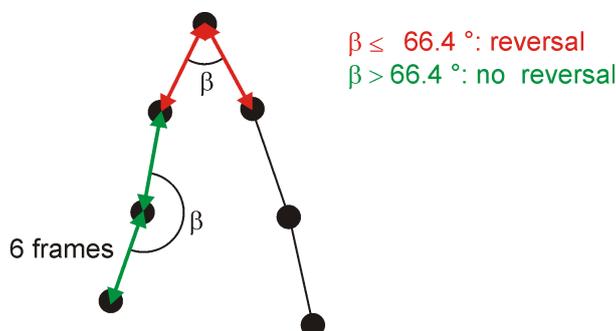


**Figure 4.1: Scheme of the double-arrow algorithm for the detection of reversals of *H. salinarum* cells.** Shown is a schematic track of a *H. salinarum* cell. Black circles indicate cell centroid positions on the track with a distance of six frames between them. For clarity, the cell centroid positions of the four frames in between are omitted. The track is scanned frame by frame by double arrows that touch each other and extend back and forth six frames, respectively from where they touch. Shown in red: double arrows that enclose an angle $\beta \leq 66.4°$ are recognized as a reversal. Shown in green: double arrows that enclose an angle $\beta > 66.4°$ are not recognized as a reversal.

In order to measure the response of the cells to light stimuli, light stimuli can be delivered through the optics of the microscope to the focus plane by two computer-controlled light sources that are coupled to the microscope via quartz fiber light guides (Fig. 4.2). The light stimuli can be applied via two separate light paths, either through the objective or the IR phase contrast condenser. Stimulation through the objective allows "local" illumination by a light spot with a diameter of 282 µm, which means that only those cells are stimulated that are in the visual field of the CCD camera. This is especially useful for pulse-shaped stimulation of the cells with blue or UV light, because a simple shift of the sample slide allows to select and stimulate a different set of cells that have not received a stimulus before. Illumination through the condenser allows "global" illumination, i.e. a spot with a diameter of 1.8 mm is illuminated which exceeds by far the visual field of the CCD camera. In this way, cells that are in the visual field as well as such that swim into the visual field during measurement are illuminated, which is useful whenever the cells are supposed to be adapted to a certain illumination, e.g. when the cells are adapted to a certain orange light intensity and then are stimulated by a step down or a shut down of orange light.

## Microscopic equipment and setup

| | |
|---|---|
| Microscope | Olympus BX51 |
| Phase contrast condenser | |
| Objective | UPlanFL 40x, N.A. 0.75, $\infty$/0.17, Olympus |
| TV adapter | U-TV1X-2, Olympus |
| C mount adapter | UCMAD-3, Olympus |
| Camera | CCD camera 4912-4000-0000, COHU, San Diego, CA, USA |
| Excitation light sources | MT20-SPA illumination system, Olympus, equipped with 150 W Hg/Xe mixed gas arc burner |

| | shutter |
| | attenuator wheels |
| | filter wheel, containing |
| Excitation filters | $360 \pm 15$ nm, AHF Analysentechnik, Tübingen, Germany |
| | $360 \pm 50$ nm, AHF Analysentechnik, Tübingen, Germany |
| | $480 \pm 15$ nm, AHF Analysentechnik, Tübingen, Germany |
| | $480 \pm 50$ nm, AHF Analysentechnik, Tübingen, Germany |
| | $580 \pm 15$ nm, AHF Analysentechnik, Tübingen, Germany |
| | $580 \pm 50$ nm, AHF Analysentechnik, Tübingen, Germany |
| Observation light source | halogen lamp |
| Infrared filter | RG780 |
| Beam splitters | DCLP650, Olympus |
| Stage | Olympus Biosystems, custom made and equipped with |
| Peltier Element | PE 94, Linkam Scientific Instruments Ltd., Surrey, England |
| Video Monitor | VM 3110, Panasonic |
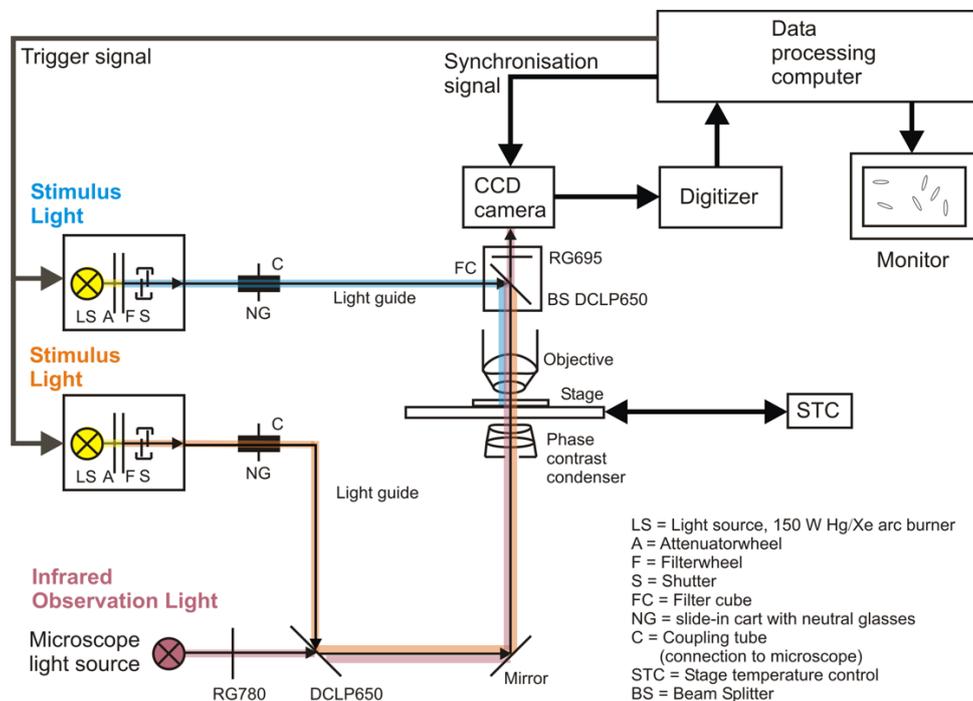


**Figure 4.2: Schematic view of the computerized cell tracking system.**

## Determination of absolute light intensities in the focus plane

In order to determine the absolute light intensities in the focus plane provided by the two MT20 light sources, a optical power meter (HT-90, HI-TOP international) was used. The power meter was equipped with a photoelectric cell that was embedded in a piece of metal with the approximate dimensions of a microscopic slide. The intensities were determined for both illumination through the condenser and through the objective for all available excitation filters (see above). The optometer measures the photocurrent

and displays the light energy in W for a chosen wavelength. In order to measure in the linear range of the power meter and to prevent saturation of the photoelectric cell, neutral density glass filters of known attenuation characteristics (see below) were used. For measurement, the photoelectric cell was placed on the microscope stage such that the maximal readout value of light energy was reached. In case of illumination through the objective the photoelectric cell was placed upright on the stage, in case of illumination through the condenser the photoelectric cell was inverted. The light spot through the objective has a fixed spotsize of 282 µm, in case of illumination through the condenser, the spotsize was set to 1.8 mm.

## Determination of transmittance of neutral density glass filters

The attenuation of light by neutral density glasses is wavelength-dependent. Therefore, the transmittance of the neutral density glasses had to be determined for all wavelengths that were used to stimulate *H. salinarum* cells. This was done by recording a spectrum (transmittance *versus* wavelength) of the filters ranging from 300 nm to 700 nm with a UV spectrophotometer (PharmaSpec UV-1700, Shimadzu). First, for baseline correction a spectrum without filter was recorded. Then, a second spectrum with the neutral filter placed in front of the measurement beam. The values of the filter spectrum were exported to an Microsoft® Excel spreadsheet.

## Determination of attenuator values

The attenuator wheels contained in the MT20 light sources are in principle rotating perforated metal disks. In contrast to neutral density filter glasses attenuation of light by the attenuator wheels is achromatic (wavelength-independent). The attenuator wheels allow to adjust 14 different degrees of attenuation.

In order to determine the actual attenuation by the attenuators, the relative light intensities of the excitation light ($480 \pm 15$ nm) that corresponded to the 14 different attenuator settings were determined by taking greyscale pictures with a CCD camera (F-view II, Olympus). The brightness of the pictures in arbitrary units was determined with the camera software and taken as a measure for the relative light intensities reflecting the attenuation. In order to avoid saturation of the camera, the integration time of the camera was varied from 3 ms to 36 ms. In addition, to countercheck linearity of the integration times neutral density glasses with known transmission ranging from 99% to 0.4% were used. The actual attenuation by the attenuator wheels of the two light sources were determined separately and in fact had different values. In case of the light source that was used for illumination through the objective, the illumination light does not pass the camera. Therefore, a trick had to be used to determine the attenuator values of this light source. A fluorescent plastic slide with fluorescence characteristics approx. like fluorescein isothiocyanate (excitation maximum at $\lambda = 495$ nm, emission maximum at $\lambda = 525$ nm) was placed under the objective. The plastic slide was excited with $480 \pm 15$ nm and the intensity of the reflecting fluorescent light determined as described. To avoid the influence of stray light coming from the excitation light, the filter cube was switched to a combination of a 505 nm dichroidic beam splitter and a 515 nm long pass blocking

filter.

## Determination of exposure times

In principle the light exposure times can be regulated by the software that sends commands to the MT20 light sources to open and close the integrated shutters. However, the actual exposure times also depend on the mechanics of the shutters. For measurement of the actual exposure times, the light fibers connected to the MT20 were removed and a photoelectric cell that was connected to an oscilloscope was placed in front of the light outlet of the MT20 light source. Opening of the shutter resulted in an increase in photocurrent to a maximum value and closing of the shutter resulted in decreased photocurrent. The time course including rise and fall of the photocurrent allowed calculation of the light exposure time.

## Preparation of microscopic slides and cover slips

To obtain reproducible phototactic behavior, the following cleaning procedure proved to be essential.

Microscopic slides (76 x 26 mm, Menzel Gläser, Braunschweig) were placed in a slide staining box and shaken three times for 1 min in deionized water. Afterwards they were shaken for 2 h in acetone and for another 2 h in ethanol at 100 rpm (Rotamax 120, Heidolph, Schwabach, Germany). Finally the slides were pulled out with pointed tweezers and wiped dry with a lint free paper cloth (Kimwipes® lite precision wipes, Kimberly-Clark®).

20 to 30 cover slips (20 x 20 mm, size 1, 0.13 - 0.16 mm thickness, Menzel Gläser, Braunschweig, Germany) were placed in a 800 ml beaker glass. The slides were shaken vigorously once in acetone for 2 min and four times for 2 min in deionized water to remove the acetone. The coverslips were then pulled out with pointed tweezers, placed upright on a filter paper circle (595, 110 mm, Schleicher & Schuell, Dassel, Germany) in a glass petri dish and dried in an oven at 80°C.

## Preparation of microscopic specimens

Cells were grown for 2 - 3 days to an $OD_{600}$ of 0.6 - 0.9. The culture was then diluted in an 25 ml Erlenmeyer flask with complex medium and complex medium supplemented with arginine to yield 10 ml of culture of an $OD_{600}$ of 0.32 - 0.35 containing arginine in a final concentration of 0.1% (w/v). The Erlenmeyer flask was then covered with an aluminum foil and placed in the dark at room temperature for at least 20 min before the first measurement.

For measurements, 5 µl cell suspension was applied to a slide and sealed under a coverslip by encircling the rim with a molten mixture of paraffin wax and vaseline (2:1 (w/w)) to prevent solvent evaporation.

## Preparation of formaldehyde treated cells to determine the minimal move radius of motile cells

Due to Brownian motion even dead or immotile cells move. In order to discriminate between motile and non-motile cells, the move radius of of formaldehyde-treated, dead cells was determined at various temeratures. The move radius is defined as a radius around the center of the whole cell track.

Cells were grown and diluted as described above. 7 µl of the diluted cells were applied to a slide that was inverted and placed on the rim of an Erlemeyer flask filled with a few milliliters of 37% (v/v) formaldehyde (Merck, Darmstadt, Germany). To prevent the cell suspension on the slide from drying out, the opening of the Erlenmeyer flask with the microsope slide on it were sealed with a piece of Parafilm "M"® (Pechiney Plastic Packaging, Chicago, IL., USA). The sample was exposed to the formaldehyde for 15 min. The cell suspension was then sealed under a coverslip as described above. The move radius of the cells was determined at various temperatures in measurements of 5 s duration as described below. The thus determined move radii were used as threshold values to discriminate between motile and immotile cells.

## General procedure of measuring the switching frequency of *H. salinarum* cells

Before starting a series of measurements consisting of 20 single measurements, the microscopic specimen was incubated on the heat stage for 5 min at 25°C and the desired background illumination. Specimens were used for measurements for 25 min at most. Background illumination was applied through the condenser with the field iris diaphragm opened as wide as possible to illuminate a maximum area of the specimen. Thus, a minimal number of non-adapted cells entering the illuminated area during a measurement could be achieved.

## Measurement of the photophobic response toward blue light pulses and step down in orange light

When the response to blue light pulses was measured, the position of the slide was changed after every single measurement to avoid repeated stimulation of the same individual cells. For the measurements in this study dark adapted cells were used.

In measurements of responses to a step down of orange light, the position of the slide was not changed, but the cells were allowed to recover for 45 s, before the next measurement was started. Thus, on the one hand the cells were optimally adapted to the orange background illumination, but on the other hand they were stimulated 20 times in a series of measurements. This procedure is therefore a compromise, because optimally one would like to measure cells that are sufficiently adapted to the constant background illumination and were not stimulated before.

## Calculation of error bars for dose-response curves

The error bars for the dose-response curves in section 3.3.1 were calculated according to Hald (1952) using the equation 4.2 below.

$$\left.\begin{array}{c} P_U \\ P_L \end{array}\right\} = \frac{1}{n+c^2} \cdot \left[ k \pm \frac{1}{2} + \frac{c^2}{2} \pm c \cdot \sqrt{\left( k \pm \frac{1}{2} \right) \left( 1 - \frac{k \pm (1/2)}{n} \right) + \frac{c^2}{4}} \right] \qquad (4.2)$$

$P_U$ and $P_L$ are the upper and lower limits of the error bars, respectively, $k$ is the number of reversing cells, $n$ is the number of evaluated cells. The value of $c$ determines the confidence interval and is equal to 1.96 for the chosen confidence interval of 95%.

### 4.5.3 Dark-field microscopy

#### Microscopic equipment and setup

Essential parts of the microscopic equipment are a dark-field immersion condenser with high numerical aperture (1.2 - 1.4), a medium power (40x), dry fluorite objective, of moderately high numerical aperture (0.75) and a high intensity light source (short-arc xenon, mercury, or xenon-mercury lamp with a power of a least 75 W).

| | |
|---|---|
| Microscope | Olympus BX50 |
| Light source | 100 W mercury lamp USH-120D, Olympus |
| Condenser | Olympus U-DCW |
| | cardioid immersion dark-field condenser |
| | N.A. 1.40 - 1.20 |
| Objective | UPlanFL 40x, Olympus, N.A. 0.75 |
| Photo tube | U-SPT, Olympus |
| Photo eye peace | PE 5 x 125 |
| TV adapter | U-PMTV, Olympus |
| C mount adapter | UCMAD-2, Olympus |
| Camera | CCD C-5405, Hamamatsu Photonics, Herrsching, Germany |
| Camera Controller | C2400, Hamamatsu Photonics, Herrsching, Germany |
| Video Monitor | WV-BM 1400, Panasonic |
| External TV card | Pinnacle PCTV Deluxe, Pinnacle |

#### Dark-field microscopy with *H. salinarum* cells

Dark-field microscopy was used to investigate two main issues, the switching frequency and the proportion of CW to CCW flagellar rotational mode in chemotaxis gene deletion mutants.

Culturing of cells and preparation of microscopic samples was done as described for computerized cell tracking with the exception that the cells were diluted to an $OD_{600}$ of 0.1. Optimally the thickness of the cover-slip should be 0.17 mm (size $1\frac{1}{2}$), because the objective is corrected for this thickness, but standard cover slips ( size 1, 0.13 - 0.16 mm thickness) worked fine.

50 µl of immersion oil ($n_e^{23}$ = 1.5180, Leitz, Wetzlar, Germany) were applied to the condenser with a cut-off pipette tip (approx. 0.5 cm of the tip was removed) to facilitate pipetting of the viscous oil. After the oil had spread evenly, the condenser was carefully approximated to the microscopic slide and positioned at its maximal height. After focusing the cells, the condenser was gradually lowered again followed by refocusing until

flagella became visible (in this position of the condenser, the diameter of the oil drop was usually about 1.2 cm). A microscopic specimen was used for 1 h at most, before a new specimen was prepared. Basic settings of the camera controller were: AGC on, high/low off, gain and offset of the contrast were between 0 and 4 and 0 and 1.5, respectively, and all shading options were at 50%. The remaining functions were shut off.

To study the switching frequency, single swimming cells were observed for a period of at least 10 min.

The flagellar rotational bias was determined by counting the number of cells that were swimming with either the flagellum behind (CW) or in front of the cell body (CCW). For counting, a "Halo-counter" software written by Stefan Streif in the MATLAB$^{®}$ environment was used. By clicking on CW and CCW buttons the software registers CW and CCW event, respectively, and saves the data in a Microsoft$^{®}$ Excel spreadsheet.

## 4.6 Electron microscopy

### 4.6.1 Growth, concentration and washing of the cells

Cells were grown under standard conditions to an $OD_{600} = 0.5$ - 0.6. 2 ml of culture were spun down (2 min, 8000·g, RT) and the supernatant removed. Residual liquid was removed with a pipette tip after another short centrifugation. The pellet was carefully resuspended in 2 portions of 500 µl Basal Salt Solution (BSS, *H. salinarum* complex medium without peptone). The resulting 1 ml cell suspension was spun down as before, the supernatant removed and residual liquid removed with a pipette tip after another short centrifugation step. Finally the pellet was carefully resuspended in altogether 1 ml of BSS.

### 4.6.2 Preparation of grids and electron microscopy

A 400 mesh carbon coated copper grid (Plano Wetzlar GmbH, S-160-4) was treated for 3 min in an evacuated plasma cleaner to render the carbon coating hydrophilic. 20 µl of the cell suspension was pipetted on the grid and incubated on the grid for 1 min before it was sucked off with a filter paper. Then 20 µl of uranyl acetate solution (2% uranyl acetate (w/v) in 100 mM maleate, pH = 6.0) were placed on the grid and left there for 1 min before it was sucked off. Finally, the grid was washed with a short jet of distilled water from a wash bottle followed by immediately sucking the water off.

Electron micrographs were taken with a Philips CM12 TEM transmission electron microscope that operated at 120 kV and was equipped with a CCD camera.

# 5 Appendix

## 5.1 Oligonucleotides

**Table 5.1: Oligonucleotides that were used in this study**. Restriction sites are underlined and the restriction enzymes are given in parantheses. Extensions added to primers to enable fusion of the upstream and downstream products to "Δ" products are italized. The position of the last is given with the following convention: +1 is the position of the 1st base of the target gene, -1 is the position of the preceding base.

| *Product name* | *Primer name* | *Primer sequence (Restriction Enzyme)* | *Pos. of last nt.* |
|---|---|---|---|
| PREFlaJ and ΔflaJ | USflaJ-1.seq | GAT CCT GCA GTC ATG GAC AAC GCC GAC GTG G (*Pst*I) | -398 |
| | USflaJ-1.rev | *GGC TCC CCG* GCT GAC TCA GAA CCC GCG TG | -1 |
| | DSflaJ-1.seq | *TCT GAG TCA GC*C GGG GAG CCA CAC TTA TGT GC | +1747 |
| | DSflaJ-1.rev | GAT CTC TAG ACA TCG CGA TGT CGT AGC TCA GC (*Xba*I) | +2186 |
| COREFlaJ | COREflaJ-1.seq | TCG CGC TCT CGT TGC CGA CG | +185 |
| | COREflaJ-1.rev | GCG CAT CCG GCA CGC GTC G | +486 |
| PREflaCE and ΔflaCE | USflaCE-1.seq | CTG ACT GCA GCG GTG CGC TCG GCA CAG C (*Pst*I) | -452 |
| | USflaCE-1.rev | *CGC AGC GGT C*CA CGA AGA CCA CGG CAG TCG G | +42 |
| | DSflaCE-1.seq | *TGG TCT TCG TG*G ACC GCT GCG AGG ACC TCC | +1474 |
| | DSflaCE-1.rev | CTG CTC TAG ACA GCG TCG ACG ACG ACA CGC (*Xba*I) | +1963 |
| COREflaCE | COREflaCE-1.seq | GGC GGT GGT GGC GGC GAC G | +118 |
| | COREflaCE-1.rev | CCA GCG GCG TTC GGA TCC AC | +458 |
| PREflaD and ΔflaD | USflaD-1.seq | GAT CCT GCA GGG CAG CGG GTT CGC CGT GG (*Pst*I) | -425 |
| | USflaD-1.rev | *CGA TCC TGT CAC* AAT GTC ATT GGC TAT CCG TGG | +9 |
| | DSflaD-1.seq | *CCA ATG ACA TTG* TGA CAG GAT CGA AAA CCG AGT C | +469 |
| | DSflaD-1.rev | CTG CTC TAG AGT TCG TTC TCG CTC CGG ACG (*Xba*I) | +915 |
| COREflaD | COREflaD-1.seq | GCG ACG AGA ACA TCC GAG AGC | +62 |
| | COREflaD-1.rev | GTG CCC CTG GAG CCG CTC G | +363 |
| *to be continued next page* | | | |

**Oligonucleotides, continued**

| *Product name* | *Primer name* | *Primer sequence (Restriction Enzyme)* | *Pos. of last nt.* |
|---|---|---|---|
| PREflgXXX and ΔflgXXX | USflgXXX-1.seq | GAT C<u>CT GCA G</u>GG AGT ACG ACA CCG CGG AGC (*Pst*I) | -401 |
| | USflgXXX-1.rev | *CAG CGT GCT GG*A CGC ATC GAC TCC ATG TAC TAG | +15 |
| | DSflgXXX-1.seq | *GTC GAT GCG T*CC AGC ACG CTG GAA CGA CGC | +640 |
| | DSflgXXX-1.rev | GTC G<u>TC TAG A</u>CT CGG CGA ACG CCG CCT GC (*Xba*I) | +1048 |
| COREflgXXX | COREflgXXX-1.seq | CGG GAT CGG AAC CTG GTG G | +27 |
| | COREflgXXX-1.rev | CGG CCC GAC CCA ATC GAC GG | +321 |
| PREcheB and ΔcheB | UScheB-1.seq | GAT G<u>CT GCA G</u>GG TCT TAC TGG TCG ACG ACT CC (*Pst*I) | -348 |
| | UScheB-1.rev | *CGT CCT CCG TAT* CAC CAG TGC CTC TGT CAT GCG | +18 |
| | DScheB-1.seq | *GGC ACT GGT G*AT ACG GAG GAC GAC GTG ACA TGG | +1027 |
| | DScheB-1.rev | CTC A<u>TC TAG A</u>CG CGT CGC GTC CAC GTC ACC (*Xba*I) | +1503 |
| COREcheB | COREcheB-1.seq | CAC CAC CGA GGA CGC CGA CG | +246 |
| | COREcheB-1.rev | CGG TCG GCG AAC CGG GAC G | +608 |
| PREcheR and ΔcheR | UScheR-1.seq | GAT C<u>CT GCA G</u>GC ACG CGA TGC TGC CGG AAG C (*Pst*I) | -333 |
| | UScheR-1.rev | *CCG CGC CGG* GCG CCG GTC GAG GTA CGA CTC | +90 |
| | DScheR-1.seq | *GAC CGG CGC* CCG GCG CGG CAG AGG AGT AAC | +808 |
| | DScheR-1.rev | CTG C<u>TC TAG A</u>CG GCG AGA GCG CGA GGT TCC (*Xba*I) | +1281 |
| COREcheR | COREcheR-1.seq | AGT GCG GCC TGC GCG GAC G | +298 |
| | COREcheR-1.rev | ACG AGG TGG CCA CCC TCA CG | +710 |
| PREcheD and ΔcheD | UScheD-1.seq | GAT C<u>CT GCA G</u>TG CCC GTC GAG CGG GTG C (*Pst*I) | -472 |
| | UScheD-1.rev | *AAA TTA CGT GCA C*CG TCA CGA CTC CTC ACT CGC G | +6 |
| | DScheD-1.seq | *AGT CGT GAC G*GT GCA CGT AAT TTG ACT GAC TTC C | +454 |
| | DScheD-1.rev | CTG C<u>TC TAG A</u>GT GCT CTC GCC AGC GCG TCC (*Xba*I) | +888 |
| PREcheC1 and ΔcheC1 | UScheC1-1.seq | GAT C<u>CT GCA G</u>GA CTC GAT GGG AGC GTC TCC (*Pst*I) | -463 |
| | UScheC1-1.rev | *TCG ACA CGC ATT* GAT TAC AGC GTA GCC ACG TCC | -1 |
| | DScheC1-1.seq | *CGC TGT AAT C*AA TGC GTG TCG ATC TCG ACG C | +589 |
| | DSCheC1-1.rev | GTC G<u>TC TAG A</u>CG TCG ATG ACC GCA GCG TCC (*Xba*I) | +1010 |
| *to be continued next page* | | | |

**Oligonucleotides, continued**

| *Product name* | *Primer name* | *Primer sequence (Restriction Enzyme)* | *Pos. of last nt.* |
|---|---|---|---|
| PREcheC3 and ΔcheC3 | UScheC3-1.seq | CAC TCT GCA GCT CGG CGC ACA CCT GGG AGC (*Pst*I) | -439 |
| | UScheC3-1.rev | *ACG ACT CCT C*TT TAG ATA CTG TTG ATC ATC GAG ACG | -1 |
| | DScheC3-1.seq | *TCA ACA GTA TCT AAA* GAG GAG TCG TGA CGA TCC GCG | +1129 |
| | DSCheC3-1.rev | GTC GTC TAG AGT CAG GTA GCC GGC GTA CTC C (*Xba*I) | +1743 |

# 5.2 Abbreviations

| | |
|---|---|
| aa(s) | amino acid(s) |
| Amp | ampicillin |
| ATP | adenosine triphosphate |
| approx., ≈ | approximately |
| bp(s) | base pair(s) |
| BLAST | Basic Local Alignment Search Tool |
| BR | bacteriorhodopsin holoprotein |
| BSA | bovine serum albumine |
| BSS | basal salt solution; *H. salinarum* complex medium without peptone |
| BSH | basal salt solution buffered with 20 mM HEPES |
| CCW | counterclockwise |
| CIC | chemical in a cuvette |
| Che | protein involved in chemotaxis |
| *che* | gene involved in chemotaxis |
| CIP | calf intestine phosphatase |
| c | concentration |
| $c_f$ | final concentration |
| CSPD | disodium 3-(4-methoxyspiro{1,2-dioxetane-3,2´-(5´-chloro)tricyclo[3.3.1.13,7]decan}-4-yl) phenyl phosphate |
| CW | clockwise |
| dATP | deoxyadenosinetriphosphate |
| dCTP | deoxycytosinetriphosphate |
| dGTP | deoxyguanosinetriphosphate |
| DIG | digoxygenin |
| DIG-11-dUTP | digoxygenin-11-2´deoxyuridine-5´-triphosphate |
| DMSO | dimethylsulfoxide |
| dNTPs | mixture of all 4 deoxy ribonucleotides dATP, dTTP, dCTP, dGTP |
| EDTA | ethylenediaminetetraacetate |
| EtOH | ethanol |

| | |
|---|---|
| Fig. | figure |
| Fla | flagellar accessory protein |
| *fla* | flagellar accessory gene |
| Flg | flagellin protein; flagellar filament structural protein |
| *flg* | flagellin gene; flagellar filament structural gene |
| HEPES | N-(2-hydroxyethyl)piperazine-N´-(2-ethanesulfonic acid) |
| HAMP | acronym out of **h**istidine kinase, **a**denylyl cyclase, **m**ethyl-accepting chemotaxis protein and **p**hosphatase |
| HK | histidin kinase |
| HM | *H. salinarum* complex medium |
| Htr(s) | halobacterial transducer protein(s) |
| *htr(s)* | halobacterial transducer gene(s) |
| HR | halorhodopsin holoprotein |
| kb | kilobase(pair)s |
| kDa | kilodalton |
| LB | Luria-Bertani |
| Mev | mevinolin (lovastatin) |
| Mb | megabase(pair)s |
| MCP(s) | methyl accecpting chemotaxis protein(s) |
| MS | mass spectrometry |
| nt. | nucleotide |
| $OD_{600}$ | optical density at 600 nm |
| ODml | one ODml corresponds to the amount of cells present in one milliliter of a halobacterial culture at an $OD_{600}$ of 1.0 |
| o.n. | over night |
| orf(s) | open reading frame(s) |
| PAGE | polyacrylamide gel elektrophoresis |
| PCR | polymerase chain reaction |
| PEG | polyethylene glycol |
| rpm | rotations per minute |
| RR | response regulator |
| RT | room temperature |
| SAM | S-adenosyl-methionine |
| SDS | sodium dodecyl sulfate |
| SMART | Simple Modular Architecture Research Tool |
| SR | sensory rhodopsin holoprotein |
| TM | melting temperature |
| Tris | tris(hydroxymethyl)aminomethane |
| T2SS | type II secretion system |
| T4P | type IV pili |
| v/v | volume per volume |
| wt | wild type |
| w/v | weight per volume |
| X-Gal | 5-bromo-4-chloro-3-indolyl-$\beta$-D-galacto pyranoside |

# 5.3 Raw data

| Mutant | measure-ment | % R spont. (No. of cells) | % R blue (No. of cells) | % R orange (No. of cells) |
|---|---|---|---|---|
| wild type | 1 | 36 (1160) | 63 (704) | 70 (797) |
| | 2 | 28 (1340) | 53 (1191) | 52 (1257) |
| $\Delta cheB$ (4) | 1 | 32 (1054) | 47 (1190) | 47 (905) |
| $\Delta cheB$ (4)/ $cheB^+$ (2) | 1 | 22 (1623) | 64 (1263) | n.d. |
| $\Delta cheR$ (5) | 1 | 11 (1282) | 12 (1239) | 10 (1365) |
| | 2 | 13 (1601) | 14 (1469) | 15 (1533) |
| $\Delta cheC1$ (2) | 1 | 24 (728) | 26 (788) | 48 (565) |
| | 2 | 16 (1356) | 32 (768) | 37 (801) |
| $\Delta cheC3$ (2) | 1 | 9 (885) | 13 (863) | 19 (863) |
| | 2 | 11 (1001) | 13 (1037) | 24 (980) |
| $\Delta cheD$ (1) | 1 | 8 (1562) | 9 (1327) | n.d. |
| $cheY^{\text{D10K,Y100W}}$ (1) | 1 | 8 (1950) | 11 (1630) | 11 (1682) |
| | 2 | 11 (1340) | 15 (1448) | 16 (1413) |

**Table 5.2: Spontaneous reversals and phototaxis determined by computerized cell tracking.** R: reversals; blue/orange: blue light/orange light stimulus; spont.: spontaneous (without stimulus, dark adapted cells); No. of cells: number of evaluated cells;

| Mutant | Date | % R spont. (No. of cells) | % R blue (No. of cells) | % R orange (No. of cells) |
|---|---|---|---|---|
| wild type | 05/07/07 | 29 (128) | 66 (97) | n.d. |
| | 05/07/13 | 27 (121) | 78 (114) | 84 (269) |
| | 05/08/08 | 4 (110) | n.d. | n.d. |
| | 05/08/17 | n.d. | 59 (108) | 76 (147) |
| | 05/11/08 | n.d. | 65 (72) | 92 (276) |
| | 05/11/21 | 22 (85) | n.d. | n.d. |
| $\Delta cheB$ (1) | 06/01/14 | 16 (769) | 24 (669) | 42 (659) |
| $\Delta cheB$ (4)/ $cheB^+$ (1) | 06/02/21 | 16 (832) | 55 (816) | 70 (953) |
| $\Delta cheR$ (5) | 06/01/12 | 4 (628) | 4 (1104) | 5 (725) |
| $\Delta cheR$ (5)/ $cheR^+$ (1) | 06/02/18 | 25 (948) | 60 (803) | 82 (828) |
| $\Delta cheD$ (1) | 05/07/07 | 3 (146) | n.d. | n.d. |
| | 05/07/13 | 5 (207) | 2 (174) | 5 (194) |
| | 05/08/17 | n.d. | 4 (159) | 5 (899) |

**Table 5.3: Spontaneous reversals and phototaxis determined by computerized cell tracking.**
R: reversals; blue/orange: blue light/orange light stimulus; spont.: spontaneous (without stimulus, dark adapted cells); No. of cells: number of evaluated cells;

| Mutant | Date | CW | CCW | % CW | Tot. CW | Tot. CCW | Av % CW |
|---|---|---|---|---|---|---|---|
| wild type | 07/01/10 | 455 | 405 | 53 | 455 | 405 | 53 |
| $\Delta cheB$ (4) | 06/09/03 | 134 | 309 | 30 | 541 | 1193 | 31 |
| | 06/10/04 | 92 | 158 | 37 | | | |
| | 06/10/05 | 69 | 107 | 39 | | | |
| | 06/11/13 | 246 | 619 | 28 | | | |
| $\Delta cheB$ (4) $/cheB^+$ (2) | 07/05/14 | 281 | 449 | 38 | 281 | 449 | 38 |
| $\Delta cheR$ (5) | 06/07/05 | 115 | 30 | 79 | 1111 | 648 | 63 |
| | 06/09/06 | 373 | 134 | 74 | | | |
| | 06/11/14 | 623 | 484 | 56 | | | |
| $\Delta cheR$ (5) $/cheR^+$ (1) | 06/07/26 | 162 | 121 | 57 | 162 | 121 | 57 |
| $\Delta cheC1$ (1) | 06/06/12 | 15 | 28 | 35 | 158 | 147 | 52 |
| $\Delta cheC1$ (2) | 06/06/12 | 63 | 54 | 54 | | | |
| $\Delta cheC1$ (2) | 06/11/14 | 80 | 65 | 54 | | | |
| $\Delta cheC3$ (1) | 06/06/13 | 165 | 84 | 66 | 707 | 277 | 72 |
| $\Delta cheC3$ (2) | 06/11/13 | 542 | 193 | 74 | | | |
| $\Delta cheD$ (1) | 06/07/25 | 180 | 35 | 84 | 605 | 98 | 86 |
| | 07/05/13 | 425 | 63 | 87 | | | |
| $cheY^{\text{D10K,Y100W}}$ (1) | 07/01/10 | 820 | 8 | 99 | 1357 | 13 | 99 |
| | 07/01/17 | 537 | 5 | 99 | | | |

**Table 5.4: Detailed overview of all high intensity dark-field microscopic experiments performed to determine the flagellar rotational bias of *che* mutants.** Numbers in parantheses following the mutant designation indicate which clone was measured. CW, CCW: cells that were found to swim with their flagella rotating in CW and CCW mode, respectively; % CW: percentage of cells swimming in CW mode. Tot. CW, Tot. CCW: sum of CW and CCW numbers of all single experiments; Av % CW: average percentage of cells swimming in CW mode.

# References

Aizawa, S. I. (1996). Flagellar assembly in *Salmonella typhimurium*. *Mol Microbiol*, 19(1):1–5.

Alam, M., Claviez, M., Oesterhelt, D., and Kessel, M. (1984). Flagella and motility behaviour of square bacteria. *EMBO J*, 3(12):2899–2903.

Alam, M., Lebert, M., Oesterhelt, D., and Hazelbauer, G. L. (1989). Methyl-accepting taxis proteins in *Halobacterium halobium*. *EMBO J*, 8(2):631–639.

Alam, M. and Oesterhelt, D. (1984). Morphology, function and isolation of halobacterial flagella. *J Mol Biol*, 176(4):459–475.

Alam, M. and Oesterhelt, D. (1987). Purification, reconstitution and polymorphic transition of halobacterial flagella. *J Mol Biol*, 194(3):495–499.

Albers, S.-V. and Driessen, A. J. M. (2005). Analysis of ATPases of putative secretion operons in the thermoacidophilic archaeon *Sulfolobus solfataricus*. *Microbiology*, 151(Pt 3):763–773.

Albers, S.-V., Szabó, Z., and Driessen, A. J. M. (2006). Protein secretion in the Archaea: multiple paths towards a unique cell surface. *Nat Rev Microbiol*, 4(7):537–547.

Allers, T. and Mevarech, M. (2005). Archaeal genetics - the third way. *Nat Rev Genet*, 6(1):58–73.

Alon, U., Surette, M. G., Barkai, N., and Leibler, S. (1999). Robustness in bacterial chemotaxis. *Nature*, 397(6715):168–171.

Appleman, J. A., Chen, L.-L., and Stewart, V. (2003). Probing conservation of HAMP linker structure and signal transduction mechanism through analysis of hybrid sensor kinases. *J Bacteriol*, 185(16):4872–4882.

Appleman, J. A. and Stewart, V. (2003). Mutational analysis of a conserved signal-transducing element: the HAMP linker of the *Escherichia coli* nitrate sensor NarX. *J Bacteriol*, 185(1):89–97.

Aravind, L. and Ponting, C. P. (1999). The cytoplasmic helical linker domain of receptor histidine kinase and methyl-accepting proteins is common to many prokaryotic signalling proteins. *FEMS Microbiol Lett*, 176(1):111–116.

Aregger, M. (2003). *Charakterisierung von cheW-Deletionsmutanten in Halobacterium salinarum*. PhD thesis, Ludwigs-Maximilians-Universität München.

## References

Barak, R. and Eisenbach, M. (1992). Fumarate or a fumarate metabolite restores switching ability to rotating flagella of bacterial envelopes. *J Bacteriol*, 174(2):643–645.

Bardy, S. L., Eichler, J., and Jarrell, K. F. (2003a). Archaeal signal peptides - a comparative survey at the genome level. *Protein Sci*, 12(9):1833–1843.

Bardy, S. L. and Jarrell, K. F. (2002). FlaK of the archaeon *Methanococcus maripaludis* possesses preflagellin peptidase activity. *FEMS Microbiol Lett*, 208(1):53–59.

Bardy, S. L. and Jarrell, K. F. (2003). Cleavage of preflagellins by an aspartic acid signal peptidase is essential for flagellation in the archaeon *Methanococcus voltae*. *Mol Microbiol*, 50(4):1339–1347.

Bardy, S. L. and Maddock, J. R. (2005). Polar localization of a soluble methyl-accepting protein of *Pseudomonas aeruginosa*. *J Bacteriol*, 187(22):7840–7844.

Bardy, S. L., Mori, T., Komoriya, K., Aizawa, S.-I., and Jarrell, K. F. (2002). Identification and localization of flagellins FlaA and FlaB3 within flagella of *Methanococcus voltae*. *J Bacteriol*, 184(19):5223–5233.

Bardy, S. L., Ng, S. Y. M., and Jarrell, K. F. (2003b). Prokaryotic motility structures. *Microbiology*, 149(Pt 2):295–304.

Barkai, N., Alon, U., and Leibler, S. (2001). Robust amplification in adaptive signal transduction networks. *C R Acad Sci (Paris)*, 2(6):871–877.

Barkai, N. and Leibler, S. (1997). Robustness in simple biochemical networks. *Nature*, 387(6636):913–917.

Berg, H. C. and Purcell, E. M. (1977). Physics of chemoreception. *Biophys J*, 20(2):193–219.

Bibikov, S. I., Grishanin, R. N., Kaulen, A. D., Marwan, W., Oesterhelt, D., and Skulachev, V. P. (1993). Bacteriorhodopsin is involved in halobacterial photoreception. *Proc Natl Acad Sci U S A*, 90(20):9446–9450.

Bibikov, S. I., Grishanin, R. N., Marwan, W., Oesterhelt, D., and Skulachev, V. P. (1991). The proton pump bacteriorhodopsin is a photoreceptor for signal transduction in *Halobacterium halobium*. *FEBS Lett*, 295(1-3):223–226.

Bischoff, D. S., Bourret, R. B., Kirsch, M. L., and Ordal, G. W. (1993). Purification and characterization of *Bacillus subtilis* CheY. *Biochemistry*, 32(35):9256–9261.

Bischoff, D. S. and Ordal, G. W. (1992). Identification and characterization of FliY, a novel component of the *Bacillus subtilis* flagellar switch complex. *Mol Microbiol*, 6(18):2715–2723.

Borkovich, K. A., Alex, L. A., and Simon, M. I. (1992). Attenuation of sensory receptor signaling by covalent modification. *Proc Natl Acad Sci U S A*, 89(15):6756–6760.

152

Borkovich, K. A., Kaplan, N., Hess, J. F., and Simon, M. I. (1989). Transmembrane signal transduction in bacterial chemotaxis involves ligand-dependent activation of phosphate group transfer. *Proc Natl Acad Sci U S A*, 86(4):1208–1212.

Bourret, R. B., Hess, J. F., and Simon, M. I. (1990). Conserved aspartate residues and phosphorylation in signal transduction by the chemotaxis protein CheY. *Proc Natl Acad Sci U S A*, 87(1):41–45.

Boyd, A. and Simon, M. I. (1980). Multiple electrophoretic forms of methyl-accepting chemotaxis proteins generated by stimulus-elicited methylation in *Escherichia coli*. *J Bacteriol*, 143(2):809–815.

Braun, T. F., Al-Mawsawi, L. Q., Kojima, S., and Blair, D. F. (2004). Arrangement of core membrane segments in the MotA/MotB proton-channel complex of *Escherichia coli*. *Biochemistry*, 43(1):35–45.

Breslauer, K. J., Frank, R., Blöcker, H., and Marky, L. A. (1986). Predicting DNA duplex stability from the base sequence. *Proc Natl Acad Sci U S A*, 83(11):3746–3750.

Brindley, G. S. (1952). The Bunsen-Roscoe law for the human eye at very short durations. *J Physiol*, 118(1):135–139.

Brooun, A., Bell, J., Freitas, T., Larsen, R. W., and Alam, M. (1998). An archaeal aero-taxis transducer combines subunit I core structures of eukaryotic cytochrome c oxidase and eubacterial methyl-accepting chemotaxis proteins. *J Bacteriol*, 180(7):1642–1646.

Brooun, A., Zhang, W., and Alam, M. (1997). Primary structure and functional analysis of the soluble transducer protein HtrXI in the archaeon *Halobacterium salinarium*. *J Bacteriol*, 179(9):2963–2968.

Brown, P. N., Terrazas, M., Paul, K., and Blair, D. F. (2007). Mutational analysis of the flagellar protein FliG: sites of interaction with FliM and implications for organization of the switch complex. *J Bacteriol*, 189(2):305–312.

Bryson, K., McGuffin, L. J., Marsden, R. L., Ward, J. J., Sodhi, J. S., and Jones, D. T. (2005). Protein structure prediction servers at University College London. *Nucleic Acids Res*, 33(Web Server issue):W36–W38.

Butler, S. M. and Camilli, A. (2005). Going against the grain: chemotaxis and infection in *Vibrio cholerae*. *Nat Rev Microbiol*, 3(8):611–620.

Chaban, B., Voisin, S., Kelly, J., Logan, S. M., and Jarrell, K. F. (2006). Identification of genes involved in the biosynthesis and attachment of *Methanococcus voltae* *N*-linked glycans: insight into *N*-linked glycosylation pathways in Archaea. *Mol Microbiol*, 61(1):259–268.

## References

Chao, X., Muff, T. J., Park, S.-Y., Zhang, S., Pollard, A. M., Ordal, G. W., Bilwes, A. M., and Crane, B. R. (2006). A receptor-modifying deamidase in complex with a signaling phosphatase reveals reciprocal regulation. *Cell*, 124(3):561–571.

Chervitz, S. A. and Falke, J. J. (1996). Molecular mechanism of transmembrane signaling by the aspartate receptor: a model. *Proc Natl Acad Sci U S A*, 93(6):2545–2550.

Chi, Y. I., Yokota, H., and Kim, S. H. (1997). Apo structure of the ligand-binding domain of aspartate receptor from *Escherichia coli* and its comparison with ligand-bound or pseudoligand-bound structures. *FEBS Lett*, 414(2):327–332.

Cline, S. W., Lam, W. L., Charlebois, R. L., Schalkwyk, L. C., and Doolittle, W. F. (1989). Transformation methods for halophilic archaebacteria. *Can J Microbiol*, 35(1):148–152.

Cohen-Krausz, S. and Trachtenberg, S. (2002). The structure of the archeabacterial flagellar filament of the extreme halophile *Halobacterium salinarum* R1M1 and its relation to eubacterial flagellar filaments and type IV pili. *J Mol Biol*, 321(3):383–395.

Correia, J. D. and Jarrell, K. F. (2000). Posttranslational processing of *Methanococcus voltae* preflagellin by preflagellin peptidases of *M. voltae* and other methanogens. *J Bacteriol*, 182(3):855–858.

Cruden, D., Sparling, R., and Markovetz, A. J. (1989). Isolation and ultrastructure of the flagella of *Methanococcus thermolithotrophicus* and *Methanospirillum hungatei*. *Appl Environ Microbiol*, 55(6):1414–1419.

del Rosario, R. C., Staudinger, W. F., Streif, S., Pfeiffer, F., Mendoza, E., and Oesterhelt, D. (2007). Modeling the $CheY^{D10K,Y100W}$ *Halobacterium salinarum* mutant: sensitivity analysis allows choice of parameter to be modified in the phototaxis model. *IET Systems Biology*, 1(4):207–221.

DeLong, E. F. and Pace, N. R. (2001). Environmental diversity of bacteria and archaea. *Syst Biol*, 50(4):470–478.

Dilks, K., Giménez, M. I., and Pohlschröder, M. (2005). Genetic and biochemical analysis of the twin-arginine translocation pathway in halophilic archaea. *J Bacteriol*, 187(23):8104–8113.

Dyer, C. M., Quillin, M. L., Campos, A., Lu, J., McEvoy, M. M., Hausrath, A. C., Westbrook, E. M., Matsumura, P., Matthews, B. W., and Dahlquist, F. W. (2004). Structure of the constitutively active double mutant CheYD13K Y106W alone and in complex with a FliM peptide. *J Mol Biol*, 342(4):1325–1335.

Engel, M. B. and Catchpole, H. R. (2005). A microprobe analysis of inorganic elements in *Halobacterium salinarum*. *Cell Biol Int*, 29(8):616–622.

154

Faguy, D. M., Jarrell, K. F., Kuzio, J., and Kalmokoff, M. L. (1994). Molecular analysis of archael flagellins: similarity to the type IV pilin-transport superfamily widespread in bacteria. *Can J Microbiol*, 40(1):67–71.

Falb, M., Pfeiffer, F., Palm, P., Rodewald, K., Hickmann, V., Tittor, J., and Oesterhelt, D. (2005). Living with two extremes: conclusions from the genome sequence of *Natronomonas pharaonis. Genome Res*, 15(10):1336–1343.

Falke, J. J. and Hazelbauer, G. L. (2001). Transmembrane signaling in bacterial chemoreceptors. *Trends Biochem Sci*, 26(4):257–265.

Feng, X., Lilly, A. A., and Hazelbauer, G. L. (1999). Enhanced function conferred on low-abundance chemoreceptor Trg by a methyltransferase-docking site. *J Bacteriol*, 181(10):3164–3171.

Ferrando-May, E., Krah, M., Marwan, W., and Oesterhelt, D. (1993). The methyl-accepting transducer protein HtrI is functionally associated with the photoreceptor sensory rhodopsin I in the archaeon *Halobacterium salinarium. EMBO J*, 12(8):2999–3005.

Fuhrer, D. K. and Ordal, G. W. (1991). *Bacillus subtilis* CheN, a homolog of CheA, the central regulator of chemotaxis in *Escherichia coli. J Bacteriol*, 173(23):7443–7448.

Garrity, G., Bell, J., and Lilburn, T. (2004). Taxonomic outline of the prokaryotes. In *Bergey´s manual of systematic bacteriology, 2nd edition*. Springer-Verlag.

Garrity, L. F. and Ordal, G. W. (1997). Activation of the CheA kinase by asparagine in *Bacillus subtilis* chemotaxis. *Microbiology*, 143(Pt 9):2945–2951.

Garrity, L. F., Schiel, S. L., Merrill, R., Reizer, J., Saier, M. H., and Ordal, G. W. (1998). Unique regulation of carbohydrate chemotaxis in *Bacillus subtilis* by the phosphoenolpyruvate-dependent phosphotransferase system and the methyl-accepting chemotaxis protein McpC. *J Bacteriol*, 180(17):4475–4480.

Gegner, J. A., Graham, D. R., Roth, A. F., and Dahlquist, F. W. (1992). Assembly of an MCP receptor, CheW, and kinase CheA complex in the bacterial chemotaxis signal transduction pathway. *Cell*, 70(6):975–982.

Gerl, L., Deutzmann, R., and Sumper, M. (1989). Halobacterial flagellins are encoded by a multigene family. Identification of all five gene products. *FEBS Lett*, 244(1):137–140.

Gerl, L. and Sumper, M. (1988). Halobacterial flagellins are encoded by a multigene family. Characterization of five flagellin genes. *J Biol Chem*, 263(26):13246–13251.

Gestwicki, J. E., Lamanna, A. C., Harshey, R. M., McCarter, L. L., Kiessling, L. L., and Adler, J. (2000). Evolutionary conservation of methyl-accepting chemotaxis protein location in Bacteria and Archaea. *J Bacteriol*, 182(22):6499–6502.

Ghosh, M. and Sonawat, H. M. (1998). Kreb's TCA cycle in *Halobacterium salinarum* investigated by $^{13}$C nuclear magnetic resonance spectroscopy. *Extremophiles*, 2(4):427–433.

Gordeliy, V. I., Labahn, J., Moukhametzianov, R., Efremov, R., Granzin, J., Schlesinger, R., Büldt, G., Savopol, T., Scheidig, A. J., Klare, J. P., and Engelhard, M. (2002). Molecular basis of transmembrane signalling by sensory rhodopsinII-transducer complex. *Nature*, 419(6906):484–487.

Grammann, K., Volke, A., and Kunte, H. J. (2002). New type of osmoregulated solute transporter identified in halophilic members of the bacteria domain: TRAP transporter TeaABC mediates uptake of ectoine and hydroxyectoine in *Halomonas elongata* DSM 2581(T). *J Bacteriol*, 184(11):3078–3085.

Hald, A. (1952). *Statistical theory with engineering applications.* Wiley, London.

Hall, T. A. (1999). BioEdit: a user-friendly biological sequence alignment editor and analysis program for Windows 95/98/NT. *Nucl Acids Symp Ser*, 41:95–98.

Hanlon, D. W. and Ordal, G. W. (1994). Cloning and characterization of genes encoding methyl-accepting chemotaxis proteins in *Bacillus subtilis*. *J Biol Chem*, 269(19):14038–14046.

Hanlon, D. W., Rosario, M. M., Ordal, G. W., Venema, G., and Sinderen, D. V. (1994). Identification of TlpC, a novel 62 kDa MCP-like protein from *Bacillus subtilis*. *Microbiology*, 140 ( Pt 8):1847–1854.

Hartmann, R., Sickinger, H. D., and Oesterhelt, D. (1980). Anaerobic growth of halobacteria. *Proc Natl Acad Sci U S A*, 77(7):3821–3825.

Henke, J. M. and Bassler, B. L. (2004). Bacterial social engagements. *Trends Cell Biol*, 14(11):648–656.

Hess, J. F., Bourret, R. B., and Simon, M. I. (1988a). Histidine phosphorylation and phosphoryl group transfer in bacterial chemotaxis. *Nature*, 336(6195):139–143.

Hess, J. F., Oosawa, K., Kaplan, N., and Simon, M. I. (1988b). Phosphorylation of three proteins in the signaling pathway of bacterial chemotaxis. *Cell*, 53(1):79–87.

Hess, J. F., Oosawa, K., Matsumura, P., and Simon, M. I. (1987). Protein phosphorylation is involved in bacterial chemotaxis. *Proc Natl Acad Sci U S A*, 84(21):7609–7613.

Hildebrand, E. and Schimz, A. (1985). *Sensing and response in microorganisms*, chapter Behavioral pattern and its photosensory control in *Halobacterium halobium*, pages 129–142. Elsevier Science Publischer B.V.

Hildebrand, E. and Schimz, A. (1987). Role of the response oscillator in inverse responses of *Halobacterium halobium* to weak light stimuli. *J Bacteriol*, 169(1):254–259.

Hoff, W. D., Jung, K. H., and Spudich, J. L. (1997). Molecular mechanism of photosignaling by archaeal sensory rhodopsins. *Annu Rev Biophys Biomol Struct*, 26:223–258.

Holmes, M. L. and Dyall-Smith, M. L. (2000). Sequence and expression of a halobacterial beta-galactosidase gene. *Mol Microbiol*, 36(1):114–122.

Hou, S., Brooun, A., Yu, H. S., Freitas, T., and Alam, M. (1998). Sensory rhodopsin II transducer HtrII is also responsible for serine chemotaxis in the archaeon *Halobacterium salinarum*. *J Bacteriol*, 180(6):1600–1602.

Hou, S., Larsen, R. W., Boudko, D., Riley, C. W., Karatan, E., Zimmer, M., Ordal, G. W., and Alam, M. (2000). Myoglobin-like aerotaxis transducers in Archaea and Bacteria. *Nature*, 403(6769):540–544.

Hughes, K. T. and Aldridge, P. D. (2001). Putting a lid on it. *Nat Struct Biol*, 8(2):96–97.

Hulko, M., Berndt, F., Gruber, M., Linder, J. U., Truffault, V., Schultz, A., Martin, J., Schultz, J. E., Lupas, A. N., and Coles, M. (2006). The HAMP domain structure implies helix rotation in transmembrane signaling. *Cell*, 126(5):929–940.

Iino, T., Komeda, Y., Kutsukake, K., Macnab, R. M., Matsumura, P., Parkinson, J. S., Simon, M. I., and Yamaguchi, S. (1988). New unified nomenclature for the flagellar genes of *Escherichia coli* and *Salmonella typhimurium*. *Microbiol Rev*, 52(4):533–535.

Jarrell, K. F., Bayley, D. P., Florian, V., and Klein, A. (1996). Isolation and characterization of insertional mutations in flagellin genes in the archaeon *Methanococcus voltae*. *Mol Microbiol*, 20(3):657–666.

Jones, D. T. (1999). Protein secondary structure prediction based on position-specific scoring matrices. *J Mol Biol*, 292(2):195–202.

Kalmokoff, M. L. and Jarrell, K. F. (1991). Cloning and sequencing of a multigene family encoding the flagellins of *Methanococcus voltae*. *J Bacteriol*, 173(22):7113–7125.

Kalmokoff, M. L., Jarrell, K. F., and Koval, S. F. (1988). Isolation of flagella from the archaebacterium *Methanococcus voltae* by phase separation with Triton X-114. *J Bacteriol*, 170(4):1752–1758.

Karatan, E., Saulmon, M. M., Bunn, M. W., and Ordal, G. W. (2001). Phosphorylation of the response regulator CheV is required for adaptation to attractants during *Bacillus subtilis* chemotaxis. *J Biol Chem*, 276(47):43618–43626.

Kates, M. (1996). Structural analysis of phospholipids and glycolipids in extremely halophilic archaebacteria. *Journal of Microbiological Methods*, 25(2):113–128.

Kehry, M. R., Bond, M. W., Hunkapiller, M. W., and Dahlquist, F. W. (1983a). Enzymatic deamidation of methyl-accepting chemotaxis proteins in *Escherichia coli* catalyzed by the *cheB* gene product. *Proc Natl Acad Sci U S A*, 80(12):3599–3603.

Kehry, M. R. and Dahlquist, F. W. (1982). The methyl-accepting chemotaxis proteins of *Escherichia coli*. Identification of the multiple methylation sites on methyl-accepting chemotaxis protein I. *J Biol Chem*, 257(17):10378–10386.

Kehry, M. R., Engström, P., Dahlquist, F. W., and Hazelbauer, G. L. (1983b). Multiple covalent modifications of Trg, a sensory transducer of *Escherichia coli*. *J Biol Chem*, 258(8):5050–5055.

Kentner, D. and Sourjik, V. (2006). Spatial organization of the bacterial chemotaxis system. *Curr Opin Microbiol*, 9:619–624.

Kessel, M., Wildhaber, I., Cohen, S., and Baumeister, W. (1988). Three-dimensional structure of the regular surface glycoprotein layer of *Halobacterium volcanii* from the Dead Sea. *EMBO J*, 7(5):1549–1554.

Kibbe, W. A. (2007). OligoCalc: an online oligonucleotide properties calculator. *Nucleic Acids Res*. Epub ahead of print.

Kim, K. K., Yokota, H., and Kim, S. H. (1999). Four-helical-bundle structure of the cytoplasmic domain of a serine chemotaxis receptor. *Nature*, 400(6746):787–792.

Kirby, J. R., Kristich, C. J., Feinberg, S. L., and Ordal, G. W. (1997). Methanol production during chemotaxis to amino acids in *Bacillus subtilis*. *Mol Microbiol*, 24(4):869–878.

Kirby, J. R., Kristich, C. J., Saulmon, M. M., Zimmer, M. A., Garrity, L. F., Zhulin, I. B., and Ordal, G. W. (2001). CheC is related to the family of flagellar switch proteins and acts independently from CheD to control chemotaxis in *Bacillus subtilis*. *Mol Microbiol*, 42(3):573–585.

Kirby, J. R., Niewold, T. B., Maloy, S., and Ordal, G. W. (2000). CheB is required for behavioural responses to negative stimuli during chemotaxis in *Bacillus subtilis*. *Mol Microbiol*, 35(1):44–57.

Kirby, J. R., Saulmon, M. M., Kristich, C. J., and Ordal, G. W. (1999). CheY-dependent methylation of the asparagine receptor, McpB, during chemotaxis in *Bacillus subtilis*. *J Biol Chem*, 274(16):11092–11100.

Kirsch, M. L., Peters, P. D., Hanlon, D. W., Kirby, J. R., and Ordal, G. W. (1993a). Chemotactic methylesterase promotes adaptation to high concentrations of attractant in *Bacillus subtilis*. *J Biol Chem*, 268(25):18610–18616.

Kirsch, M. L., Zuberi, A. R., Henner, D., Peters, P. D., Yazdi, M. A., and Ordal, G. W. (1993b). Chemotactic methyltransferase promotes adaptation to repellents in *Bacillus subtilis*. *J Biol Chem*, 268(34):25350–25356.

Klare, J. P., Gordeliy, V. I., Labahn, J., Büldt, G., Steinhoff, H.-J., and Engelhard, M. (2004). The archaeal sensory rhodopsin II/transducer complex: a model for transmembrane signal transfer. *FEBS Lett*, 564(3):219–224.

Klein, A. (2005). *Vergleichende Analyse halophiler Genome.* Diploma thesis, Fachhochschule Bingen.

Klein, C., Garcia-Rizo, C., Bisle, B., Scheffer, B., Zischka, H., Pfeiffer, F., Siedler, F., and Oesterhelt, D. (2005). The membrane proteome of *Halobacterium salinarum*. *Proteomics*, 5(1):180–197.

Koch, M. K. (2005). *Investigations on halobacterial transducers with respect to membrane potential sensing and adaptive methylation.* PhD thesis, Fakultät für Chemie und Pharmazie der Ludwigs-Maximilians-Universität München.

Koch, M. K. and Oesterhelt, D. (2005). MpcT is the transducer for membrane potential changes in *Halobacterium salinarum. Mol Microbiol*, 55(6):1681–1694.

Koch, M. K., Staudinger, W. F., Siedler, F., and Oesterhelt, D. (2007). Physiological sites of deamidation and methyl esterification in sensory transducers of *Halobacterium salinarum.* Submitted.

Kokoeva, M. V. and Oesterhelt, D. (2000). BasT, a membrane-bound transducer protein for amino acid detection in *Halobacterium salinarum. Mol Microbiol*, 35(3):647–656.

Kokoeva, M. V., Storch, K.-F., Klein, C., and Oesterhelt, D. (2002). A novel mode of sensory transduction in archaea: binding protein-mediated chemotaxis towards osmoprotectants and amino acids. *EMBO J*, 21(10):2312–2322.

Kollmann, M., Løvdok, L., Bartholomé, K., Timmer, J., and Sourjik, V. (2005). Design principles of a bacterial signalling network. *Nature*, 438(7067):504–507.

Koonin, E. V. (1993). A superfamily of ATPases with diverse functions containing either classical or deviant ATP-binding motif. *J Mol Biol*, 229(4):1165–1174.

Kornfeld, R. and Kornfeld, S. (1985). Assembly of asparagine-linked oligosaccharides. *Annu Rev Biochem*, 54:631–664.

Kristich, C. J., Glekas, G. D., and Ordal, G. W. (2003). The conserved cytoplasmic module of the transmembrane chemoreceptor McpC mediates carbohydrate chemotaxis in *Bacillus subtilis. Mol Microbiol*, 47(5):1353–1366.

Kristich, C. J. and Ordal, G. W. (2002). *Bacillus subtilis* CheD is a chemoreceptor modification enzyme required for chemotaxis. *J Biol Chem*, 277(28):25356–25362.

Kunst, F., Ogasawara, N., Moszer, I., Albertini, A. M., Alloni, G., Azevedo, V., Bertero, M. G., Bessières, P., Bolotin, A., Borchert, S., Borriss, R., Boursier, L., Brans, A., Braun, M., Brignell, S. C., Bron, S., Brouillet, S., Bruschi, C. V., Caldwell, B., Capuano, V., Carter, N. M., Choi, S. K., Codani, J. J., Connerton, I. F., and Danchin, A. (1997). The complete genome sequence of the gram-positive bacterium *Bacillus subtilis. Nature*, 390(6657):249–256.

Kupper, J., Marwan, W., Typke, D., Grünberg, H., Uwer, U., Gluch, M., and Oesterhelt, D. (1994). The flagellar bundle of *Halobacterium salinarium* is inserted into a distinct polar cap structure. *J Bacteriol*, 176(16):5184–5187.

Langworthy, T. A. and Pond, J. L. (1986). Archaebacterial ether lipids and chemotaxonomy. *System Appl Microbiol*, 7(3):253–257.

LaPointe, C. F. and Taylor, R. K. (2000). The type 4 prepilin peptidases comprise a novel family of aspartic acid proteases. *J Biol Chem*, 275(2):1502–1510.

Le Moual, H. and Koshland, D. E. (1996). Molecular evolution of the C-terminal cytoplasmic domain of a superfamily of bacterial receptors involved in taxis. *J Mol Biol*, 261(4):568–585.

Lechner, J., Wieland, F., and Sumper, M. (1985a). Biosynthesis of sulfated saccharides *N*-glycosidically linked to the protein via glucose. Purification and identification of sulfated dolichyl monophosphoryl tetrasaccharides from halobacteria. *J Biol Chem*, 260(2):860–866.

Lechner, J., Wieland, F., and Sumper, M. (1985b). Transient methylation of dolichyl oligosaccharides is an obligatory step in halobacterial sulfated glycoprotein biosynthesis. *J Biol Chem*, 260(15):8984–8989.

Lee, S. Y., Cho, H. S., Pelton, J. G., Yan, D., Henderson, R. K., King, D. S., Huang, L., Kustu, S., Berry, E. A., and Wemmer, D. E. (2001). Crystal structure of an activated response regulator bound to its target. *Nat Struct Biol*, 8(1):52–56.

Letunic, I., Copley, R. R., Pils, B., Pinkert, S., Schultz, J., and Bork, P. (2006). SMART 5: domains in the context of genomes and networks. *Nucleic Acids Res*, 34(Database issue):D257–D260.

Li, M. and Hazelbauer, G. L. (2004). Cellular stoichiometry of the components of the chemotaxis signaling complex. *J Bacteriol*, 186(12):3687–3694.

Li, M. and Hazelbauer, G. L. (2005). Adaptational assistance in clusters of bacterial chemoreceptors. *Mol Microbiol*, 56(6):1617–1626.

Lukat, G. S., Lee, B. H., Mottonen, J. M., Stock, A. M., and Stock, J. B. (1991). Roles of the highly conserved aspartate and lysine residues in the response regulator of bacterial chemotaxis. *J Biol Chem*, 266(13):8348–8354.

Lupas, A. and Stock, J. (1989). Phosphorylation of an N-terminal regulatory domain activates the CheB methylesterase in bacterial chemotaxis. *J Biol Chem*, 264(29):17337–17342.

Macnab, R. M. (1976). Examination of bacterial flagellation by dark-field microscopy. *J Clin Microbiol*, 4(3):258–265.

Macnab, R. M. (1996). *In Escherichia coli and Salmonella: Cellular and molecular biology.*, chapter Flagella and motility, pages 123–145. ASM press, 2nd edition.

Macnab, R. M. (1999). The bacterial flagellum: reversible rotary propellor and type III export apparatus. *J Bacteriol*, 181(23):7149–7153.

Macnab, R. M. (2003). How bacteria assemble flagella. *Annu Rev Microbiol*, 57:77–100.

Macnab, R. M. and Koshland, D. E. (1972). The gradient-sensing mechanism in bacterial chemotaxis. *Proc Natl Acad Sci U S A*, 69(9):2509–2512.

Macnab, R. M. and Ornston, M. K. (1977). Normal-to-curly flagellar transitions and their role in bacterial tumbling. Stabilization of an alternative quaternary structure by mechanical force. *J Mol Biol*, 112(1):1–30.

Maddock, J. R. and Shapiro, L. (1993). Polar location of the chemoreceptor complex in the *Escherichia coli* cell. *Science*, 259(5102):1717–1723.

Mao, H., Cremer, P. S., and Manson, M. D. (2003). A sensitive, versatile microfluidic assay for bacterial chemotaxis. *Proc Natl Acad Sci U S A*, 100(9):5449–5454.

Marg, B.-L., Schweimer, K., Sticht, H., and Oesterhelt, D. (2005). A two-alpha-helix extra domain mediates the halophilic character of a plant-type ferredoxin from halophilic archaea. *Biochemistry*, 44(1):29–39.

Martin, A. C., Wadhams, G. H., and Armitage, J. P. (2001a). The roles of the multiple CheW and CheA homologues in chemotaxis and in chemoreceptor localization in *Rhodobacter sphaeroides*. *Mol Microbiol*, 40(6):1261–1272.

Martin, A. C., Wadhams, G. H., Shah, D. S., Porter, S. L., Mantotta, J. C., Craig, T. J., Verdult, P. H., Jones, H., and Armitage, J. P. (2001b). CheR- and CheB-dependent chemosensory adaptation system of *Rhodobacter sphaeroides*. *J Bacteriol*, 183(24):7135–7144.

Marwan, W., Alam, M., and Oesterhelt, D. (1987). Die Geißelbewegung halophiler Bakterien. *Naturwissenschaften*, 74(12):585–590.

Marwan, W., Alam, M., and Oesterhelt, D. (1991). Rotation and switching of the flagellar motor assembly in *Halobacterium halobium*. *J Bacteriol*, 173(6):1971–1977.

Marwan, W., Hegemann, P., and Oesterhelt, D. (1988). Single photon detection by an archaebacterium. *J Mol Biol*, 199(4):663–664.

Marwan, W. and Oesterhelt, D. (1987). Signal formation in the halobacterial photophobic response mediated by a fourth retinal protein (P480). *J Mol Biol*, 195(2):333–342.

Marwan, W. and Oesterhelt, D. (1990). Quantitation of photochromism of sensory rhodopsin-I by computerized tracking of *Halobacterium halobium* cells. *J Mol Biol*, 215(2):277–285.

# References

Marwan, W., Schäfer, W., and Oesterhelt, D. (1990). Signal transduction in *Halobacterium* depends on fumarate. *EMBO J*, 9(2):355–362.

Mattick, J. S. (2002). Type IV pili and twitching motility. *Annu Rev Microbiol*, 56:289–314.

McCain, D. A., Amici, L. A., and Spudich, J. L. (1987). Kinetically resolved states of the *Halobacterium halobium* flagellar motor switch and modulation of the switch by sensory rhodopsin I. *J Bacteriol*, 169(10):4750–4758.

McGuffin, L. J., Bryson, K., and Jones, D. T. (2000). The PSIPRED protein structure prediction server. *Bioinformatics*, 16(4):404–405.

Merz, A. J., So, M., and Sheetz, M. P. (2000). Pilus retraction powers bacterial twitching motility. *Nature*, 407(6800):98–102.

Metlina, A. L. (2004). Bacterial and archaeal flagella as prokaryotic motility organelles. *Biochemistry (Mosc)*, 69(11):1203–1212.

Milburn, M. V., Privé, G. G., Milligan, D. L., Scott, W. G., Yeh, J., Jancarik, J., Koshland, D. E., and Kim, S. H. (1991). Three-dimensional structures of the ligand-binding domain of the bacterial aspartate receptor with and without a ligand. *Science*, 254(5036):1342–1347.

Miller, M. B. and Bassler, B. L. (2001). Quorum sensing in bacteria. *Annu Rev Microbiol*, 55:165–199.

Milligan, D. L. and Koshland, D. E. (1988). Site-directed cross-linking. Establishing the dimeric structure of the aspartate receptor of bacterial chemotaxis. *J Biol Chem*, 263(13):6268–6275.

Müller, J., Schiel, S., Ordal, G. W., and Saxild, H. H. (1997). Functional and genetic characterization of mcpC, which encodes a third methyl-accepting chemotaxis protein in *Bacillus subtilis*. *Microbiology*, 143 ( Pt 10):3231–3240.

Montrone, M., Marwan, W., Grünberg, H., Musseleck, S., Starostzik, C., and Oesterhelt, D. (1993). Sensory rhodopsin-controlled release of the switch factor fumarate in *Halobacterium salinarium*. *Mol Microbiol*, 10(5):1077–1085.

Montrone, M., Oesterhelt, D., and Marwan, W. (1996). Phosphorylation-independent bacterial chemoresponses correlate with changes in the cytoplasmic level of fumarate. *J Bacteriol*, 178(23):6882–6887.

Morton-Firth, C. J., Shimizu, T. S., and Bray, D. (1999). A free-energy-based stochastic simulation of the Tar receptor complex. *J Mol Biol*, 286(4):1059–1074.

Motallebi-Veshareh, M., Rouch, D. A., and Thomas, C. M. (1990). A family of ATPases involved in active partitioning of diverse bacterial plasmids. *Mol Microbiol*, 4(9):1455–1463.

Moukhametzianov, R., Klare, J. P., Efremov, R., Baeken, C., Göppner, A., Labahn, J., Engelhard, M., Büldt, G., and Gordeliy, V. I. (2006). Development of the signal in sensory rhodopsin and its transfer to the cognate transducer. *Nature*, 440(7080):115–119.

Murphy, G. E., Leadbetter, J. R., and Jensen, G. J. (2006). *In situ* structure of the complete *Treponema primitia* flagellar motor. *Nature*, 442(7106):1062–1064.

Ng, S. Y. M., Chaban, B., and Jarrell, K. F. (2006). Archaeal flagella, bacterial flagella and type IV pili: A comparison of genes and posttranslational modifications. *J Mol Microbiol Biotechnol*, 11(3-5):167–191.

Ninfa, E. G., Stock, A., Mowbray, S., and Stock, J. (1991). Reconstitution of the bacterial chemotaxis signal transduction system from purified components. *J Biol Chem*, 266(15):9764–9770.

Nordmann, B., Lebert, M. R., Alam, M., Nitz, S., Kollmannsberger, H., Oesterhelt, D., and Hazelbauer, G. L. (1994). Identification of volatile forms of methyl groups released by *Halobacterium salinarium*. *J Biol Chem*, 269(23):16449–16454.

Nutsch, T. (2006). *Die Phototaxis von Halobacterium salinarum - Mathematische Beschreibung stochastischer Prozesse*. PhD thesis, Institut für Systemdynamik und Regelungstechnik Universität Stuttgart.

Nutsch, T., Oesterhelt, D., Gilles, E. D., and Marwan, W. (2005). A quantitative model of the switch cycle of an archaeal flagellar motor and its sensory control. *Biophys J*, 89(4):2307–2323.

Oesterhelt, D. (1998). The structure and mechanism of the family of retinal proteins from halophilic archaea. *Curr Opin Struct Biol*, 8(4):489–500.

Oesterhelt, D. and Krippahl, G. (1983). Phototrophic growth of halobacteria and its use for isolation of photosynthetically-deficient mutants. *Ann Microbiol (Paris)*, 134B(1):137–150.

Oesterhelt, D. and Marwan, W. (1987). Change of membrane potential is not a component of the photophobic transduction chain in *Halobacterium halobium*. *J Bacteriol*, 169(8):3515–3520.

Oesterhelt, D. and Marwan, W. (2005). Salz in der Suppe des Lebens. *Biospektrum*, 1:60–62.

Oesterhelt, D. and Tittor, J. (1989). Two pumps, one principle: light-driven ion transport in halobacteria. *Trends Biochem Sci*, 14(2):57–61.

Olszewska, E. and Jones, K. (1988). Vacuum blotting enhances nucleic acid transfer. *Trends Genet*, 4(4):92–94.

## References

Oren, A. (1991). Anaerobic growth of halophilic achaeobacteria by reduction of fumarate. *J Gen Microbiol*, 137:1387–1390.

Oren, A. and Trüper, H. G. (1990). Anaerobic growth of halophilic archaeobacteria by reduction of dimethysulfoxide and trimethylamine N-oxide. *FEMS Microbiology Letters*, 70(1):33–36.

Otomo, J., Marwan, W., Oesterhelt, D., Desel, H., and Uhl, R. (1989). Biosynthesis of the two halobacterial light sensors P480 and sensory rhodopsin and variation in gain of their signal transduction chains. *J Bacteriol*, 171(4):2155–2159.

Paggi, R. A., Martone, C. B., Fuqua, C., and Castro, R. E. D. (2003). Detection of quorum sensing signals in the haloalkaliphilic archaeon *Natronococcus occultus*. *FEMS Microbiol Lett*, 221(1):49–52.

Park, S.-Y., Borbat, P. P., Gonzalez-Bonet, G., Bhatnagar, J., Pollard, A. M., Freed, J. H., Bilwes, A. M., and Crane, B. R. (2006a). Reconstruction of the chemotaxis receptor-kinase assembly. *Nat Struct Mol Biol*, 13(5):400–407.

Park, S.-Y., Chao, X., Gonzalez-Bonet, G., Beel, B. D., Bilwes, A. M., and Crane, B. R. (2004). Structure and function of an unusual family of protein phosphatases: the bacterial chemotaxis proteins CheC and CheX. *Mol Cell*, 16(4):563–574.

Park, S.-Y., Lowder, B., Bilwes, A. M., Blair, D. F., and Crane, B. R. (2006b). Structure of FliM provides insight into assembly of the switch complex in the bacterial flagella motor. *Proc Natl Acad Sci U S A*, 103(32):11886–11891.

Parkinson, J. S. (1976). *cheA*, *cheB*, and *cheC* genes of *Escherichia coli* and their role in chemotaxis. *J Bacteriol*, 126(2):758–770.

Parkinson, J. S. (1978). Complementation analysis and deletion mapping of *Escherichia coli* mutants defective in chemotaxis. *J Bacteriol*, 135(1):45–53.

Patenge, N., Berendes, A., Engelhardt, H., Schuster, S. C., and Oesterhelt, D. (2001). The *fla* gene cluster is involved in the biogenesis of flagella in *Halobacterium salinarum*. *Mol Microbiol*, 41(3):653–663.

Patenge, N., Haase, A., Bolhuis, H., and Oesterhelt, D. (2000). The gene for a halophilic beta-galactosidase (*bgaH*) of *Haloferax alicantei* as a reporter gene for promoter analyses in *Halobacterium salinarum*. *Mol Microbiol*, 36(1):105–113.

Peabody, C. R., Chung, Y. J., Yen, M.-R., Vidal-Ingigliardi, D., Pugsley, A. P., and Saier, M. H. (2003). Type II protein secretion and its relationship to bacterial type IV pili and archaeal flagella. *Microbiology*, 149(Pt 11):3051–3072.

Perazzona, B. and Spudich, J. L. (1999). Identification of methylation sites and effects of phototaxis stimuli on transducer methylation in *Halobacterium salinarum*. *J Bacteriol*, 181(18):5676–5683.

Perez, E. and Stock, A. M. (2006). Characterization of the *Thermotoga maritima* chemotaxis methylation system that lacks pentapeptide-dependent methyltransferase CheR:MCP tethering. *Mol Microbiol*, 63(2):363–378.

Porter, S. L., Wadhams, G. H., Martin, A. C., Byles, E. D., Lancaster, D. E., and Armitage, J. P. (2006). The CheYs of *Rhodobacter sphaeroides*. *J Biol Chem*, 281(43):32694–32704.

Porter, S. L., Warren, A. V., Martin, A. C., and Armitage, J. P. (2002). The third chemotaxis locus of *Rhodobacter sphaeroides* is essential for chemotaxis. *Mol Microbiol*, 46(4):1081–1094.

Prasad, K., Caplan, S. R., and Eisenbach, M. (1998). Fumarate modulates bacterial flagellar rotation by lowering the free energy difference between the clockwise and counterclockwise states of the motor. *J Mol Biol*, 280(5):821–828.

Pyatibratov, M. G., Leonard, K., Tarasov, V. Y., and Fedorov, O. V. (2002). Two immunologically distinct types of protofilaments can be identified in *Natrialba magadii* flagella. *FEMS Microbiol Lett*, 212(1):23–27.

Rao, C. V., Kirby, J. R., and Arkin, A. P. (2004). Design and diversity in bacterial chemotaxis: a comparative study in *Escherichia coli* and *Bacillus subtilis*. *PLoS Biol*, 2(2):239–252.

Reuter, C. J. and Maupin-Furlow, J. A. (2004). Analysis of proteasome-dependent proteolysis in *Haloferax volcanii* cells, using short-lived green fluorescent proteins. *Appl Environ Microbiol*, 70(12):7530–7538.

Rollins, C. and Dahlquist, F. W. (1981). The methyl-accepting chemotaxis proteins of *E. coli*: a repellent-stimulated, covalent modification, distinct from methylation. *Cell*, 25(2):333–340.

Rosario, M. M., Fredrick, K. L., Ordal, G. W., and Helmann, J. D. (1994). Chemotaxis in *Bacillus subtilis* requires either of two functionally redundant CheW homologs. *J Bacteriol*, 176(9):2736–2739.

Rosario, M. M., Kirby, J. R., Bochar, D. A., and Ordal, G. W. (1995). Chemotactic methylation and behavior in *Bacillus subtilis*: role of two unique proteins, CheC and CheD. *Biochemistry*, 34(11):3823–3831.

Rosario, M. M. and Ordal, G. W. (1996). CheC and CheD interact to regulate methylation of *Bacillus subtilis* methyl-accepting chemotaxis proteins. *Mol Microbiol*, 21(3):511–518.

Rose, R. W., Brüser, T., Kissinger, J. C., and Pohlschröder, M. (2002). Adaptation of protein secretion to extremely high-salt conditions by extensive use of the twin-arginine translocation pathway. *Mol Microbiol*, 45(4):943–950.

## References

Rudolph, J., Nordmann, B., Storch, K. F., Gruenberg, H., Rodewald, K., and Oesterhelt, D. (1996). A family of halobacterial transducer proteins. *FEMS Microbiol Lett*, 139(2-3):161–168.

Rudolph, J. and Oesterhelt, D. (1995). Chemotaxis and phototaxis require a CheA histidine kinase in the archaeon *Halobacterium salinarium*. *EMBO J*, 14(4):667–673.

Rudolph, J. and Oesterhelt, D. (1996). Deletion analysis of the *che* operon in the archaeon *Halobacterium salinarium*. *J Mol Biol*, 258(4):548–554.

Rudolph, J., Tolliday, N., Schmitt, C., Schuster, S. C., and Oesterhelt, D. (1995). Phosphorylation in halobacterial signal transduction. *EMBO J*, 14(17):4249–4257.

Ruepp, A. and Soppa, J. (1996). Fermentative arginine degradation in *Halobacterium salinarium* (formerly *Halobacterium halobium*): genes, gene products, and transcripts of the *arcRACB* gene cluster. *J Bacteriol*, 178(16):4942–4947.

Samatey, F. A., Imada, K., Nagashima, S., Vonderviszt, F., Kumasaka, T., Yamamoto, M., and Namba, K. (2001). Structure of the bacterial flagellar protofilament and implications for a switch for supercoiling. *Nature*, 410(6826):331–337.

Saulmon, M. M., Karatan, E., and Ordal, G. W. (2004). Effect of loss of CheC and other adaptational proteins on chemotactic behaviour in *Bacillus subtilis*. *Microbiology*, 150(Pt 3):581–589.

Sauvonnet, N., Vignon, G., Pugsley, A. P., and Gounon, P. (2000). Pilus formation and protein secretion by the same machinery in *Escherichia coli*. *EMBO J*, 19(10):2221–2228.

Scharf, B., Pevec, B., Hess, B., and Engelhard, M. (1992). Biochemical and photochemical properties of the photophobic receptors from *Halobacterium halobium* and *Natronobacterium pharaonis*. *Eur J Biochem*, 206(2):359–366.

Scharf, B. E., Fahrner, K. A., Turner, L., and Berg, H. C. (1998). Control of direction of flagellar rotation in bacterial chemotaxis. *Proc Natl Acad Sci U S A*, 95(1):201–206.

Schäfer, G., Engelhard, M., and Müller, V. (1999). Bioenergetics of the Archaea. *Microbiol Mol Biol Rev*, 63(3):570–620.

Schimz, A. and Hildebrand, E. (1985). Response regulation and sensory control in *Halobacterium halobium* based on an oscillator. *Nature*, 317:641– 643.

Schobert, B. and Lanyi, J. K. (1982). Halorhodopsin is a light-driven chloride pump. *J Biol Chem*, 257(17):10306–10313.

Schultz, J., Milpetz, F., Bork, P., and Ponting, C. P. (1998). SMART, a simple modular architecture research tool: identification of signaling domains. *Proc Natl Acad Sci U S A*, 95(11):5857–5864.

Schuster, M., Zhao, R., Bourret, R. B., and Collins, E. J. (2000). Correlated switch binding and signaling in bacterial chemotaxis. *J Biol Chem*, 275(26):19752–19758.

Schuster, S. C., Swanson, R. V., Alex, L. A., Bourret, R. B., and Simon, M. I. (1993). Assembly and function of a quaternary signal transduction complex monitored by surface plasmon resonance. *Nature*, 365(6444):343–347.

Segall, J. E., Block, S. M., and Berg, H. C. (1986). Temporal comparisons in bacterial chemotaxis. *Proc Natl Acad Sci U S A*, 83(23):8987–8991.

Silverman, M. and Simon, M. (1974). Flagellar rotation and the mechanism of bacterial motility. *Nature*, 249(452):73–74.

Sourjik, V. (2004). Receptor clustering and signal processing in *E. coli* chemotaxis. *Trends Microbiol*, 12(12):569–576.

Sourjik, V. and Berg, H. C. (2000). Localization of components of the chemotaxis machinery of *Escherichia coli* using fluorescent protein fusions. *Mol Microbiol*, 37(4):740–751.

Sourjik, V. and Berg, H. C. (2002a). Binding of the *Escherichia coli* response regulator CheY to its target measured in vivo by fluorescence resonance energy transfer. *Proc Natl Acad Sci U S A*, 99(20):12669–12674.

Sourjik, V. and Berg, H. C. (2002b). Receptor sensitivity in bacterial chemotaxis. *Proc Natl Acad Sci U S A*, 99(1):123–127.

Speranskii, V., Novikova, A. L. M. T., and Bakeyeva, L. Y. (1996). Bacterial and archaeal flagella as prokaryotic motility organelles. *Biochemistry (Mosc)*, 41(1):167–173.

Spudich, J. L. and Stoeckenius, W. (1979). Photosensory and chemosensory behavior of *Halobacterium halobium*. *Photobiochemistry and Photobiophysics*, 1:43–53.

Staudinger, W. F. (2001). *Funktionsanalyse des Gens flaK in Halobacterium salinarum durch Deletion und Komplementation*. Diploma thesis, Julius-Maximilians-Universität Würzburg.

Stock, J., Kersulis, G., and Koshland, D. E. (1985). Neither methylating nor demethylating enzymes are required for bacterial chemotaxis. *Cell*, 42(2):683–690.

Stoeckenius, W. and Rowen, R. (1967). A morphological study of *Halobacterium halobium* and its lysis in media of low salt concentration. *J Cell Biol*, 34(1):365–393.

Storch, K. F., Rudolph, J., and Oesterhelt, D. (1999). Car: a cytoplasmic sensor responsible for arginine chemotaxis in the archaeon *Halobacterium salinarum*. *EMBO J*, 18(5):1146–1158.

Streif, S., Joanidopoulos, K., Staudinger, W. F., Seel, M., Marwan, W., and Oesterhelt, D. (2007). Quantitative analysis of signal transduction in motile and phototactic archaea by computerized light stimulation and tracking. In preparation.

## References

Sugimoto, N., Nakano, S., Yoneyama, M., and Honda, K. (1996). Improved thermodynamic parameters and helix initiation factor to predict stability of DNA duplexes. *Nucleic Acids Res*, 24(22):4501–4505.

Sumper, M. (1987). Halobacterial glycoprotein biosynthesis. *Biochim Biophys Acta*, 906(1):69–79.

Sundberg, S. A., Alam, M., Lebert, M., Spudich, J. L., Oesterhelt, D., and Hazelbauer, G. L. (1990). Characterization of *Halobacterium halobium* mutants defective in taxis. *J Bacteriol*, 172(5):2328–2335.

Szabó, Z., Sani, M., Groeneveld, M., Zolghadr, B., Schelert, J., Albers, S.-V., Blum, P., Boekema, E. J., and Driessen, A. J. M. (2007). Flagellar motility and structure in the hyperthermoacidophilic Archaeon *Sulfolobus solfataricus*. *J Bacteriol*, 189(11):4305–4309.

Szurmant, H., Bunn, M. W., Cannistraro, V. J., and Ordal, G. W. (2003). *Bacillus subtilis* hydrolyzes CheY-P at the location of its action, the flagellar switch. *J Biol Chem*, 278(49):48611–48616.

Szurmant, H., Muff, T. J., and Ordal, G. W. (2004). *Bacillus subtilis* CheC and FliY are members of a novel class of CheY-P-hydrolyzing proteins in the chemotactic signal transduction cascade. *J Biol Chem*, 279(21):21787–21792.

Szurmant, H. and Ordal, G. W. (2004). Diversity in chemotaxis mechanisms among the bacteria and archaea. *Microbiol Mol Biol Rev*, 68(2):301–319.

Tarasov, V. Y., Pyatibratov, M. G., Tang, S. L., Dyall-Smith, M., and Fedorov, O. V. (2000). Role of flagellins from A and B loci in flagella formation of *Halobacterium salinarum*. *Mol Microbiol*, 35(1):69–78.

Tatusova, T. A. and Madden, T. L. (1999). BLAST 2 Sequences, a new tool for comparing protein and nucleotide sequences. *FEMS Microbiol Lett*, 174(2):247–250.

Tebbe, A., Klein, C., Bisle, B., Siedler, F., Scheffer, B., Garcia-Rizo, C., Wolfertz, J., Hickmann, V., Pfeiffer, F., and Oesterhelt, D. (2005). Analysis of the cytosolic proteome of *Halobacterium salinarum* and its implication for genome annotation. *Proteomics*, 5(1):168–179.

Thanassi, D. G. and Hultgren, S. J. (2000). Multiple pathways allow protein secretion across the bacterial outer membrane. *Curr Opin Cell Biol*, 12(4):420–430.

Thar, R. and Kühl, M. (2003). Bacteria are not too small for spatial sensing of chemical gradients: an experimental evidence. *Proc Natl Acad Sci U S A*, 100(10):5748–5753.

Thomas, N. A., Bardy, S. L., and Jarrell, K. F. (2001a). The archaeal flagellum: a different kind of prokaryotic motility structure. *FEMS Microbiol Rev*, 25(2):147–174.

Thomas, N. A., Chao, E. D., and Jarrell, K. F. (2001b). Identification of amino acids in the leader peptide of *Methanococcus voltae* preflagellin that are important in posttranslational processing. *Arch Microbiol*, 175(4):263–269.

Thomas, N. A. and Jarrell, K. F. (2001). Characterization of flagellum gene families of methanogenic archaea and localization of novel flagellum accessory proteins. *J Bacteriol*, 183(24):7154–7164.

Thomas, N. A., Mueller, S., Klein, A., and Jarrell, K. F. (2002). Mutants in *flaI* and *flaJ* of the archaeon *Methanococcus voltae* are deficient in flagellum assembly. *Mol Microbiol*, 46(3):879–887.

Thomas, N. A., Pawson, C. T., and Jarrell, K. F. (2001c). Insertional inactivation of the *flaH* gene in the archaeon *Methanococcus voltae* results in non-flagellated cells. *Mol Genet Genomics*, 265(4):596–603.

Thompson, S. R., Wadhams, G. H., and Armitage, J. P. (2006). The positioning of cytoplasmic protein clusters in bacteria. *Proc Natl Acad Sci U S A*, 103(21):8209–8214.

Trachtenberg, S., Galkin, V. E., and Egelman, E. H. (2005). Refining the structure of the *Halobacterium salinarum* flagellar filament using the iterative helical real space reconstruction method: insights into polymorphism. *J Mol Biol*, 346(3):665–676.

Trachtenberg, S., Pinnick, B., and Kessel, M. (2000). The cell surface glycoprotein layer of the extreme halophile *Halobacterium salinarum* and its relation to *Haloferax volcanii*: cryo-electron tomography of freeze-substituted cells and projection studies of negatively stained envelopes. *J Struct Biol*, 130(1):10–26.

Turner, L., Samuel, A. D., Stern, A. S., and Berg, H. C. (1999). Temperature dependence of switching of the bacterial flagellar motor by the protein CheY(13DK106YW). *Biophys J*, 77(1):597–603.

Turner, L. R., Lara, J. C., Nunn, D. N., and Lory, S. (1993). Mutations in the consensus ATP-binding sites of XcpR and PilB eliminate extracellular protein secretion and pilus biogenesis in *Pseudomonas aeruginosa*. *J Bacteriol*, 175(16):4962–4969.

Ullrich, A. and Schlessinger, J. (1990). Signal transduction by receptors with tyrosine kinase activity. *Cell*, 61(2):203–212.

Voisin, S., Houliston, R. S., Kelly, J., Brisson, J.-R., Watson, D., Bardy, S. L., Jarrell, K. F., and Logan, S. M. (2005). Identification and characterization of the unique *N*-linked glycan common to the flagellins and S-layer glycoprotein of *Methanococcus voltae*. *J Biol Chem*, 280(17):16586–16593.

Wadhams, G. H. and Armitage, J. P. (2004). Making sense of it all: bacterial chemotaxis. *Nat Rev Mol Cell Biol*, 5(12):1024–1037.

# References

Wadhams, G. H., Warren, A. V., Martin, A. C., and Armitage, J. P. (2003). Targeting of two signal transduction pathways to different regions of the bacterial cell. *Mol Microbiol*, 50(3):763–770.

Wagner, G., Hartmann, R., and Oesterhelt, D. (1978). Potassium uniport and ATP synthesis in *Halobacterium halobium*. *Eur J Biochem*, 89(1):169–179.

Wagner, G., Oesterhelt, D., Krippahl, G., and Lanyi, J. K. (1981). Bioenergetic role of halorhodopsin in *Halobacterium halobium* cells. *FEBS Lett*, 131:341–345.

Wall, D. and Kaiser, D. (1999). Type IV pili and cell motility. *Mol Microbiol*, 32(1):1–10.

Weidinger, E. (2007). *Herstellung und Charakterisierung von Chemotaxiemutanten von Halobacterium salinarum*. Diploma thesis, Fachhochschule München.

Whitchurch, C. B., Hobbs, M., Livingston, S. P., Krishnapillai, V., and Mattick, J. S. (1991). Characterisation of a *Pseudomonas aeruginosa* twitching motility gene and evidence for a specialised protein export system widespread in eubacteria. *Gene*, 101(1):33–44.

Wieland, F., Lechner, J., and Sumper, M. (1986). Iduronic acid: constituent of sulphated dolichyl phosphate oligosaccharides in halobacteria. *FEBS Letters*, 195(1-2):77–81.

Wieland, F., Paul, G., and Sumper, M. (1985). Halobacterial flagellins are sulfated glycoproteins. *J Biol Chem*, 260(28):15180–15185.

Woese, C. R. and Fox, G. E. (1977). Phylogenetic structure of the prokaryotic domain: the primary kingdoms. *Proc Natl Acad Sci U S A*, 74(11):5088–5090.

Woese, C. R., Kandler, O., and Wheelis, M. L. (1990). Towards a natural system of organisms: proposal for the domains Archaea, Bacteria, and Eucarya. *Proc Natl Acad Sci U S A*, 87(12):4576–4579.

Wolfe, A. J. and Berg, H. C. (1989). Migration of bacteria in semisolid agar. *Proc Natl Acad Sci U S A*, 86(18):6973–6977.

Wolfgang, M., Lauer, P., Park, H. S., Brossay, L., Hébert, J., and Koomey, M. (1998). PilT mutations lead to simultaneous defects in competence for natural transformation and twitching motility in piliated *Neisseria gonorrhoeae*. *Mol Microbiol*, 29(1):321–330.

Wu, S. S., Wu, J., and Kaiser, D. (1997). The *Myxococcus xanthus pilT* locus is required for social gliding motility although pili are still produced. *Mol Microbiol*, 23(1):109–121.

Yonekura, K., Maki, S., Morgan, D. G., DeRosier, D. J., Vonderviszt, F., Imada, K., and Namba, K. (2000). The bacterial flagellar cap as the rotary promoter of flagellin self-assembly. *Science*, 290(5499):2148–2152.

Zhang, W., Brooun, A., McCandless, J., Banda, P., and Alam, M. (1996). Signal transduction in the archaeon *Halobacterium salinarium* is processed through three subfamilies of 13 soluble and membrane-bound transducer proteins. *Proc Natl Acad Sci U S A*, 93(10):4649–4654.

Zhu, X., Amsler, C. D., Volz, K., and Matsumura, P. (1996). Tyrosine 106 of CheY plays an important role in chemotaxis signal transduction in *Escherichia coli*. *J Bacteriol*, 178(14):4208–4215.

Zimmer, M. A., Szurmant, H., Saulmon, M. M., Collins, M. A., Bant, J. S., and Ordal, G. W. (2002). The role of heterologous receptors in McpB-mediated signalling in *Bacillus subtilis* chemotaxis. *Mol Microbiol*, 45(2):555–568.

Zimmer, M. A., Tiu, J., Collins, M. A., and Ordal, G. W. (2000). Selective methylation changes on the *Bacillus subtilis* chemotaxis receptor McpB promote adaptation. *J Biol Chem*, 275(32):24264–24272.

# Lebenslauf

**Wilfried Franz Staudinger** (Dipl.-Chem.)

Geburtsdatum:     07.01.1973
Geburtsort:       Heibronn am Neckar, Deutschland

Adresse:          Am Klopferspitz 14c
                  82152 Martinsried

Familienstand:    ledig

Nationalität:     deutsch

## Schulausbildung

09/1979 - 07/1983    Grundschule Massenbachhausen
09/1983 - 05/1992    Gymnasium Eppingen
                     Abschluss: Allgemeine Hochschulreife

## Berufsausbildung

09/1992 - 06/1994    Kerschensteinerschule Stuttgart-Feuerbach
                     Abschluss: Staatlich geprüfter chemisch-technischer Assistent

## Zivildienst

10/1994 - 09/1995    Deutscher Paritätischer Wohlfahrtsverband, Heilbronn

## Studium und Promotion

10/1995 - 09/2001    Diplomstudiengang Chemie, Julius-Maximilians-Universität Würzburg
                     Abschluss: Diplom-Chemiker
                     Thema:    Funtionsanalyse des Gens *flaK* in
                               *Halobacterium salinarum* durch
                               Deletion und Komplementation
                     Betreuer: Prof. Dr. Dieter Oesterhelt

seit 10/2001         Promotion am Max-Planck-Institut für Biochemie, Martinsried
                     Thema:    Investigations on Flagellar Biogenesis, Motility
                               and Signal Transduction of *Halobacterium salinarum*
                     Betreuer: Prof. Dr. Dieter Oesterhelt

# Danksagungen

Mein Dank gilt...

meinem Doktorvater Dieter Oesterhelt für die interessante Thematik, sein nachhaltiges Interesse an meinen Ergebnissen, die stets hilfreichen Diskussionen und Erläuterungen sowie die langjährige finanzielle Unterstützung.

Prof. Dr. Wolfgang Marwan für die Einweihung in die Geheimnisse der halobakteriallen Phototaxis und der Bewegungsanalyse, die zahlreichen Diskussionen und seine spontane Bereitschaft, das Zweitgutachten zu schreiben.

meinem langjährigen Laborkollegen Matthias Koch für so vieles wie die Betreuung des praktischen Teils meiner Diplomarbeit, seine Hilfsbereitschaft und Kollegialität, die ausgedehnten wissenschaftlichen und nichtwissenschaftlichen Diskussion bei unzähligen gemeinsamen Abendessen und allerlei unvergessliche Erlebnisse, die ich nicht missen möchte.

Stefan Streif für seine Freundschaft und Kollegialität, sein Interesse an meiner Arbeit, seine ständige Diskussionsbereitschaft, seine Unterstützung und Nachsicht während der schweren Zeit des Schreibens und natürlich für die Entwicklung von "Halo-Track".

Peter Palm für die angenehme Atmosphäre im Büro und seine allgegenwärtige Hilfsbereitschaft.

Jens Twellmeyer für seine Freundschaft und die zahlreichen nichtwissenschaftlichen Unternehmungen, die mich mal wieder auf andere Gedanken gebracht haben.

"meiner" Diplomandin Elisabeth Weidinger für die tatkräftige Unterstützung und äußerst angenehme Zusammenarbeit.

Bettina Brustmann für ihre Freundschaft und ihre Bereitschaft, ihr molekularbiologisches Wissen insbesondere bezüglich *H. salinarum* weiterzugeben und Erfahrungen auszutauschen sowie die eine oder andere außerdienstliche Unternehmung.

den Kollegen und Freunden Peter Reichelt, Barbara Mulinacci, Katrin Krzak, Stefanie Zorbas-Seifried und Haralabos "Akis" Zorbas, Brigitte Keßler, Florian Wimmer, Judith Müller und Mirit Kolog Gulko.

den ehemaligen Benjamin Quest, Christian Klein, Steffi Offermann, Hüseyin Besir, Matthias Pfeiffer, Bianca Marg und allen anderen, die mir jetzt gerade entfallen sind.

Torsten Nutsch für die aus meiner Sicht viel zu kurze Zeit der Zusammenarbeit.

Friedhelm Pfeiffer für so manche anregende Diskussion über archaeale Motilität und Signaltransduktion und nicht zuletzt für das Korrekturlesen der Arbeit.

den Praktikanten Esther Lange, Christine Rothmund, Philipp Wild, Daniel Fleck, Anne Dueck und Jonas Müller, die mich nicht nur im Labor tatkräftig unterstützt haben, sondern auch Abwechslung und gute Stimmung in den Alltag brachten.

Günter Pfeifer für die Einweisung in die Elektronenmikroskopie.

Karin Rodewald und "Kiki" Weyrauch für ihre Sequenzierexpertise.

all jenen, die sozusagen die "Infrastruktur" der Abteilung darstellen:
Frau Haack, die so manches Problem unbürokratisch aus der Welt geschafft hat.
Jörg Tittor, als erfahrenen Wissenschaftler, Chefplaner und rechte Hand des Chefs.
Walter Erhardt, dem technischen Genie der Abteilung, der mit einer unglaublichen Geduld und Gelassenheit für die kniffligsten Probleme eine praktikable Lösung gefunden hat.

Stefan Benkert, der mich nach längerer Abstinenz dazu überredet hat, wieder regelmäßig die Fußballschuhe zu schnüren.

dem harten Kern der MPI-Kickers Herbert, Gerd, Sigi, Petschko, Peter, Hansi und Gunther für die herzliche Aufnahme eines "Studierten" ins Team, ihre Kameradschaft und die unvergesslichen Ausflüge und Sommerfeste.

zuletzt allen, die nicht unmittelbar beteiligt waren, ohne die diese Arbeit jedoch nie zustande gekommen wäre:

meinen Eltern für ihre Liebe, die Finanzierung meines Studiums und die ungebrochene moralische Unterstützung während der gesamten Zeit des Studiums und der Promotion.

meiner Familie: meinen Schwestern Sabine und Birgit, meinen Neffen Simon und David und schließlich meinen Schwägern Bertram und Holger.

meinen Freunden
aus der Schulzeit: Thorsten Dörr, Dominik Ziegler und Tobias Häberlein.
aus der Studienzeit: Franz Köhler, Matthias und Christiana Hofmann, Patrick Musch, Marco Erdmann, Simon Otter und Stefan Holzner.